Doctoral Dissertation
Doctoral Program in Metrology (34th Cycle)

Study of antimicrobial and antioxidant properties of new materials for development of active food packaging

By

Giulia Barzan

******

Supervisors:
Dr. A.M. Rossi, Supervisor, Dr. A.M. Givannozzi, Co-Supervisor

Doctoral Examination Committee:
Prof. M.P. Aznar Ramos, Referee, University of Zaragoza, Zaragoza, Spain
Prof. R. Gavara, Referee, Polytechnic University of Valencia, Valencia, Spain

Politecnico di Torino
2022

Declaration

I hereby declare that the contents and organization of this dissertation constitute my own original work and do not compromise in any way the rights of third parties, including those relating to the security of personal data.

Giulia Barzan

2022

* This dissertation is presented in partial fulfillment of the requirements for **Ph.D. degree** in the Graduate School of Politecnico di Torino (ScuDo).

I would like to dedicate this thesis to my loving parents who always remain my guide in the night

Acknowledgments

For the realization of this Doctoral thesis work I would like to acknowledge Prof. Francisco Jesús Salafranca Lázaro, of the Analytical Chemistry department of the University of Zaragoza (Spain), who was my tutor during the period I spent in Spain. He and his group, the GUIA (University Group for Analytical Research) I3A, allowed the realization of the third part of this work regarding the actual production of active food packaging polymeric materials with natural extracts. His support and precious advices, together with his kindness, willingness and moral encouragement, were fundamental to continue the advancement of the project in INRiM after the COVID-19 pandemic breakout.

I would like to acknowledge Prof. Paul Williams and Dr. James Brown from the University of Nottingham (UK), who allowed me to visit Nottingham and the Centre for Biomolecular Sciences. There I had the possibility of furthering my knowledge about many advanced microbiological techniques, which resulted fundamental to carry out the first part of this work, and to see the Robin Hood castle for real and eat fish and chips in the oldest English Inn.

My acknowledgements go also to Prof. Angelo Taglietti, from the University of Pavia, Prof. Ivana Fenoglio and Dr. Ida Kokalari, from the University of Turin, for their precious collaboration for the development of silver and carbon-based nanomaterials and nanosystems.

I would like to mention also the fundamental collaboration and advices about plastic materials for food packaging and current related normative of Dr. Paolo Ciocca, Valeria Viganò and Shirley Barrera Cardenas, from SealedAir company (Rho, Italy).

Finally, I would like to thank my supervisors Dr. Andrea Mario Rossi and Dr. Andrea Mario Giovannozzi to have allowed and sustained the realization of my PhD project in INRiM. Special thanks go to all the group of Quantum Metrology and Nanotechnology where I had the opportunity to meet very nice people, some of whom I can now call friends and also family.

Abstract

This work is focused on the design, production and characterization of sustainable active food packaging materials with antimicrobial and antioxidant properties to ensure the safety and quality of foods and prolong their shelf-life.

Firstly, a microfluidic device combining dielectrophoresis (DEP) and Raman spectroscopy was developed for a fast and dynamic characterization of different bacterial strains, including food-related pathogens (i.e. *E. coli* and *S. aureus*), directly in planktonic suspension. Predictive models to identify bacterial cross-induced resistance to antibiotic within few hours were built using this method, overcoming the overnight incubation required by classical microbiological assays. Furthermore, Raman imaging was employed to detect the spatial distribution of different biomolecules at single cell level.

Then, the antibacterial properties of innovative silver and carbon-based nanosystems and their inclusion in prototype packaging materials were studied.

Differently sized silver nanoparticles, from 6 to 50 nm, were compared for their antibacterial efficacy in suspension and immobilized on glass. For the first time, the surface minimal bactericidal concentration (SMBC) of silver needed to kill 99.9999% of bacteria, was determined by ISO 22196, thereby facilitating the comparison between measurements and minimizing the amount of silver on the materials surface (0.023-0.034 μg/cm2) as well as their cost of production and toxicity.

Colloidal carbon nanoparticles (CNP), obtained by a green chemistry synthesis, were tested against Gram + and a Gram – bacteria, by classical microbiological assays and the DEP-Raman system, revealing a rapid interaction with the bacteria but not significant bactericidal effects. Thus, CNP were loaded with an antimicrobial peptide which increased their antibacterial activity, especially against *S. aureus*.

Finally, new antioxidant packaging modified with grape and olive industrial waste products and *Moringa oleifera* leaves obtained by different extractive procedures were produced and characterized. The antioxidant efficacy of many fractions of the plants extracts were analyzed by multiple standard assays and the results were correlated with their content of polyphenols obtaining higher values for anti-solvent and maceration extract fractions. The latter, resulting from a more sustainable extraction procedure, were included in cellulose-based active packaging systems. The antioxidant properties of such films were measured by

indirect and direct analytical methods demonstrating good free radical scavenging properties for all the three kind of active agents and a higher radical reduction capacity of moringa. Additionally, the ability of the packaging coated with moringa (5% w/w) of delaying fresh ground beef oxidation was tested. This film was chosen as the best alternative to obtain the highest oxidative protection of meat on the basis of the *in vitro* results and ensuring a direct food-contact mechanism of action. This packaging revealed to prevent meat from lipid oxidation by at least 60% after 16 days compared to simple cellulose. Additionally, *in situ* analysis of the meat performed by vibrational spectroscopies evidenced also a protective action against protein and lipid degradation.

This work could be considered valuable in the field of food packaging because the use of sustainable and degradable materials to prolong the food shelf-life perfectly fits in the actual compelling need to reduce pollution and global waste production. This is in accordance with the 12th Sustainable Development Goal of the European Green Deal purpose to halve the global food waste production per capita by 2030, ensuring an efficient and sustainable use of natural resources. Hence, an innovative way to recover food industry waste is proposed and their antioxidant efficacy in active food packaging was demonstrated even on real food matrices with many different techniques strengthening the reliability of the results.

Contents

List of Figures

List of Tables

List of Abbreviations

AAPH: 2,2'-azobis(2-amidinopropane) dihydrochloride

Ac: acetone

AgNPs: silver nanoparticles

AMP: antimicrobial peptide

ANOVA: analysis of variance

AOAC: association of official analytical chemists

AP: antioxidant power

ASCA: ANOVA simultaneous component analysis

AST: antibiotic susceptibility test

ATR: attenuated total reflection

AUC: area under the curve

BHA: butylated hydroxyanisole

BHT: butylated hydroxytoluene

C: catechin

CA: cellulose acetate

CAF: caffeine

CG: catechin gallate

CNP: carbon nanoparticles

CP: ciprofloxacin

CTRL: control

DCM: dichloromethane

DEP: dielectrophoresis

DHB: 2,5-dihydroxybenzoic acid

DHPEA: dihydroxyphenylethanol

DOC: Controlled Designation of Origin

DOCG: Controlled and Guaranteed Designation of Origin

DPPH: 2,2-diphenyl-1-picrylhydrazyl radical

EC: epicatechin

***E. coli*:** *Escherichia coli*

EC_{50} : maximal effective concentration

ECHO: Educational Concerns for Hunger Organization

ECG: epicatechin gallate

ECNM: elemental carbon nanomaterials

EFSA: European Food Safety Authority

EGC: epigallocatechin

EGCG: epigallocatechin gallate

EO: essential oils

ESI : electrospray ionization

Et : ethanol

EU: European Union

EVO: extra virgin olive oil

FAO: Food and Agricultural Organization

FDA: Food and Drug Administration

FT-IR: Fourier Transform infrared

G: grape

GA: gallic acid

GC: gallocatechin

GCG: gallocatechin gallate

GC-MS: gas chromatography-mass spectrometry

H%: percentage of hydroxylation

HTC: hydrothermal carbonization

INRiM: Istituto Nazionale di Ricerca Metrologica

IR: infrared

ISO: International Organization for Standardization

LB: Luria-Bertani

LBA: Luria-Bertani agar

M: moringa

MAE: microwave assisted extraction

MAC: maceration

MAP: modified atmosphere packaging

MBC: minimal bactericidal concentration

MCP: mixture critical point

MCR-ALS: multivariate curve resolution-alternating least squares

MDA: malondialdehyde

MDR: multi-drug resistance

MDRO: multi-drug resistant organism

Met: methanol

MH: Muller Hilton

MHA: Muller Hilton agar

MIC: minimal inhibitory concentration

NA: numerical aperture

NIAS: non-intentionally added substances

NIR: near infrared

NIST: National Institute of Standards and Technology

NMI: National Measurement Institutes

NPL: National Physical Laboratory

O: olive

OD_{600}: optical density at 600 nm

OH•: hydroxyl radical

O/N: overnight

ORAC: oxygen radical absorbance capacity

***P. aeruginosa*:** *Pseudomonas aeruginosa*

PBS: phosphate-buffered saline

PCA: principal component analysis

PCR: polymerase chain reaction

PD: photo-dynamic

PDMS: polydimethylsiloxane

PDO: Protected Designation of Origin

PE: polyethylene

PET: polyethylene terephthalate

PG: propyl gallate

PGI: Protected Geographical Indication

PLS-DA: Partial least square discriminant analysis

PP: polypropylene

PT: photo-thermic

PTB: Physikalisch-Technische Bundesanstalt

PVC: polyvinyl chloride

RI: Raman Imaging

ROS: reactive oxygen species

RS: Raman spectroscopy

***S. aureus*:** *Staphylococcus aureus*

SA: salicylic acid

SAE: anti-solvent extraction

SC: supercritical

SCA: sickle cell anemia

SERS: surface enhanced Raman spectroscopy

SFE: supercritical fluid extraction

SI: international system of units

SMBC: surface minimal bactericidal concentration

SML: specific migration limits

SOP: standard operating procedures

TBA: thiobarbituric acid

TBARS: thiobarbituric acid reactive substances

TBHQ: tertiary butyl hydroquinone

TCA: trichloroacetic acid

TCS: triclosan

TE: Trolox equivalent

TSG: Traditional Specialty Guaranteed

UAE: ultrasound-assisted extraction

UPLC-MS: ultra-performance liquid chromatography-mass spectrometry

UPLC-TQ-MS: ultra performance liquid chromatography-triple quadrupole mass spectrometry

UTI: urinary tract infection

UV: ultraviolet

UV-VIS: ultraviolet-visible

30d: 30 days

10d: 10 days

Chapter 1

Introduction

1.1 Thesis aim

The aim of this thesis is to develop and characterize new active food packaging materials based on biopolymers functionalized with biocides and natural antioxidants. These agents include nanostructures and natural plant extracts, in order to increase the shelf-life of food products, to guarantee the food safety and quality, ensuring compliance with international regulations and providing strong and reliable dataset based on standard measurement procedures.

1.2 Food packaging

1.2.1 What is food packaging?

The food package plays three fundamental roles: to contain the food, to protect and preserve it from the external environment influences and damages and to provide consumers with ingredients and nutritional information [1]. Besides, the importance of ensuring traceability, convenience and tamper indications are issues of growing interests in this field. The goal of food packaging is to satisfy customers and industry requirements containing the food in a cost-effective and appealing way, while maintaining intact the safety and quality of the product and minimizing the environmental impact [2]. In the past two centuries, under the pressure of military and commercial requirements, there has been an evolution of

the food packaging from being a simple container for the product to becoming a critical challenge to prolong the product shelf-life as much as possible while maintaining integral or even improve its quality, nutritional values and safety upon international standards. Nowadays, led by the increasing demand of ready-to-eat products due to the busy lifestyle of the consumers, protection, hygiene and food safety have been the major drivers of advances in food technology and packaging innovation.

1.2.2 Active, smart and improved food packaging

In this frame, the importance of food shelf-life prolongation and safety preservation has driven technology advancements and innovations in the direction of development of new food packaging materials declined into three major areas of research and application: active, smart or intelligent, and improved packaging. All three of these functions work in synergy to ensure correct packaging and storage of food, each one focusing on a specific aspect of these phases.

Active food packaging can be defined as the positive interaction process that occurs between food, its package and the environment to improve the shelf-life and product safety [3]. As defined in the European regulation (EC) No 450/2009, active packaging systems are designed to "deliberately incorporate components that would release or absorb substances into or from the packaged food or the environment surrounding the food". Indeed, the term "active" can be used referring to a food packaging when it represents more than a simple inert barrier to the external environmental conditions, performing a specific role in food preservation [4, 5]. It is important not to confuse "active packaging" with "intelligent" or "smart packaging" because these last two terms are related to the packaging that is able to sense and provide information about the function and properties of the packaged food throughout special devices or materials which are incorporated in the package. These devices could be time and temperature indicators, gas sensing dyes, microbial growth and physical or thermal shock indicators, etc. which are all very useful for products requiring an uninterrupted cold chain [6]. They could either rely on the migration of a dye through a porous material, which is temperature and time dependent, or employ a chemical reaction (initiated when the label is applied to the packaging) which results in a colour change that alert the consumer or the seller. More recent developments include oxygen indicators based on TiO_2 nanoparticles or nanocrystalline SnO_2 [7] or freshness indicators and pathogen sensors which are able to detect food-spoilage organisms such as *Bacillus cereus*, *Vibrio parahaemolyticus* and *Salmonella.*

Therefore, on the one hand active packaging usually improves the packed food product reducing its oxidation or degradation processes resulting in its shelf-life extension, on the other hand intelligent or smart packaging is a material that monitors the food and its surrounding environment providing qualitative information through visual colorimetric changes.

Finally, improved packaging consists in the common practice of optimizing the packaging material characteristics by adding, for example, nanofillers to increase their stiffness, flexibility, gas barrier properties and temperature/moisture stability. The advantages, as said above, originate mainly from the type, amount and effective distribution of the fillers, as well as from the level of adhesion to the matrix.

In summary, improved packaging provides high performance materials with enhanced characteristics to contain food and beverage; smart packaging ensures the proper detection of storage conditions and the presence of pathogens; active packaging offers effective solutions to avoid product deterioration.

Thus, according to regulation 1935/2004/EC and 450/2009/EC active materials and articles are intended to extend the shelf-life or to maintain or improve the condition of packaged food applying different strategies like oxygen removal, moisture and temperature control or addition of chemical or natural compounds with particular properties, such as bactericidal or antioxidant efficacy [8, 9]. Indeed, active packaging is designed to deliberately incorporate various substances that would release or adsorb substances into or from the packaged food or the surrounding environment [10, 11]. The package can be functionalized with the active compounds in many different ways in order explain its properties with the highest efficacy: through direct food-contact, including the substances on the internal surface of the package, or acting on the atmospheric concentration of gaseous compounds inside the packaging manipulating the selectivity. The latest can be obtained by coating, micro perforation, lamination, co-extrusion or polymer blending [12]. In this thesis the research is focused on the development and characterization of natural and nanofabricated compounds with antibacterial and antioxidant properties in order to develop new prototype materials for active food packaging [13].

1.2.3 Biopolymers for the development of new environmentally sustainable packaging materials

Since the mid-1920s, petroleum-based plastic materials have been widely used among other classical packaging materials like glass, paper and metal thanks

to their cost effectiveness, good aesthetic quality, and excellent physical, chemical and mechanical properties.

However, the rising of global concern about environmental problems has recently drawn the attention on the dangerous consequences of plastic materials impact, especially the disposal of plastic wastes, on the planet health. This serious issue has driven to a drastic reduction of the demand of classical plastic containers and packaging materials bringing to a switch of the consumers' inclination toward more environmentally sustainable and more easily biodegradable products possibly obtained from renewable biological sources such as biopolymers.

Nowadays, biopolymers are considered as the best candidates to substitute non-biodegradable and non-renewable packaging materials thanks to their environmentally friendly characteristics [14]. To better clarify, biopolymers should be distinguished in natural biopolymers, which spontaneously occur in nature (such as polypeptide, cellulose, starch, natural rubber, chitin/chitosan, etc.) which can be produced by plants or animals, or bio-based polymers that are artificially synthesized from natural renewable resources (vegetal, animal or fungal) [15].

Biodegradable materials could be defined as "materials that are part of the earth's innate cycles like the carbon cycle and capable of decomposing back into natural elements" [16]. Indeed, biodegradable polymers are those materials whose chemical and physical characteristics deteriorate and completely degrade when exposed to microorganisms, aerobic, and anaerobic processes [17].

ISO 14855 defines biodegradability as "aerobic biodegradability under controlled composting conditions"

All natural biopolymers are biodegradable under open atmospheric conditions for definition [18].

On the other hand, even if bio-based polymers derive from natural resources it does not mean that they are biodegradable, since biodegradability is a special functionality conferred to a material which is not entailed in bio-based polymers. However, most of the polymers obtained from biological systems and bio-based products, such as vegetable oils, animal fats and extracts of plant products, are biodegradable.

It is important not to confuse the term biodegradable with compostable: "which is capable of undergoing biological decomposition in a compost site such that the material is not visually distinguishable and breaks down into carbon dioxide, water, inorganic compounds and biomass at a rate consistent with known compostable materials" (US standard ASTM D 6002).

In Europe, biodegradable plastics normative is CEN/TR 159325. It states that the characteristics of biopolymers and bioplastics can be applied to: i) bio-genic or bio-based plastic, in regard to the origin of raw materials (renewable sources); ii) biodegradable plastics, in terms of their functionality; iii) biocompatible plastics, in terms of compatibility with the human or animal body (medical applications only).

Compostable materials in Europe must meet eight criteria stated by the European Union standard (EN 13432:20006 for packaging and EN 14995:20067 for non-packaging) regarding:

- Chemical composition: volatile matter and heavy metals as well as fluorine should be limited.
- Biodegradability: more than 90% of the original material should be converted into CO_2, water and minerals by biological processes within 6 months.
- Disintegrability: at least 90% of the original mass should be decomposed into particles that are able to pass through a 2 mm × 2 mm sieve.
- Quality: absence of toxic substances and other substances that impede composting.

In addition, ISO 17088:2012 currently defines plastics suitable for recovery through aerobic composting and ISO 18606:2012 standardize the recycling of biodegradable plastics.

Table 1 summarizes the main characteristics of the composition and principal properties of biopolymers classified for their origin as natural, bio-based biodegradable and microbial.

Table 1: Most common biodegradable polymeric packaging materials and their properties

Natural biopolymers	Composition	Properties	Uses	Reference
starch	alpha-glucan, amylose, amylopectin	tasteless, odourless, insoluble in water or alcohol	laundering of clothes, papermaking, manufacturing process, adhesives, glues	[19]
cellulose	Linear chain of β(1,4)linked D-glucose	odourless, hydrophilic, chiral and biodegradable	paper products, textiles, emulsifiers, stabilizers	[20]

			in processed foods.	
chitosan	β (1,4) linked D-glucosamine and N-acetyl-D-glucosamine	positive charged polysaccharide, biocompatible, non-toxic, biodegradable	antimicrobial and wound healing biomaterials, agricultural field, food processing	[21]
agar	linear agarose and agropectin	porous gel, stable, flexible	impression material in dentistry, histopathology processing, bacteriological plates.	[22]
alginate	ester salts of alginic acid, calcium sulphate, zinc oxide, potassium titanium fluoride	flexibility, elasticity, strength, poor dimensional stability	duplicating material for artificial prosthesis	[23, 24]
Biodegradable (chemically modified) polymers	**Composition**	**Properties**	**Uses**	**Reference**
thermoplastic starch (TPS)	native starch	flexibility, elasticity, tensile strength of less than 5 MPa	biodegradable food containers, compostable films and bags, disposable eating utensils	[25]
cellulose acetate (CA)	esterification of cellulose by acetic acid, resulting in the substitution of the hydroxyl groups of cellulose by acetyl groups	valuable fibre, soft, resilient	food packaging, dresses, home furnishings, surgical products and diapers, cigarette filters	[26]
poly (L-lactide) (PLA)	dimerization of lactic acid	soluble in solvents, amorphous and semi-crystalline polymer, biodegradable, bioresorbable,	medical implants, bone screws, surgical sutures, tissue engineering, controlled drug delivery,	[27]

		biocompatible	compostable packaging	
Natural microbial polyesters	**Composition**	**Properties**	**Uses**	**Reference**
poly (hydroxybutyrate) (PHB)	linear polyester of 3-hydroxybutyric acid	natural, renewable, non-toxic, biodegradable, biocompatible, thermoplastic, soluble in chloroform and other chlorinated hydrocarbons	packaging material, medical applications (sutures, cardiovascular grafts, bone and cartilage scaffolds, drug delivery, nerve guides	[28]
poly (3-hydroxybutyrate co-3 -hydroxyvalerate) (PHBV)	monomers of 3-hydroxybutanoic acid and 3-hydroxypentanoic acid, copolymerization of PHB with 3-hydroxyvalerate (HV) through bacterial fermentation	flexibility and strength, reduced chain packing and toughness, amorphous structure	medical implants, controlled release of drugs, packaging	[29, 30]

Biopolymers are indeed one of the most dynamic polymer area and the current production of these materials is around 15 Mt/year [15].

Nonetheless, despite the many advantages that those new materials could bring, several issues remain unsolved, like the production costs of these innovative materials that are usually too expensive to be fabricated at an industrial level. In addition, they often present poorer mechanical and barrier properties if compared with traditional synthetic polymers and some problems could be created by their characteristic odour such as starch-by materials.

These issues have prevented the complete replacement of petroleum-based polymers such as polyethylene (PE), polypropylene (PP), polyvinyl chloride (PVC) and polyethylene terephthalate (PET) [31] with biopolymers as food packaging and beverage containers. Despite the enormous effort of the scientific and industrial community in this field and the continuous consumers' awareness campaign pursued by productive sectors and social media, plastics still remain

essential in modern life [32] thanks also to their lightness, versatility and flexibility properties.

In this thesis, a cellulose-based polymer was chosen as a eco-friendly biopolymer, which can be easily obtained from industrial, agricultural and green landscaping waste after separation of hemicellulose [33, 34]. Cellulose is very promising for its use in innovative food packaging systems thanks to its ability to form films at room temperatures, its absence of odour, non-toxicity and biodegradability, very low affinity for water vapour and insolubility in water [35].

Furthermore, it is reported that secondary cellulose acetate (53-56% of acetyl groups) presents good thermoplastic properties, and the substitution of common plasticizers by specific esters and other low molecular components (at least 30% by weight) can accelerate its biodegradability in soil and water, or under appropriate composting conditions of anaerobic fermentation, while maintaining nearly the same thermoplastic characteristics. Moreover, cellulose polymers such as cellulose acetate can also be recycled or incinerated without residue formation, and it can be processed into granular materials, films and strips by injection molding or extrusion. Its physical and mechanical properties are similar to those of known cellulose ester-based plastics and conventional packaging materials with a good level of transparency of films and thin-walled hollow bodies. In addition, this material shows moderate resistance to oils and fats and, for short times, even to weak acids and alkalies [36].

1.3 Antimicrobial active food packaging

1.3.1 Definition and methods of inclusion of antimicrobial additives in the packaging material

The microbial growth is one of the main reasons of rapid deterioration of food. It is often accompanied by changes in the colour, the flavour or the texture of the product and leads to loss of nutritive values, reducing the shelf-life and quality of foods and increasing the risk of food-borne diseases [13, 37].

In this context, it results clear the great potential of antimicrobial to reduce microbial growth in non-sterile foods, by minimizing the hazard of post-contamination especially of pasteurized products [5] and enhancing the safety and quality measures already adopted by food industry. The primary interest is to counteract the possible formation of a biofilm on the packaging material, which must therefore be able to resist the adhesion of biocontaminants, degrade or kill them. All these functions can be optimized thanks to proper control and tuning of

surface hydrophobicity and roughness, electrostatic interactions, and surface conformity. It is well known, in fact, that bacterial attachment to a surface is mediated by several mechanisms that can vary throughout different bacterial species and even change within a particular bacterial strain due to internal mutations: among them, hydrophobic and electrostatic interactions are the most relevant. It can also occur through a layer of adsorbed protein. Thus, surfaces that resist adsorption of proteins should be chosen to minimize bacterial adhesion. There are two kinds of antimicrobial packaging systems, that can be classified as migrating or non-migrating, depending on the antimicrobial agent used and its interaction with the matrix [38, 39, 40]. For example, the antimicrobial package that explains its effects only in direct contact with the surface of the food matrix is mainly functionalized with active agents that are effective without migrating. This kind of system is very suited for vacuum-packed or film-wrapped products. On the other hand, if the active agents are volatile substances, even if the package is not in direct contact with the surface of the product, they can migrate onto the food to explain their properties or they can modify the surrounding environment. This kind of packaging includes different technologies, like vacuum or modified atmosphere packaging (MAP) [41, 42, 43] or the employment of active substances that can inhibit the microorganisms growth in an indirect way including ethanol, carbon dioxide, silver ions, chlorine dioxide, antibiotics, bacteriocins, organic acids, essential oils and spices [37, 39, 44]. Inserting antimicrobial agents and food preservatives in the packaging material instead of their direct addition in the food presents many advantages. Firstly, a slow migration of the antimicrobial agents from the packaging material, where they are more concentrated, to the surface of the product, where the concentration is lower [45], is useful to maintain high concentration of the antimicrobials where they are needed [46]. In this way, only the necessary amount would come into contact with the food at very low levels. Furthermore, food matrices are complex because they are composed by lipids, proteins and salts. These components could cross-react with active agents directly added on the food, leading to a reduction of their efficacy. Conversely, the inclusion of the antimicrobial agent in the packaging could result more efficient. Its slow release into food, does not only induce an initial inhibition of the microorganisms extending their lag period, but also explains a residual activity over time, improving the food shelf life during transport, storage and distribution [47]. In this thesis, polymeric packaging materials have been taken into account. In this field, other than inherently antimicrobial polymers like chitosan, there are two basic approaches to produce antimicrobial films: incorporating the active compound directly into the film material, or coating the packaging with a subtle

layer of a resin containing the antimicrobial substance. The coating could be on the inner surface of the package in direct contact with the food or incorporated in the adhesive between the layers of different materials in a multi-layer system. Some of the most used antimicrobial packaging systems include the release of the active agents through diffusion, evaporation or releasing into the headspace. In the latter case, often the specific headspace concentration of the antimicrobials is maintained by a control layer with specific properties and width, which regulate the permeation of volatile active compounds [48].

1.3.2 Nanomaterials: a safer alternative to antibiotics as antibacterial food packaging additives

To satisfy the market requirements in order to successfully implement new antimicrobial packaging systems it is essential to choose carefully the right packaging for the selected antimicrobial agent, taking into consideration the environmental conditions faced by a particular food product. These issues are fundamental to create antimicrobial agents with a promising future in the food packaging industry, and need the expertise of many fields of research such as microbiology, biotechnology, food technology, material science and engineering [37]. Recently, there is a growing interest in the development of new antimicrobial packaging using natural or biologically-derived antimicrobials such as bacteriocins, enzymes and plant extracts. This tendency is driven by the consumer rising demand of minimally processed food products, as well as higher concerns about health-related issues regarding synthetic or chemical preservatives and about environmental issues, including biodegradability properties. In particular, numerous studies have focused their attention on the antimicrobial activity of plant essential oils (EO) including thyme, rosemary, cumin, laurel, mint, marjoram, clove, cinnamon, garlic, onion, etc. [49]. However, the application of essential oils in antimicrobial food packaging still presents some limitations [44] because their antimicrobial efficacy is highly influenced by pH, temperature and level of food microbial contamination [50]. Furthermore, their release on the food surface or in the environment surrounding the product may cause negative sensory effects due to their intense aroma, which can partially limit their use as food preservatives.

Nanotechnology constitutes the other research field that has demonstrated an enormous potential in multi-disciplinary areas to develop new improved, smart and active food packaging systems. Besides their proved bactericidal effects, the application of nanomaterials in the food packaging presents quite a few

advantages. For example, they can improve the thermal, mechanical and gas-barrier properties of the original polymeric material increasing their elasticity and stability under different temperature and moisture conditions [51]. Moreover, in the last few decades the overuse and misuse of antibiotics and bactericidal products in human, animal and vegetal healthcare have led to a rapid widespread of drug-resistant organisms. The multi-drug resistance has become a global emergency in many fields, but nano-additives can be considered as valid alternatives to reduce this issue. Furthermore, nanomaterials, thanks to their high surface-to-volume ratio, can be used as carriers of additives to obtain a controlled release, and they exhibit improved physical, chemical, and biological properties compared to bulk materials.

In general, the antimicrobial activity of nanomaterials is mainly dependent on their shape, size and concentration [52], as well as the cell wall structure of the bacteria. Gram-positive cell walls are thick and composed of multilayer peptidoglycan, while the Gram-negative ones are composed of complex structures with thin peptidoglycan layer surrounded by an outer membrane.

Antibacterial nanomaterials can be incorporated in or coated onto the food packaging to slow down or stop bacterial growth. The mechanism of action could occur by a first interaction of the antibacterial agent with the microorganisms' external structures obtaining a mechanical damage. Then, some other strategies can intervene such as the release of ions by metallic nanoparticles. These ions can physically and electrochemically damage the bacterial outer membrane, increasing its permeability allowing reactions with cell's internal components which can promote the production of reactive oxygen species (ROS) with consequent oxidative damage of the microorganisms [53].

There are two categories of nanomaterials generally applied in food packaging: organic and inorganic materials. While the former are typically phenols, halogenated compounds, quaternary ammonium salts, plastic polymers with natural polysaccharide or protein materials (like chitin, chitosan, zein and peptides) [54, 55], the latter includes metals, metal oxides and clay nanoparticles [56, 57]. Inorganic materials involve metal and metal oxide nanoparticles such as CuO, ZnO, TiO_2, MgO and Fe_3O_4, but the more studied, and currently applied in some commercially available packaging materials, are silver nanoparticles (AgNPs). Indeed, among all developed and characterized nanoparticles, AgNPs have risen great interest for their application in many fields and are currently extensively studied. The main reasons are their largely known broad spectrum bactericidal properties [58], low tendencies to develop microbial resistances [59] and characteristic plasmonic properties in the visible region [60]. The bactericidal

effect of silver is known from ancient times. Silver-salt materials are broadly used to preserve human health from different dangerous pathogens infections [61] and are considered, even if with some reserve, as environmental friendly. In addition, it was demonstrated that very low concentrations of silver, as 0.1 mg/m^3 for metallic silver and 0.01 mg/m^3 for soluble compounds of silver (threshold limits established by the American Conference of Governmental Industrial Hygienists, 0.01 mg/m^3 is also the permissible exposure limit (PEL) recommended by the Occupational Safety and Health Administration and the Mine Safety and Health Administration and the recommended exposure limit established by the National Institute for Occupational Safety and Health for all forms of silver), are not toxic for human and animal cells [62, 63, 64]. As a result, AgNPs, thanks to their unique antibacterial and antiviral effects [65], that can target both the microorganism's cell membrane or intracellular metabolic activity [66], and their improved physical, chemical, and biological properties with respect to bulk silver [67], have become the most widely used nano-antimicrobial additive in many consumer products. These include cosmetics, surgical coatings and medical implants [68], textiles, water disinfection applications [69] and last but not least, food packaging [70].

Another nanomaterials that are rising a noticeable interest in many fields, especially in medical and food packaging, are elemental carbon nanomaterials (ECNMs) such as carbon nanotubes [71], graphene [72], fullerene [73] and carbon nanoparticles (CNP). In particular, polysaccharide-derived CNP are an emerging class of CNMs because of their characteristic physical, photo-thermic (PT) and photo-dynamic (PD) properties, which make them very suitable for many applications. For example, in nanomedicine, they are applied as carrier of drugs and for punctual tumour phototherapy due to their ability to produce ROS and heat upon irradiation with a NIR laser beam [74, 75], as carrier of antibacterial agents [76], adsorbents for heavy metals [77] or composites for energy storage [78], and as antioxidant agents due to their ability to scavenge hydroxyl radicals. Their composition, like other carbonaceous particles (soot, carbon black, etc.) consists principally of amorphous carbon with some graphitic domains embedded in the amorphous matrix. They present many advantages: firstly, they can be obtained by hydrothermal carbonization of glucose (HTC) [74] which is considered a green synthesis process, very reproducible and useful to obtain a high yield of nanoparticles without long purification processes and expensive reagents. By modifying some parameters of this synthesis, like the precursor concentration or the temperature, it is easy to tune the CNP size. Furthermore, as their surface is negatively charged, they present a very high stability in water and

other aqueous media, and ready to use for surface functionalization. Moreover, one of the main obstacles for the translation of nanomaterials for biomedical or food applications to the market is their biopersistency, which is related to a possible accumulation in the body and could lead to short and long term harmful effects. In this sense, some studies have already demonstrated *in vitro* and *ex-vivo* their non-cytotoxicity, biocompatibility and degradability in the human body [79]. Finally, in other works CNP were shown to remain stable also in human plasma and blood, suggesting good hematocompatibility [80]. Therefore, they are very promising candidates for the active food packaging technology as carriers of antimicrobial agents or for the thermal killing of pathogens.

1.3.3 Safety of food packaging with nanomaterials

Although nanomaterials are very promising for the development of new antimicrobial food packaging solutions, there are still considerable issues to face to translate the new materials from a laboratory-scale to real-application. For instance, there is the issue that real food presents many compositional differences in comparison with synthetic laboratory food matrices or simulants. In addition, as said before, real food contains carbohydrates, fats and proteins which can interact with the antimicrobials [81, 82, 83]. All these factors, together with regulatory issues and technical constraints are some of the main reasons limiting the commercialization of nanomaterials-based antimicrobial packaging systems [37, 43]. Furthermore, many safety concerns are associated to the application of nanomaterials in food contact systems, such as their possible migration from the packaging to the food matrix [84], indeed their absorption, distribution metabolism, excretion and toxicological assessment are currently important research focuses [85]. The more dynamic behaviour of nanomaterials compared to their corresponding bulk materials has been correlated to their structural characteristics like size, shape, surface charge, presence of surface functional groups and aspect ratio. All these properties strongly influencing their circulation in bloodstream, their site-specific extravasation and their clearance profiles within organs are strictly correlated with their possible toxicity. So, they must be carefully analysed when developing a new food packaging system.

Nonetheless, higher migration properties could be beneficial to obtain more efficient antimicrobial or antioxidant effect on the food product, by releasing for example higher concentrations of silver ions against pathogen microorganisms. Consequently, it is important to take into account the limits dictated by European regulations to guarantee food safety. In general, Commission Regulation EU No

10/2011 of 14 January 2011 on plastic materials and articles intended to come into contact with food establishes specific migration limits (SML) that cannot be exceed. According to article 12 about overall migration limits "Plastic materials and articles shall not transfer their constituents to food simulants in amounts exceeding 10 milligrams of total constituents released per dm^2 of food contact surface (mg/dm^2)". It states also that during the manufacture and use of plastic materials and articles, non-intentionally added substances (NIAS) can be formed, but any potential health risk in the final material or article arising from NIAS should be assessed by the manufacturer in accordance with internationally recognized scientific principles of risk assessment [86]. In particular, for nanomaterials no SML are present in this normative since they need to be evaluated individually by specific toxicological studies and approved by the Panel on Food Contact Materials, Enzymes and Processing Aids (CEP). However, EFSA has developed a Guidance on Technical Requirements (Guidance on Particle-TR), defining the criteria for assessing the presence of a fraction of small particles, and setting out information requirements for applications in the regulated food and feed product areas (e.g. novel food, food/feed additives, food contact materials and pesticides). These requirements apply to particles requiring specific assessment at the nanoscale in conventional materials that do not meet the definition of engineered nanomaterial as set out in the Novel Food Regulation (EU) 2015/2283. Specifically, as regards silver and ZnO nanoparticles, which are the most commonly used in active food packaging systems, EFSA has published regulatory guidelines. As regards the migration of Ag into foods from silver containing materials, the European Union states a SML of 0.05 mg Ag/kg of food, while the migration of soluble ionic zinc should respect the SML of 5 mg Zn/kg food (Commission Regulation (EU) 2016/1416 amending 10/2011, Annex II).

Moreover, consumers shall be informed about the presence of innovative nanomaterials into the food packaging in order to ensure their information with respect to specific types or categories of foods. In this regard, article 18 of the Regulation (EU) No 1169/2011 of the European Parliament and of the Council of 25 October 2011, introduces that every food product should have the list of ingredients with the clear indication of "all ingredients present in the form of engineered nanomaterials shall be clearly indicated in the list of ingredients. The names of such ingredients shall be followed by the word 'nano' in brackets".

1.3.4 Standard methods for the characterization of the antibacterial efficacy of active food packaging

Since the commercialization of antimicrobial materials requires the proof of their efficacy, different *in vitro* assays are normally employed to test their antimicrobial activity. Even if most of these methods are quite simple, reproducible and inexpensive, they might differ significantly in their properties and hence in their outcome, making difficult the comparison of the results between different materials and laboratories. Main inconsistencies usually rely on the selected technique, the choice of the microorganisms as well as the extraction method and the degree of solubility or diffusivity of each test-compound [87]. Therefore, standard test methods were developed to allow objective comparison of active materials in respect of their antimicrobial properties such as those proposed by the International Organization for Standardization (ISO). In this context, the ISO 22196:2011 is widely accepted as a standard and reliable method for measuring the antibacterial activity of daily goods, as already indicated in previous works [88, 89]. Therefore, in this thesis this standard procedure, together with classical microbiological methods such as disk and well diffusion, was chosen to establish the antibacterial activity of the developed packaging systems. However, even if the international standard protocols are quite strictly defined, specific changes are allowed, based, for example, on the physio-chemical of the active materials, the microorganism to be tested for a specific application, the incubation time to follow specific kinetics of antibacterial efficacy and the growth condition and concentration of the starting inoculum. As well descripted in the work of Wiegand et al. [90], some critical physiological factors mainly influence the outcome of antimicrobial testing. It emerged that these factors are the (i) incubation time, (ii) bacteria starting concentration, (iii) the physiological state of bacteria (stationary or exponential phase of growth), and (iv) nutrient concentration. If these factors are not accurately defined and followed in the protocol, different antibacterial efficacies can be calculated, especially for a material with intermediate antibacterial effects, leading to less reliable and comparable results.

1.3.5 Dielectrophoresis-Raman method to rapidly identify bacterial drug resistances

The use of antibiotics or synthetic antimicrobial additives in food packaging innovative systems can contribute to the rising of the global issue of multi-drug

resistant organisms (MDROs) development [91]. Various studies demonstrated that also the extensive use of antimicrobial agents in everyday life, including biocides, could lead to the development of resistant bacteria to other antimicrobial agents or even to antibiotics [92]. The mechanism by which a microorganism resistant to one antimicrobial confers the resistance to other related, or even unrelated, antimicrobials is called cross-resistance, in which the same mechanism of resistance is applicable to both drugs. Nowadays, this tendency has even been aggravated by the Covid-19 pandemic outbreak which have bring the people fear of germs to an extreme limit, leading to an irrational overuse of consumer products containing antibacterial and antimicrobial agents.

Indeed, continuous exposition to little amounts of these compounds, which could remain on the surfaces, in the environment or be ingested or absorbed would inevitably be diluted to sub-lethal concentrations in the organism, promoting the activation of bacterial resistance mechanisms also among the human microflora [93].

Therefore, it is clear how the development of new techniques able to rapidly detect bacterial resistance or sensitivity to specific treatments, together with the reduction of the indiscriminate use of antibiotics, also in the food preservation, results essential to slow down the escalation of further resistances. Many research fields are devoting their efforts in the development of new antibiotic susceptibility test (AST) methods which are able to overcome the time-consuming steps, such as overnight incubation of bacterial cultures required by classical microbiological techniques, like disk diffusion, gradient diffusion and agar/broth dilution [94]. Most of the recent approaches are based on molecular methods, i.e. polymerase chain reaction (PCR) [95], or mass spectrometry techniques [96], which, however, are not cheap, because they need expensive reagents, long sample preparations and experienced operators.

However, vibrational spectroscopy and in particular Raman spectroscopy (RS), as a label-free, non-contact and cultural independent method, has emerged among other spectroscopic techniques as a good alternative for fast identification, characterization of bacteria and antibiotic resistances detection [97]. RS is very suitable to provide fast phenotype-related information of single bacterial cells, allowing direct analysis of clinical specimens. Furthermore, it does not require any toxic immunochemical staining, and sample preparation is easy and reduced to a minimum. Thus, RS as a non-invasive and non-destructive method instantly delivers a complete molecular fingerprint of the bacterial cells in their natural environment in a fast and highly specific manner, proposing itself as a rapid bacterial detection and classification technique. However, RS has a very low

cross-section (10^{-28}–10^{-30} cm^2) and its performances are constrained by the diffraction limit of the light (Abbe limit ~200 nm for visible light). Therefore, Raman analysis on dispersed bacteria can be difficult to achieve, but it was demonstrated that dielectrophoresis (DEP) can be employed in combination with RS in order to aggregate bacteria. Indeed, applying the appropriate voltage and frequency, bacteria from suspension can be directly captured in the focus of the Raman microscope, thus increasing their local concentration and optimizing the Raman signal-to-noise ratio [98, 99].

DEP is a phenomenon that describes the movement of dielectric particles when subjected to a non-uniform electric field. The basis for generating the DEP force is the interaction between the particle's dipole and the spatial gradient of the electric field.

A dielectric particle placed in an electric field becomes electrically polarized as a result of partial charge separation, which leads to an induced dipole moment. The magnitude of the induced dipole depends on the polarizability of the particle with respect to that of the medium [100]. An electrode generates the non-uniform electric field that provides the DEP effects. Current platforms utilize advanced microfabrication technologies to produce microelectrode arrays that are capable of generating strong DEP forces with small applied voltages. This method allows to perform Raman analyses dynamically on living planktonic cells in liquid culture using an integrated microfluidic device or directly on bacterial biofilms [99].

In this thesis, a combined DEP-Raman approach to rapidly test bacterial sensitivity to the most common fluoroquinolone, ciprofloxacin, was developed, further improving the total time for samples analysis and using for the first time statistical predictive models to evaluate bacterial viability in a situation of cross-induced tolerance.

1.4 Antioxidant active food packaging

1.4.1 Definition and methods of inclusion of antioxidant additives in the packaging material

As well as reducing bacterial growth, removing the oxygen from the package headspace is another one of the most desirable goals of food-packaging researchers because it is a crucial point to improve the quality of the products. Indeed, high levels of O_2 in the atmosphere surrounding the food can facilitate the oxidation of lipids and pigments present in the product modifying its colour, texture and important nutritive values due to the loss of vitamins A, C and E,

which are oxygen-sensitive. Furthermore, the presence of oxygen can lead to a faster growth of aerobic microorganisms, leading to a quicker degradation of the packaged food. Thus, the rapid deterioration of the product due to its oxidation can render its aspect intolerable for human consumption. Moreover, it can also become unsafe for the human health because of the formation of toxic aldehydes from the degradation of polyunsaturated fatty acids, which have been demonstrated to be positively correlated with some cardiovascular diseases [41, 43, 101, 102].

Lipid oxidation is one of the most important phenomena that leads to food degradation. Lipids like triglycerides and phospholipids are present in most of the commercialized food products and their auto-oxidation, caused by their spontaneous reaction with the oxygen present in the environment, is frequently associated with the development of bad odour, bad taste, darkening of their colour and rancidity. Besides lipids, also other molecules present in organic matrices could promote the formation of free radicals by photo-oxidation such as riboflavin, porphirins, bilirubin, lipoxygenase, etc. If only one ring of the chain of oxidative reactions is removed, the propagation could not take place. This fact underlines the importance of the employment of antioxidant agents in the food packaging to prolong food's shelf-life and improve its quality and safety.

The five different mechanisms of action of antioxidants are summarized in Table 2.

Table 2: Mechanisms of action of antioxidants

Name	Mechanism of action	Target	Examples	Reference
Radical scavenger	to break the chain reaction of radicals to avoid further propagation steps	free radicals	phenols	[103, 104]
Peroxide scavenger	to decompose peroxides into stable compounds	peroxides	tioethers, methionine, tiodipropionic acid, glutation peroxidase and glucose oxidase	[105]
Inhibitor of oxidation	to avoid catalytic effect of metals in	transition metals	citric acid, ascorbic acid,	

	oxidation process		tartaric acid, oxalic acid, succinic acid, oxalate, phosphate, EDTA (ethylendiamintetr acetic acid)	[105]
Singlet oxygen scavenger	to inactivate singlet oxygen and propelling molecules dissipating the energy as heat in the photo-oxidation process	singlet form of oxygen	tocopherols, carotenoids	[105]
Autoxidation protector	to prevent the enzymatic activity required for autoxidation	lipoxygenase	flavonoids, phenolic acids, gallates	[105]

There are two categories of food-related antioxidant systems: the oxygen scavengers, separate antioxidant devices which are attached to a conventional not-active packaging, like labels, pads or sachets [101] and actual antioxidant active packaging materials. The first ones are currently applied and commercialized, mainly based on the oxidation of ferrous and iron fine powders. Nevertheless, to avoid unpleasant metallic taste of the packaged food, the research is turning towards non-metallic oxygen scavengers such as catechol, citric and ascorbic acids and enzymes (like ethanol and glucose oxidases) [12, 106]. In some cases, the O_2 scavengers need to be activated, for example using particular light sources like UV or IR for photosensitive materials, or by different levels of moisture for the iron-based ones, to prevent their premature action due to the ubiquitous presence of oxygen in the environment [107]. As already said in paragraph 1.3 for the bactericidal agents, also antioxidants can be added directly into the food matrix during the production steps but this could change the foodstuffs' organoleptic properties or quality, which may negatively influence the consumer acceptance of the final product. In addition, if directly added to the food, the active antioxidant agents may exploit all their effect immediately and the preservative efficacy would conclude prematurely, leading to a faster degradation of the food. To overcome all these limitations, incorporating the antioxidant additives in the packaging material results to be the most desirable solution

because, like it was said for the antibacterial packaging, it presents many advantages. Firstly, the release of the antioxidant agents can be gradual and controlled, their action could be localized, and less amounts of the active compounds and manufacturing process steps are needed. The addition of the antioxidants in the package could also improve the safety of the oxygen scavengers technology because it avoids the accidentally ingestion of the preservatives present in the sachet in the event of a rupture. Moreover, it can expand the effective removal of the O_2 already performed by standard vacuum packaging combined with an oxygen barrier, because any little leaking from the sealing or residual oxygen could led to a premature deterioration of the food, which is not the case in the presence of a controlled release of antioxidant additives [106, 108, 109]. All these positive features render this technology the most commercially applied. The antioxidants can also be incorporated into the polymer matrix of the packaging material or coated on its internal surface in order to explicate their action modifying the headspace atmosphere [101, 106]. Indeed, the inclusion of the antioxidants in the packaging material can be performed in three different ways: i) by extrusion, previously mixing the melted polymer with the antioxidant. In this case, the highest risk is to lose or degrade most of the antioxidants due to the high temperatures during the proces; ii) by introducing the antioxidant agents as an internal layer in a multilayer structure, for example melting them in the adhesive between two layers. Usually, the antioxidant layer contains an oxygen absorber. Although this technology is already on the market, sometimes it can be expensive, since a special activation is needed when used in the food industry; iii) by coating technique, melting the antioxidant in a resin to be spread on the internal surface of the package [110]. In particular, this thesis is focused on the last two techniques because they are the most interesting for an industrial application. However, the existing antioxidant agents commonly included in the polymers usually consist of heavy metals such as chromium, and can be harmful both to human and environment health. Thus, increasing interest is focusing on plant extracts as natural additives for coating applications as safe, non-toxic and environmentally friendly. Moreover, many recent studies demonstrated that plant extracts can improve functional properties of the packaging material such as anti-corrosion, antimicrobial, antifouling, self-healing and UV-shielding [111].

Nevertheless, it is important to keep in mind that the physical, mechanical, optical and barrier properties of the material could change after the incorporation of the antioxidant compounds [112, 113, 114]. Thus, the influence of the addition of an antioxidant agent on the mechanical and physical characteristics of the

packaging material and coatings need to be assessed carefully before the incorporation. Moreover, the kind of polymeric material and of antioxidant substances should be taken into consideration to choose the best process of production in order to maintain intact the antioxidant efficacy and to permit the activation of the agents. For example, if the antioxidant needs to migrate into the food matrix, the active agents have to be allowed as food additives and it is necessary that their maximum migrated amount results within the limits prescribed by European regulations [41]. Moreover, some studies report that the relationship between the amount of antioxidant and its protective effect on the food is not always linear, and this could be due to the interaction between the active agent and the material matrix, or an overload of the antioxidant [115, 116]. Briefly, the diffusion rate of the compounds needs to be controlled to maintain the correct concentration of antioxidant in the package headspace or on the food to allow the maximum preservative efficacy. In conclusion, for each kind of food it is necessary to find the correct combination of packaging and active material [117].

1.4.2 Natural and sustainable alternatives to synthetic antioxidants for active food packaging: *Moringa oleifera* leaves, and industrial waste of grape and olive

Nowadays, consumer request for safer foods based on natural ingredients and production processes has opened the way to a growing interest on natural antioxidants to replace synthetic ones. Butylated hydroxytoluene (BHT), butylated hydroxyanisole (BHA), propyl gallate (PG), tertiary butyl hydroquinone (TBHQ), organophospate and thioester compounds are currently widely used in food packaging as antioxidant agents.

However, due to their potentially toxic effects on human health, the addition of synthetic antioxidants in foodstuffs is restricted and finely regulated by Codex Alimentarius (FAO/WHO Food Standards, 2005) as well as by European Regulation (Directive 2006/52/EC, 2006) and FDA Food Additive Status List (US Food and Drug Administration, 2006). For instance, the concentration of BHA and TBHQ in oil and fats should not exceed 200 mg/kg (individually or in combination with other added antioxidants) and 100 mg/kg for BHT (EC, 2011). These limitations could be a relevant issue in the industrial fabrication of antioxidant food packaging. Furthermore, since potential risks of carcinogenic effects on the consumers lately emerged to be related to synthetic antioxidants, natural additives such as plant extracts, essential oils from herbs and spices, and

tocopherol can be considered as a valid alternative in active food packaging production [43, 118]. In particular, essential oils and plant extracts incorporated in the packaging can offer an antioxidant and antibacterial efficacy not only through the packaged food but also in the human body if ingested, improving health benefits for the consumers [41, 106].

Recently, in compliance with the concept of circular economy and of reducing environmental problems and improve the clearance of waste, many research fields have drawn their attention on natural extracts derived from industrial waste as safer and cost-effective alternatives.

Among them, many studies demonstrated that the extracts of many plants (like green tea, *Moringa oleifera*, cocoa, grape and olive) or of fruit and vegetables peel and seeds are very rich of polyphenolic compounds and flavonoids such as quercetin, morin, catechin and epicatechin. Thus, they are the most effective and very attractive candidates to replace synthetic antioxidants and to preserve the food package's contents thanks to their high bio-compatibility, safety and possibility to obtain them from the wastes of industrial production process of common goods such as olive oil or wine [119]. Phenolic compounds, thanks to their chemical structure, are able to scavenge ROS and free radicals donating hydrogen atoms, chelating metal cations, quenching singlet oxygen or acting as substrates for attack by superoxide. Furthermore, the primary function of phenolic antioxidants is stopping the free radical reaction chain propagation rapidly donating an hydrogen atom to lipid radicals [120]. Due to their volatile nature they perform their effectiveness on the atmosphere surrounding the food and the direct contact with the food or their release from the package is not strictly necessary [121], however their action decreases with the ageing of the film. Flavonoids, instead, are non-volatile and emerging as easier to insert in the package by extrusion or injection and capable of increase the content of bioactive compounds in the product when they are put in contact with the food or released into it.

In this work, natural extracts of moringa leaves and industrial wastes of grape and olive were taken into consideration.

Viticulture and consequently winemaking is one of the major productive industrial sectors worldwide but especially in Italy, in particular in Piedmont which is the motherland of wine excellences such as Barolo, Barbera and Moscato. However, since the yield of winemaking is about 80% of the weight of all the processed grapes and grape harvest is about 60 million tons per year worldwide, this process leads inevitably to the production of huge amounts of waste (which are about 5-9 million tons per year worldwide) [122]. Furthermore,

from 100 kg of grapes 3 kg are of seeds and since around 1.4 kg of grapes are needed to obtain 1 l of wine and the world wine production has reached 264 000 000 of hl in 2008, it is an easy conclusion that the valorisation of winery waste represents an attractive opportunity and appealing business for green chemistry and associated technologies. This is even more urgent if we consider that the clearance of these waste inevitably results in an increasing of pollution due to the high content of organic substances (sugars, polyalchols, lipids, pectins, tannins, etc.) that drives to an increasing of the oxygen demand with very negative effects on the environment and on the economy. Thus, as the management of the winery waste is a global and severe environmental issue, it is clear how important is the research of innovative ways to use them other than as animal feed or fertilizers. For example, they can be a source of polyphenols and flavonoids which, as said before, are the plant secondary metabolites with the highest antioxidant properties. Nonetheless, other than to be good antioxidant, polyphenols have also demonstrated to have properties against cancer, allergies, DNA mutations and ageing [123, 124].

Another kind of food industry related waste, which can be very valuable for its high amount of phenolic compounds, is the one derived from olive oil production. As already said for the winery waste, also the olive oil by-products, especially those derived from the production of extra virgin olive oil (EVO), which is a very treasured production field in Italy and a precious source of antioxidant and others important nutrients in the human diet (such as vitamins), are extremely interesting in the perspective of using them as natural antioxidant additives in other food products thanks to their structure and biological properties. The administration of olive oil industry wastes, which consist at least of the 10% of the total olive weight, has been attentively studied in order to maximize the recovery of phenolic and other active compounds, which remain almost entirely in the discarded parts of the olives (98%) [125]. These wastes can be obtained in many forms depending on the method used for the oil extraction and their extraction phase, which always include the elimination of soil, leaves and dust from the fruit, the pressing, the malaxation and three or two-phase centrifugation and filtration steps. They can be in form of: i) “olive pomace” or “olive cake”, which is the solid waste speared from the liquid phase due to the addition of water; ii) wet solid residues, composed by both the olive pomace and the oil waste water together obtained without the addition of supplementary water; iii) olive leaves; iv) residues of the oil filtration [126, 127, 128]. The yield of the phenolic compounds content depends on the industrial process the oil faces during its production. The most valuable phenolic olive oil by-products in economical,

antioxidant and antimicrobial terms are oleuropeine (produced during the malaxation) and its derivates like hydroxytyrosol (3,4-dihydroxyphenylethanol (3,4-DHPEA)) which was reported to reach the 70% of the total phenolic content of olive mills waters [129, 130] but they are both present also in olive leaves. Nonetheless, there are other phenolic compounds such as alpha-tocopherol, caffeic acid, vanillin, apigenin, luteolin, etc. which are present in lower amounts both in the fruit and leaves [131]. Furthermore, hydroxytyrosol demonstrated to have not only a very high antioxidant efficacy, thanks to its o-diphenolic structure which stabilize radicals by the formation of an intramolecular hydrogen bond [132], but also positive effects on the prevention of cardiovascular diseases, as it is able to inhibit lipid peroxidation on low-density lipoprotein (LDL) molecules, Alzheimer's diseases and proliferation of carcinogenic cells. Moreover, it showed some antimicrobial properties against many bacterial strains which are strictly related to food-borne diseases such as *Staphylococcus aureus*, *Pseudomonas aeruginosa*, *Listeria monocytogenes* and *Helicobacter pylori* [133]. On the other hand, both oleuropeine and the other phenolic compounds like luteolin are known to be related to antitumoral activity promoting the apoptosis of carcinogenic cells and inhibiting their proliferation [134]. In summary, phenolic compounds derived from fruits and vegetables industry waste, such as wine and olive oil, own high potentiality to be employed as food preservatives in the packaging material to prolong the shelf-life of the products and maintain intact or eventually improve their safety and quality [135, 136].

In this thesis also extracts of *Moringa oleifera* leaves, a tropical perennial tree which has demonstrated to have valuable antioxidant and nutritional properties, were analysed. *Moringa oleifera* is one of the 13 species in the moringa genus and is mostly cultivated in tropical and subtropical countries, in particular in Jamaica but it is native to the Himalaya and very well known in India as Drumstick or Sohanjana. Most parts of the plant are edible but in particular its leaves and pods present fundamental nutraceutical properties since they are rich of fibres, carbohydrates, proteins, vitamins, amino acids, minerals and other important nutrients [137]. Indeed, many non-governmental organizations such as FAO (Food and Agricultural Organization) and ECHO (Educational Concerns for Hunger Organization) have recognised this plant as a very highly valuable nutritional source for undernourished populations in order to combat protein energy malnutrition problems all over the world especially among infants [138]. Other than its nutritional value, *Moringa oleifera* demonstrated to have many therapeutic properties [139] thanks to its high content of natural antioxidants such as phenolic compounds. The ability of leaves extracts to neutralize free radicals or

decompose peroxides [140] is due to the presence of carboxylic groups on the conjugated ring structures of their polyphenols, flavonoids and vitamins which have been reported to inhibit lipid peroxidation [141]. These antioxidant properties have been demonstrated to be useful as medical treatment of pathologies caused by oxidative stress such as sickle cell anaemia (SCA) [142]. Moreover, many studies have reported anti-inflammatory and antibacterial properties of moringa leaves extracts against many food-related pathogenic bacterial strains and mould, such as *Staphylococcus*, *Streptococcus* and *Candida albicans,* suggesting its possible use as a natural antimicrobial agent with reasonable safety margins in pharmaceutical and food applications [143]. The interest on moringa arouse around the 2000s but is still developing and wide spreading worldwide.

1.4.3 Industrial importance of natural extracts: extraction techniques and quantitative analysis of active compounds

Extraction means to separate active portions of plants and soluble plants' metabolites from the insoluble cellular residue using selective solvents and standard procedures [144]. The crude extracts contain complex mixtures of plant molecules such as alkaloids, glycosides, phenols, terpenoids and flavonoids. The extraction of active compounds from plants and other natural sources is a very important step to obtain the maximum antioxidant efficacy and need to be finely tuned on the basis of the molecules of interest, the type of plant or fruit and all the influential factors like temperature, solvents, agitation speed, etc. which might enhance the extraction yield but, if used without the proper evaluation, may also cause the degradation of the active substances.

In the case of plants extraction, like it was done in this work, it is important to consider also the form of the materials (leaves, barks, roots, fruits and flower) before the extraction, because the pre-preparation processes, as if the sample is fresh or dried or if it is grinded or reduced in powder, can influence the final extracts efficacy and the preservation of the active compounds. In most cases, since fresh samples are difficult to maintain and they could easily deteriorate, dried samples are preferable. For instance, studies on *Moringa oleifera* leaves showed that the total phenolic content is not affected by the drying but the dried extracts presented higher amounts of flavonoids if compared with the fresh ones [145].

Among the traditional extraction methods, maceration, percolation, infusion, decoction and Soxhlet extraction are commonly applied at a small manufacturing

level. There are also some advanced methods such as supercritical fluid extraction (SFE), microwave assisted extraction (MAE), ultrasound-assisted extraction (UAE) and accelerated solvent extraction. These methods are developed and constantly modified to translate plant extraction at an industrial scale level, increasing the yield and lowering the costs of the processes. It results clear how the selection of the appropriate extraction method is fundamental. Some of the most used extraction methods are briefly explained below [146].

Maceration, a classical technique often used for wine making, involves the soak of the plant components in a solvent inside a plugged container at room temperature for a time period (minimum 3 days) under frequent agitation [144]. This procedure leads to the rupture of plants' cell wall and the subsequent release of soluble compounds in the solvent. After the incubation with the solvent, the mixture is usually pressed or filtrated and the solvent can be allowed to evaporate by air-drying. In this method the solvent is chosen specifically to obtain some kind of molecules in the extracts instead of others. This is the easiest extraction technique even if a good disposal of large amounts of organic solvent waste needs to be considered. Infusion and decoction are based on the same principle as maceration but in these techniques plants materials are soaked in cold or boiled water. The choice of one method over the other should be done based on the temperature stability of the compounds of interest and the availability of solvents.

Another classical method is the Soxhlet or hot continuous extraction which involves an apparatus composed by a boiling flask, a condenser and the extractor body with a siphon arm in which the plant materials contained in a filter or "thimble" are soaked in the heated solvent. The solvent is evaporated, and the condensed vapour fills the extractor body until discharged to the flask by the siphon arm, thus continuing the process. Even if this method requires less amounts of solvent compared to maceration, it presents more risks for the operators because they are exposed to flammable liquid organic solvents and possible toxic exhalation during the extraction. Furthermore, this technique results more expensive due to the required purity of solvents and less environmentally friendly than advanced methods such as SFE. In addition, many factors such as temperature and solvent-sample ratio need to be taken into consideration. Some studies on *Moringa oleifera* reported that this procedure applied on its leaves resulted in lower phenolic compounds and flavonoids yield [145] if compared with maceration.

Among the advanced techniques, MAE employs microwave radiation energy to interact with the dipoles of polar or polarizable compounds, heating the surface and causing the disruption of hydrogen bonding, thus allowing an easier migration

of molecules from the plant matrix to the solvent. This method reduces the volume of solvent and time of extraction and is selective for polar molecules and solvents with high dielectric constants. Using this technique, it is important to consider the thermo-degradability of the compounds of interest and that this method is limited to small phenolic compounds which are stable under microwave conditions (i.e gallic acid, quercetin, isoflavin, trans-resveratrol). Thus, this technique is not suitable for the extraction of tannins and anthocyanin.

On the other hand, UAE uses the mechanic effect of ultrasound (from 20 kHz to 2000 kHz) to increase the contact surface between the solvent and the matrix and desegregate plants' cell wall. This is a simple and relatively low cost technique really suitable for large scale extractions because it reduces the solvent volume and extraction time. However, ultrasound energy may affect the active compounds promoting the formation of free radicals [147].

SFE involves the use of substances such as carbon dioxide, nitrogen, methane, ethane, propane, etc. in supercritical state, which have the physical properties of both liquid and gas over their critical point, to extract active agents. The plant materials are put in a container under controlled temperature and pressure conditions. When both temperature and pressure are lower than the solvent critical point, the active compounds dissolved in the fluid are separated. The important factor is the mass transfer of the active components in the supercritical fluid. To obtain this, the temperature and pressure fine regulation is fundamental because the rising of the pressure correspond to a higher density of the supercritical fluid which enhance the solubility of the matrix components. The biggest issue for the employment of this method is the initial cost of the equipment, which is very expensive (from about 10 000 to 20 000 $ depending on the size of the extractor). An example of supercritical fluid that is often used for this extraction method is CO_2. CO_2 thanks to its low cost and toxicity represents an interesting source for SFE and it is able to extract non-polar compounds. However, the addition of small amount of matrix modifiers, such as ethanol or methanol can increase the solubility of polar substances. Furthermore, as CO_2 vaporizes at room temperature the concentration of active compounds in the extracts is high. The SC-solvents' strength can be tuned by changing not only temperature and pressure conditions but also with the addition of modifiers or co-solvent to reduce the extraction time. Often more than 10% w/w co-solvents are added to modify the SC-CO_2 solvent properties losing the advantages of using a solventless technique. In the case of compounds that are slightly or not soluble in CO_2 an alternative is to employ the anti-solvent extraction (SAE). CO_2, thanks to its lipophilic character, is very useful to fractionate non-polar compounds from organic solution, indeed it can easily be

mixed with organic solvents like methanol, ethanol, acetone, chloroform etc. reaching a mixture critical point (MCP) around 9-10 MPa at 40 °C [148]. At higher pressures these compounds are completely miscible and the supercritical mixture is formed as soon as the overall composition overcome the MCP. Thus, if some compounds are not soluble in SC-CO_2 but they are dissolved in the organic solvent they can be easily extracted with it and separated from the solvent by precipitation. This is very useful to separate for example flavonoids, which are more soluble in the mixture CO_2 and ethanol than in pure CO_2, from more polar or heavier molecules. In this case SC-CO_2 behave both as an antisolvent to precipitate higher molecular mass molecules and as a solvent to extract ethanol with the components dissolved in it. In summary, SAE is a hybrid process composed by organic solvent extraction followed by SC-CO_2 elimination of the solvent. The mechanism consists of maintaining continuous contact between SC-CO_2 and the organic liquid mixture in a pressurized precipitation container. A spray of the liquid solution is produced in the supercritical fluid and can be fractionated by SC-CO_2 which cause the precipitation of the compounds insoluble in CO_2 at the bottom of the pressurized vessel as powder. This method is very flexible because the solvent can be changed in function of the molecules of interest and it does not require large amounts of raw materials, reducing most of the costs of SFE. Many studies have underlined the usefulness of this technique to extract polyphenols and anthocyanin from grape residues and oleuropein from olive leaves [149, 150]. When the molecules of interest are relatively soluble in SC-CO_2, it is very important to carefully chose the pressure, the temperature and the molar fraction of CO_2 to employ in order to precipitate them, avoiding their extraction from the precipitator. The limit in this case is that the organic solvent can act as a co-solvent increasing the solubility of the compounds in SC-CO_2.

Among all these methods, in this thesis the extracts of the active antioxidant molecules from *Moringa oleifera* leaves, olive pomace and leaves and grape fruits after pressing residues, were obtained by maceration as classical technique, and SFE and SAE as advanced methods. In particular, the attention was focused on maceration as the more eco-friendly and less expensive extraction method compared to the other [145]. Since the factor that influence most the yield extraction of active agents such as polyphenols and flavonoids is the solvent kind and strength, in this thesis a comparison between fractions of extracts using many different organic solvents such as ethanol, methanol, acetone and dichloromethane was done and also two different time periods of maceration were considered.

1.4.4 Standard methods for the characterization of the antioxidant efficacy of natural extracts and of active food packaging

Extracts' antioxidant efficacy could be qualitative and quantitative measured by colorimetric or fluorescence-based methods such as diphenyl-1-picrylhydrazyl radical (DPPH) and oxygen radical absorbance capacity (ORAC) assays.

They are both optical approaches based on the detection of a differential highness of intensity signal at a specific wavelength. These two assays are often used as standard methods to characterize the antioxidant efficacy of active agents in food industry. The first is based on the measurement of the ability of an antioxidant to donate hydrogens and thus reduce DPPH radical molecules over time. The results are expressed as the concentration of antioxidant agent necessary to reduce the 50% of the initial amount of DPPH (EC_{50}) on the basis of a calibration curve built on an antioxidant standard molecule. On the other hand, ORAC is a more standardized method, it is based on the capacity of a certain antioxidant to protect a fluorescent probe from fluorescence quenching induced by the addition of peroxyl radicals in the reaction room. In this case the results are expressed as equivalent moiety of an antioxidant standard, such as Trolox, per gram of sample.

In this work, both methods were applied to evaluate the antioxidant efficacy of all the fractions of the natural extracts since they can measure two different antioxidant principles. The details of the techniques are described in section 5.2.5.

As regard the active food packaging materials, their antioxidant efficacy needs to be measured in a quantitative and objective manner to support manufacturers selecting the best new materials and for quality control of raw materials. The antioxidant efficacy of the packaging materials can be obtained by non-destructive techniques in order to maintain intact their properties and a good correspondence with the reality. Some of these are based on an indirect measurement such as the DPPH assay, mentioned above for the crude extracts. It can be applied also for the final material, by cutting a defined area of the active film and putting it in the DPPH methanol solution making sure that the resin or the polymer are not soluble in this solvent.

The research group of Nerín [151] developed a very efficient technique able to measure the free OH• radical scavenging ability of active polymers by an indirect reaction with salicylic acid (SA). Briefly, an atmosphere enriched in OH• radicals is driven in bags made of the active polymers to be tested then let bubble in aqueous solution of SA. The amount of 2,5-dihydroxybenzoic acid (2,5-DHB)

generated by hydroxylation of SA, as well as the remaining SA are quantitatively measured by UPLC after 48 h of exposure. Thus, if the active polymer is a good radical scavenger, that is, it has a good antioxidant efficacy, the radicals remain entrapped in the bags without the possibility to react with SA. See section 5.2.7 for the details of the method. Therefore, the concentration of 2,5-DHB is inversely proportional to the efficacy (or amount, if several concentrations are tested) of the active agent. Also in this case, a comparison with an antioxidant standard, such as Trolox or gallic acid, inserted in the polymer in the same way of the analysed samples is needed.

In this thesis work, the antioxidant capacity against OH• radicals of active cellulose polymers coated with the natural extracts was measured in the Zaragoza University using this technique.

In food industry the thiobarbituric acid reactive substances (TBARS) assay is commonly used as a standard method to evaluate the preservative efficacy of an antioxidant agent or packaging material indirectly by measuring the level of lipid oxidation of the food. This technique is a colorimetric assay based on the reaction of thiobarbituric acid with a secondary product of lipid oxidation. See section 5.2.7 for further details. This method is quantitative and provides a sound indication of the antioxidant performance of the active materials on packaged food.

On the other hand, there are also some destructive procedures that involve an extraction of the antioxidant agents from the polymer to analyse the efficacy of the final product. These methods are not designed for a direct measurement of the polymeric active material because they often require to work with measurands in the form of liquid solutions. Obviously, the results could be different from that obtained on the proper active material because the behaviour of the antioxidant could change in the presence of the polymeric matrix. Among these methods the most employed ones are ORAC and DPPH performed on the solution obtained after an extraction of active compound from the produced active film. Other indirect methods based on the measurement of hydrogen atoms exchange and electron transfer like TRAP and FRAP [152] can be performed but, since they are not specific for active packaging testing, they were not considered in this work.

However, methods which measure the antioxidant efficacy in a more direct way avoiding any chemical modification of the sample which can influence the chemical behaviour of the active compounds, are present. Among them there is Raman spectroscopy. As a vibrational spectroscopic technique, Raman presents many advantages: it allows rapid and non-destructive measurements and it is quantitative. Studies that measured the reduction of the specific Raman band of

fatty acid around 1445 cm^{-1}, which represents the CH_2 vibrational modes, caused by their oxidation directly on foodstuffs packaged in the polymer with the active compounds vs. traditional packaging over different time spans, were published [136].

In the present work, both TBARS and vibrational spectroscopies including Raman and FT-IR were employed to assess the antioxidant efficacy of newly developed antioxidant packaging materials, confirming the reliability of this more direct techniques.

1.5 Industrial application of new active packaging

1.5.1 Commercial availability of antimicrobial and antioxidant active packaging

Although antimicrobial and antioxidant active packaging possess very promising and appealing characteristics, they still have a limited commercial availability in Europe and very few are produced on an industrial scale. However, several kinds of antimicrobial packaging have already been commercialized [39, 41, 106] and silver-based antimicrobial materials are commonly used in many other countries such as in the United States and in Japan [43]. As regards those with antioxidant properties, on the market there are some multilayer systems that act as oxygen absorber like Oxyguard, which needs to be activated after the production of the material by UV radiation and requires to be on the internal layer because it needs protection from external environment. Furthermore, new active materials containing essential oils which act as radical scavenger produced by two Spanish companies: Artibal (Sabiñánigo, Spain) and Repsol-Rylesa (Madrid, Spain) have recently appeared on the market. They are able to directly scavenge molecular oxygen in the atmosphere, do not require further protection layers and have demonstrated to be very efficient in food protection from oxidation for more than one year. Moreover, the Research group GUIA of the Zaragoza University, which is one of the collaborators for the production of this thesis work, together with the company Repsol-Rylesa (Spain) have developed several paraffin coating formulations with essential oils for paper and board packaging.

1.5.2 Particularly interesting foods for the industrial development of active food packaging

Some foods are more predisposed to promote rapid oxidative process, such as dried nuts, fatty food, and bakery products with a high fat or butter content, or pathogen bacterial infections, such as *Listeria monocytogene*s and *Salmonella,* than others. In particular, many companies are focusing their attention on the correct preservation and prolongation of the shelf life of fresh meat, fresh fish and fresh milk. In particular, milk is still a big problem due to its massive production in the third countries which consume it before pasteurization, risking very dangerous foodborne-diseases. As regards fresh meat, USA and Spain are still fighting against the severe problem of *Listeria monocytogene*s infection which, today, affects many countries with serious impact on public healthcare and on the economy. For all these issues, the development of active antioxidant and antibacterial packaging systems are very important and also better accepted by the public opinion. Since, as described before, the addition additives directly in the food, to maintain the freshness period of the product, is less efficient, the introduction of natural additives in the coating results the best solution. In the case of fresh meat, the development of packaging with, for example, carbon nanoparticles which display photothermic activity if irradiated with particular light wavelength can be very interesting to reduce the bacterial growth on the meat surface because they can be simply activated by the light present in the cold display stands of the supermarket. Moreover, if the coating contains natural antioxidants that do not change any organoleptic properties of the product, are not toxic, do not require high barrier materials and are able to react with molecular oxygen, then the characteristic red colour of fresh meat could be maintained for longer times. This is a very good improvement on the shelf-life prolongation and safety of the food with a high economical value for the food industry. This gains an even more interesting prospective by using biodegradable biopolymers, and active agents obtained from industrial wastes in a concept of environmentally sustainable and circular economy.

Chapter 2

Introduction to the experimental part

2.1 Importance of metrology in food industry

2.1.1 Food Metrology

Since food is now a trading good in a global market the issue of guarantee food safety, security and traceability has led to an emerging need of standard and reliable methods to ensure and measure its quality, the safety of each component and to confirm its provenance and authenticity [153]. On this purpose metrology, the science of measurement, and in particular the area concerning food metrology, offers a great support to assure measurements traceability, compliance with international regulations and reference to certified standards. Metrology, based on the decimal metric-system, was born in France during the French revolution but it is well known that metrical issues have interested most of the human activities from ancient times [154]. Besides food metrology, other areas of study have developed from fundamental metrology, such as applied metrology and legal metrology. Their activities spread over wide areas of interests, from scientific research to many industrials fields to people's everyday life, confirming the relevance of clear and reliable measurements in both experimental and theoretical determinations considering any level of uncertainty. Among the science regarding health and quality of life, food metrology is recently emerging as fundamental to

respond both to verification requests by the regulatory authorities and to assure consumer protection.

The main outcomes of food metrology are: i) control and safety, which is fundamental to determine the unintentionally added substances (NIAS) present in the product or in the packaging material and their possible migration into food; ii) development of new suitable reference materials that can be used by industrial companies all over the world to ensure full traceability of measurements related to the international system of units (SI); iii) contribution to create new standard operating procedures (SOP); iv) validation of analytical methods with a whole uncertainty budget declaration, and last but not least v) performance of accurate and precise measurements of food composition and detection of eventual presence of contaminants, supporting companies and ensuring compliance with international regulations. Furthermore, metrological institutions are fundamental for: i) the distribution of standardized calibration procedures for laboratories and industrial instruments based on primary calibration standard reference materials; ii) organizing inter-laboratory comparison studies on hot research topics to obtain measurements independent from the analysis method; iii) to ensure the authenticity of food labels and provenience especially if the products are declared to be under these categories: PDO (Protected Designation of Origin), DOC (Controlled Designation of Origin), DOCG (Controlled and Guaranteed Designation of Origin), PGI (Protected Geographical Indication). Nevertheless, metrology has also the difficult task of developing new reliable and metrological techniques to describe the organoleptic properties of food and beverages. In summary, the principal goal of food metrology is to provide standardized methods to determine food composition, to detect the presence of any toxic elements, even in minimal traces, to ensure the final product quality, safety and provenance [155], inferring authority on the analytical results, supporting public health decisions and enhancing the consumers' confidence.

2.1.2 Food safety, food security and food traceability

Food safety is related to the prevention of all the potential chemical, physical and microbiological health hazards that could harm the consumers or provoke food-borne diseases and it interest all the food-related steps, from its preparation to its packing, transport, storage and handling up to its consumption. Food safety regards all the procedures of labelling, certification, import and export guidelines, biotechnology policies and hygiene of food and also the determination of the presence of additives or pesticide residues [156]. To avoid all the possible health

hazards, the developed countries elaborate standard procedures for food production and commercialization which, in the EU, are included in the Integrated Food Safety policy. Their objectives are ensuring effective control systems to establish compliance of food safety and quality; animal health, welfare and nutrition and plant health with the European standards, and administrate international relations with third countries on those sectors, supporting the European Food Safety Authority (EFSA) and ensuring science-based risk management. The main achievement of the European commission for Food Safety is to highly protect human health in respect of food industry. This fundamental was primarily expressed in the Commission's White Paper on Food Safety: "apply an integrated approach from farm to fork covering all sectors of the food chain".

In the context of this work, new active food packaging are developed incorporating antibacterial and antioxidant agents in resins or adhesives that can come in contact with the food product. Consequently, it is very important to underline that the detection of the possible presence of hazardous chemicals in food represents one of the main points of food safety assurance. As already said, nowadays, food additives have become an integral part of food production chain, so a strict and efficient infrastructural control is necessary to prevent food safety related accidents which can easily reach the global market with very negative consequences on global economy and human health. Metrology may again be an essential support to industries providing new efficient and reliable analytical methods with improved sensitivity, selectivity and narrow uncertainty intervals.

A second topic of food metrology regards food security, which is "the condition in which all people, at all times, have physical, social and economic access to sufficient safe and nutritious food, that meets their dietary needs and food preferences for an active and healthy life" (United Nations' Committee on World Food Security) [157]. In a frame of climate changes and continuous growing of the global population, a good management of the primary resources and the guarantee of the primary needs at costs accessible to everyone is necessary and it is strictly bound to a sustainable economic growth, essential to ensure food security all over the world. The foundations on which food security is based are four and were identified by FAO: i) availability, ii) access, iii) utilization, and iv) stability, intended as the stability of the first three points over time. Once more metrology, together with other scientific fields, plays a central role in the persecution of the objectives of food security. It is worth to mention the balance of the nutritional benefits of foods with the ecological costs of their production, offering a common language based on standards and referable measurements to deal with the experts of the productive sectors. So, it will be

possible to find new sustainable and environmental friendly food security strategies such as, for example, the introduction of insects as a novel food and feed [158].

The third but not less important pillar on which food metrology is founded regards food traceability, which, as was stated by the ISO is "the ability to verify the history, location or application of an item by means of documented recorded identification". This definition explains the need to track any feed, food, food-related animal or compound that will be used for consumption through all their production, processing and distribution chain to protect public health and confidence [159] following the European Committee's guidelines and sector-specific legislations. Food traceability should not be confused with metrological traceability, which regards the calibration and determination of the measurements' bias, precision and accuracy of an instrument by an uninterrupted chain of comparisons of the measurements related to a well-known standard. This function can be performed only by a few National Measurement Institutes (NMI) spread all over the world such as NPL (National Physical Laboratory) in UK, NIST (National Institute of Standards and Technology) in the USA, PTB (Physikalisch-Technische Bundesanstalt) in Germany and INRiM (Istituto Nazionale di Ricerca Metrologica) in Italy). On the other hand, food traceability is based on two areas of expertise, one concerning food safety and the other regarding food quality and authenticity [160]. Indeed, traceability is needed to identify any food-related risk or food declared as unsafe and trace it back to the source isolating it and preventing the consumers from contaminated products before they reach them. Furthermore, traceability is fundamental to provide the consumers with accurate information about the provenance and authenticity of all the food products. This allows targeted withdrawals and rapid intervention of the competent authorities in case of risk identification. As regards the quality of food products, traceability is needed to protect the consumers against imitations and frauds and that the quality designations explained by the Europeans Commission's Regulation 1151/2012 (i.e. Traditional Specialty Guaranteed (TSG), PDO, and PGI [161]) are real when declared. Thus, labelling the products is essential to attest the economic value, the safety, quality and authenticity of the product. In this context, metrology is needed, for the development of reliable analytical techniques to correlate the food with their geographical provenience in order to confirm their authenticity.

In conclusion, in the context of new food packaging materials and technologies development, food metrology is fundamental to guarantee compliance with international regulations and to support companies for the measurements. Indeed, food metrology can provide support to those actives in the

sector who must respond both to verification requests by the regulatory authorities and to consumer protection. As food safety is a global priority and one of the major concerns of consumers, new active packaging systems, such as antimicrobial or antioxidant ones may be launched into the European market if they comply with the restrictions set out in European Regulations (EC) 1935/2004 and (EC) 450/2009.

Furthermore, since in this thesis a possible sustainable reuse of food industry waste, such as wine and olive oil production waste, is proposed, the work fits perfectly in a frame of circular economy. In addition it results in compliance with one of the 17 Sustainable Development Goals of the recently signed European Green Deal [162], in particular the number 12th regarding "responsible consumption and production" which states that to fight pollution and reduce the overall waste generation, the global food waste per capita should be halved by 2030 ensuring the efficient and sustainable use of natural resources.

Chapter 3

Raman-based methods to rapidly characterize food-pathogens and antibiotic resistance

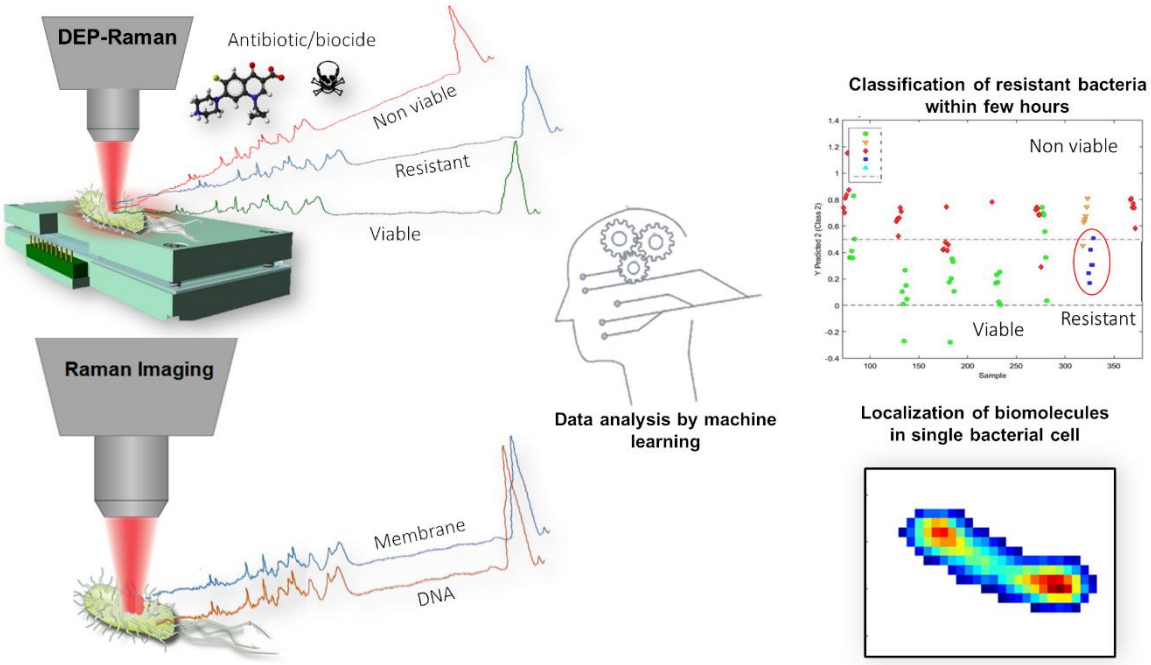

3.1 Raman spectroscopy as an advantageous alternative to classical microbiological techniques

A key factor to consider when developing materials with antimicrobial properties to reduce the growth rate of target microorganisms (i.e. *E. coli*, *Salmonella* and *Listeria monocytogenes*, which are the most important strains related to foodborne diseases) is the possible insurgence of bacterial resistances. In this frame, a direct non-destructive method which allows to detect, discern and characterize resistant bacteria in few hours, instead of the 24 required by classical microbiological cultures, without the need of any staining or difficult sample preparation results very attractive.

Among other techniques, vibrational spectroscopy presents many advantages for its use in the field of life sciences. In particular, for its short times of analysis, cost efficacy and easiness of sample preparation it has brought a positive innovation, compared with classical microbiological methods [163, 164]. Vibrational spectroscopy, like Fourier transform-infrared spectroscopy (FT-IR), near-infrared spectroscopy (NIR) or Raman spectroscopy, is a non-contact and culture-independent technique based on the analysis of the vibrational modes of functional groups and bonds between atoms and molecules, which allow to obtain a chemical fingerprint of the analysed sample. The principle is centred on the interaction of an incident electromagnetic radiation, produced by an intense light source such as a laser, which can be absorbed (IR) or scattered (Raman) by the sample. The non-absorbed photons that exit from the sample after the interaction with the incident beam are collected by a detector which is connected to a software that elaborates the signals and returns a spectrum as the output. The spectrum presents the characteristic peaks and bands specific for the analysed sample and their intensity is quantitatively proportional to the presence of the specific functional group or chemical bond. The light beam can interact with the sample without or with an energy transfer. In the first case the light can be scattered by the sample in an elastic manner (Rayleigh scattering) and it is emitted from the sample at the same wavelength of the incident photon. On the other hand, if the light beam, when interacting with the sample, gains or loses some energy, the scattered light that reaches the detector can have a lower (Stokes) or higher (anti-Stokes) frequency than the incident beam producing an inelastic or Raman scattering (Figure 1).

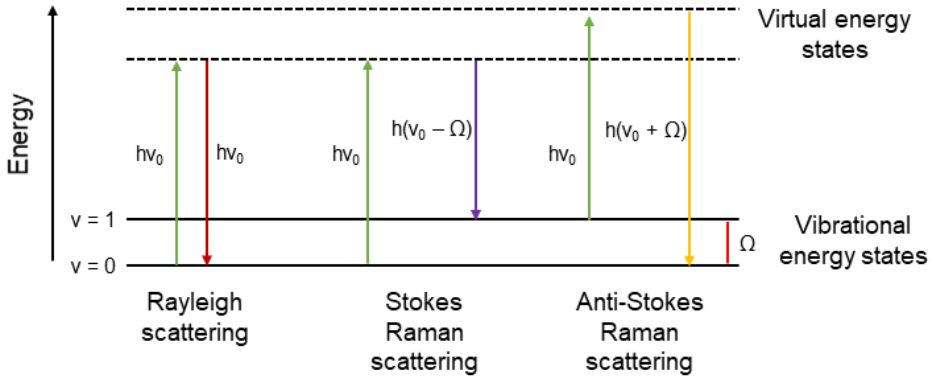

Figure 1: Scheme of the energy states.

The energy difference between the incident and the scattered light strictly depends on the sample chemical structure. This phenomenon was postulated theoretically in 1923 by Smekal [165] but the first experimental observation of Raman scattering effect was reported by two Indian physicists, Raman and Krishnan [166] and, independently, by Mandelstan and Landsberg [167] in Soviet Union in 1928. Raman spectroscopy and infrared spectroscopy are complementary techniques based on two different phenomena: the first one consists on the inelastic scattering of light, while the second one on selective absorbance of radiations that provoke energy transitions in the IR region. Moreover, the selection rules on which the two techniques are based that determine which vibrational modes of a molecule are active, are different. Indeed, while IR spectroscopy detects the vibrations due to the changes in the dipole moments of a molecule, Raman active molecules require a change in their polarizability which depends on the deformation of the electron cloud, so some vibrational modes that are IR active are not Raman active and vice-versa. However, compared to infrared, Raman spectroscopy offers many advantages especially for biological investigations allowing real-time and dynamic analysis of living samples which can also be dispersed in aqueous media, simulating their natural environmental conditions, or deposited on commercial microscope glasses since water and glass signals are negligible in Raman spectroscopy, which is not the case for IR spectroscopy. Furthermore, as already mentioned in section 1.3.5 Raman is very suitable for microbiology because it is direct, non-invasive and it does not require any labelling process. Moreover, a very small amount of sample

is needed and its preparation is minimized [168], indeed the most time-consuming step required by quite all the classical microbiological techniques, which is the overnight incubation of the analysed microorganisms, is not necessary here. In addition, spatial information of molecules or other microbiological constituents can be obtained at a single cell level with high resolution providing evidences about the cell status, composition, history and metabolic information [169]. These kinds of analysis can be done by coupling Raman spectroscopy with multivariate statistical post-process techniques [170] in order to easily manage the huge amount of data generated by the spectroscopic technology in a very short time and for improving the interpretation of biological samples-derived Raman spectra which are often very complex and could easily lead to misinterpretation. In order to overcome these issues, some disciplines such as chemometrics, image processing, machine learning and computational intelligence techniques come to a help for data analysis [171, 172]. All these aspects, render this technique very suitable for its application in the field of food packaging where rapid and reliable characterization of the antimicrobial properties of the materials and of the active agents are fundamental, together with the analysis of the mode of action of newly developed antimicrobials that need to be added or inserted in the packaging materials [173, 176]. Indeed, many food-born related issues have still very severe consequences on public healthcare like for example the *Listeria monocytogenes* infection which, today, affects many countries including USA and Spain with serious impact on food safety and food security. Thus, it is clear how the rapid detection of bacteria and their resistances to antimicrobials results of great importance in the field of food packaging.

Figure 2 shows a scheme of the Raman apparatus and a photograph of the instrument used for this thesis work.

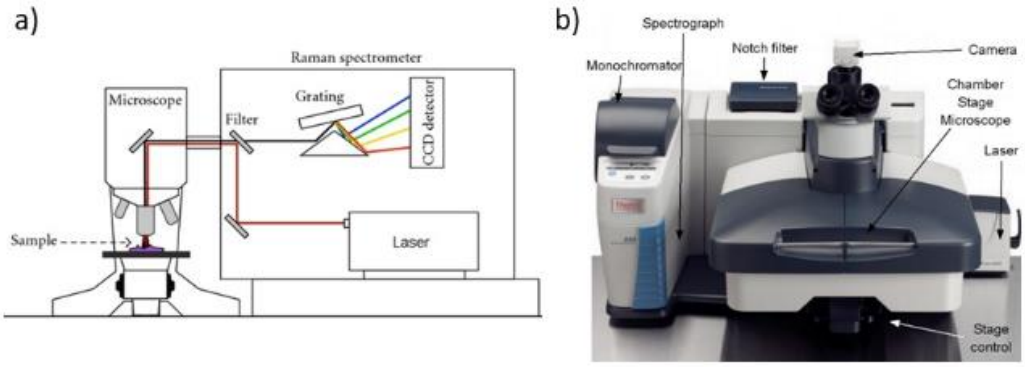

Figure 2: Raman spectroscopy apparatus.
a) Scheme of the Raman spectroscopy apparatus components. Reprinted with permission from [174]. b) Image of the instrument used in this work.

3.2 Materials and Methods

3.2.1 Reagents

The antibiotic Ciprofloxacin (CP) and the antimicrobial agent Triclosan (TCS) (Sigma-Aldrich, Milan), necessary for the DEP-Raman AST method and the cross-induced resistance experiments, were diluted in HCl 0.1 M (Sigma-Aldrich, Milan) and in absolute ethanol (Carlo Erba, Cornaredo, Milan) respectively, to prepare stock solutions. The solutions were then diluted in Milli-Q® water (Milan) to obtain the correct concentrations needed for the two assays.

Luria-Bertani (LB) broth and agar (Sigma-Aldrich) were used as bacterial culture media. PBS solution was obtained dissolving tablets (Sigma-Aldrich, for 200 ml, pH 7.4) in Milli-Q® water. All the solutions and culture media used for bacteria were sterilized in autoclave for 20 min at 121 °C.

For the fluorescent microscopy analysis of bacteria DAPI (4',6-diamidino-2-phenylindole, dihydrochloride, D1306) and FM™5-95 (*N*-(3-trimethylammoniumpropyl)-4-(6-(4-(diethylamino)phenyl)hexatrienyl)pyridinium dibromide, T23360) were purchased from Thermo Fisher Scientific, Milan, and were used as fluorescent dyes diluting them in PBS.

Absolute ethanol and acetone (Carlo Erba, Cornaredo, Milan) were used to wash the silicon substrates required for Raman Imaging analysis of bacteria.

3.2.2 Bacterial strains and cultivation

For these experiments different bacterial strains were taken into account:

- *Escherichia coli* MG1655, as a CP susceptible strain;
- *Escherichia coli* PSA-I, as a CP resistant strain;
- *Pseudomonas aeruginosa* PAO-1 (by Matthew Avison; University of Bristol, UK);
- *Staphylococcus aureus* SH1000;
- *Escherichia coli* ATCC 8739, as a standard strain for Raman Imaging (RI) experiments.

The first two *E. coli* strains together with *P. aeruginosa* PAO-1 and *S. aureus* SH1000 were kindly provided by the University of Nottingham.

All the strains were provided like a frozen stock culture. Each strain was revitalized plating it on LB agar and incubating the plates at (37 ± 1) °C overnight. Then a single colony was taken with a sterile loop and let grow overnight in 5 ml of LB broth at (37 ± 1) °C under agitation (150 rpm). The following day, the optical density at 600 nm (OD_{600}) of the bacterial culture was measured by UV-Vis spectrophotometer (Lange DR500, Lainate, Milan) in the single wavelength mode, employing LB broth without bacteria as a blank. The OD_{600} of the bacterial suspension was adjusted to 0.05 with fresh LB medium and let grow at (37 ± 1) °C under agitation (150 rpm) for at least 2 hours, when the OD_{600} reached the value of about 0.3, approximately in the middle of the exponential phase of bacterial growth curve, where bacteria are more sensitive to treatments.

Bacteria were then purified from the culture media before each experiment by successive centrifugations. 1 ml of each sample was taken and harvested by centrifugation at 6000 rpm for 5 min, then bacteria were washed twice with PBS 0.5×, for the DEP-RS experiments, or Milli-Q® water, for RI experiments, by two centrifugation cycles at 15000 rpm for 1.5 min. The new OD_{600} was measured and adjusted with fresh PBS or water to 0.3 and 0.1 for DEP-RS and for RI respectively.

3.2.3 DEP-Raman analysis

3.2.3.1 Design and fabrication of the DEP cell

A home-made DEP sample holder was made. The manufactured DEP cell, showed in Figure 3 consisted of: i) a rigid outer shell made of aluminium needed

as scaffold and for the manipulation of the device. A window was carved out from this shell in order to inject and remove the bacterial suspensions and to render visible the aggregating bacteria during DEP experiments; ii) a polydimethylsiloxane (PDMS) gasket which formed together with a microscope cover glass a sealed volume in the cell; and iii) an active chip containing the electrodes. The chip was fabricated by laser photolithography, starting from RCA-cleaned corning glass, which was spin-coated with a photoresist. This glass was then selectively exposed to the laser light to trace out the electrode geometry. After the development, resulting in the formation of a mask, a 5 nm layer of titanium was deposited on it, then a gold film 500 nm thick was sputtered on the chip. Then, the mask was removed, leaving (on clean glass) electrodes forming quadrupoles and traces, which were wired for polarization as shown in Figure 3 after being connected to the sinusoidal voltage generator. The applied voltage generates the electric field which drives bacterial cells aggregation in the centre of the four electrodes due to DEP forces (blue arrows). The distance between the tips of the two electrodes with same polarity (V+, V+) is 40 µm, while the gap between the two electrodes with opposite polarity (V+, V-) is 20 µm.

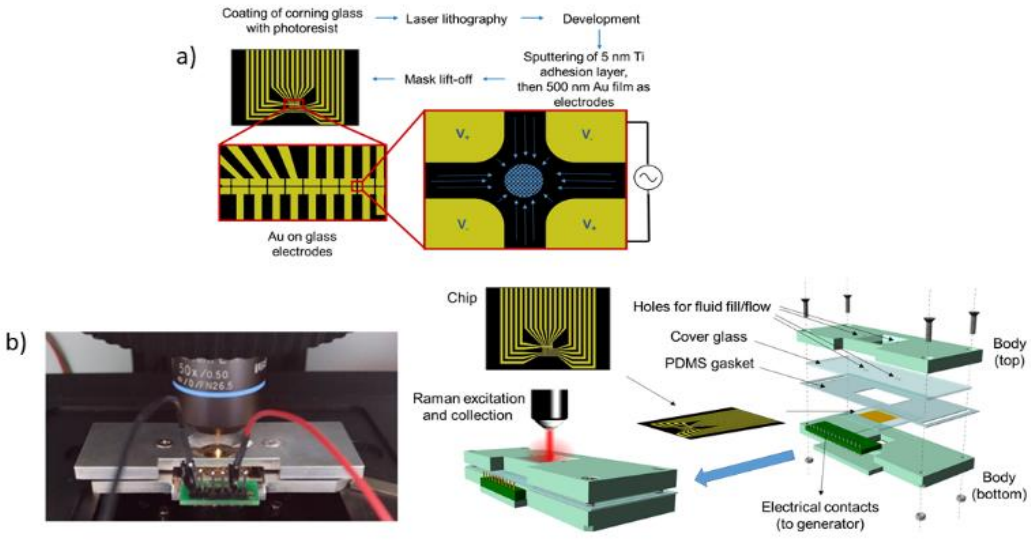

Figure 3: DEP-Raman in-house manufactured cell.
a) Scheme of active chip preparation. b) Image of the in-house manufactured DEP device and its positioning in the Raman instrument sample holder with the voltage connections (left) and scheme of the cell composition. Planktonic dispersed bacteria are injected into the holes near the window, the voltage applied, and the laser beam focused into the center of the window. Reprinted with permission from [175].

3.2.3.2 Bacterial characterization by the DEP-Raman device

About 100 µl of the culture medium purified bacterial suspensions were injected into the DEP-Raman microfluidic device and Raman spectra were collected in the centre of the cell. The samples were analysed by a Thermo Fisher Scientific™ DXR™ (Rodano, Milan) dispersive Raman microscope equipped with an Nd-YAG laser. Each spectrum was acquired using an excitation wavelength of 532 nm, a laser power of 10 mW, an exposure time of 2.5 s for 24 scans (1 min total integration time per spectrum) and a spectrograph confocal pinhole aperture of 50 µm in diameter. Spectra were collected with the dispersive Raman system with a 5 cm^{-1} spectral resolution and a spectral range between (500-3100) cm^{-1} acquiring 3489 points per spectrum. The objective employed in this study was an Olympus™ 60× water immersion with a numerical aperture of 1.1 (model LUMFLN60XW).

The calibration and alignment of the instrument was performed before every measurement by the calibration tool provided by Thermo Scientific. The grating resolution of 5 cm^{-1} determined the frequency uncertainty while the intensity uncertainty was established using a polystyrene standard and resulted lower than 5%. Monocrystalline silicon was used as standard taking a spectrum each time and comparing its characteristic Raman band at 520 cm^{-1} with that of a reference spectrum acquired in the same conditions to verify the success of the process.

The bacteria agglomeration conditions of the DEP cell used for each bacterial strains were: 5 V peak-to-peak sinusoidal voltage between the electrodes with a frequency of 800 kHz for *E. coli*, the same waveform with an amplitude of 4 V peak-to-peak and a frequency of 1 MHz was employed for *S. aureus* and a voltage of 5 V peak-to peak and a frequency of 1.5 MHz for *P. aeruginosa.*

3.2.3.3 Ciprofloxacin MIC and MBC determination towards E. coli by classical microbiological assays

CP MIC (minimum inhibitory concentration) and MBC (minimum bactericidal concentration) towards *E. coli* MG1655 were determined by broth dilution (BDM) method, following the protocol explained in details by Wiegand et al. [177] and by performing a viability assay respectively, as described by the National Committee for Control of Laboratory Standards (NCCLS) guidelines [178]. *E. coli* was revitalized and let grow in LB broth at (37 ± 1) °C under agitation (150 rpm) as described in paragraph 3.2.2 until it reached an OD_{600} of 0.3 using a starting inoculum of ($1.3 \times 10^8 – 3 \times 10^7$) CFU/ml. Then, the bacterial planktonic culture was divided in many different sterile tubes: one for each CP

concentration to test and one for the negative control (CTRL–), and different concentrations of the antibiotic (0.015, 0.025, 0.1, 0.25, 0.5, 1, 2) μg/ml were inoculated in each culture. Then, they were let grow at (37 ± 1) °C under agitation (150 rpm) and the OD_{600} of each tube was measured every hour for 7 hours and one was taken after 24 hours. At each time span one aliquot of each culture was serially diluted in PBS 1× and plated on LB agar. The plates were incubated overnight at (37 ± 1) °C, the colonies were counted the following day and the $\log_{10}$ of the calculated CFU/ml was plotted against the relative collection time point. The MIC was calculated as the lowest concentration of CP at which bacterial growth is inhibited with a statistical significance of $\alpha = 5\%$. All the experiments were carried out in triplicate and the mean and the standard deviation were calculated for each measurement. Moreover, in order to measure the bactericidal effects of CP, the MBC was considered as the lowest concentration of antibiotic to cause a reduction of 3 $\log_{10}$ in the CFU with respect to the MIC.

3.2.3.4 Bacterial exposure to antimicrobials for the DEP-Raman assays

Before being washed *E. coli* suspension at OD_{600} of 0.3 was splitted in two aliquots: one was let untreated as a negative control (CTRL–) while in the other CP at the desired concentration was added. The incubation at (37 ± 1) °C under agitation (150 rpm) was continued and one aliquot of 1 ml was removed from both the samples at intervals of (1, 2, 3) h from the antibiotic injection, the OD_{600} was measured and bacterial suspensions were purified from the culture medium, as described in detail in paragraph 3.2.2, to be analysed with DEP-RS.

Viability assay of bacteria was performed after each time span for both the treated and the CTRL– samples counting the colony forming units (CFU). Each bacterial suspension was serially 10-fold diluted in PBS 1×. For the enumeration of CFU both the 'whole plate' and the 'dot' plating methods were used. In the first case 100 μl of each correct dilution were spotted on the surface of a sterile antibiotic-free LB-agar plate, while for the dot plating, 10 μl of multiple dilutions were spotted on the same plate. All the plates were incubated overnight at (37 ± 1) °C, then colonies were manually counted and the total number of bacteria was calculated for each sample in triplicate.

In the cross-induced tolerance experiment, *E. coli* MG1655 was let grow in LB broth until it reached an OD_{600} of 0.1, then the suspension was divided into four aliquots, two were treated with 0.2 μg/ml of TCS and cultured for additional 30 min. Then, when the OD_{600} of 0.3 was reached, 0.5 μg/ml of CP were added to one of the two cultures pre-treated with TCS and to one of the remaining two

untreated cultures as positive control (CTRL+) while the other remained untreated (CTRL–). From the addition of CP (time 0), one sample from each aliquot was collected for the CFU assay and for the parallel DEP-RS analysis at each time point over a 3 h period.

3.2.3.5 Morphological analysis by fluorescence microscopy

2 µl of the fluorophore FM5-95 (Sigma-Aldrich; 200 µg/ml) were added to 30 µl of bacterial culture to stain bacterial membranes; 1 µl of DAPI solution (1 mg/ml) was added to 6 µl of the culture in order to stain the DNA in the nucleoids. Little drops of stained bacteria were then mounted on a microscope slide coated with a thin film of 1.2% agarose.

A Nikon Digital (Amsterdam, Netherlands) Sight DS-Fi1 camera was used to acquire the images attaching it to a Nikon Eclipse 50i microscope equipped with an Intensilight C-HGFI light source.

3.2.3.6 Data analysis and multivariate modelling

The chemometric analysis was performed using the PLS Toolbox (Eigenvector Research, Inc., Manson, WA) for Matlab R2015a (Mathworks, Natick, MA).

Firstly, the spectra obtained by the DEP-Raman setup were pre-processed by a 35 points window width Savitsky-Golay smoothing (polynomial order 2), a baseline correction was performed by weighted least squares (polynomial order 2), then spectra were mean centred and the signals intensity was normalized for the CH_x vibrational modes at 2940 cm^{-1} eliminating possible spectral differences due to a variation of bacterial cells concentration under the laser spot. To analyse spectral variations due to diverse experimental parameters, such as i) “time” (1, 2 and 3 h); ii) “treatment”, (untreated (class 0, control) or treated (class 1, test)); iii) “experiment” (the different cell culture batches), Analysis of variance-simultaneous component analysis (ASCA) was employed [179] considering 2-way correlations between the factors. The statistical significance was determined calculating the *p-values* through permutation tests by randomizing the levels belonging to the factor under consideration within the levels of each other factor [180]. The H0 hypothesis of no experimental effect, with a confidence level of *p* was tested.

A training set of independent experiments was built conducting them at different times and PLS-DA classification models were developed on them and validated by predicting independent spectra acquired from new experiments. The sensitivity [true positive / (true positive + false negative)], specificity [true

negative / (true negative + false positive)], and classification error (1 – accuracy) where accuracy is the ratio (correctly classified samples) / (total samples as classification) were calculated.

3.2.4 Raman Imaging analysis

3.2.4.1 Sample preparation for Raman analysis

Virgin silicon wafers, coated with a 5 nm layer of titanium and covered by a 60 nm layer of pure gold were prepared as described in details by Sacco et al. (Sacco et al., 2018) and used as reflective substrates. Gold, as an inert material which do not present any Raman signals in the molecular fingerprint region of *E. coli*, was chosen to avoid Raman enhancement from the surface. The substrates were cleaned by sonication in a bath of acetone for 10 min followed by a bath of absolute ethanol for another 10 min. Then, 20 µl of the tested bacterial suspension were spotted on the substrates' surface and while some samples were let to air-dry under the bio-safety cabinet, other samples were freeze-dried without adding any cryoprotective substances. The freeze-dried samples were produced using a K775X Liquid Nitrogen Cooled, Turbo-Pumped EM Freeze Dryer (GlobalSpec, United States). A drop of bacteria was instantly frozen on a pre-cooled gold slice surface by its immersion in liquid nitrogen. Then the frozen samples were put in the freeze-dryer machine setting 10 different temperature steps. The whole process required 8 hours and the temperatures followed different cooling and heating steps from -115 °C to +25 °C (Table 3).

Table 3: Scheme of the freeze dry process applied to bacteria.

Instrumental process	Time	Temperature
Constant	1 h	-115 °C
Ramp	1 h	-115 °C / -75 °C
Constant	1 h	-75 °C
Ramp	1 h	-75 °C / -50 °C
Constant	1 h	-50 °C

Ramp	1 h	-50 °C / +25 °C
Constant	-	+25 °C

3.2.4.2 Bacterial characterization by Raman Imaging

E. coli ATCC 8739, prepared as described in paragraph 3.2.2, was measured by a DXR™xi confocal Raman microscope (Thermo Scientific) using a laser excitation wavelength of 532 nm and a power of 8 mW. An exposure time of 0.033 s for 100 scans using a confocal pinhole aperture of 50 µm diameter was applied for each spectral acquisition. Single bacterial cells were analysed collecting chemical Raman maps in the spectral range of 3300–50 cm^{-1} with a spectral resolution of 5 cm^{-1} using a 100× objective (0.9 NA). The instrument was calibrated before every measurement as described in detail in the previous paragraph. Indeed, accurate calibration processes are fundamental to identify chemical compounds based on using references and literature data, and to compare measurements acquired in different conditions (for instance, in case of environmental and instrumental parameters changes) especially for the comparisons between freeze-dried and air-dried samples. The total uncertainty obviously includes some systematic biases between measurements as well as random contributions influencing each spectrum. However, since the intra-image variability is lower than the total one it can be assumed that multivariate analysis on single Raman maps is not affected by the former, and is intrinsically robust against the latter. For the bacterial spectral band assignment, a 6^{th} order polynomial fit was applied to the average spectra of each sample to delete any fluorescence effects. Spectral regions of interest were analysed by deconvolving specific peaks in order to obtain the wavenumber of each maximum and a chemical meaning was assigned to each signal. The Raman chemical images lateral resolution was of 0.1 µm and they were acquired using the step size of the sample stage obtaining a resolution greater than the laser spot-size, which is approximately of 0.45 µm.

3.2.4.3 Data analysis and multivariate modelling

Data reduction and analysis was performed by the Hypertools open source interface for hyperspectral image analysis. The noisy background around single bacterial cells was removed using an image mask created on the basis of a k-

means clustering setting k = 6. The 4 classes ascribed to background by the model were removed, therefore the pixels formed an image which was related only to the bacterial chemical signals.

Then PCA was performed after pre-processing the Raman spectra in the range between 666 cm^{-1} and 3120 cm^{-1} by correction of the baseline (by least squares fitting using 2^{nd} order polynomial), smoothing of 41 points window (2^{nd} order Savitsky-Golay method) and mean centering.

Two PCs emerged to contain relevant data, so the multivariate curve resolution-alternating least squares (MCR-ALS) method was applied to resolve 2 components. This method is based on the resolution of the discernment of a two-variable model $D = CS^T + E$, where D is the raw measurement, C is the matrix of concentration profiles and S^T the matrix of related pure spectra. E encompasses the experimental noise and the background unrelated to the ideal components. The number of image components was determined by PCA. The alternating optimization started by using the original pre-processed measurement, D, and an initial guess of either the C or the S^T matrices. Non-negativity constraint was imposed for the two model components (MCR1 and MCR2).

3.3 DEP-Raman spectroscopy: a novel approach to rapidly characterize bacteria and detect antibiotic resistances

As introduced in chapter 1, paragraph 1.3.5, some strategies can be applied in order to facilitate the Raman analysis of samples which are dispersed in liquid solutions. In particular, dielectrophoresis (DEP) can be used in combination of Raman spectroscopy to increase the number of bacteria under the focus spot of the microscope aggregating them thanks to spatial non-uniform alternate electric fields. This results in a maximization of the Raman signal and an increasing of the signal- to-noise ratio [98, 99].

The detection and characterization of the different bacterial species dispersed in human samples of body fluids and the development of rapid, sensitive and specific methods to determine antibiotic susceptibility of bacteria represent two of the most important issues to avoid sepsis deaths, prescribe targeted effective therapies and reduce the widespread misuse of antibiotic and multi-drug-resistance related problems. Thus, a combined DEP-Raman approach is here proposed as an innovative technique for bacterial strain characterization and antibiotic susceptibility test (AST). The developed Raman-based method allows to

reduce the total time of liquid sample analysis to few hours instead of the 24 h required by classical microbiological assays.

In the following paragraphs, firstly three different bacterial strains: *Escherichia coli*, *Pseudomonas aeruginosa* and *Staphylococcus aureus* were characterized by Raman using an in-house constructed DEP-Raman microfluidic device. The two firsts are Gram – while the third is Gram +. These two kinds of bacteria present many structural differences due to their different cell wall chemical composition.

Then, the susceptibility of *E. coli*, a model bacterial strain which is usually associated to urinary tract infection (UTI) diseases [181], towards the commonly employed second-generation fluoroquinolone ciprofloxacin (CP) [182] was dynamically analysed over time by the same DEP-Raman device.

The purpose was to develop a statistically robust and reliable classification model based on the analysis of spectral signal variance to rapidly determine the viability of *E. coli* when treated with the antibiotic, detecting spectral changes in the bacterial chemical fingerprint over time due to the mode of action of the drug in comparison with an untreated control, which could be applied for the prediction of bacterial susceptibility to CP or other drugs. The systematic differences present in the Raman spectra were thus identified, using supervised multivariate tools such as Partial least square discriminant analysis (PLS-DA) and PLS-regression, as a function of experimental replicates, time of exposure to the treatment and antibiotic action and a statistical significance was assigned by ANOVA simultaneous component analysis (ASCA). The sensitivity and predictive power of the built model was successfully proved twice testing the viability of *E. coli* treated with CP at sub-MIC and the viability of an *E. coli* strain genetically modified to be resistant to CP (*E. coli* PSA-I) demonstrating its good accuracy. Furthermore, for the first time, this predictive model was applied to evaluate *E. coli* susceptibility to CP in a situation of cross-induced tolerance obtained by its pre-treatment with sub-MIC concentration of a common used biocide agent: triclosan (TCS), which was recently withdrawn from the market due to its positive relation with the occurrence of multi-drug resistance (MDR) process [183]. The results presented in the following paragraphs were published in 2020, and are accessible through the reference [175].

3.3.1 Characterization of *E. coli*, *S. aureus* and *P. aeruginosa* by DEP-Raman spectroscopy

The sensitivity of the manufactured DEP-Raman setup was tested analysing three different bacterial strains *E.coli* MG1655, *S. aureus* SH1000 and *P. aeruginosa* PAO1-N. These strains were chosen because of their great interest in medical and microbiological fields due to their connection with drug resistance studies. At least 20 Raman spectra for each bacterial strain were collected optimizing the DEP cell acquiring conditions for each strain as explained in detail in paragraph 3.2.3. Raman specific signals in the regions of the bacteria chemical fingerprint, between (500-3100) cm^{-1}, were analysed and a chemical assignment was made for each peak or band (Figure 4).

Figure 4 shows that although all the analysed bacterial strains present a similar Raman profile in the molecular fingerprint region due to the same basic compositional structures, some differences are evident between the three spectra. In particular, bands around 750 cm^{-1} and 787 cm^{-1} can be ascribed to the relative content of nucleic acids. The intensities of the bands at 1445 cm^{-1} and 1660 cm^{-1}, which are due to the C-H and the amide I vibrational modes respectively, can be useful to calculate lipid/protein ratio, an information that can help to the detection of structural composition changes of microbial cells due to environmental factors such as temperature or pH of the culture medium or they can be an indications of the growth time. The peak at 1008 cm^{-1} is typical of the phenylalanine and is always very narrow and intense in all Raman spectra of bacteria. However, there are some molecular constituents, like pigments, that produced the formation of additional peaks in the Raman spectra which, even if their amount is very small, provided a noticeable intensity due to pre-resonance phenomena.

For instance, Raman spectra of *S. aureus* displayed two specific peaks around 1525 cm^{-1} (ν(C=C)) and at 1160 cm^{-1} (ν(C-C)) which could be ascribable to the signals of carotenoid structure [184] which are cellular pigments present in this particular bacterial strain and responsible of the characteristic orange colour of its colonies. It was found in literature that the amount of this pigment production is time-dependent and can be easily related to the stage of growth of the bacterial cells comparing the relative intensities of the two peaks with the amide I band as an internal standard [185].

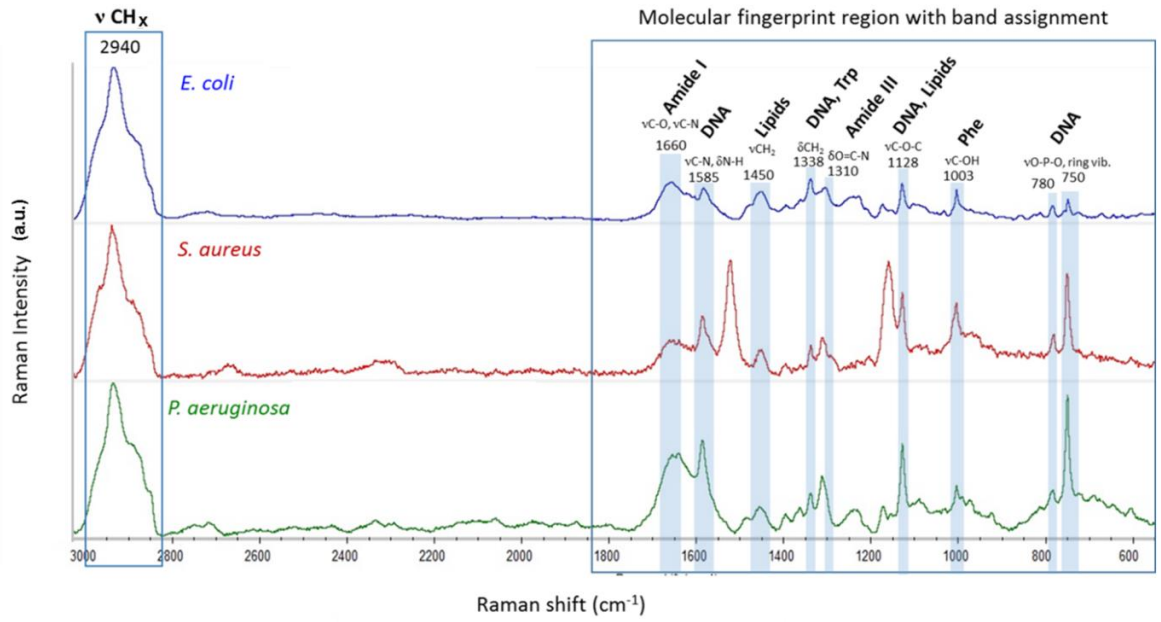

Figure 4: DEP-Raman characterization of *E. coli* MG1655, *S. aureus* SH1000 and *P. aeruginosa* PAO1.

Raman spectra of *E. coli* MG1655 (blue), *S. aureus* SH1000 (red) and *P. aeruginosa* PAO1 (green). The most significant bacterial spectral regions are highlighted in blue and a chemical assignment was done for each signal. The CH_x region and the molecular fingerprint region are squared. Reprinted with permission from [175].

The attention was then focalized especially on *E. coli* and its Raman spectrum obtained using this DEP-Raman technique was more accurately analysed (Figure 5). A tentative assignment of each significant Raman signal was performed and is summarized in Table 4.

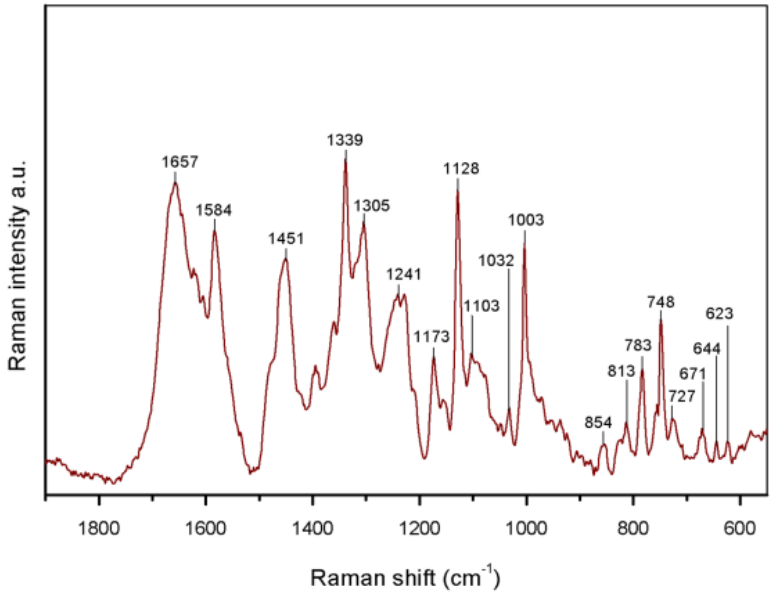

Figure 5: Raman spectrum of *E. coli* MG1655 with signal assignment.
Spectrum of *E. coli* MG1655 obtained using the DEP cell. The spectral collection conditions are described in Material and Methods section.

Table 4: *E. coli* MG1655 Raman signals and their tentative assignment.

Raman shift (cm^{-1})	**Assignment**	**Chemical compound**	**Reference assignement (cm^{-1})**
2940	$\nu(CH_2)$ asym. $\nu(CH_3)$ sym.	carbohydrates, amino acids, proteins, lipids	2935 [186] 2935 [187]
1657	amide I band $\nu(C=C)$	nucleic acids	1666 [188] 1663 [187]
1584	amide II band		1565 [189]

	δ(NH); ν(CN)	nucleic acids (G, A)	1575 [186]
1440-1480	$\delta(CH_2/CH_3)$	lipids, amino acid, side chains of proteins and carbohydrates	1440-1460[186]; 1450 [188]
1338-1316	ring vibration	nucleic acids (G, A), Trp	1337 [186]
	$\delta(CH_2)$	proteins	1337 [186]
1241	ν(C-C), ν(C-O)	nucleic acids (A, T)	1250-1000 [189]
	amide III band		1245 [186]
	$\nu(PO_2^-)$ asym.	DNA bases	1243 [186]
	ν(C-O-S)	sulpholipids	1240 [189]
1100-1035	ring stretching	saccharide components (lipid, DNA and RNA backbone); phenylalanine	1115-1005 [189]
	ν(C-O-C) sym. glycosidic link; ν(C-N); ν(C-C);		1104 [187] 1125 [186]; 1099 [187]
1003	ν(C-OH)	Phenylalanine	1008 [185]

854	ν(C-N-C) sym.	aminoacids (Tyr)	850[189]
813	ν(C-O-S)	sulpholipids	800-815 [189]
783	ring breathing modes	nucleic acids (C, T, U), phenylalanine, pyranose compounds	786-780 [187]
750-620	ring vibration	DNA (A,G,C)	748 [187]
		amminoacids (Phe)	615 [185]

*ν: stretching mode, δ: deformation mode, G: guanine, A: adenine, T: thymine, C: cytosine, U: uracil

These results show that with the developed Raman-DEP setup different bacterial strains dynamically dispersed in their liquid medium as planktonic culture can be analysed in a very short time. Raman spectra allows to obtain chemical information about their time of growth or other microbiological conditions and different bacterial strains could be discriminate and recognized on the basis of their specific Raman signals. However, even if macro differences such as the presence of pigments in the cells can be easily detected by the naked eye, modern machine learning techniques and multivariate statistics such as classification models and cluster analysis are very useful to analyse larger number of Raman spectra simultaneously and identify the most significant spectral regions of variance to achieve optimal classifications. However, these preliminary results were fundamental to confirm the successful working of the developed DEP cell.

3.3.2 Determination of MIC and MBC of ciprofloxacin towards *E. coli* MG1655 by DEP-Raman

In order to study the changes in the Raman spectra of *E. coli* MG1655 due to its treatment with the most prescribed second generation fluoroquinolone

ciprofloxacin (CP) and its mode of action, firstly the MIC and MBC of this antibiotic toward *E. coli* were determined using classical microbiological assays, like BDM and viability assay. Bacteria were let grown until they reached the mid of their exponential growth phase, OD_{600} around 0.3, where they were demonstrated to be more sensitive to external treatments. Indeed, since at this stage of growth bacteria are rapidly multiplying, the chance of developing advantageous mutations that would confer resistance to antibiotics or other antimicrobial is higher [190]. Then they were treated with different concentrations of CP (0.015-2) µg/ml.

As shown in Figure 6, it emerged that, under these culture conditions, the MIC and MBC of ciprofloxacin for *E. coli* MG1655 are 0.5 µg/ml and 1 µg/ml, respectively.

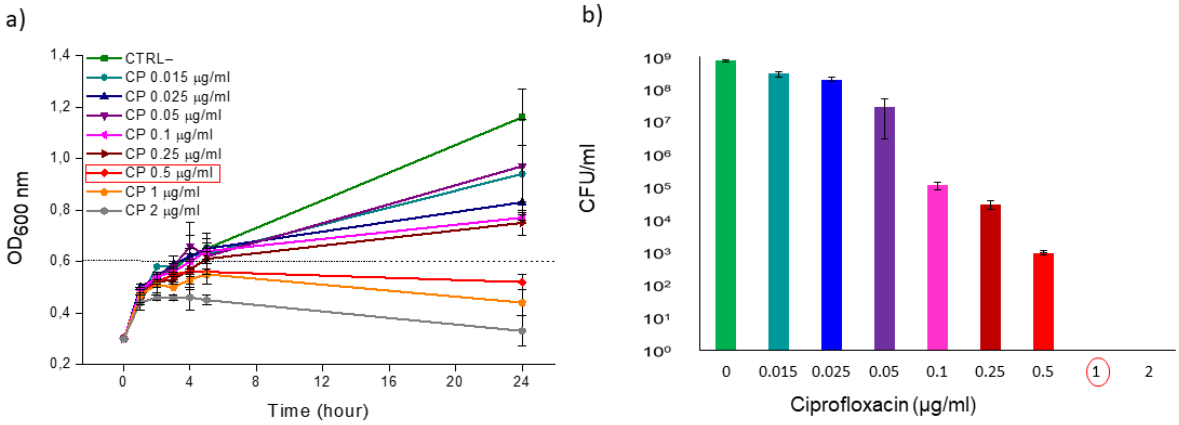

Figure 6: CP MIC and MBC determination for *E. coli* MG1655.
a) Turbidity assay results of the CP MIC determination for *E. coli* MG1655 by BDM. The OD_{600} of the cultures measured were plotted against time. Concentrations of CP between 0.015 µg/ml and 2 µg/ml were tested. b) Viability assay results of the CP MBC determination for *E. coli* MG1655. The CFU enumeration was performed using the same concentrations of CP employed for the BDM. The red box (a) and red circle (b) indicate the MIC and MBC values, respectively. Reprinted with permission from [175].

Raman analyses of E. coli MG1655 were then performed using the DEP-Raman setup and comparisons between bacterial treated (Test) and untreated samples (CTRL–) were performed at the CP MBC (1 µg/ml) for four different time points (0, 1, 2, 3) h. The volume of analysis of the confocal Raman microscope was 4.7 μm^3 under the conditions of this experiment. Samples of

CTRL– *E. coli* MG1655 cells were analysed by optical microscopy and it was calculated that performing the DEP-Raman measurements no more than 10 cells were investigated (bacteria treated with CP have higher, variable volumes, so in these cases the number was reduced). Standard microbiological assays such as OD600 measurements, viability assay and fluorescence microscopy analysis were performed simultaneously with Raman analysis as reference methods to correlate the observed Raman response. Differences between the spectra of treated and untreated bacteria were detected (Figure 7).

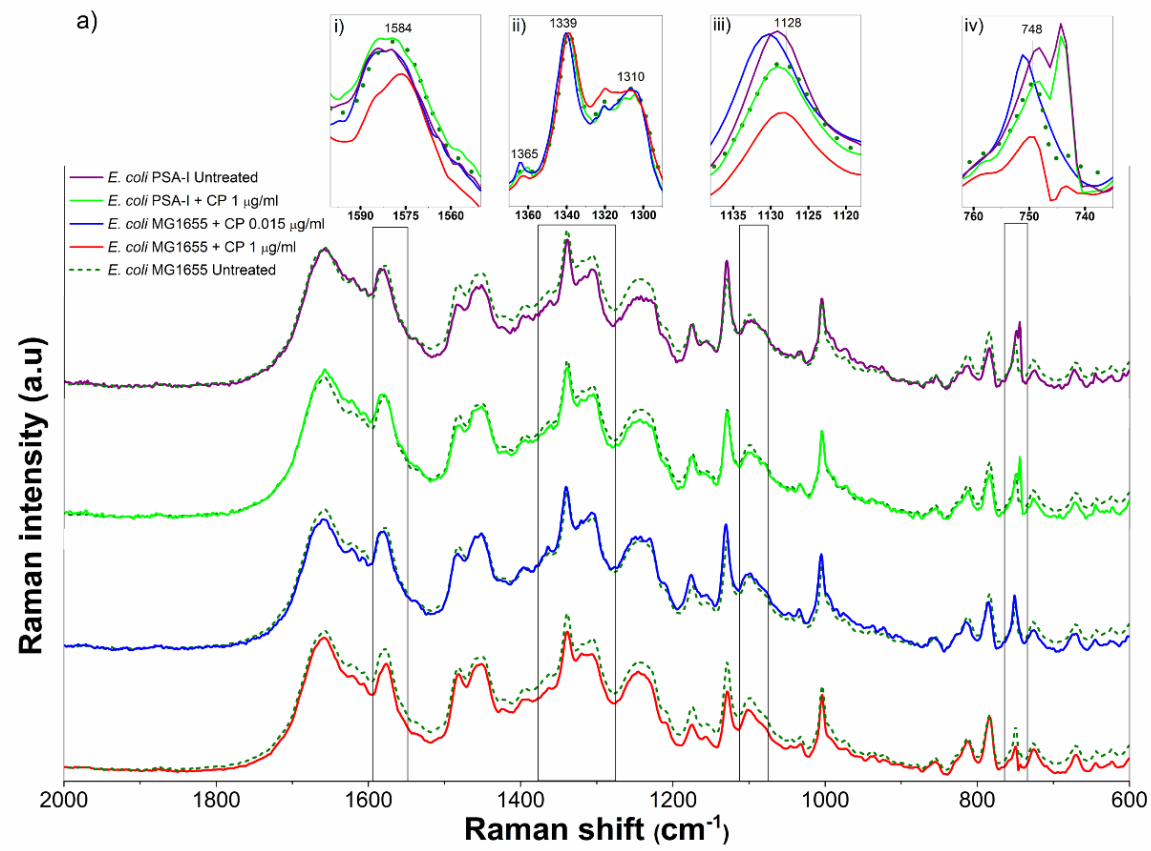

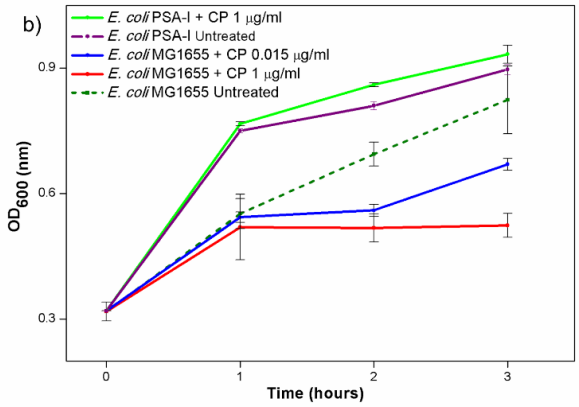

Figure 7: DEP-Raman and turbidity assays measurements of different *E. coli* strains treated at different concentrations of CP or untreated over 3 hours.
a) *E. coli* MG1655 and *E. coli* PSA-I DEP-Raman spectra. Samples are: *E. coli* MG1655 untreated (dash dark green), treated with CP at 1 µg/ml (red) and treated with CP 0.015 µg/ml (blue); *E. coli* PSA-I untreated (purple) and treated with CP at 1 µg/ml for 1h (green). Inserts: spectral regions which display the most relevant differences. In insert ii): spectra were normalized against the peak at 1339 cm^{-1} (tryptophan vibrational modes). b) Turbidity assay of *E. coli* strains MG1655 and PSA-I showing their growth under the same treatment conditions and colour coding described for panel a. The OD_{600} of the cultures is plotted against incubation time Reprinted with permission from [175].

Figure 7b showed that *E. coli* MG1655, the strain sensitive to CP, when treated with the MBC of the antibiotic stopped its growth already after 1 h of treatment. This is due to the cell replication inhibition due to the mode of action of the drug which induces the arrest of the DNA gyrase/topoisomerase activity.

These results were confirmed by the viability assay which demonstrated that bacteria exposed for 24 h to CP at 1 µg/ml showed a viability reduction of 99.9% in comparison with the negative control (Figure 6b). Therefore, in the following paragraph bacterial cells treated with MBC of CP will be referred as “non-viable” while the untreated ones (CTRL–), which maintained all their vitality and viability, as “control”.

3.3.3 Multivariate data analysis and classification model building

Even though the spectral profile of treated and control samples was very similar, statistical differentiation due to minor changes dependent on drug treatment were highlighted exploring Raman data performing a Principal

Component Analysis (PCA) (Figure 8). This technique helps in the visualization of non-random variation in spectral data. In general, multivariate statistical analysis helps in finding the spectral regions of maximum variance to focus on, in order to make a better spectral interpretation.

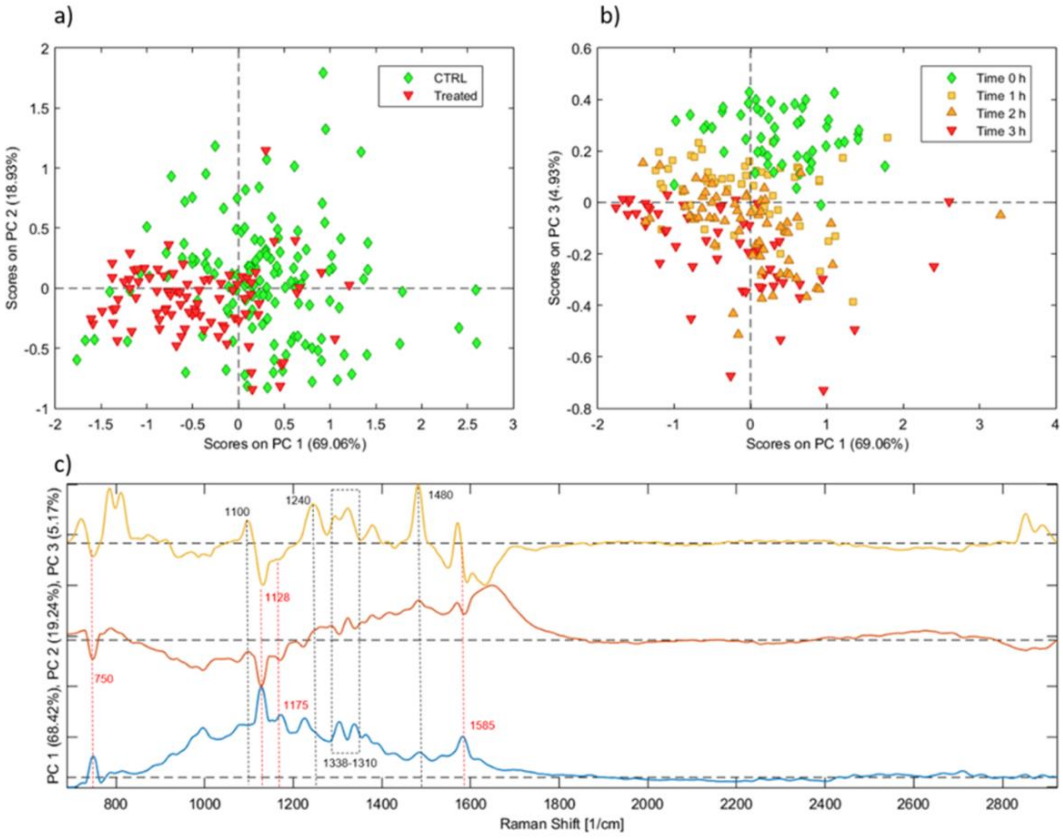

Figure 8: PCA model built on Raman spectra of *E. coli* MG1655 treated with CP at MBC over 3 h.

a) Scores plot of PC2 vs PC1. Groups were coloured by treatment: control samples (green) and treated samples (red), each point represents one Raman spectrum. b) Scores plot of PC3 vs PC1. Groups were coloured by time: starting point (green), 1 h (yellow), 2 h (orange), 3 h (red). Each point represents one Raman spectrum. c) Loading profile of PC1, PC2 and PC3, highlighting the more meaningful spectral bands represented in the first three PCs. Red dashes display the relevant bands related to treatment (represented mostly in PC1 and PC2); black dashes display relevant bands that vary due to the effect of time (represented mostly in PC1 and PC3). Reprinted with permission from [175].

PCA results showed that changes to the Raman spectra of *E. coli* due to the CP treatment were visible already after 1 h of antibiotic treatment (Figure 8a). This analysis allowed to detect also spectral changes due to the passing of time (Figure 8b). However, the spectral regions involved in each of these two effects revealed to be different, indeed they were mostly represented by different PCs (Figure 8c).

It was found that Raman signals variations driven by the antibiotic treatment were those corresponding to the vibrational modes of nucleic acids (Figure 9a), which is in line with the CP mode of action as it targets cellular DNA. Specifically, spectral changes were found in the region at 1584 cm^{-1} which corresponds to the ν(C-N), δ(N-H) of guanine and adenine [191]; in the peaks around (748–750) cm^{-1} due to ν(O-P-O) and aromatic ring vibration of nucleic acids [187]; and in the spectral region between (1300–1370) cm^{-1} corresponding to deformation of adenine and guanine (1302–1315) cm^{-1} [192], tryptophan (1339 cm^{-1}), (CH_2/CH_3) twisting, wagging, bending modes of lipids (1313–1307) cm^{-1} [187] and cytosine (1362 cm^{-1}) [193] (Figure 9a).

Conversely, spectral regions affected by the passing of time were more related to protein and lipids. In particular, variations were identified in the spectral region around 1100 cm^{-1}, related to ν(C-N) and other ring breathing modes of phenylalanine (Phe). Other ones were present in the band at 1240 cm^{-1} referring to amide III and asymmetric ν(PO_2) of DNA bases. Many differences were found in the region between (1338–1310) cm^{-1} corresponding to δ(CH_2) of tryptophan (Trp), C-H bending modes of lipids and ring vibration of guanine and adenine, and in the peak at 1480 cm^{-1} which refers to CH_2 stretching modes of lipids. Specifically, the band at 1240 cm^{-1} was found to be influenced more by the time of incubation, than by the presence of the antibiotic, which is in accordance with literature data [97] (Figure 9b).

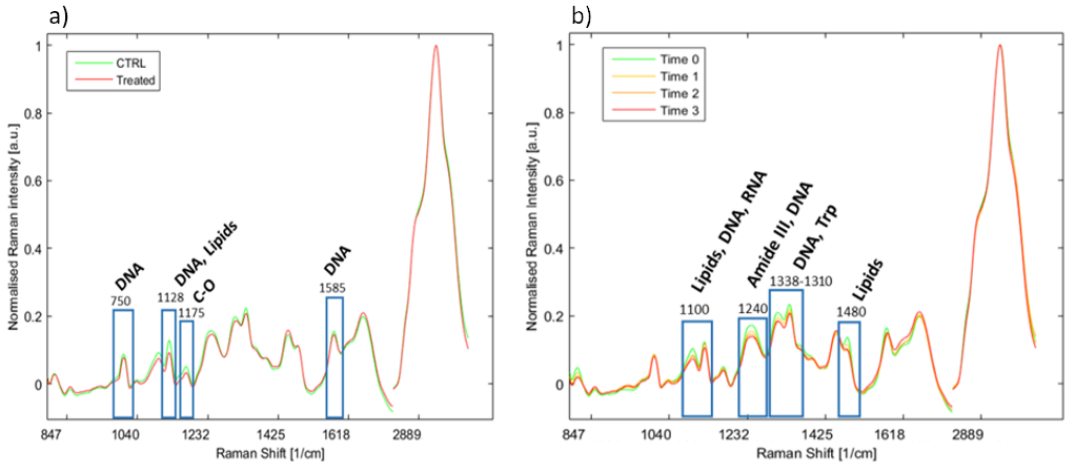

Figure 9: Raman average spectra of *E. coli* MG1655 treated with MBC of CP. a) Raman spectral differences between *E. coli* MG1655 untreated (green) or treated with 1 µg/ml of CP for 1 h (red). b) Raman spectral difference between *E. coli* MG1655 treated for 0 h (green), 1 h (yellow), 2 h (orange) and 3 h (red) with 1 µg/ml of CP. Chemical meaning was assigned to the bands which changed the most. Reprinted with permission from [175].

To evaluate the statistical significance of those spectral variation emerged from PCA an ASCA was performed on the same dataset. This statistical technique is highly appropriate for time-resolved multigroup (such as viable or non-viable *E. coli*, treated for the three different time spans), multi-subject (data of several culture batches) and multivariate data (such as Raman spectra). It results that both bacterial growth time and CP effects together with experimental replicates led to statistically significant chemical changes. The variations due to each of these three factors ("time", "drug" and "experiment") were detected and quantified by ASCA. It emerged that the effects of factor "experiment" produced from data of different replicate samples are the prevalent with 16.27% of spectral variance with p = 0.001, while the factor "time" produced a variance of 12.56% with p = 0.001 and the factor "drug" presented 11.73% of variance with p = 0.001. Furthermore, also the combination of the two factor "time × drug" was analysed and resulted significant, meaning that the antibiotic action toward bacterial cells was not constant over time but the cells responded differently to the drug after different time of treatment.

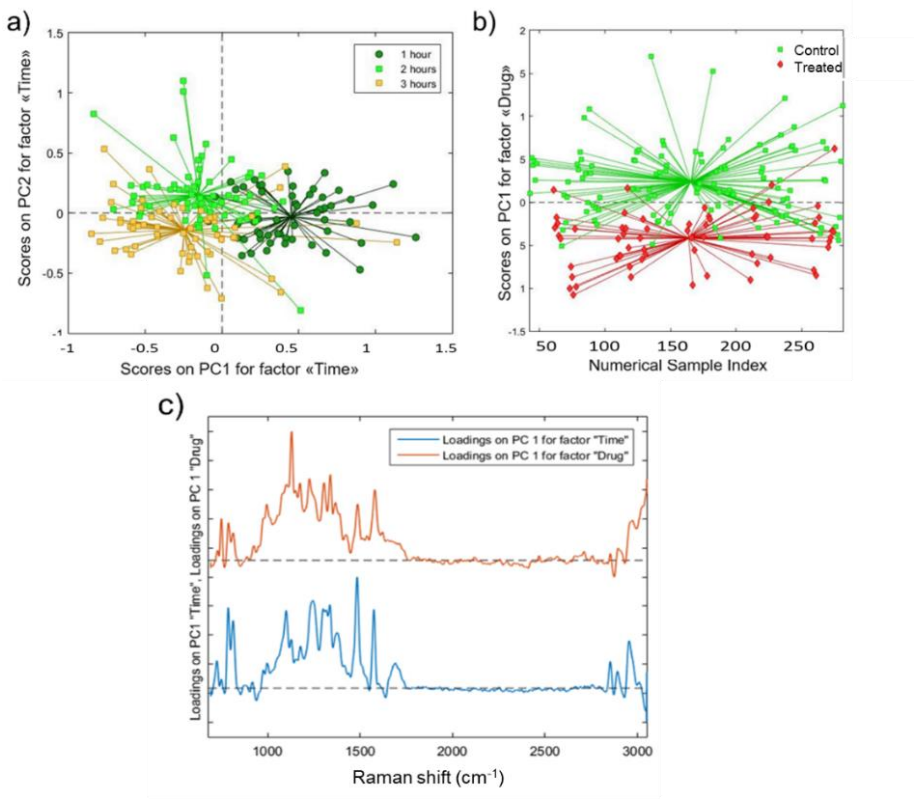

Figure 10: ASCA scores plots built on the first two PCs relevant experimental factors. a) ASCA score plot relative to factor "time" b) ASCA score plot relative to factor "drug". c) Loading profile of PC1 for factors "time" and "drug". Reprinted with permission from [175].

Figure 10 panel a) and b) show the scores plot of the PCA models built for the two effects "time" and "drug" exhibiting a statistical significant separation between the groups. Figure 10 panel c) displays the loading profiles of PC1 for these two factors revealing the different contribution of original spectral bands in the separation. These results demonstrated that the impact of bacterial physiology and stage of growth are not negligible and that the antibiotic action can be successfully detected by Raman spectroscopy. Moreover, ASCA on the PC1 of the PCA model was performed colouring the data groups on the basis of the concentration of CP used for the treatments (Figure 11) revealing a correlation between Raman spectra and different concentrations of the antibiotic confirming with Raman the results obtained with classical microbiological methods used for MIC and MBC determination. For this experiment four different concentrations of

CP were analysed over a 3 h time span. ASCA model of normalized and mean centred spectra was calculated to better understand the effect of CP concentration in combination with other experimental factors. Factor 1 represents "CP concentration", its levels are: 0 µg/ml (untreated control bacteria), 0.015 µg/ml (sub-MIC treatment), 0.5 µg/ml (MIC treatment), 1 µg/ml (MBC treatment). Factor 2 represents "time", its levels are (1, 2, 3) h (6 spectra were collected for each experimental level).

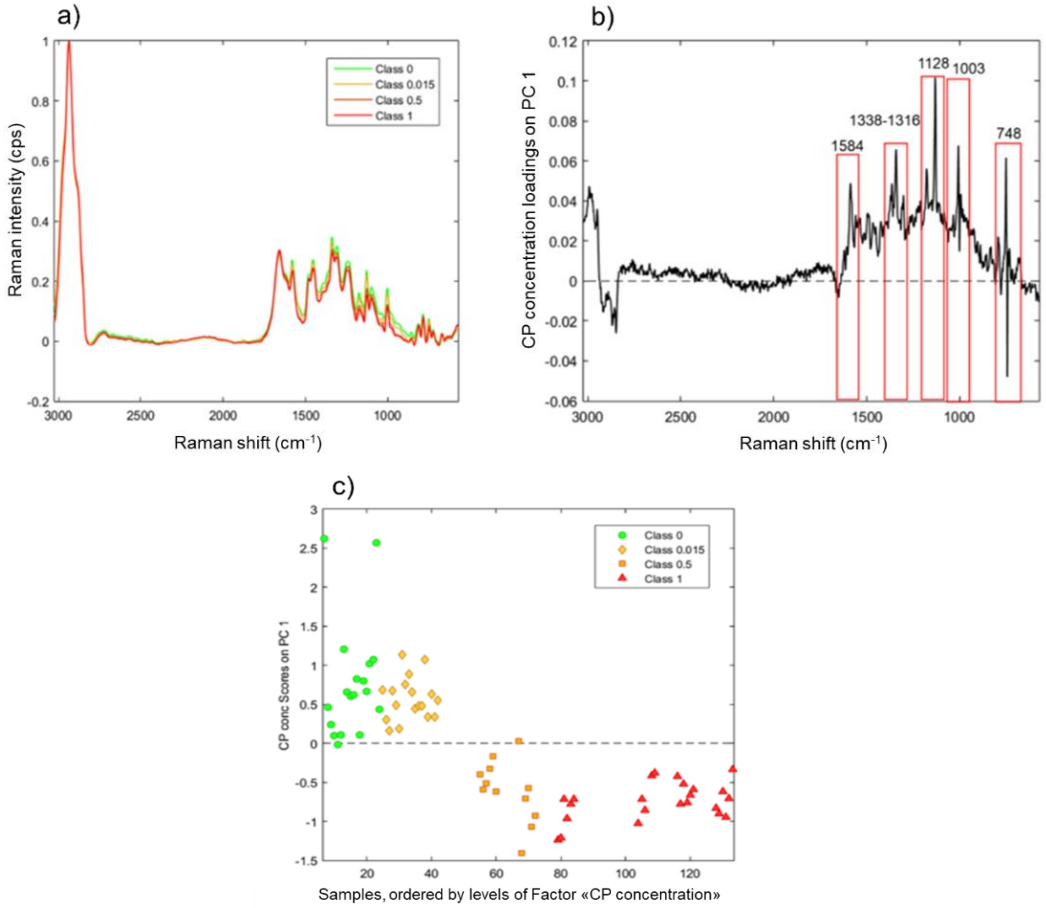

Figure 11: Evaluation of the effect of CP concentration on *E. coli* MG1655 Raman spectra by ASCA.

a) Average spectra of bacteria treated at the same concentration of CP (at all the three time points); b) Loading shape of the PC1 of the PCA model related to the "CP concentration" factor of the ASCA model; c) ASCA plot of PC1 resulted from Raman spectral data of *E. coli* replicates untreated (green), treated with 0.015 µg/ml of CP (yellow rhombi), treated with 0.5 µg/ml of CP (orange squares) and treated with 1 µg/ml of CP (red triangles). Reprinted with permission from [175].

The CP concentration factor resulted to have a significant effect on spectral variance (52%) with a *p-value* of 0.001. In Figure 11 the normalized average spectra of the four concentration levels are showed (panel a) together with the profile of the calculated CP concentration factor (loadings on PC1 of factor "CP concentration") (panel b), and the scatter plot of the scores on this factor for 12 measurement batches (panel c).

Since these results were very promising, PLS-DA classification models were developed to obtain a predictive method to detect bacterial cells responses to the CP treatment. It was built one model for each time span, since it was found that the time of incubation with CP and the time of growth significantly influenced bacterial Raman spectra of both treated and controls.

Class 1 or "positive" regards bacterial samples treated with the MBC of the antibiotic and are considered as "non-viable", while class 0 or "negative" is related to untreated bacteria considered as "viable". The sensitivity, specificity and classification error calculated for this model are summarized in Table 5. It emerged that a good discrimination between viable and non-viable bacteria can be obtained already after 1 h of treatment with CP. It is evident that the bacterial susceptibility to the antibiotic increases over time, indeed after 2 h and 3 h of treatment, all treated samples were classified as non-viable without any false negatives. However, the highest prediction's specificity was obtained after only 1 h of treatment, that is due to the sum-up of the factors "time" and "treatment" effects, resulting in an increasing of false positives, i.e. erroneously classified as non-viable. Since the total error rate increases over time, the analysis was focused on 1 h of treatment because it presented the lowest classification error. Indeed, while performing an AST for investigating antibiotic tolerance, the possible miss of a tolerant culture is considered more dangerous than an overestimation of false negatives (i.e. erroneously classified as viable), so high specificity is required for this kind of analysis. Moreover, Raman spectroscopy demonstrated to be more sensitive in comparison with classical microbiological techniques as major differences between the spectra of treated and untreated bacteria were detectable already after 1 h of treatment while the growth curves built by the turbidity assay, almost overlap at this time point (Figure 7b).

Table 5: Susceptibility, specificity and classification error of PLS-DA models built for each time point of CP treatment.

Validation	1 h (%)	2 h (%)	3 h (%)
Sensitivity (prediction)	67	100	100
Specificity (prediction)	100	50	33
Classification Error (prediction)	17	25	33

3.3.4 Classification model validation

The predictive strength of this classification model was tested performing the same experiment but treating bacteria with other two CP concentrations: 0.5 µg/ml, which is the founded MIC for *E. coli* MG1655 at OD_{600} = 0.3, and 0.015 µg/ml, which is definitely under the MIC.

Since CP mechanism of action is to inhibit DNA gyrase and topoisomerase IV (both involved in DNA replication), thereby blocking bacterial cell division [194], as showed in the turbidity assay, bacteria treated with MIC of CP (Figure 7b red line) showed an inhibition of replication after 1 h of treatment (which is the time required from bacteria for at least two complete cycles of replication and from CP to affect the total cell population). On the other hand, bacteria treated with 0.015 µg/ml of CP continue to grow (Figure 7b, blue line), although a slowdown in the growth is visible if compared to the untreated bacteria (Figure 7b green line), which is maybe due to bacterial stress response to the introduction of the antibiotic, even if this concentration is not sufficient to stop bacterial replication.

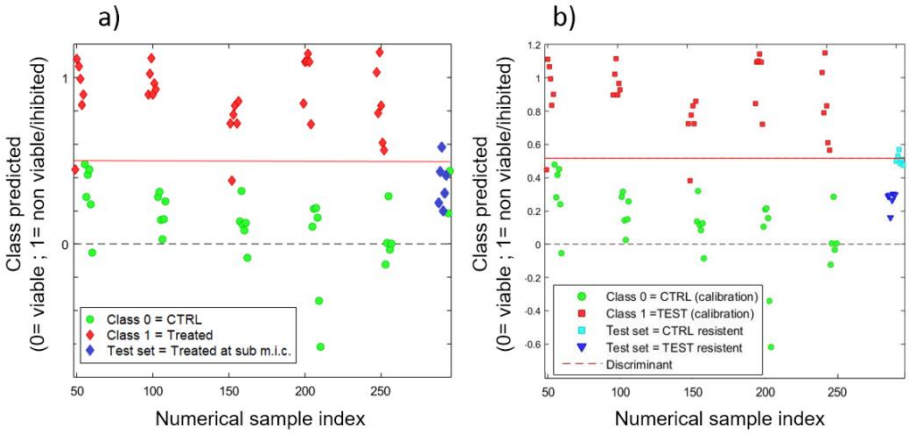

Figure 12: Evaluation of *E. coli* viability by PLS-DA classification model. a) Prediction of *E. coli* MG1655 susceptibility after the treatment with CP 0.015 µg/ml (dark blue diamonds); b) Prediction of E. coli PSA-I susceptibility after the treatment with CP 1 µg/ml (dark blue triangles). In both plots, the training data were reported as green circles (negative) and red squares/diamonds (positive). Reprinted with permission from [175].

The PLS-DA model was then applied to the Raman spectra obtained from these samples at the three time points and it classified the spectra obtained from *E. coli* treated with CP at MIC as non-viable (positive) with 83% of accuracy. Furthermore, 83% of bacteria treated at sub-MIC were classified as viable (negative) (Figure 12a).

Moreover, the viability assay performed for the MBC determination (Figure 6b) showed a significant reduction of bacterial vitality after 24 h of treatment with 0.5 µg/ml of CP, whereas with 0.015 µg/ml of CP no significant differences were visible in comparison with untreated bacteria, which confirmed the classification results. These results evidenced that RS can be used to test the viability of bacteria with adequate accuracy after only 1 h of treatment at different CP concentrations, which is in accordance with previous literature data [98]. Noticeably, the spectral signals which varied the most in correlation with CP concentration are the same as those that were revealed to be related to the effect of the antibiotic (Figure 11).

In order to further validate the classification model, it was applied to classify an environmental isolate CP resistant strain of *E. coli* (*E. coli* PSA-I), which demonstrated to be morphologically very similar to *E. cli* MG1655 [195], untreated and after a treatment with CP at 1 µg/ml.

The turbidity assay (Figure 7b) revealed that as expected *E. coli* PSA-I replication was not inhibited by this CP treatment, but continued to grow at the same rate as the untreated *E. coli* PSA-I. This was confirmed by the Raman spectra profile of *E. coli* PSA-I treated with CP at 1 μg/ml (green line), which highlight more similarities with *E. coli* MG1655 negative control (olive dash line) than with the treated one (red line, Figure 7a). After only 1 h of antibiotic treatment 100% of *E. coli* PSA-I bacteria were correctly classified by the model as viable (Figure 12b) as well as 89% of the untreated *E. coli* PSA-I samples. This test is a very important result since it demonstrated the versatility of the model on different bacterial strains, even though they can slightly differ from the training set. So, the statistical robustness of the model was confirmed since the scores of the resistant *E. coli* strain were positioned below the discriminant line, nearer to negative control cells (viable). Moreover, from this experiment emerged that the model can successfully be applied to predict the susceptibility of bacteria to a specific antibiotic.

3.3.5 Application of the model to a biocide cross-induced tolerance experiment

It was previously demonstrated that some biocide products such as triclosan (TCS), which was one of the most widely used antimicrobial agents for personal hygiene purposes, are able to induce cross-tolerance to antibiotics in different bacterial species even at concentrations commonly found in the environment [196]. Westfall et al [197], demonstrated by both *in vitro* and *in vivo* in murine models that TCS exerts an impressive protective effect on *E. coli*, increasing its survival in the presence of ciprofloxacin even at concentration around three times the MIC (100 ng/ml). In this thesis *E. coli* MG1655 was pre-treated with TCS at a concentration usually found in the urine of individuals using products containing TCS (0.2 μg/ml) [198, 199] promote a biocide induced antibiotic tolerance. Then, the susceptibility of the developed DEP-RS method to detect antibiotic tolerance insurgence was tested.

Simultaneously, fluorescence microscopy and viability assays were performed on each bacterial samples as reference methods to support the Raman results (Figures 13 and 14).

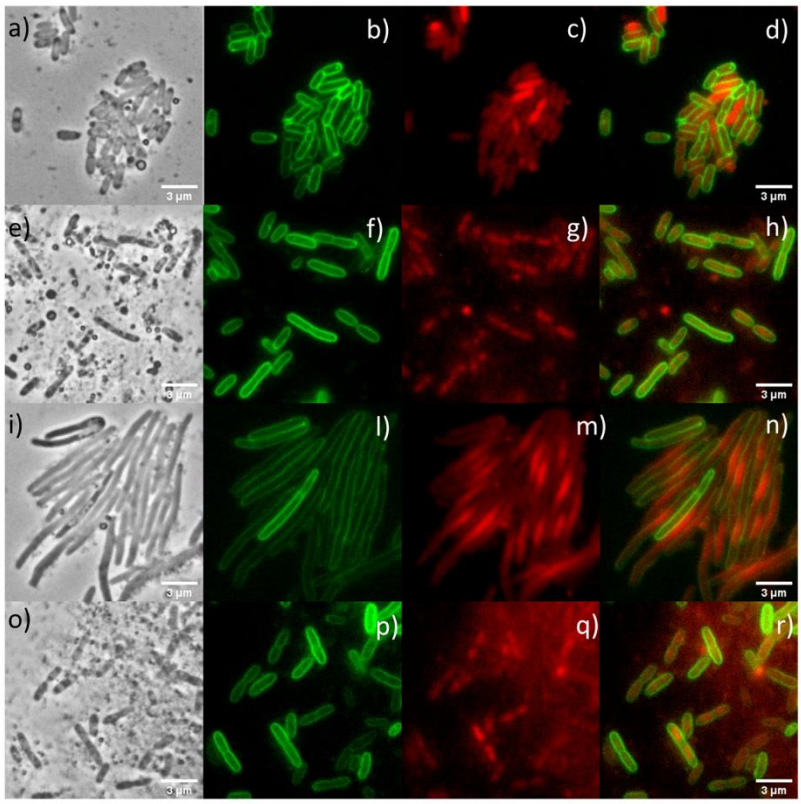

Figure 13: Fluorescence microscopy of *E. coli* MG1655 subject to different treatment.

a-d) *E. coli* MG1655 untreated. e-h) *E. coli* MG1655 treated with 0.2 µg/ml of TCS for 1 h. i-n) *E. coli* MG1655 treated with 0.5 µg/ml of CP. o-r) *E. coli* MG1655 pre-treated for 30 min with 0.2 µg/ml of TCS and then treated with 0.5 µg/ml of CP. Each sample is shown in bright field (a,e,i,o), stained for bacterial membranes (b,f,l,p; green), for DNA (c,g,m,q; red) or with membrane and DNA stains overlaid (d,h,n,r). reprinted with permission from [175].

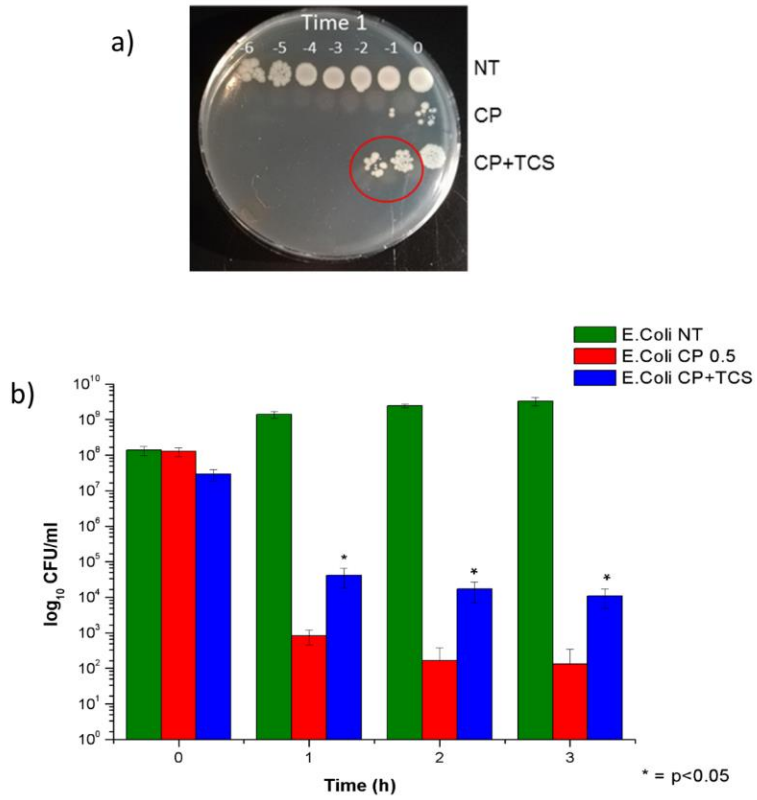

Figure 14: *E. coli* MG1655 viability assay to confirm the cross-induced tolerance. a) Photo of a representative plate of *E. coli* MG1655 untreated (NT), pre-treated with 0.2 µg/ml TCS then treated with CP at 0.5 µg/ml (CP+TCS) for 1 h, or treated only with CP at 0.5 µg/ml (CP) for 1 h. b) Viability assay results representation of *E. coli* MG1655 NT (green), CP + TCS (blue), CP (red) after (1, 2, 3) h of treatment with CP. The tolerance was evident after 24 h at a significant level for all the 3 time points (star: *p-value* < 0.05). Each experiment was replicated three independent times and error bars are shown. Reprinted with permission from [175].

In Figure 13, it is evident that CP treatment at the MIC (0.5 µg/ml) for 1 h induces visible filamentation and changes in the DNA localization in *E. coli* MG1655 (Figure 13 i-n) if compared with the untreated ones (Figure 13 a-d). This is due to the bacterial response to the mechanism of action of the antibiotic which blocking the cell division induces an SOS DNA repair response. It is important to notice that the bacterial samples treated for 1 h with CP after a pre-treatment with sub-MIC concentration of TCS maintain the typical morphology of untreated bacterial cells (Figure 13 p–r). These results confirmed the successful induction of

CP tolerance since bacterial cells recover their ability to divide themselves even in presence of the MIC of CP. It was also demonstrated that 1 h of treatment with ciprofloxacin at this concentration is sufficient to observe its influence on cell morphology and intracellular DNA distribution. Furthermore, it was confirmed that bacteria pre-treated with TCS at sub-MIC concentration are able to develop a cross-tolerance to CP after just 1 h of exposure to the antibiotic. This was supported by viability assay data (Figure 14) where a statistically significant (*p-value* < 0.05) increase in growth of bacteria pre-treated with TCS and then treated with CP at all the three time points if compared with those treated only with CP.

The DEP-RS spectra of the same samples were analysed with the previously validated PLS-DA model (Figure 15).

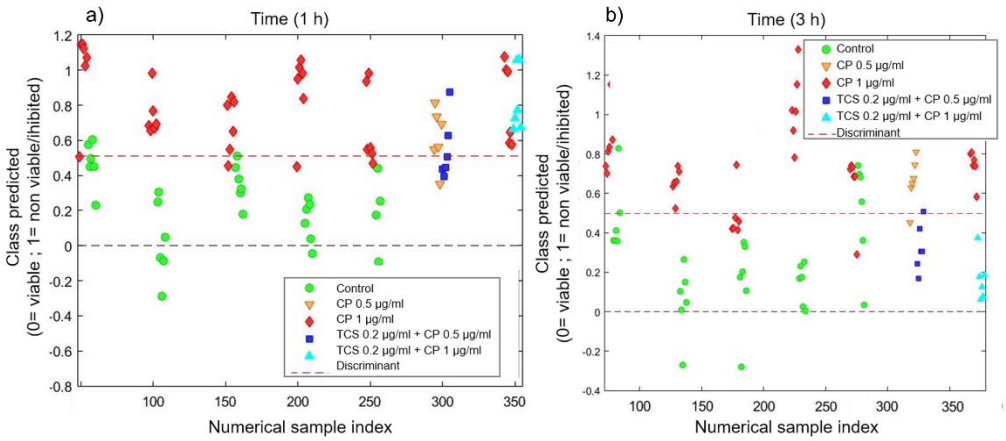

Figure 15: PLS-DA plots of *E. coli* MG1655 cross-induced resistance experiment. a) PLS-DA classification of *E. coli* MG1655 spectra collected after 1 h of CP treatment. b) PLS-DA classification of *E. coli* MG1655 spectra after 3 h of CP treatment. *E. coli* MG1655 samples: pre-treated with TCS then treated with CP at MIC (dark blue squares) or MBC (light blue triangles), treated only with CP at MIC (yellow triangles) or MBC (red diamonds). The training set data are also reported as green circles and red diamonds for "viable" (untreated) and "non-viable" (treated with CP at 1 µg/ml) bacteria, respectively. Reprinted with permission from [175].

As it is shown in Figure 15 most of bacteria treated with MIC of CP (yellow triangles) were classified by the PLS-DA model as "non-viable". This was a control test and those samples represented the negatives for the model sensitivity and specificity calculation. Bacteria treated with both drugs were successfully

classified as tolerant near the group of "viable" bacteria after 1 h of treatment with MIC of CP with a sensitivity of 66% (panel a) which rises to 83% after 3 h of treatment (panel b). This confirmed that the DEP-RS approach is able to reveal the TCS-induced tolerance after only 1 h of antibiotic treatment, as confirmed by the biological assays results. In addition, the induced tolerance was detected more sensitively after prolonged time of CP treatment. This might be due to the greater adaptability of bacterial cells to CP after 3 h, clearly showing the TCS-induced tolerance. The same experiment was performed using the MBC of CP and evaluating its effect using the validated DEP-RS method. In this case, 1 h of treatment revealed to be insufficient to observe bacterial tolerance effects which, however, appeared evident after 3 h of treatment with a sensitivity of 100%. This supports that prolonged time of treatment with the antibiotic allows the detection of the insurgence of cross-induced tolerances also at higher CP concentrations, i.e. at the MBC.

3.4 Raman Imaging for bacterial structures analysis and their localization at a single cell level

Another method to improve Raman performance in the field of microbiological analysis is to combine it with hyperspectral imaging technology, which allows to acquire both spectral and spatial information at the same time. Indeed, Raman imaging in respect to conventional spectroscopy presents a higher spatial resolution, and it is really suited for biological purposes because there is no interference by water, enabling direct measurements on wet tissues, alive cells or bacterial biofilms. The specific chemical fingerprints of the molecules explained in the electromagnetic spectrum in a defined area are recorded pixel by pixel in the resulting image. This technique could be very useful for the characterization of the composition and homogeneity of materials and the identification of their spatial features. Also in this case, statistical data processing techniques, like machine learning and chemometrics, are fundamental to reduce spectral interpretation complexity and data dimensions and to improve the management of the huge amount of chemical and physical information resulting from the images facilitating the detection of important information and the classification of the areas of interest during post-processing [200]. In this way, data regarding different stages of cells cycles or structural features of microorganisms can be rapidly obtained and accurately processed without time-consuming steps [201].

In this thesis, the ability of Raman hyperspectral imaging to detect the spatial distribution of the biological components in a single bacterial cell at a sub-micron level based on their Raman spectral differences is demonstrated. A single *E. coli* cell, in his mid-exponential growth phase, was here investigated using this technique in order to localize the intracellular elements, such as membrane proteins and DNA molecules, and identify the phase of the cell replication cycle thanks to the Raman imaging high resolution and molecular specificity.

Firstly, a comparison between an *E. coli* sample let to air-dry and one lyophilized was performed at a single cell level in order to determine with Raman the preservation conditions of the cells structures if they undergo or not a thermal shock due to the instantaneous freezing required in the freeze-dry process without the addition of any cryoprotectant.

The obtained Raman hyperspectral imaging maps were then analysed throughout multivariate statistical methods such as PCA, to reduce data dimensionality, and MCR-ALS to solve the mixed spectra. Indeed, this last statistical technique allows to provide a chemically meaningful additive bilinear model of pure contributions from the sole information of an original data matrix including a mixed measurement [170].

In the following paragraphs the use of Raman imaging to detect and map the DNA segregation of a single replicating bacterial cell at a sub-micrometre level is explained, the results presented here were published in 2021, and are accessible through the reference [202].

3.4.1 *E. coli* single cell sub-diffraction Raman Imaging

The spatial distribution of biocomponents of an *E. coli* ATCC 8739, a standard bacterial strain, single cell was here analysed by Raman imaging. *E. coli* planktonic culture at a concentration of 1×10^8 CFU/ml was spotted on a golden substrate and an isolated cell was selected randomly and its Raman fingerprint was acquired using the Raman imaging DXR-xi instrument. The mean Raman spectrum resulted to be almost overlapped to that obtained with the DXR so the signals chemical assignment can be referred to Table 4.

Then, one sample of *E. coli* was let air dry (Figure 16Aa) while one was freeze dried (Figure 16Ab) as described in material and methods. These two samples were analysed by sub-micrometrical Raman imaging to determine changes in the distribution of cells biological components due to the different treatment without the need of any molecular staining. Images of each single *E. coli* cell were obtained scanning areas of about 6 µm × 5 µm. The spectra

collection conditions were optimized for each sample maximizing the Raman signal at 2940 cm^{-1} relative to CH_2/CH_3 vibrational modes [186, 187]. The resulting maps were colored according to the intensity of the peak of interest from blue to red as the Raman signal increased, to easily localise the corresponding biomolecules within the cell area.

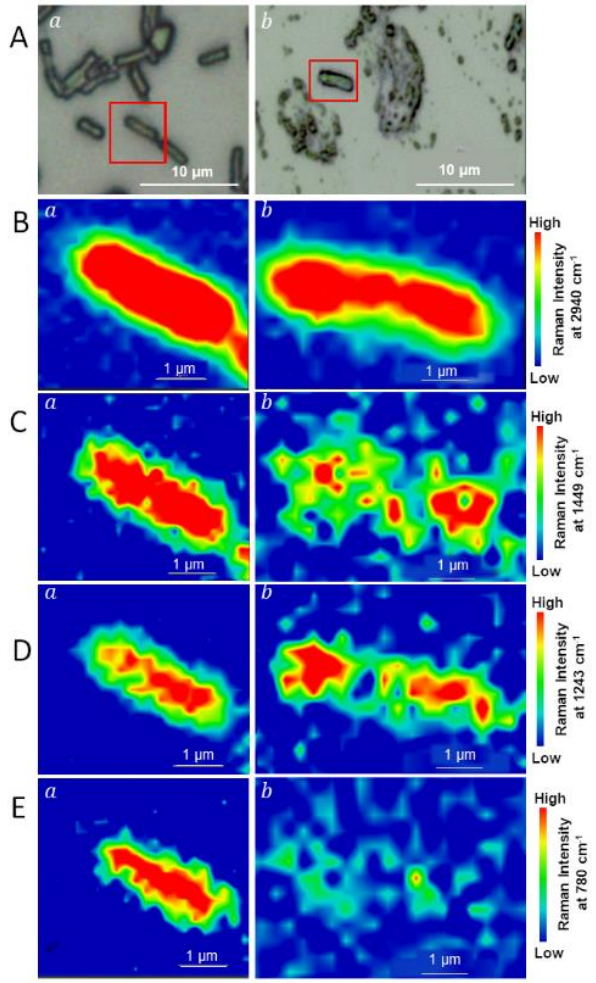

Figure 16: Comparison of Raman Imaging maps of an air dried and a freeze dried single *E. coli* cell at molecular level.

A) Image of representative *E. coli* samples spotted on gold surfaces taken by confocal microscopy with a 100× magnification. (a) Air dried cells, (b) freeze dried cells. B) Single *E. coli* cell's chemical Raman map, the colour scale is based on the intensity of the Raman signal at 2940 cm^{-1} related to generic biomaterial. C) Chemical Raman map at 1449 cm^{-1} relative to cell membrane. D-E) Chemical Raman map at 1243 and 780 cm^{-1} relative to nucleic acids. Adapted with permission from [202].

Figure 16B shows chemical Raman maps of the two differently treated *E. coli* cells coloured with respect to the intensity of the Raman signal at 2940 cm^{-1}, which is the most intense when biomaterials are analysed, attesting that both the air dried and the freeze dried cells remain mostly intact. However, greater differences between the two samples could be detected focusing on the signal at 1449 cm^{-1} (Figure 16C) corresponding to $\delta(CH_2/CH_3)$ modes of C-H functional groups of lipids, proteins' amino acid side chains and carbohydrates, which are all principally paced on the bacterial membrane region [203]. Since freeze-dried bacteria undergo a very fast freezing process when instantly immerged in liquid nitrogen, without the addition of any cryoprotectant in the culture medium, differences in the integrity of the cell's membrane if compared to simply air dried ones were expected. Even though in the optical image of the freeze dried cell (Figure 16Ab) evident cellular damages are not detectable, Raman imaging maps revealed a difference in the biocomponents distribution between the two samples which can be ascribed to membrane damage due to the sudden thermal shock (Figure 16B-C-D-Eb). In this preliminary study the cryoprotective agent was omitted on purpose to demonstrate that Raman images allows to capture the real distribution of the compounds within the bacterial cell at a molecular level, revealing differences in the case of proper or poor preparation method. Noticeably, the air dried sample (Figure 16Ca) presented more homogeneity of the highest Raman intensity areas (red to yellow) toward the cell in respect to the freeze-dried sample (Figure 16Cb). Indeed, in this case the membrane appears damaged resulting in a less defined outer shape. To confirm these findings, the line profiles of intensity across the cell (both longitudinal and transversal) were obtained for the same Raman signals and normalized.

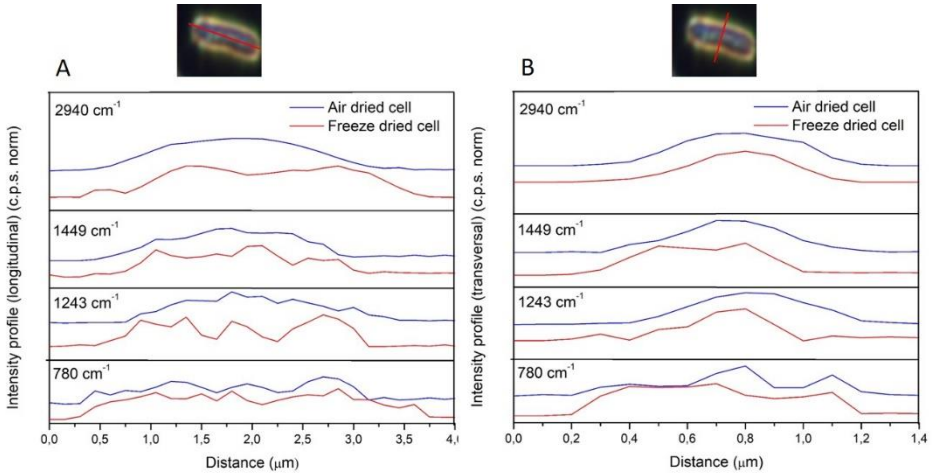

Figure 17: Profiles of the main Raman signals intensities across the air dried and the freeze dried *E. coli* cells.
Intensity profiles of the 4 characteristic peaks at (2940, 1449, 1243) cm^{-1} and 780 cm^{-1} extracted from the air dried (blue) and the freeze dried (red) *E. coli* cells. A) longitudinal section; B) transversal section. Reprinted with permission from [202].

The same analysis were repeated colouring the Raman map in respect to the signal intensity at 1243 cm^{-1} (Figure 16D) and 780 cm^{-1} (Figure 16E) which are specific for nucleic acids vibrational modes [187, 189, 203]. From Figure 16D and 16E it results evident that the spatial localization of the regions related to DNA vibrational modes are different from those regarding the highest intensity of C-H signals. Once more the air dried cell (Figure 16Da and 16Ea) presented a higher homogeneity of the main intensity regions than the freeze-dried one (Figure 16Dφ and 16Eb, respectively). Furthermore, membrane disruption of the freeze dried sample is even more evident if it is considered that while the air dried cell presented nucleic acids signals mostly condensed in the centre of the cell, in accordance with the biological distribution of genetic material, in the freeze-dried one it is unevenly spread around and the peak at 780 cm^{-1} is nearly undetectable, whereas it can be mapped in the air dried cell. Many other samples were analysed in the same way (Figure 18) and they all support these results.

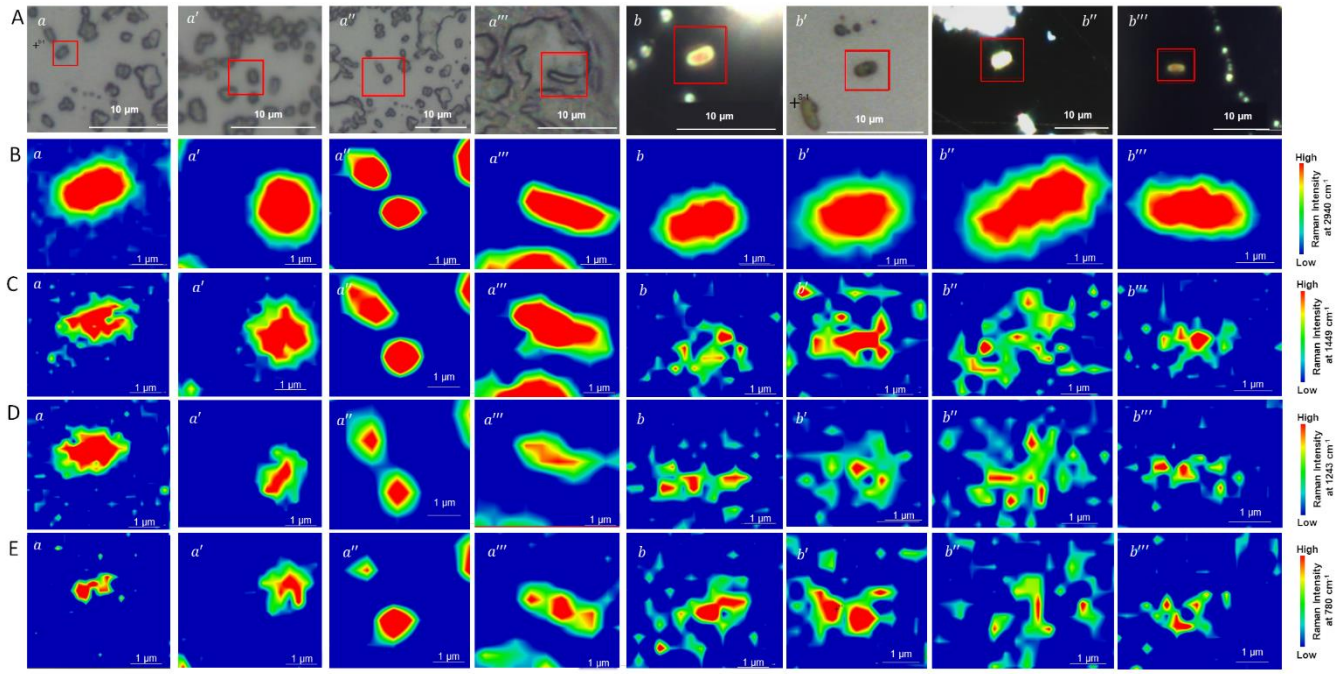

Figure 18: Raman imaging maps of other 4 air dried and 4 freeze dried *E. coli* single cells samples.
A) Confocal Microscope images of (a) air dried cells, (b) freeze dried *E. coli* cells taken with a 100× magnification. B-E) Chemical Raman maps of the single bacterial cells, the colour scale is based on the intensity of the Raman signal at B) 2940 cm^{-1}, generic biomaterials. C) 1449 cm^{-1}, cell membrane. D-E) 1243 and 780 cm^{-1}, nucleic acids. Adapted with permission from [202].

Multivariate analysis of the obtained Raman imaging data was performed to further investigate the differences in the spatial distribution of the bacterial molecules at single cell level considering the variations of all the Raman vibrational fingerprint at the same time and increasing the specificity of the findings.

3.4.2 Principal component analysis to detect dividing cells

Since *E. coli* samples were let grow to reach their mid-exponential growth phase, as explained in paragraph 3.2.2, the probability to find bacterial cells that are duplicating are maximized in this stage of growth. Therefore, Raman imaging analysis was performed on an air-dried cell that showed bigger dimensions

(Figure 19A) in comparison with other observed samples in order to enhance the possibility of detecting actually dividing bacterial cell and to localize the signals of the different cellular molecules. The hypothesis of observing a real-time cellular duplication was supported by the fact that the Raman signal at 2940 cm^{-1}, evidenced an accumulation of biomaterials at both ends of the bacterial cell while in the centre it resulted very low (Figure 19B). To identify unsupervised grouping of image pixels based on their Raman spectral similarities a PCA was performed on the spectra composing the map. This analysis helped to better visualize spectral variance in the different cell's regions focusing on non-random variations. Figure 19C and 19D show the maps of the PCA revealing the spatial distribution of the two first components.

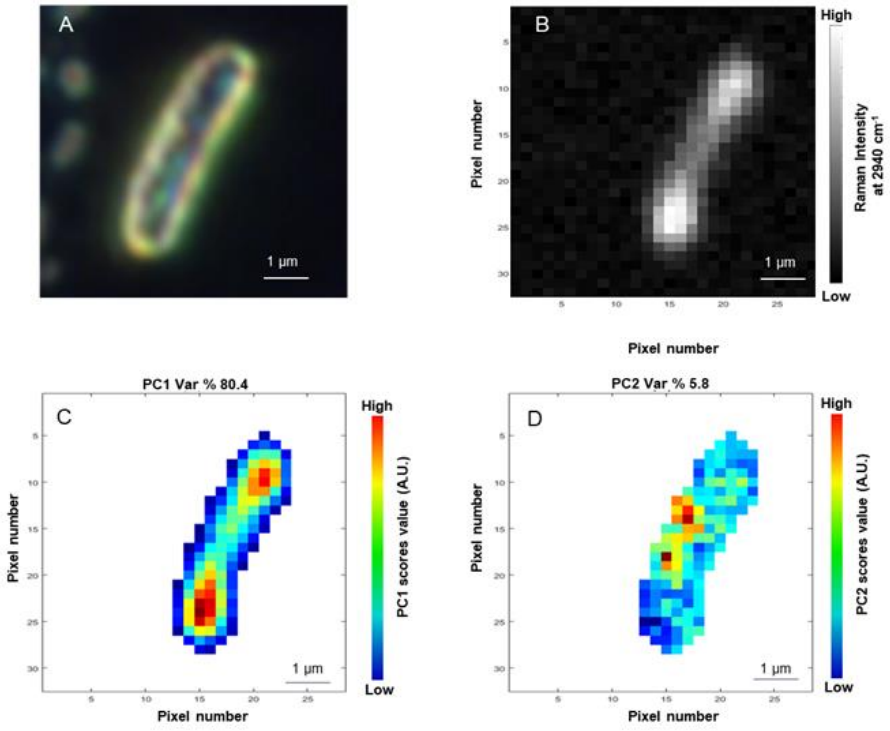

Figure 19: Raman chemical map and PCA scores distribution of a replicating *E. coli* single cell.

A) Image of a replicating *E. coli* cell obtained by confocal microscopy with a 100× magnification in dark field. B) Raman chemical map of the cell described in A coloured for the intensity of the Raman signal at 2940 cm^{-1}. C) PC1 scores intensity distribution from lowest (blue) to highest (red). D) PC2 scores intensity distribution from lowest (blue) to highest (red). Reprinted with permission from [202].

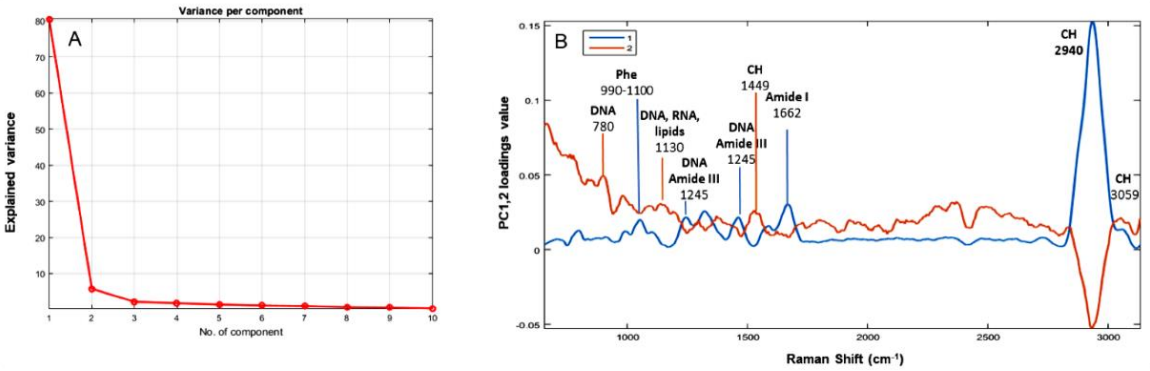

Figure 20: Explained variance and PC1 and PC2 loadings profile.
A) Explained variance of the first 10 PCs. B) Loadings profile of PC1 (blue) and PC2 (orange) in the range between 666 cm^{-1} and 3120 cm^{-1} with corresponding chemical meaning assignment Reprinted with permission from [202].

The first two principal components (PCs) were explaining the 86.2% of the total variance of Raman spectral data (Figure 20A) so they were chosen to model the chemical images. The chemical differences of bacterial composition were interpreted on the basis of these 2 PCs loadings profiles (Figure 20B) performing a chemical assignment for the highest scores, thus revealing the chemical species more represented by each PC (see Table 4). Each pixel of the map was coloured from yellow to red depending on the highness of each PC's scores value which correspond to a lower or higher representation of this PC in the Raman spectral profile (Figure 19C and D). In particular, both PCs are dominated by the C-H stretching signal at 2940 cm^{-1}. This fact confirms the inhomogeneity of biomaterial distribution within the cell, also supported by the different scores intensity distribution revealed by each PC. Especially, PC1 highest scores distribution (Figure 19C) confirmed that the main amount of biomaterial is condensed at the edges of the cell, as already revealed by the Raman chemical map (Figure 19B), supporting that it is undergoing duplication.

However, a simple interpretation of chemical information brought by the PCs, even if detailed, is not always sufficient because the vibrational modes of the molecules are not always represented by the PCs loading. Indeed, they appear in their original Raman spectral profile since the shape of the bands resulted from a mathematical elaboration of data and also negative signals can appear. Furthermore, PCs explaining larger amounts of information are preferentially chosen over the others but considering biological systems it is not so simple because it is well known that large changes may be triggered by very small

differences [204]. Therefore, MCR-ALS analysis was performed on these data to identify more components with lower information to support PCA results [205]. This technique, in fact, allows to maintain the chemical meaning of the original spectrum in the loadings profile of each component providing estimations of the pure deconvolved spectral shapes in an iterative modelling of mixed spectra.

3.4.3 Multivariate Curve Resolution-Alternating least squares

The first two components of the MCR-ALS analysis demonstrated to include the most representative information and their profiles revealed to be in accordance with the score plots of PC1 and PC2 of the PCA (Figure 21). However, MCR1 and MCR2 granted a more detailed understanding of biomolecules distribution and higher specificity considering a whole spectral pattern instead of a single peak at a time and allowing a better spectral signals analysis removing the negative ones (Figure 22).

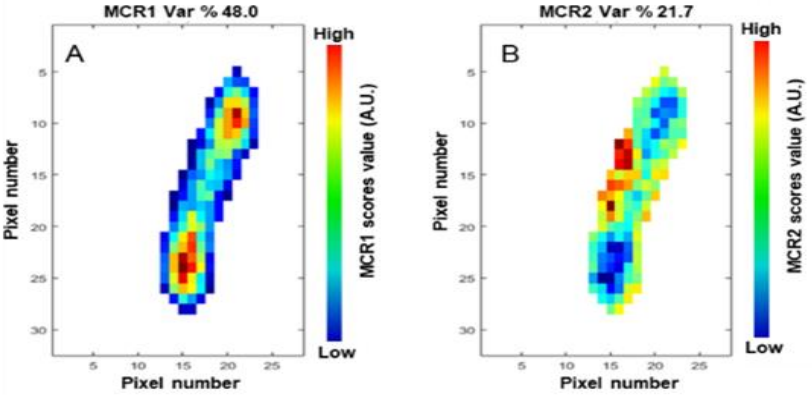

Figure 21: MCR1 and MCR2 scores plot of a single replicating *E. coli* cell. A) MCR1 scores plots coloured for its intensity from lowest (blue) to highest (red). B) MCR2 scores plot coloured for its intensity from lowest (blue) to highest (red). Reprinted with permission from [202].

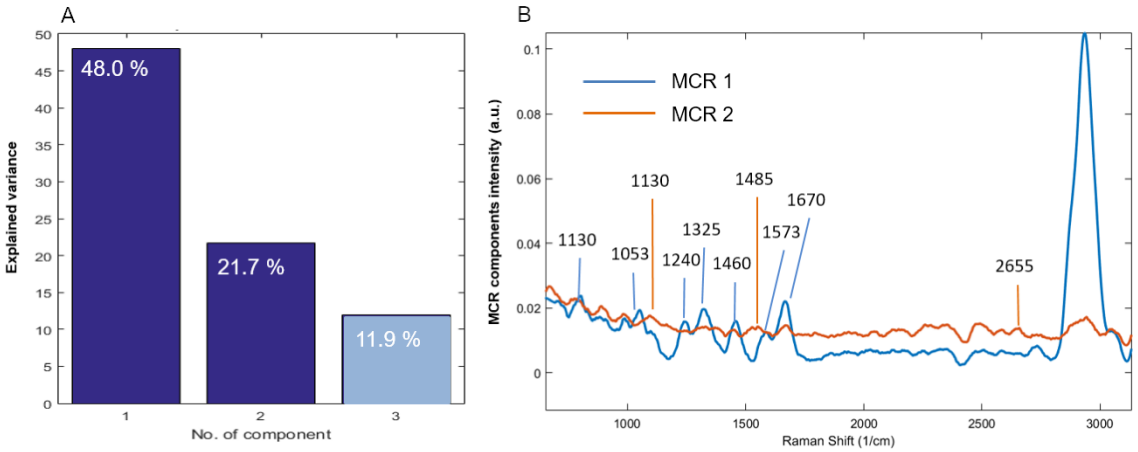

Figure 22: MCR explained variance and loadings plot of the first two components. A) First 10 MCR components' explained variance. B) MCR1 (blue) and MCR2 (orange) loadings plot in the range between 666 cm^{-1} and 3120 cm^{-1}. Chemical band assignment is reported in Table 4. Reprinted with permission from [202].

As already said for PCA, also in this case, the MCR1 component mainly represented spectral data located at the opposite edges of the *E. coli* cell, with the highest contribution of the CH signals (2940 cm^{-1}) confirming the hypothesis of the replication. On the other hand, MCR2 contribution is mainly represented in the central area of the cell with higher scores in the cell's borders suggesting a correlation with the bacterial membrane.

The hypothesis of observing an actually dividing *E. coli* cell is supported by literature studies on proteins and genetic materials dynamic localization performed on *E. coli* based on fluorescence microscopy [206]. Indeed, they sustained that at the earliest stage of segregation, origin duplicate in the middle of the cell, then the two sisters' origins rapidly relocate toward the opposite cell's extremities establishing polarity. After DNA replication and condensation, the bulk of the chromosomes move towards their respective origins [207]. Briefly, during DNA replication, newly duplicated chromosomes separate from each other and form two large masses, the nucleoids, at the two poles of the cell with a DNA-free zone in between. This supported the accumulation of generic biomaterial observed by both PCA and MCR analysis, attested by intense C-H stretching signals, at the two extremities of the observed *E. coli* cell, as they are target for chromosome as well as for proteins.

At this point, at the centre of the cell, assembles a cytokinesis ring made of tubulin-like proteins (FtsZ), known as Z-ring, which is fundamental for bacterial replication to recruit additional proteins needed for cell division. In the space between the two genetic materials masses generated by chromosomes segregation takes place the polymerization of the Z-ring proteins. Therefore, dynamic protein and nucleic acid determinants work together to ensure that the cell finds its precise mid-point when it undergoes binary fission [208]. Therefore, since during cellular division, a bacterial cell's pole can be the targeted by both genetic material as well as by proteins, this explains the higher concentration of biological material in these regions, proved by intense C-H stretching signals.

Indeed, a part from these signals MCR1 is mostly represented by proteins and nucleic acids signals at 780, 1000-1100 and 1243 cm^{-1}, which confirm the theory of observing the actually segregation of the chromosomes at the two opposite poles of the cell together with the two replication origins and the proteins needed for the division. Thus, Raman signals due to the two nucleoids are here captured. Although, MCR2 in (Figure 22, orange) which seems to be more represented in the cell's middle seems to be more related to the cellular membrane components like proteins, lipids and carbohydrates. This interpretation supported the theory that the centre of a divisional bacterial cell, between the two nucleosomes, is a DNA-free zone (Figure 21B). Indeed, in this region, a major presence of membrane-associated signals could be due to the assembly of the Z-ring proteins to mediate the cytokinesis, as said before.

3.5 Conclusions of Part I

In this section of the thesis Raman spectroscopy was employed as new and faster alternative to classical microbiological techniques to characterize bacteria and develop new ways to test their sensitivity to antibiotics and biocides. In fact, a Raman-based method was here developed to detect possible resistances directly measuring planktonic cultures in few hours instead of the typical 24 h of incubation required by standard methods. Saving time is fundamental to prevent or reduce the selection of advantageous resistance mechanisms by the organisms [209].

Firstly, an integrated microfluidic device was built to combine dielectrophoresis with Raman spectroscopy to maximize bacterial concentration under the focus of the laser thus optimizing their signals. Using this DEP-Raman technique three different bacterial strains (*E. coli*, *P. aeruginosa*, *S. aureus*) were

well characterized directly in suspension with high specificity. Raman spectral results were processed by multivariate data analysis and spectral differences between *E. coli* treated with the antibiotic ciprofloxacin (CP) at its MIC ("non-viable" bacteria) or untreated (as negative control or "viable") were modelled at a molecular level after only 1 h of treatment. This model based on Raman data was built to predict the bacterial viability (as well as bacterial susceptibility to antibiotic treatment), and was successfully validated by correctly classifying as non-susceptible (or "viable") bacteria treated with a sub-MIC concentration of CP and bacteria in which a tolerance to the antibiotic was induced by a pre-treatment with the biocide TCS at very low concentrations. Furthermore, *E. coli* PSA-I, a strain naturally resistant to CP and treated with the MBC of CP, was correctly predicted as non-susceptible after only 1 h with an accuracy of 100%. All these results were confirmed by standard microbiological assays supporting the cross-induction of antibiotic tolerance at the analysed time points and the definition of the CP MIC and MBC for *E. coli* MG1655 at its middle exponential growth phase.

Therefore, the combined DEP-Raman method here explained could open the way to faster ways to identify bacterial resistances to antibiotics, without the need of time-consuming sample preparation with high accuracy and versatility for several applications.

Furthermore, Raman chemical imaging was here applied to investigate single *E. coli* cells at sub-micrometrical level to identify and localize the distribution of different biocomponents throughout the bacterium.

It was demonstrated that bacterial membrane and genetic material can be distinguished and localized within the bacterial cell by Raman without the need of any labelling or complex sample preparation. *E. coli* samples which were freeze-dried or simply let to air-dried on a microscope slide showed different chemical map patterns related to the integrity of the bacterial membrane. Moreover, performing statistical multivariate analysis on the Raman imaging data, the possibility to visualize the chromosomes segregation and the Z-ring formation during an actually replicating single bacterial cell was demonstrated. Specifically, MCR-ALS analysis showed one component dominated by DNA signals while the others, mainly representing membrane proteins signals (which could be due to the Z-ring assembly), confirmed a different localization of these two types of bacterial compounds. Thus, Raman spectroscopy enables to observe bacterial duplication with sufficient specificity and sensitivity to catch the faithful segregation of the newly duplicated genetic material. These findings could open the door to real-time molecular analysis on cells in their natural environment.

Chapter 4

Nanomaterials as novel antimicrobial additives for active food packaging

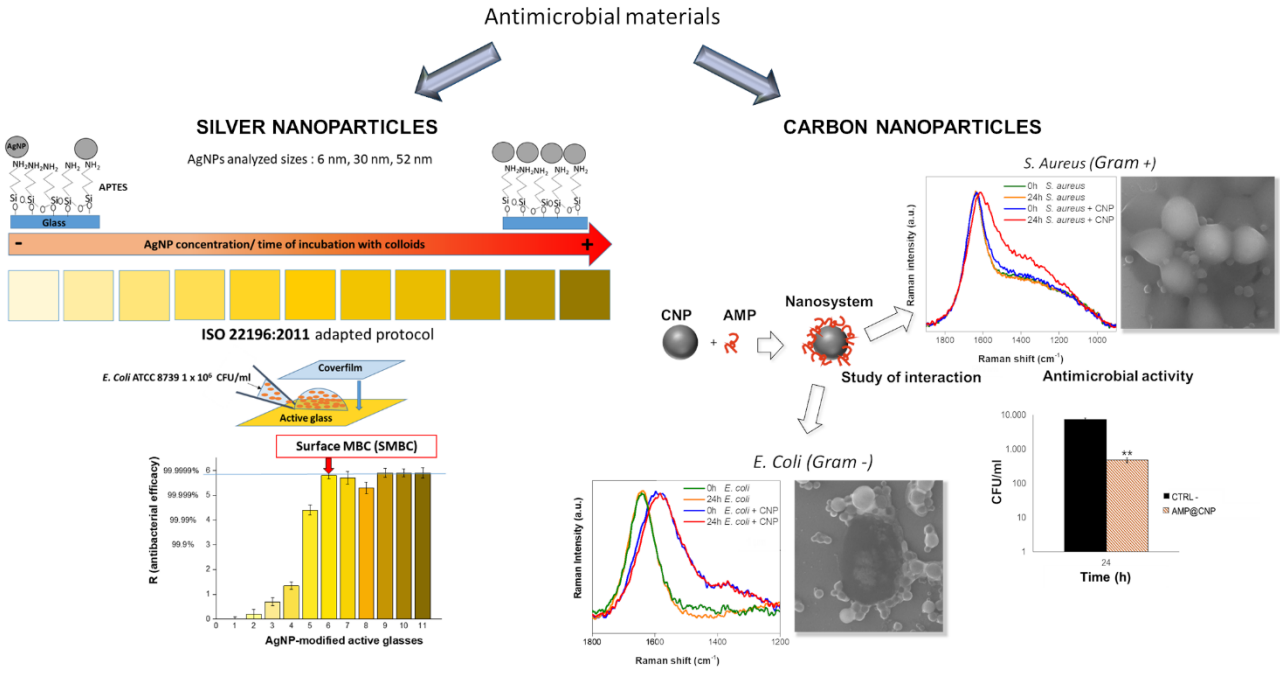

4.1 Silver and carbon nanoparticles as antimicrobial agents in novel active food packaging materials

Silver nanoparticles (AgNPs) are already well known and widely employed in many fields from medicine [68], to cosmetics, to water disinfection [69] and to food packaging industry [70]. Indeed, they have demonstrated to be a very effective alternative to classical antibacterial chemical products or to antibiotics since they seemed to be less related to the development of microbial resistances [59] together to their characteristic bactericidal, antiviral and optical properties and their non-toxicity for human cells at low concentrations [63]. Even if colloidal silver was employed for its antibacterial properties from ancient times the potential of silver nanoparticles remains today still not fully exploited also because it depends on many factors. Firstly, the size of the AgNPs is a variable that has a great impact on their bactericidal effects since it seems to be inversely proportional to their efficacy [210, 211, 212], which is mainly due to an higher exposed metallic surface and a faster ion release from smaller nanoparticles [213, 214]. Furthermore, another factor that greatly influence their antibacterial activity is their shape. Many studies revealed that truncated triangular nanosilver exhibited the highest biocidal activity followed by silver nanospheres and nanorods [215]. In addition also their dispersion, chemical stability and the presence of surface modifiers can influence the results of the tests of their antimicrobial efficacy since they are usually suspended in aqueous media [216, 217]. However, the relations between size and antimicrobial properties of AgNPs immobilized on substrates is still far from being completely understood. In literature many examples of AgNPs coated or incorporated on/in different materials such as bio/polymers [68, 218], fabrics, textiles [219] or glass [220] could be found but a proper evaluation of the correlation between the nanoparticles' size, their amount on the surface and their bactericidal properties conducted by standard and referable methods is not present.

Thus, three different sized AgNPs (6 ± 3, 30 ± 6, 52 ± 7) nm were synthetized for this thesis work and their shape, dimensions, surface properties and content of silver were characterized by different techniques. Their bactericidal properties were tested in liquid suspension against *E. coli* ATCC 8739 and their MIC and MBC were found for all the three sizes. Then, glass surfaces were functionalized with monolayers of all the three sizes by the "layer-by-layer" (LbL) approach [220], with different percentage of coverage. The antibacterial properties of this obtained model active glasses were evaluated against *E. coli* by the international

standard ISO 22196. The correlation between the AgNPs antibacterial effects and their size was here analysed and for the first time surface MBC (SMBC) was quantified for each type of AgNPs-modified surface. Furthermore, the MBC and the SMBC were compared to a better understanding of the different mechanisms of action and the overall antibacterial performance of suspended or immobilized AgNPs.

Moreover, a second kind of nanoparticles based on carbon were here considered for their possible application as antimicrobial agents in innovative active packaging. As already explained in the introduction of this thesis, carbon nanoparticles (CNP) are arising great interest in many fields of application thanks to the biocompatibility of the material, low environmental impact and high mass/surface ratio which make them very suitable as innovative drug delivery systems and nanomedicine [221, 222]. In particular, the CNP employed in the present work were obtained from hydrothermal carbonization of glucose, which is considered a simple green chemistry process that allows to prepare particles of a defined size, which presented a spheroidal shape, a high stability in suspension and a negatively charged surface. Furthermore, they demonstrated to have photothermic and photodynamic activities when irradiated with a NIR laser source (945 nm) [74] and to be degradable by human monocytes *in vitro* [79], which is important to avoid bioaccumulation in the human body. These characteristics render them very interesting for their application in targeted and punctual tumoral therapies because they allow to enhance the efficacy of the treatment and to reduce the side effects of chemotherapy. Thanks to the presence of many functional groups at their surface they can be functionalized by physical adsorption or covalent biding with many antimicrobial compounds or cationic peptides by electrostatic interaction with their surface negative charges.

In this thesis CNP were physically conjugated with a cationic antimicrobial peptide derived from bactenecin Bac8c^{2,5Leu}, and the antibacterial activity and mode of interaction of both the CNP alone and the peptide-loaded CNP was analysed against *Staphylococcus aureus* SH1000 and *Escherichia coli* MG1655 as models of Gram + and Gram – organisms, respectively. The eight aminoacids long peptide Bac8c^{2,5Leu} was chosen for its low production costs and its relevant bactericidal properties. It revealed a low concentration MIC against *S. aure*us (8 μg/ml, 6.75 μM) and other medically relevant bacteria and demonstrated to be effective *S. aureus* biofilm infections eradication *in vitro* [223].

4.2 Materials and Methods

4.2.1 Reagents

Silver nitrate (>99.8%), sodium borohydride (>99.0%), sodium citrate (>99.0%) and (3-mercaptopropyl)trimethoxysilane (≥98%, APTES) were purchased from Sigma Aldrich.

For bacterial cultivation Luria Barthani (LB) and Muller Hilton (MH) broth and agar, PBS tablets at pH 7.4 (for 200 ml), nutrient broth (NB) components (Sigma Aldrich) and plate count agar (PCA) (Lickson) were employed and all were diluted in Milli-Q® water. Soybean casein digest broth and polyoxyethylene sorbitan monooleate (Tween 80) by Scharlau Microbiology with lecithin (SCDLP) was prepared.

The pH of each culture medium was corrected to be in the range between 6.8 and 7.2 (at 25 °C) by the addition of NaOH and HCl 0.1 M solutions.

Phosphate-buffered physiological saline (PPS) was prepared adding sodium chloride in Milli-Q® water and this solution was used to dilute PBS 800 fold. All the solutions used for the bacterial analysis were autoclaved.

For the glass substrates commercial microscope glass slides (26 mm × 76 mm, 1.0-1.2 mm thick) purchased from Aptaca (Canelli, Asti) were used.

4.2.2 Bacterial strains and cultivation

Escherichia coli ATCC 8739 was employed for the microbiological experiments on AgNPs, while *Escherichia coli* MG1655 and *Staphylococcus aureus* SH1000 were chosen for the experiments on CNP.

Each bacterial strain was revitalized and cultured in LB medium for the AgNPs experiments and in MH medium for the CNP experiments until they reached an OD_{600} of 0.3 as described in details in paragraph 3.2.2.

4.2.3 Active glass functionalized with different-sized silver nanoparticles

4.2.3.1 Silver nanoparticles preparation

The synthesis of spheroid shaped AgNPs was adapted from a previously reported preparation method [224, 225, 226]. Briefly, starter seeds of about 6 nm of diameter were produced by the reduction of silver nitrate induced by sodium borohydride under controlled temperature conditions. These seeds were used as

starters for growing larger nanoparticles (30 nm and 52 nm) by the stepwise seeded-growth method.

4.2.3.2 Chemical characterization of AgNPs

Colloidal AgNPs were analysed by UV-VIS spectrophotometer (Lange DR500) and absorbance spectra were obtained in the range between (200-1000) nm using water as blank.

A Jeol JEM-3010 UHR (Tokio, Japan) transmission electron microscope (TEM) equipped with monocrystalline LaB6 as thermo-ionic source was used to take images of the colloidal AgNPs with a point resolution of 0.17 nm, employing a voltage of 300 kV. A drop of AgNPs suspension, prepared as described, was air dried on a copper grid (3 mm) coated by a perforated carbon thin film. Using the ImageJ software [227] the relative diameter and the function of dimensions distribution of each suspension were obtained from TEM images of at least 200 NPs for each AgNPs size.

The content of silver in each AgNPs preparation was quantified by Thermo Fisher Scientific ICP-MS ICAP-Qs. Before the measurements the samples were sonicated for 20 min at 180 W, filtered with a 0.2 µm nylon filter and washed three times with Milli-Q® water, precipitating them by centrifugation as described in details in the following paragraph. 0.5 ml of each suspension were then mineralized in hot concentrated HNO_3 to completely dissolve silver and they were diluted up to 1:10 000 in a 2% (v/v) final nitric acid concentration. A 7 points calibration curve was made using (100, 50, 25, 10, 5, 1 and 0.3) µg/l with a linear correlation coefficient >0.999. The polyatomic ions interference was cancelled by using the collision cell in He mode with kinetic energy discrimination (He - KED). The isotope ^{107}Ag was used for quantitation. Other operating parameters were as follows: RF power 1450 W; main Ar flow 15 l/min; Ar auxiliary flow 1.0 l/min; nebulizer flow 0.90 l/min; concentric nebulizer with impact sphere; collision cell He flow 5.0 ml/min. Extraction lens voltages and KED bias were auto-optimized with the tuning solution suggested by the vendor.

4.2.3.3 Cleaning and concentration of AgNPs

The three kind of AgNPs batches were cleaned, concentrated and sterilized. After a 20 min sonication bath at 180 W they were filtered with a 0.2 µm nylon filter and suspensions at the different concentrations to be tested (from 0.2 µg/ml to 10 µg/ml) were prepared in Milli-Q® water. Three calibration curves, one for

each size of AgNPs, based on their extinction UV-VIS spectra were built considering the maximum of each typical plasmonic peak (391 nm for 6 nm AgNPs, 398 nm for 30 nm AgNPs and, 419 nm for 52 nm AgNPs). AgNPs were precipitated at 4 °C by different centrifugations protocols for each size (90 min at 21000 RCF for AgNPs 6 nm, 30 min at 4500 RCF for AgNPs 30 nm, and 20 min at 2500 RCF for AgNPs 52 nm). AgNPs were washed three times with Milli-Q® water, sterilized by autoclavation, and the final concentration of the suspensions after the cleaning was measured on the basis of the calibration curves by Lambert-Beer formula. Then the final concentration of each AgNPs stock was adjusted to 2 mg/ml with Milli-Q® sterilized water.

4.2.3.4 MIC and MBC determination of colloidal AgNPs

The MIC and the MBC of colloidal AgNPs of the three sizes against *E. coli* ATCC 8739 were obtained adapting the method described by Ortiz et al. (Ortiz, Torres and Paredes, 2014). The three differently sized AgNPs were put in different tubes within the desired test concentrations in 15 ml of LB medium: (0.65, 1.3, 2.6, 6.4, 10.4, 13, 26, 39) µg/ml were tested for the (6 ± 3) nm AgNPs; (6.05, 12.1, 24.2, 36.4, 60.5, 97, 121, 146, 182) µg/ml for the (30 ± 6) nm AgNPs and (6.6, 13.2, 26.5, 66, 106 132, 158, 198) µg/ml for the (52 ± 7) nm AgNPs. All the suspensions were sonicated at 180 W for 20 min. The bacterial culture prepared as described in paragraph 4.2.2 was diluted in fresh LB broth to an OD_{600} of 0.1 (which correspond to about 1×10^8 CFU/ml) and each tube was inoculated with a volume of bacteria to reach a final concentration of 1×10^6 CFU/ml. A negative control of *E. coli* in LB without AgNPs and two positive controls prepared by adding 10 µg/ml of $AgNO_3$ and 10 µg/ml of TCS in the culture medium were tested as well. All the tubes were vortexed and incubated horizontally at (37 ± 1) °C under agitation at 200 rpm. The OD_{600} was measured every hour for 6 hours and one point was taken after 24 h. Then, each concentration tested was serially diluted in PBS and plated on LB agar in triplicate. The plates were incubated overnight at (37 ± 1) °C and the formed bacterial colonies were counted.

4.2.3.5 Immobilization of the AgNPs on the glasses surface

Squares of 25 mm × 25 mm were manually cut from microscopy glass slides 26 mm × 76 mm, (1.0–1.2) mm thick. They were cleaned by sonication in acetone bath for 10 min, then in ethanol bath for other 10 min. They were immersed in aqua regia (3:1 HCl 37%:HNO_3 65%) for 15 min and washed three times with

Milli-Q® water. Then they were soaked in piranha solution (3:1 H_2SO_4 96%: H_2O_2 30%) for 30 min at 80° C to generate superficial –OH groups, and washed other three times with Milli-Q® water. A 3% (v/v) solution of (3-aminopropyl)triethoxysilane (APTES) was prepared in methanol and put in a polytetrafluorethylene (PTFE) samples holder where 4 glasses at time were put vertically for 1 h at room temperature to promote the formation of superficial amino-groups. The volume of APTES put in each holder was calculated to obtain at least a monolayer of molecules on each surface of each glass. Then, the amino-modified glasses were washed by sonicating them in methanol bath, dried using a nitrogen stream, moved to a 4-place glass holder and kept thermostatically at 150°C for 1 hour. They were let cool to room temperature, and incubated in 30 ml of colloidal AgNPs of the desired size and dilution for different times. The AgNPs were diluted in Milli-Q® water in a concentrations range of (1.9–60) μg/ml and they were incubated with the modified glasses for different time spans from 15 min to overnight. After the incubation, the functionalized glasses were washed three times with Milli-Q® water and air dried vertically under the sterile cabinet.

4.2.3.6 Characterization of active glasses

The silver modified glasses were analysed by UV-VIS spectrophotometer (Lange DR500) equipped with a film holder taking absorbance spectra in the (200 -1000) nm range. A non-functionalized cleaned glass was used as blank.

The glasses were then observed by SEM using a SEM FEI Inspect F (Thermo Scientific) in UHV sputtering them with 10 nm of Au film to prevent their charging. To estimate the average distribution of the nanoparticles on the glasses surface, at least 5 images in different samples areas were taken using an acceleration potential of 10 kV, with a spot size of 3.5 and a magnification of 10000×. The images were analysed with ImageJ and converted to binary to obtain the percentage of area covered by AgNPs.

The glasses silver coverage was quantified for each AgNPs size on selected glasses in duplicate. Glasses without AgNPs, only functionalized with APTES, were analysed as well as blank. Silver was recovered from the substrates by soaking the slides in HNO_3 65% for 3 hours and sonicating them for 2 minutes, then the final volume was brought to 25 ml with HNO_3. Samples were then treated in microwave for 30 min at 150°C to dissolve the residual AgNPs and finally diluted to obtain a HNO_3 concentration of 5%. The solutions were then measured with the ICP-MS instrument described in paragraph 4.2.3.2.

4.2.3.7 Antibacterial efficacy characterization of silver-modified glasses

The antibacterial activity of the silver-modified glasses was principally tested in accordance with ISO 22196:2011 which states the standard procedure for testing antibacterial activity of plastics and other non-porous substrates setting the test parameters. It regulates the test specimen's preparation, bacterial culture conditions, the incubation time, the content of nutrient medium, and the analytical method. To avoid any legal repercussions this work refers to the standard, all changes to this protocol are given in detail to clarify the experimental procedures. Non-functionalized glasses were used as controls. All the tested glasses were sterilized bathing them in 70% ethanol for 20 min. The inoculum volume was reduced to 100 µl in proportion to the area of the sterile cover film, which in this case was reduced to 20 mm × 20 mm to maintain the correct dimensionality in relation to that of the glasses, in line with the ISO requirements. *E. coli* ATCC 8739 at a concentration 1×10^6 CFU/ml was inoculated on each glass surface. The time of contact of bacteria with the glasses was reduced to 5 h to appreciate better the kinetics of the killing efficacy when the AgNPs surface coverage was higher.

4.2.4 *S. aureus* and *E. coli* interaction study with AMP loaded carbon nanoparticles

4.2.4.1 CNP and AMP stock

CNP with a diameter around 132 nm (CNP-S) and around 243 nm (CNP-L) were synthetized by hydrothermal carbonization (HTC) of glucose, purified and characterized for their physiochemical properties, as described in details in the work of Kokalari et al. [79], by the chemical department of the University of Turin, which provided us also the antimicrobial peptide $Bac8c^{2,5Leu}$ and the nanosystem $Bac8c^{2,5Leu}$@CNP.

4.2.4.2 Viability assay of S. aureus and E. coli treated with CNP

The interaction of *E. coli* MG1655 and *S. aureus* SH1000 with three CNP concentrations: (53.3, 26.7, 13.3) µg/ml was analysed performing a CFU counting of vital colonies after (0, 24, 48) h of exposition. To do this, 1 ml of the synthesis batch of CNP was sonicated at 180 W for 20 min and was diluted in PBS to obtain the three desired concentrations of CNP. The suspensions were incubated for 1 h at (37 ± 1) °C under shaking at 150 rpm. 2 ml of each suspension and a negative control, consisting in PBS only, were placed in a 12 wells plate in triplicate. Two

plates were made simultaneously: one for each bacterial strain. The bacterial culture prepared as described in paragraph 4.2.2, was diluted in fresh MH to reach a final OD_{600} of 0.1 (1×10^8 CFU/ml) and each well was inoculated with 2 µl of bacterial suspension to obtain a final concentration of 1×10^5 CFU/ml in each sample. A plate with 2 ml of CNP only, at each of the three concentrations in triplicate, without the bacterial inoculum was prepared as well and treated in the same way of the other samples to be used as control for the DEP-Raman analysis. The plates were incubated at (37 ± 1) °C under shaking at 150 rpm. To avoid evaporation of the samples the plates' lids were sealed with Parafilm® M and the pates were inserted in autoclavable plastic bags during the incubation. An aliquot of each sample was collected at each time span, serially diluted in PBS and plated on MH agar. The plates were incubated overnight at (37 ± 1) °C. Bacterial colonies were counted and the $\log_{10}$ of the calculated CFU/ml was plotted against the relative collection time point.

4.2.4.3 DEP -Raman spectroscopy

The association between bacteria and CNP was analysed by the DEP-Raman method and sample holder device developed and described in details in chapter 3. At each time point 1 ml of each samples from both the plate inoculated with *S. aureus* and that with *E. coli* and the PBS and CNP only controls were collected. Bacteria were precipitated at 3000 rpm for 5 min and five-fold concentrated in order to reach the limit of detection of the technique. Samples were then washed twice with PBS 0.5× by two centrifugation cycles at 14000 rpm for 1.5 min. The pellets were suspended in 200 µl of PBS 0.5× and 100 µl of each sample were injected in the DEP cell. *E. coli* was agglomerated using this parameters of the DEP device: 5 V peak-to-peak sinusoidal voltage between the electrodes with a frequency of 800 kHz. For *S. aureus* the same waveform was employed but using an amplitude of 4 V peak-to-peak and a frequency of 1 MHz. The aggregation time before Raman measurements was 6 minutes for both strains. The micro Raman instrument and collection conditions were the same described in paragraph 3.2.3. The integration times used to acquire each Raman spectrum were 60 scans of 2.5 s each (2.5 min total integration time per spectrum).

4.2.4.4 Bacteria-CNP interaction characterization by SEM

SEM was employed to further analyse bacterial behaviour in the presence of the CNP. Aliquots of the same samples prepared for DEP-Raman analysis,

described before, were collected immediately after the inoculum or after 24 h. Bacteria and the interacting CNP were precipitated by centrifugation at 3000 rpm for 5 min, the supernatant was discarded and bacteria were suspended in 500 µl of Milli-Q® water and washed by a second centrifugation at 14000 rpm for 1.5 min. Supernatant was discarded and the pellets were suspended in 40 µl of Milli-Q® water. 10 µl of each sample were spotted on virgin silicon wafers, which were previously cleaned in hydrofluoric acid 15% (w/v), and left to air-dry. The images were acquired using a SEM FEI Inspect F in UHV with an acceleration potential of 10 kV, with a spot size of 3.5 and a magnification of 10000×.

4.2.4.5 Test of the antimicrobial activity of Bac8c^{2,5Leu}@CNP

The bactericidal activity of the novel nanosystem Bac8c^{2,5Leu}@CNP was measured over time performing a time-kill kinetic assay as described by the standard procedure developed by the Clinical and Laboratory Standards Institute (CLSI), USA. This test was performed on the same kind of CNP described above but with a smaller diameter (CNP-S) in order to obtain the maximum available loading surface. The same CNP concentrations used for the bacteria interaction experiments (53.3, 26.7, 13.3) µg/ml were loaded with (16, 8, 4) µg/ml of the antimicrobial peptide (AMP) Bac8c^{2,5Leu}, respectively. The same concentrations of AMP alone and of the CNP-S unloaded were tested as well as controls. All the suspensions were prepared in PBS and incubated at (37 ± 1) °C for 1 h under agitation at 150 rpm. Plates of 12 wells with 2 ml of each sample in triplicate, including a negative control with PBS only one for each bacterial strain were prepared as described in details for the viability assay, inoculated with 1.0×10^5 CFU/ml and incubated at (37 ± 1) °C, under shaking at 150 rpm. 100 µl of each sample were taken after (2, 5, 24) h, serially diluted in PBS, plated on MH agar and incubated overnight at (37 ± 1) °C. Then, the CFU were counted and the calculated bacterial concentrations (CFU/ml) were plotted against their collection time point.

4.3 Active glass functionalized with different-sized silver nanoparticles

Spheroidal citrate-capped silver nanoparticles (AgNPs) with a nominal diameter of (6, 30, 52) nm were synthetized by the stepwise seeded growth synthesis method described in material and method section. Their physical and chemical characteristics were analysed by different analytical techniques. TEM

was used to determine their shape and dimensions (Figure 23a-b-c), while their absorbance spectra revealed their optical properties and agglomeration state. (Figure 23d-e-f); finally, the Ag content in solution for each AgNPs size was quantified by ICP-MS. All the characteristics of these three sized AgNPs are summarized in Table 6.

Table 6: AgNPs physiochemical characterization.

AgNPs nominal size (nm)	Diameter TEM (nm)	λ LSPR main peak (nm)	[Ag] ICP-MS (µg/ml)	Single AgNP surface area (nm^2)*	Number of AgNPs (NPs/ml)*	Total surface area (nm^2/ml)*	Specific surface area (nm^2/µg)*
6	6 ± 3	391	152 ± 2	1.13×10^2	1.28×10^{14}	1.45×10^{16}	9.52×10^{13}
30	30 ± 6	398	424 ± 12	2.83×10^3	2.86×10^{12}	8.1×10^{15}	1.9×10^{13}
52	52 ± 7	419	208 ± 4	8.49×10^3	2.54×10^{11}	2.3×10^{15}	1.1×10^{13}

* The values were calculated assuming a spherical shape of the AgNPs using the formulas reported in the text.

To calculate the area of AgNPs their shape was approximated to a sphere and the following formulas were used:

Equation 1: Single AgNP surface area : A_{sphere} (nm^2) = $4\pi r^2$

Equation 2: Numbers of AgNPs : NPs/ml = [Ag] (µg/ml) / single NP mass (µg)

NB: The single NP average mass was calculated by multiplying the calculated volume of a single NP (V_{sphere} (nm^3) = $4/3\pi r^3$) by the Ag density: $1.0^5 \times 10^{-20}$ (g/nm^3) and the results were converted from g to µg.

Equation 3: Total surface area: A_s (nm^2/ml) = A_{sphere} (nm^2) × NPs/ml

Equation 4: Specific surface area: A_{ss} (nm^2/µg) = A_{sphere} (nm^2) / single NP mass (µg)

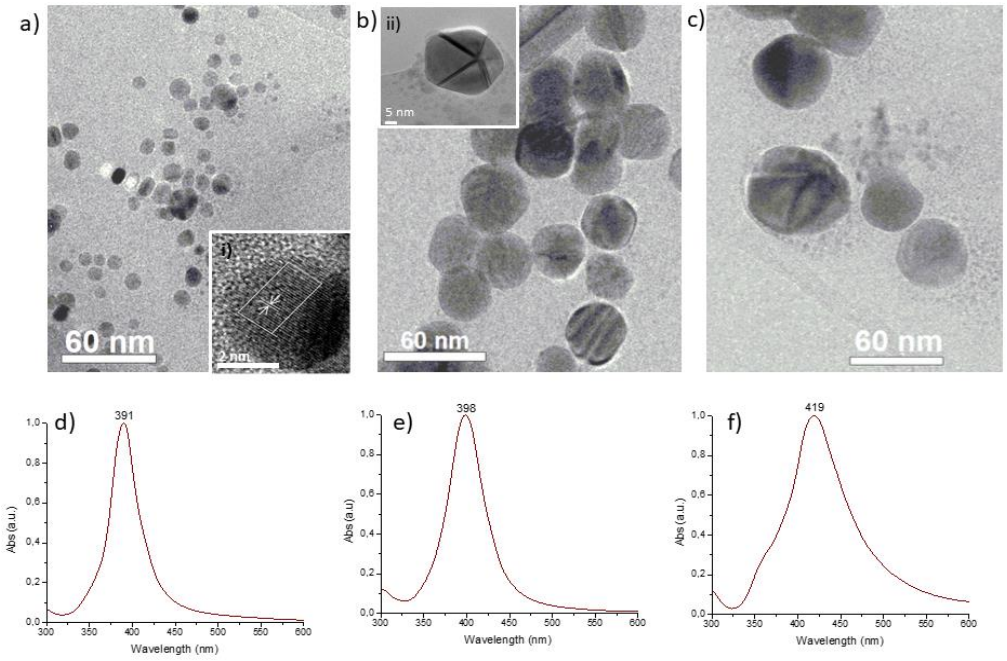

Figure 23: TEM and UV-VIS characterization of colloidal AgNPs.
a)-b)-c) TEM photograph of colloidal AgNPs (6, 30, 52) nm respectively. Insert i) High Resolution TEM image displaying the lattice fringes of a 6 nm nanoparticle. Insert ii) TEM image showing a particular pyramidal shape of a 30 nm nanoparticle. d)-e)-f) UV-VIS absorbance spectra of colloidal AgNPs (6, 30, 52) nm from left to right respectively, with the reference maximum absorbance peaks. Reprinted with permission from [228].

All the three sizes of AgNPs analysed by TEM revealed to be mainly spheroidal shaped and the measured average diameters corresponded to expectations (Figure 23a-c). Insert i) in Figure 23 shows the evaluation of the crystallinity degree performed by TEM and, in accordance with literature data on single crystalline AgNP [229], all the three kind of AgNPs displayed a *d-spacing* between the lattice fringes of 2.4 Å corresponding to the plane of silver. Larger AgNPs (30 nm and 52 nm), which were obtained from the growing of seeds, showed the presence of multiple-twinned crystalline planes in HRTEM images. Particularly, in insert ii) in Figure 23b a five-fold multiple twinned decahedron crystal, which could be due to the growth of silver, is visible. Indeed, the formation of multiple twinned particles is normally considered as an indicator of the formation of silver nuclei/particles which firstly undergo Ostwald ripening and then are transformed into larger silver nanoparticles completing the growth process [210, 230].

The size distribution, shape and above all the agglomeration state of the three kinds of AgNPs produced were analysed also by UV-VIS. In Figure 23d-e-f the extinction spectra with λ_{max} of the differently sized AgNPs are displayed. A red-shift from 391 nm to 417 nm of the Local Surface Plasmon Resonance (LSPR) peak is noticeable as the relative particle size increase from 6 nm to 52 nm [231]. The homogeneity of the size distribution and shape of all the three batches, in accordance with the TEM results, was confirmed by the single, narrow and symmetric absorption peaks.

To determine the linearity of the absorbance at their typical LSPR in water a calibration curve was built for each AgNPs size. As emerged from Figure 24 the resultant calibration curves were good for each of the three AgNPs size in a range of concentrations that includes the concentrations analysed in the bacterial experiments.

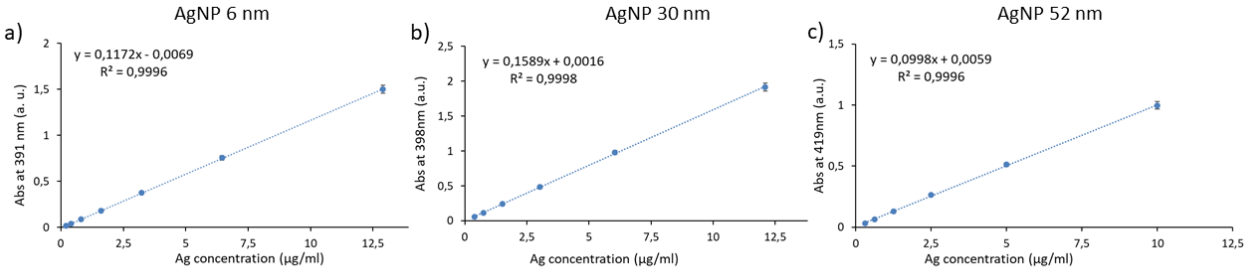

Figure 24: AgNPs calibration curves. Reprinted with permission from [228].

4.3.1 AgNPs MIC and MBC determination against *E. coli*

The MIC and MBC of the three different AgNPs was determined against *E. coli* ATCC 8739 by both broth dilution method (BDM) and viability assay following the standard procedures already adopted for the ciprofloxacin experiments [178]. The results are showed in Figure 25 and summarized in Table 7 and they are in good agreement with literature data of similar AgNPs with comparable sizes.

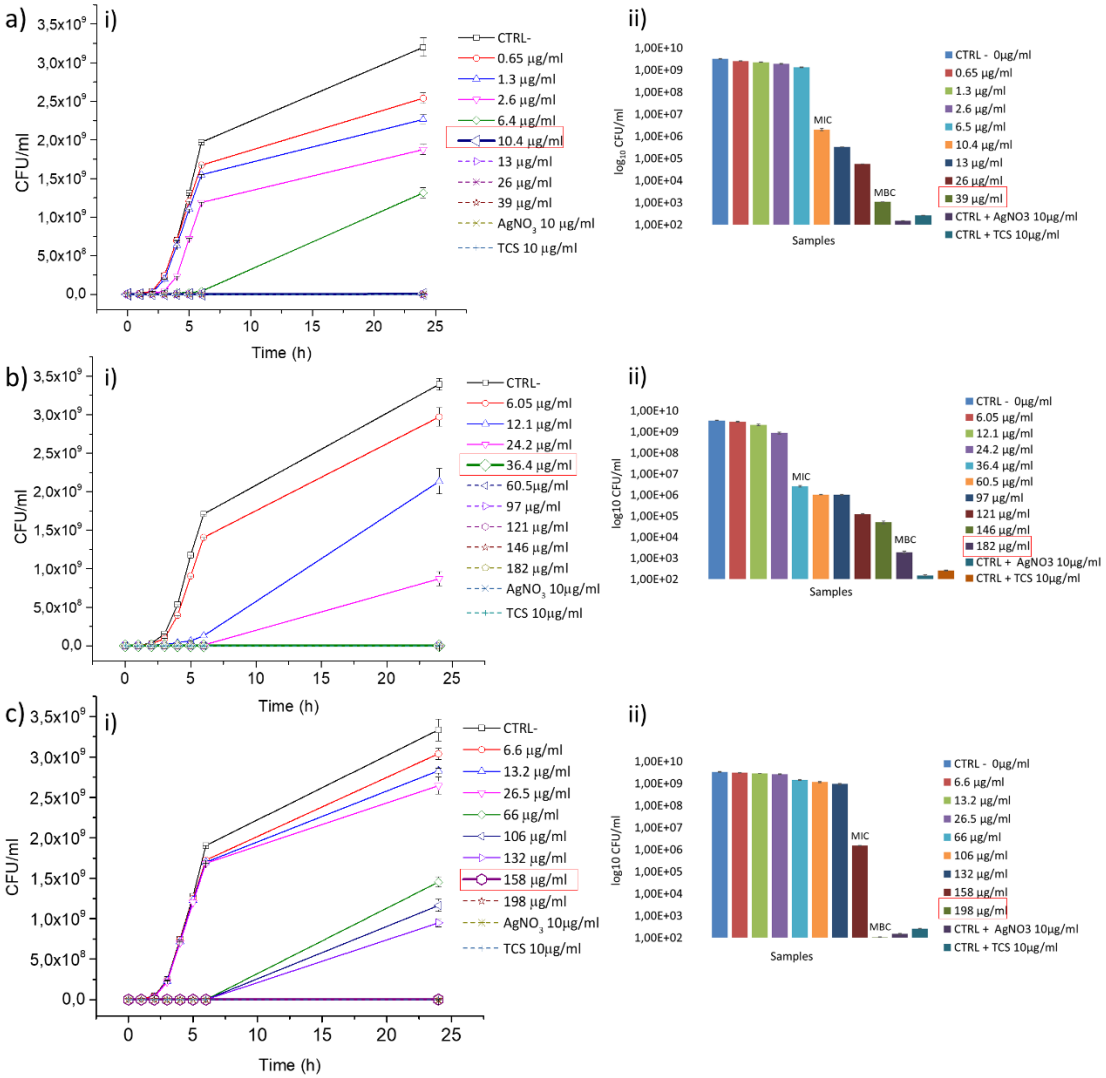

Figure 25: Colloidal AgNPs MIC and MBC determination towards *E. coli*. a) AgNPS 6 nm, b) AgNPS 30 nm and c) AgNPS 52 nm. Left panels i): BMD test results of AgNPs against *E. coli* ATCC 8739 the CFU/ml was calculated from the OD_{600} measured after 24 h of exposure and plotted against time. 10 µg/ml of TCS and $AgNO_3$ were used as positive controls. Red squares: MIC values. Right panels ii): histograms of *E. coli* ATCC 8739 viability assay. The AgNPs concentrations and the controls were the same used for the MIC. Red squares: MBC values. Reprinted with permission from [228].

Table 7: Bactericidal activity of colloidal AgNPs.

AgNPs nominal size (nm)	MIC (µg/ml)	Number of AgNPs at the MIC (NPS/ml)*	Surface area AgNPs at the MIC (nm^2/ml)*	MBC (µg/ml)	Number of AgNPs at the MBC (NPs/ml)*	Surface area AgNPs at the MBC (nm^2/ml)*
6	10.4	8.67×10^{12}	9.80×10^{14}	39	3.25×10^{13}	3.68×10^{15}
30	36.4	2.45×10^{11}	6.92×10^{14}	182	1.22×10^{12}	3.46×10^{15}
52	158	1.94×10^{11}	1.7×10^{15}	198	2.42×10^{11}	2.14×10^{15}

* The values were calculated assuming a spherical shape of the AgNPs using the formulas reported in the previous paragraph.

Furthermore, the highest antibacterial effect of smaller AgNPs was confirmed and even more evident in the plot showed in Figure 26, which supports that the AgNPs killing trend against *E. coli* after 24 h of exposure is strictly size-dependent, in particular the 6 nm AgNPs demonstrated a higher killing efficacy followed by the 30 nm and the 52 nm.

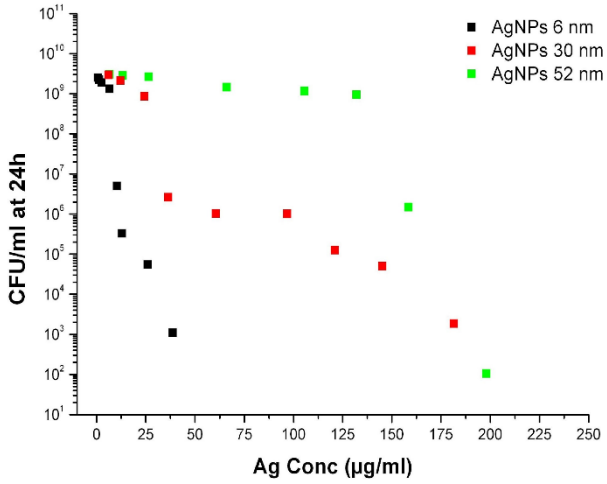

Figure 26: Comparison of the antibacterial effects of the three kinds of AgNPs in respect to the silver concentration.
E. coli CFU/ml after 24 h of incubation with the colloidal AgNPs 6 nm (black squares), 30 nm (red squares) and 52 nm (green squares) plotted against the silver concentrations used for the MIC and MBC experiments. Reprinted with permission from [228].

Moreover, their aggregation state was studied by monitoring the profile of the UV-VIS spectra at different concentrations of AgNPs both in water and in LB broth.

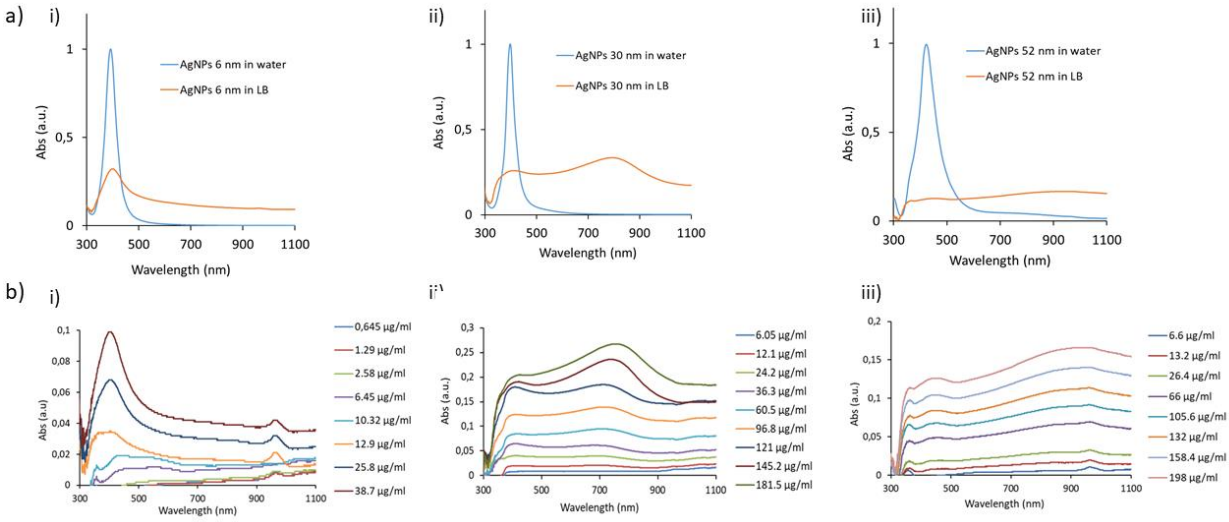

Figure 27: AgNPs aggregation study in bacterial culture medium.
a) Extinction spectra of colloidal AgNPs in water and in LB broth. From left to right: AgNPs i) 6 nm, ii) 30 nm, iii) 52 nm, respectively. b) Extinction spectra of different concentrations of colloidal AgNPs diluted in LB broth. From left to right: AgNPs i) 6 nm, ii) 30 nm, iii) 52 nm. Reprinted with permission from [228].

It emerged that AgNPs aggregation phenomena are really evident when they are suspended in bacterial culture medium in respect to the water, and they increase proportionally with the size and the concentration of the nanoparticles. This is sustained by the formation of broad plasmonic bands in the spectral region between (450–800) nm (Figure 27). These results support the hypothesis that the killing efficacy associated with the smaller NPs could be mostly reduced by their agglomeration, while bigger AgNPs displayed a comparable bactericidal effect due to their higher silver content, as showed in the plot in Figure 26. It could possible that above a certain concentration even the smallest AgNPs are no longer capable of penetrating in bacterial cells because they are stuck together. Consequently, the formation of agglomerate that become bigger together with the increasing of the AgNPs concentration in the liquid medium, the exposed surface areas become nearly the same for each of the three sizes. This could lead to a predomination of the Ag^+ ions release and direct contact, as main bactericidal effects, which led to a flattening of the sizes-related differences. Furthermore,

since the AgNPs were suspended in LB, a complex medium rich in salts and proteins, the availability of silver ions can be affected by their presence. That together with the occurring agglomeration events, might negatively influence their antibacterial activity [217, 232, 233, 234].

Thus, in order to avoid all these negative occurrences and better elucidate the bactericidal activity of the AgNPs in respect to their size, they were anchored forming monolayers on amino-silanized glass surfaces.

4.3.2 Preparation and characterization of AgNPs-modified glasses

Metallic nanoparticles can be immobilized on glass surfaces by silanizing them with amino-groups as previously reported [220, 235]. The glasses prepared by cutting commercial microscope glass slides (as described in material and methods paragraph) were functionalized with different coverage percentages of AgNPs by changing the NPs concentration and/or the incubation time. Firstly, the immobilization of the different sized AgNPs on the amino-modified glasses was characterized by UV-VIS and SEM to evaluate the surface coverage over time (Figure 28).

In Figure 28 four representative amino-modified glasses exposed to AgNPs for different time spans are shown. It is easy to notice that the yellow colour of the AgNPs-modified surfaces darkened together with the increasing of the exposure time which is ascribable to a higher percentage of surface coverage (Figure 28a). This is further proved by the UV-VIS results (Figure 28b), indeed a progressive increase of the intensity of the extinction which is correlated with the increasing of the time of incubation was observed especially for the AgNPs 30 nm and 52 nm. Furthermore, as the time of exposure increased a broad band centred at (600–800) nm appeared for both the bigger sized nanoparticles. This signal is linked to the plasmonic coupling of proximal AgNPs and thus to the formation of aggregates on the surface. This was confirmed also by SEM analysis of these glasses (Figure 28c), it was observed that at lower exposure times (1 h and 2 h), all AgNPs were well separated with only few nanoclusters of three to six nanoparticles visible on the surfaces, confirming the single LSPR signal in the extinction spectra at the corresponding time spans.

The immobilization protocols were optimized for each size of AgNPs by changing the exposure time in order to find the optimal conditions to produce a homogeneous and stable monolayer together with a maximized surface coverage.

As showed in Figure 28b lower incubation times were required for smaller AgNPs to reach their highest surface coverage.

For the glasses functionalized with AgNPs 30 nm and 52 nm the average percentage of covered area was calculated from five SEM images per incubation time using the software ImageJ. The images were converted to binary and the areas occupied by AgNPs were measured. The results are summarized in Tables 8 and 9. The highest coverage rate was calculated and revealed to be around 25-30% for both the two sizes. From the comparison between SEM and UV-VIS measurements it resulted that the optimal surface coverage for 30 nm AgNPs was obtained after 30 min of incubation, while AgNPs 52 nm required almost 1 h. Longer exposure times only increase the formation of aggregates on the surface without really changing their coverage. As regards AgNPs 6 nm, they were too small to reach the resolution limit of SEM, thus the evaluation of the surface coverage rate was only conducted by UV-VIS analysis and it resulted that the maximum coverage rate was reached already after 15 minutes, since the spectra were almost overlapped for longer times (Figure 28b plot i).

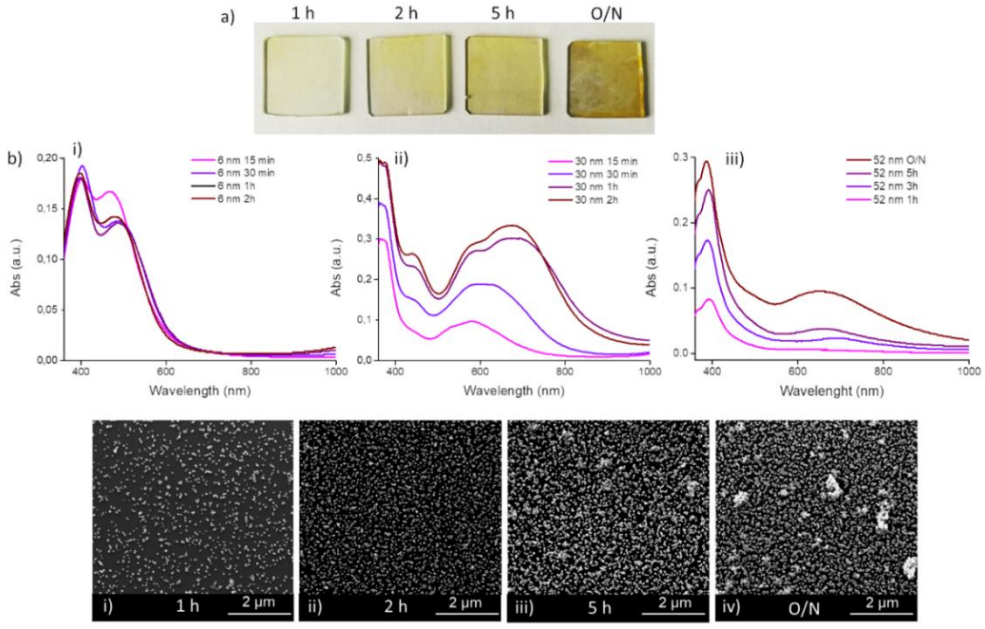

Figure 28: Characterization of AgNPs -modified glasses by UV-VIS and SEM. a) Images amino-modified glasses incubated with AgNPs 52 nm at a concentration of 59.3 µg/ml for four different time spans (1 h, 3 h, 5 h, O/N from left to right respectively) b) UV-VIS absorbance spectra four representative functionalised glasses with AgNPs i) 6 nm, ii) 30 nm, iii) 52 nm for four different exposure times. c) SEM images of the glasses described in a). Reprinted with permission from [228].

Table 8: Calculated percentage of glasses surface coverage for AgNPs 30 nm.

AgNPs	Time of incubation	Covered area%	Standard deviation	Observations
30 nm	15 min	19.9	1.7	
	30 min	26.5	3.9	
	1 h	30.0	2.6	Aggregates

Table 9: Calculated percentage of glasses surface coverage for AgNPs 52 nm.

AgNPs	Time of incubation	Covered area%	Standard deviation	Observations
52 nm	1 h	13.9	2.6	
	3 h	29.2	5.8	Small aggregates
	5 h	32.3	5.3	More aggregates
	O/N	37.0	5.6	More aggregates

4.3.3 Antibacterial properties of AgNPs-modified glasses

ISO 22196:2011 method was employed to test the antibacterial properties of AgNPs-modified glasses produced as previously described. This procedure is a standard and reliable method widely adopted for measuring the antibacterial activity of daily goods [88] and to facilitate the measurements comparison between different materials and laboratories. However, some critical environmental and physiological factors can have some impact on the outcome of the microbiological results, as reported in the work of Wiegand et al. [90], in this thesis every change from the standard protocol is specified. For instance, to better appreciate the difference between differently covered surfaces, the incubation time of bacteria with active glasses was reduced to 5 h since after 24 h all the tested substrates reached a bacterial killing rate of 99.9999% with almost no

bacterial colony present on the agar plates, thus all resulting in R values ≥ 5. The R value represent the decimal logarithmic reduction rate of viable bacteria, thus an active surface that reaches an R > 4 is considered an optimum antibacterial material.

The antibacterial properties based on the different AgNPs sizes and the SMBC of silver value were established for each kind of AgNPs-modified glasses, preparing a wide series of samples differently covered using progressive dilutions of the starting AgNPs suspensions concentration and exposing them to these suspensions for different time spans (Figure 29). A first evaluation of the glasses silver coverage was performed by UV-VIS analysis of the glasses (Figure 29 i). Then, their antibacterial activity was quantified using the following formula:

Equation 5: $R = (U_t - U_0) - (A_t - U_0) = U_t - A_t$

where U_t is the average of the common logarithm of the number of viable bacteria (cells/cm^2), recovered from the untreated test specimens after 5 h; U_0 is the average of the common logarithm of the number of viable bacteria (cells/cm^2), recovered from the untreated test specimens immediately after inoculation; At is the average of the common logarithm of the number of viable bacteria (cells/cm^2), recovered from the treated test specimens after 5 h.

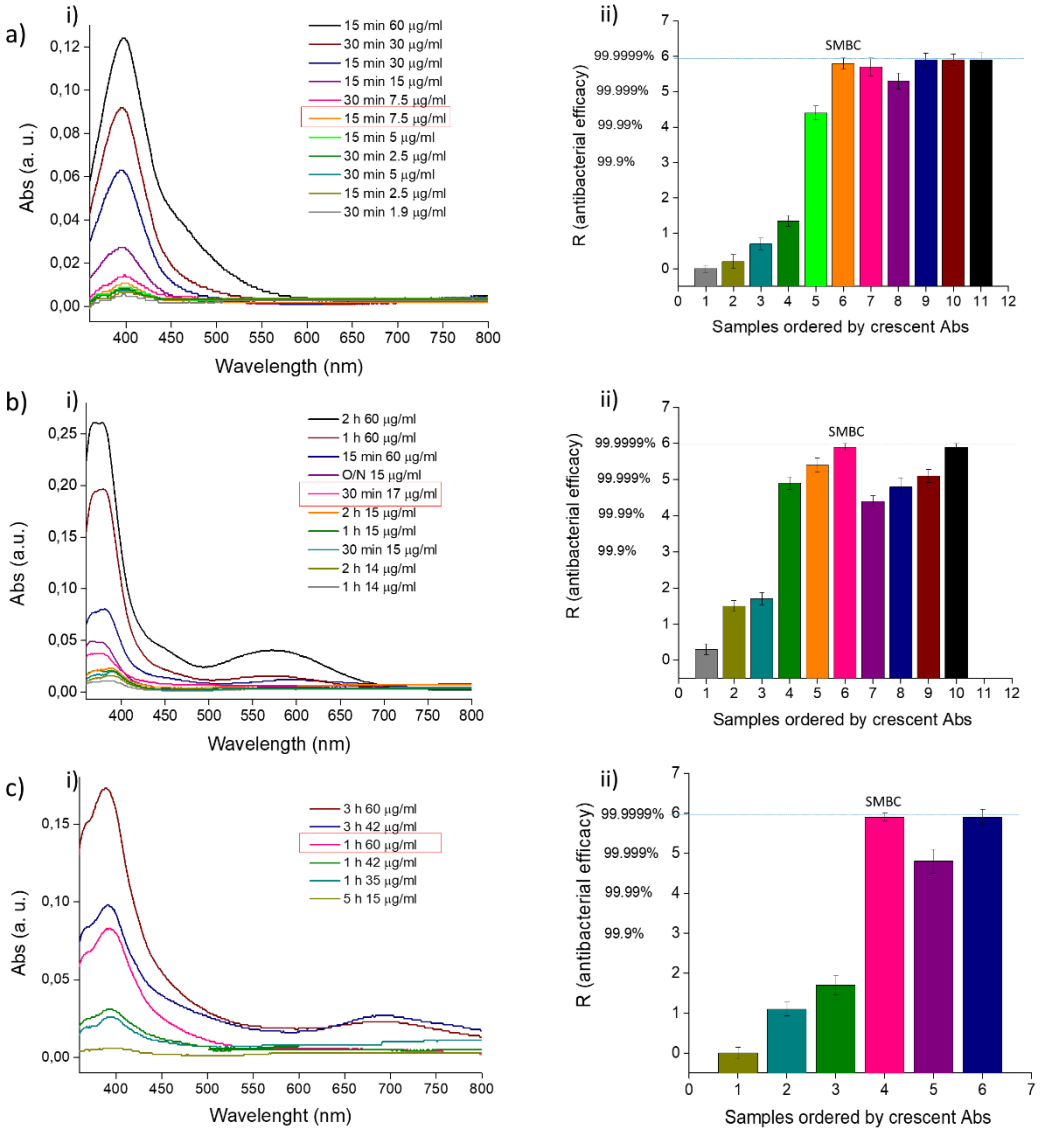

Figure 29: UV-VIS and antibacterial characterization of AgNPs-modified glasses. Characterization of glasses functionalized with AgNPs a) 6 nm, b) 30 nm and c) 52 nm, respectively. Left plots i): UV-VIS extinction spectra of glasses functionalized with different concentrations of AgNPs incubated for different time spans. Right histograms ii): graphical representation of calculated R values of glasses analysed by UV-VIS ordered by crescent absorbance.

In Figure 29 the proportionality between the antibacterial efficacy and the AgNPs coverage is appreciable, with an increasing trend between the extinction intensity of the UV-VIS spectra and the calculated R value. It resulted that when a certain value of AgNPs coverage was reached, the R value touched its maximum (around 5.9) and do not rose any further. At this point a bacterial killing ≥ 99.9999% was obtained and was taken as the SMBC (Figure 29 ii). These values were obtained from glasses exposed for 15 min to 7.5 μg/ml of AgNPs 6 nm (R = 5.8), for 30 min to 17 μg/ml AgNPs 30 nm (R = 5.9) and for 1 hour to 60 μg/ml of 52 nm AgNPs (R = 5.8).

The amount of silver present on the surface of these three selected active glasses was quantified by ICP-MS and resulted to be (0.023 ± 0.004) μg/cm^2 AgNPs 6 nm, (0.026 ± 0.002) μg/cm^2 AgNPs 30 nm, and (0.034 ± 0.007) μg/cm^2 AgNPs 52 nm, respectively. However, Pallavicini et al., [236, 237] already published an analysis of the antibacterial efficacy of similar AgNPs-modified glasses against *E. coli* ATCC 10356, which resulted to be nearly the same of that we have obtained but they employed an amount of silver on the surfaces which was at least fifteen times higher than the calculated SMBC for 6 nm AgNPs explained in this work. Therefore, it emerged that the knowledge of the SMBC plays an essential role in reducing the amount of silver needed for a relevant antibacterial efficacy to its minimum. Furthermore, a comparison between the antibacterial properties of immobilized and colloidal AgNPs was made converting the MBC values reported in Table 7 in μg/cm^2 by considering the hypothetical experiment in which 0.1 ml of dispersed AgNPs and 1 × 10^6 CFU/ml of *E. coli* were placed on the top of a non-functionalized glass. Indeed, 0.1 ml represent the volume of the inoculum used for the SMBC experiments. All these results are summarized in Table 10 and 11.

Table 10: ICP-MS calculation of anchored AgNPs MBC.

AgNPs size (nm)	MBC (μg/cm^2)*	Number of AgNPs at the MBC in 0.1 ml	Surface area AgNPs at the MBC (nm^2)	SMBC (μg/cm^2)	Number of AgNPs at the SMBC	Surface area AgNPs at the Surface MBC (nm^2)
6 ± 3	0.96	3.25 × 10^{12}	3.68 × 10^{15}	0.023	7.73 × 10^{10}	8.74 × 10^{12}
30 ± 6	4.5	1.22 × 10^{11}	3.46 × 10^{15}	0.026	7.02 × 10^{8}	1.98 × 10^{12}
52 ± 7	4.7	2.42 × 10^{10}	2.14 × 10^{15}	0.034	1.66 × 10^{8}	1.47 × 10^{12}

* The values were calculated using the formulas reported in the text

Table 11: Comparison between MBC and SMBC.

AgNP nominal size (nm)	N° at the MBC (NPs/ml)	mass single AgNP (μg)	N° AgNPs in 0.1 ml*	Total mass AgNPs in 0.1 ml (μg)*	Coverfilm area (cm^2)	MBC* (μg/cm^2)	SMBC (μg/cm^2)
6	3.25×10^{13}	1.187×10^{-12}	3.25×10^{12}	3.86	4	0.96	0.023
30	1.22×10^{12}	1.484×10^{-10}	1.22×10^{11}	18.1	4	4.5	0.026
52	2.42×10^{11}	7.726×10^{-10}	2.42×10^{10}	18.7	4	4.7	0.034

* The values were calculated assuming a spherical shape of the AgNPs using the formulas reported in the text.

Equation 6: Number of NPs in 0.1 ml = N° NPs at the MBC (NPs/ml) /0.1 ml

Equation 7: Total mass NPs in 0.1 ml = N° NPs in 0.1 ml × mass single NP (μg)

Equation 8: MBC (μg/cm^2) = Total mass NPs in 0.1 ml (μg) / coverfilm area (cm^2)

Once more, smaller AgNPs demonstrated greater bactericidal properties which decreased progressively with the increasing of the size, confirming the observations for suspended AgNPs. However, the ratio of the MBC values reported for the two forms of AgNPs (colloidal or anchored) are quite different. Indeed, the MBC value found for colloidal AgNPs 6 nm was almost five times lower than that reported for 30 nm and 52 nm, respectively. Although this difference resulted greatly reduced considering immobilized AgNPs that demonstrated a statistically significant difference ($p < 0.05$) among the SMBC in respect of the 52 nm AgNPs, while almost no difference was evident between AgNPs 6 nm and 30 nm. This could be driven by a reduction of the ability of smaller AgNPs to penetrate inside the bacterial cells since they are anchored to the glass surface, even if the number of 6 nm AgNPs and their exposed surface area remains higher than the 30 nm and 52 nm AgNPs (Table 10).

In addition, comparing the founded MBC and SMBC it resulted that the SMBC are almost two to three orders of magnitude lower than the corresponding values of MBC derived from tests on colloidal AgNPs. These findings suggested that the immobilization of the AgNPs greatly enhances their bactericidal effects since their aggregation is prevented their contact with bacteria is maximized. This is supported by previous studies conducted by Aghinotri group on citrate capped AgNPs (8.6 ± 1.2) nm seized. Indeed, they demonstrated that those AgNPs showed higher bactericidal activity when anchored on glass in respect to the same

colloidal AgNPs [235]. Furthermore, the enhancement of the antibacterial activity of immobilized AgNPs in respect to the suspensions led by the reduction of the aggregation phenomena, which normally occur in liquid media, could maximize the AgNPs exposed specific superficial area to bacteria as well as augmenting the Ag^+ ions release. Moreover, the reduction of the bactericidal properties differences between the sizes observed for immobilized might be desirably to reduce cytotoxicity related to smaller NPs [88].

4.4 *S. aureus* and *E. coli* interaction study with AMP loaded carbon nanoparticles

The CNP used for this work were synthetized and characterized by the chemical department of the University of Turin and presented a spherical shape, a mostly amorphous carbon composition, a high stability in aqueous media, and a negatively charged surface.

Two batches of CNP were selected, which presented two different hydrodynamic diameters distributions one smaller, with a mean diameter of 132 nm, called here CNP-S, and one bigger with a mean diameter of 243 nm, called here CNP-L (Figure 30). Both CNP-S and CNP-L showed to be monodispersed (PDI = 0.1) and with a narrow size range.

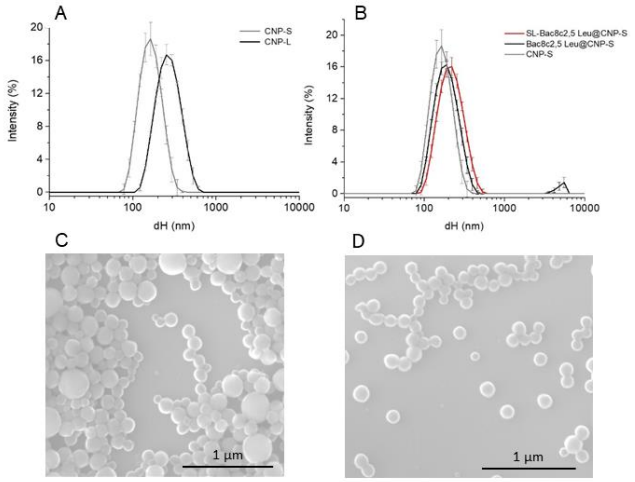

Figure 30: Size distribution characterization of CNP-S and CNP-L.
A) Hydrodynamic diameter distribution of CNP-S and CNP-L measured by DLS; B) Hydrodynamic diameter distribution changes following functionalization of CNP-S with Bac8c^{2,5Leu} or SL-Bac8c^{2,5Leu}. Hydrodynamic diameters (dH) distribution (% intensity) is expressed as mean value of 3 measurements ± SD. C-D) Representative SEM image of CNP-L and CNP-S respectively.

The interaction of *S. aureus* SH1000 and *E. coli* MG1655 with three different concentrations (53.3, 26.7, 13.3) µg/ml of both CNP-S and CNP-L over time was firstly evaluated by performing a kinetic assay in PBS, as a less complex culture medium. The vitality of bacteria at three different time points from the inoculation (0, 24, 48) h was determined. The viability assay is a method commonly applied as standard for the evaluation of possible bactericidal effects induced by the presence of nanoparticles dynamically over time [238]. In this case PBS was chosen instead of MH broth as bacterial growth medium to obtain a simpler, repeatable and more controlled system and to avoid the insurgence of aggregation phenomena due to the presence of nutrients and salts.

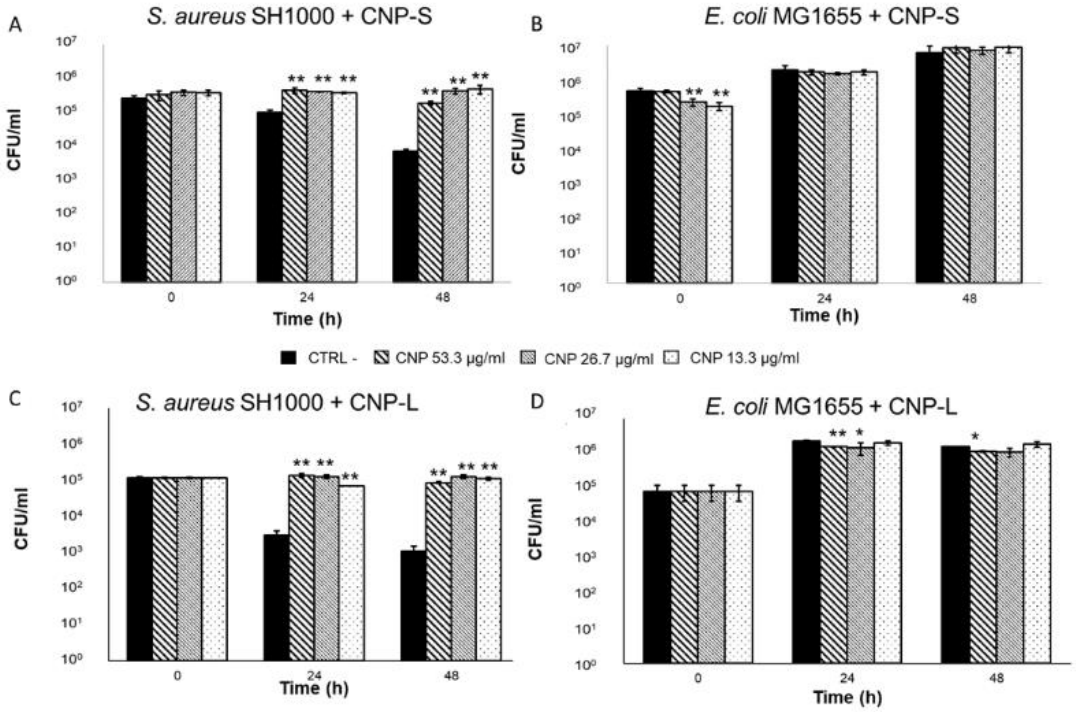

Figure 31: viability assay of *S. aureus* and *E. coli* exposed to CNP-S and CNP-L. Vitality of: left panels: *S. aureus* SH1000 and right panels: *E. coli* MG1655 exposed for 0 h, 24 h and 48 h to CNP-S (A, B) and CNP-L (C-D) in PBS. A CTRL– without CNP was included. Both the CNP were tested against the two bacteria at three concentrations (53.3, 26.7, 13.3) µg/ml. Each experiment was replicated three independent times. * *p-value* < 0.05; ** *p-value* < 0.01

As shown in Figure 31 it emerged that both the differently sized CNP demonstrated to have similar effects on the two bacterial strains. In particular, *S. aureus* vitality (left panels), if the bacterium was grown in PBS instead of a complex culture medium, decreased over time (CTRL–), that is possibly due to the lack of nutrients. It is evident that both CNP-S and CNP-L did not demonstrate any particular bactericidal effects, against *S. aureus*. On the contrary they seem to maintain the bacterial vitality similar to that of the inoculum suggesting that CNP might be used by Gram + bacteria as a carbon and energy source. Indeed, although no data were found in literature on the possible degradation of CNP by *S. aureus*, few works report the capability of some bacteria to degrade other carbon nanomaterials [239, 240, 241]

On the other hand, *E. coli* (Figure 31, right panels) did not seem to suffer for the lack of nutrients in the medium. However, a statistical significant decrease of the bacterial vitality was evidenced, in comparison with the CTRL–, for higher CNP concentrations at shorter times of exposition, albeit this effect seems to diminish for longer times for both the two sizes of CNP.

The low bactericidal activity observed for these CNP was in line with the expectations since they are spherical shaped and present a smoothed, negatively charged and highly hydrophilic surface. Conversely, other carbon-based nanomaterials which demonstrated high bactericidal effects such as CNTs [242] or graphene or graphene oxide (GO) [243] exploit their action by extracting phospholipids from the bacterial membranes inducing cell death, a property that is strictly related to their needle/sheet-or needle-like shape [244].

4.4.1 Study of the interaction of CNP-L with *S. aureus* and *E. coli*

To further investigate the CNP-bacteria interaction DEP-Raman spectroscopy and SEM techniques were adopted.

Even if, as said before, these NPs are mainly composed by elemental carbon in the amorphous form, they exhibit graphite patches, visible using Raman spectroscopy [79]. Therefore, this technique results very suitable to rapidly and directly detect and characterize interactions between bacteria and CNP especially using the DEP-Raman setup explained in the first part of this thesis, without the need of any particular sample processing. In Figure 32 the Raman fingerprints of the two bacteria, of PBS and of a suspension of CNP-L in water are showed. Since the viability assays showed before demonstrated that the behaviour of

bacterial growth didn't change between the two different sizes of CNP only CNP-L were considered for these interaction analysis.

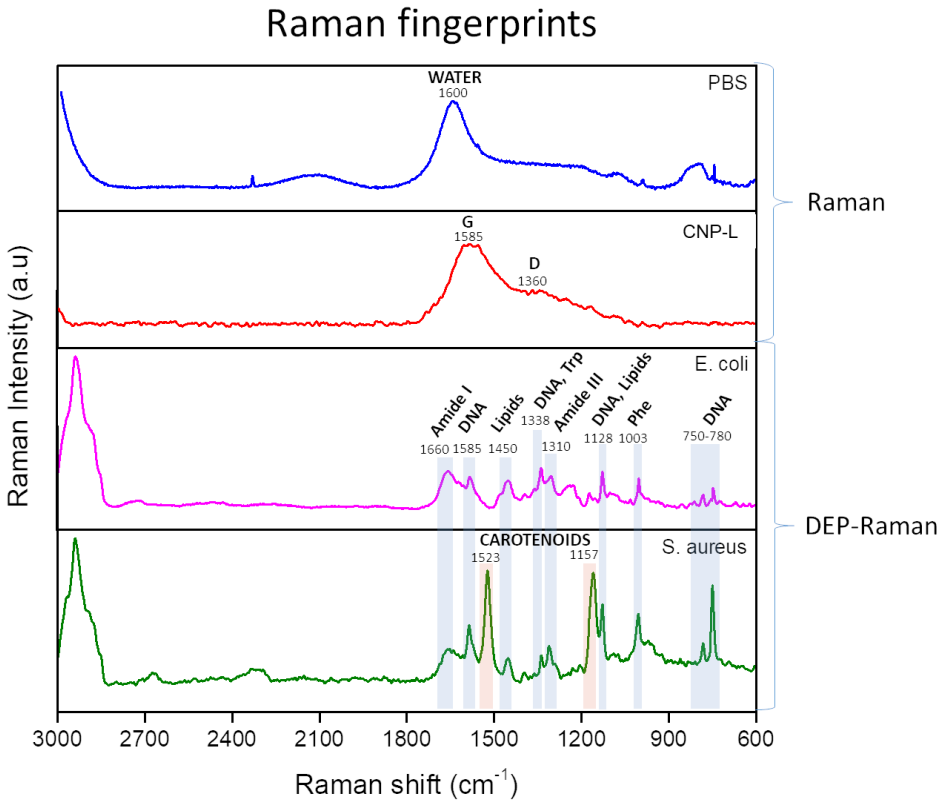

Figure 32: Raman fingerprints of PBS, CNP-L, and the two selected bacteria From the top to the bottom: Raman spectra of phosphate buffered saline solution; CNP-L; *E. coli* MG1655 and; *S. aureus* SH1000 with relative bands assignment.

From figure 32 it is evident that the spectrum of PBS presented the vibrational band of water at 1600 cm^{-1} as dominant Raman signal. On the other hand, CNP-L exhibited the typical G and D bands proper of the graphite (1585 cm^{-1} and 1360 cm^{1}) [74]. The band were broad, and with a low G/D intensity ratio confirming a preponderant amorphous carbon atomic structure.

The Raman spectra of bacteria showed the typical signals referred to bacterial cells structures and the chemical assignment referred to Table 4.

Then, *S. aureus* and *E. coli* were analysed by DEP-Raman immediately after the addition of the highest concentration of CNP-L (53.3 µg/ml) or after 24 h of exposition (Figure 33A, B and 33C, D respectively). As expected the Raman spectra of the two bacterial samples without CNP showed no differences at the

two time points because in the considered range only the vibrational signal of water is visible (Figure 33 yellow and green lines).

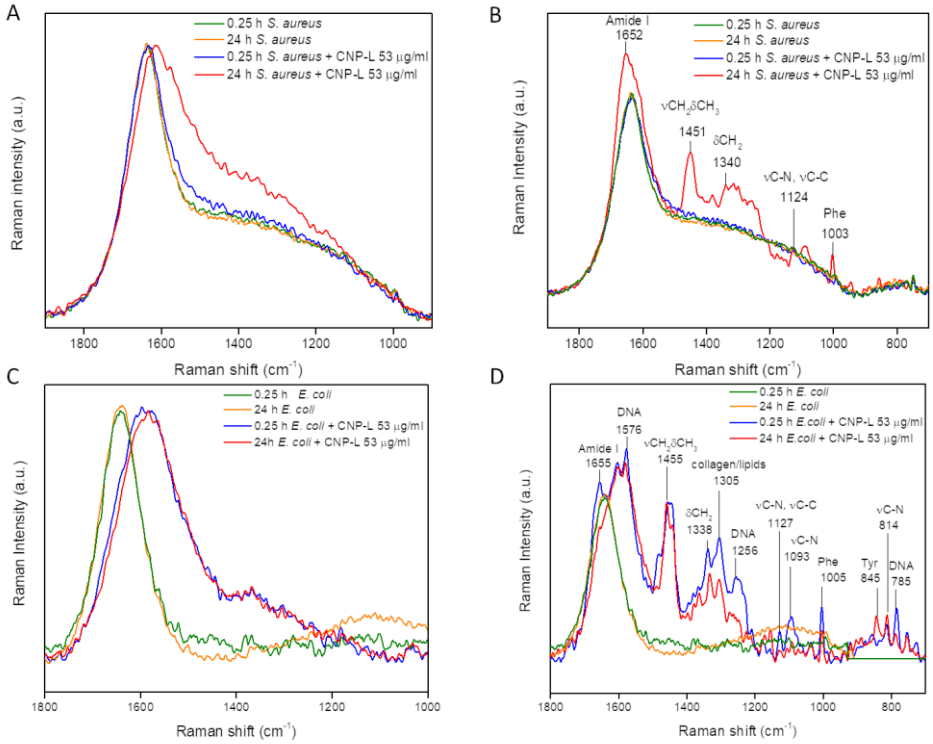

Figure 33: DEP-Raman analysis of the interaction of CNP-L with *S. aureus* and *E. coli*.

DEP-Raman spectra of A,B) *S. aureus* SH1000 and C,D) *E. coli* MG1655 in the absence or presence of CNP-L (53 µg/ml) immediately and after 24 hours from the addition of CNP. For each bacterial sample two different signals were recorded focalising the Raman microscope in different regions of the same sample: i) Raman signal of CNP (panel A red line and C red and blue lines); ii) Raman signal of ECM is visible in both the bacteria (left panels). Each line represents the normalized average of three Raman spectra recorded during three independent experiments..

On the other hand, after 24 h of exposition to the CNP the Raman spectra of both the bacteria presented signals which are ascribable to extracellular matrix (ECM) components [245] (Figure 33B, D red lines). In particular, *E. coli* (Figure 33D) showed the presence of these signals already immediately after the addition of the CNP, indicating a faster interaction between this kind of bacterium and the CNP than what observed for *S. aureus*. To investigate if the production of the

ECM matrix was promoted by the presence of the CNP, Raman spectra were recorded in area in which the ECM signals were not visible (Figure 33A, C).

If only the Raman signals of the CNP are considered, it resulted that for *S. aureus*, after 24 h of exposition, an increase of the band intensity in the 1600-1200 cm^{-1} region, corresponding to the summation of the G and D bands, was observed. Since bacteria were precipitated and washed before each DEP-Raman measurements, all the CNP present in suspension in the media were eliminated, so the presence of this signal is an evidence of the association between bacteria and CNP. In fact, even if a small moiety of free CNP was still present in the samples, negative dielectrophoresis (nDEP) forces employed for these analysis act selectively on the bacterial cells, this resulted in the agglomeration in the analysis volume only of bacterial cells and what is strictly attached to them, either bound to the bacterial walls or internalized, and not of free CNP. This claim was furtherly sustained by the fact that no carbon signal was observed with the voltage turned off. From figure 33 D it results evident that also in this case, for *E. coli* the interaction with the CNP occurs earlier than what observed for *S. aureus*, as this signal is visible already at time 0 h, supporting the results observed for the formation of ECM.

To further analyse the physical interaction of CNP-L with both the bacteria, SEM analysis was performed on the same samples measured by DEP-Raman (Figure 34). Since *S. aureus* cells exhibit a spherical shape similar to that of CNP-L, and also a very similar composition, mostly carbon-based, it resulted difficult to distinguish them from the CNP. This issue which was overcame considering the size of bacterial cells which is almost three time bigger than that of the CNP-L (red circles).

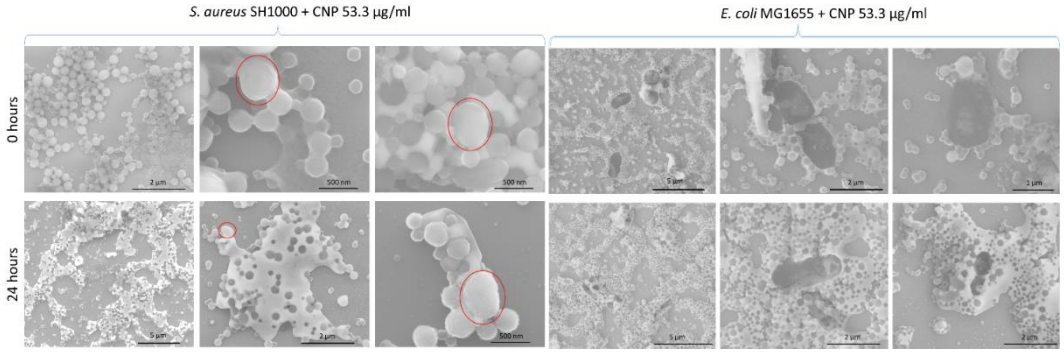

Figure 34: SEM analysis of the interaction of CNP-L with *S. aureus* and *E. coli*. Representative SEM images of *S. aureus* SH1000 (left) and *E. coli* MG1655 (right) after 0 h (top) and 24 h (bottom) of exposition to 53.3 µg/ml of CNP-L. The red circles indicate the bacterial cells of *S. aureus* SH1000.

Also this kind of analysis evinced that the formation of large amount of extracellular matrix around both CNP and bacteria is visible for both the strains especially after 24 h of exposition to the CNP. This phenomenon is even more evident for E. coli, confirming what already observed with Raman measurements confirming the fast interaction between bacteria and CNP which drives bacteria to produce the ECM, which is enhanced over time.

In general, the results of these measurements showed the ability of CNP to interact with both Gram + and Gram – bacteria, albeit with a different rate of association. Even if a possible uptake of the CNP by the bacterial cells was not possible to be detected with these techniques, the strong interaction between CNP and bacterial cells suggests the possibility of transporting bactericidal compounds strictly near the cells loading them to the CNP surfaces. This idea renders particularly suitable the CNP-S because their higher exposed surface area can allow a higher loading. Furthermore, since the viability assay demonstrated that CNP-L and CNP-S exhibited similar activity toward the two bacteria, CNP-S can be used on the basis of the interaction analysis observed for the CNP-L.

Therefore, in this thesis, the bactericidal efficacy of the cationic bactenecin-derived peptide Bac8c^{2,5Leu} was tested against both the bacterial strains as a Gram + and Gram – models and then was physically adsorbed by electrostatic interaction on the CNP-S surface to form a Bac8c^{2,5Leu}@CNP-S nanosystem.

Indeed, recent studies had demonstrated the wide range of advantages of peptide-based drugs like their ability of killing bacteria and other microorganisms resistant to common antibiotics [223] and more specifically of cationic antimicrobial peptides (AMPs), characterized by a net positive charge and a high proportion of hydrophobic residues which give them amphipathic properties [246]. Furthermore they demonstrated to be less linked to bacterial resistances insurgence thanks to their high efficacy, rapid, broad and synergic mode of action toward bacteria, fungi and viruses, as compared with other antimicrobial compounds [247], thus they have been proposed as a valid alternative to conventional antibiotics.

However, since AMPs' antimicrobial effects *in vivo* are often reduced due to their degradation by proteases or to low pH environments, i.e. stomach, its loading onto CNP surface could overcome these issues providing enhanced antimicrobial efficacy and selectivity, lower cytotoxicity and extended biostability [248, 249]. Moreover, this novel nanosystem could be promising as a drug delivery system considering to include sustained drug release, improving the bioavailability and biodistribution of the treatment.

4.4.2 In vitro antibacterial efficacy of Bac8c^{2,5Leu}@CNP-S

The kinetic of the interaction between the Bac8c^{2,5Leu}@CNP-S system at three different concentrations (53.3, 26.7, 13.3) µg/ml of loaded CNP-S) and the two bacterial strains of *E. coli* and *S. aureus* was evaluated over 24 h and compared with the free Bac8c^{2,5Leu} at the same concentrations loaded on the CNP at concentrations of (16, 8, 4) µg/ml (Figure 35). The effects of the CNP-S alone on the two bacteria were represented as well to better appreciate the differences between the three systems (CNP, AMP and AMP@CNP).

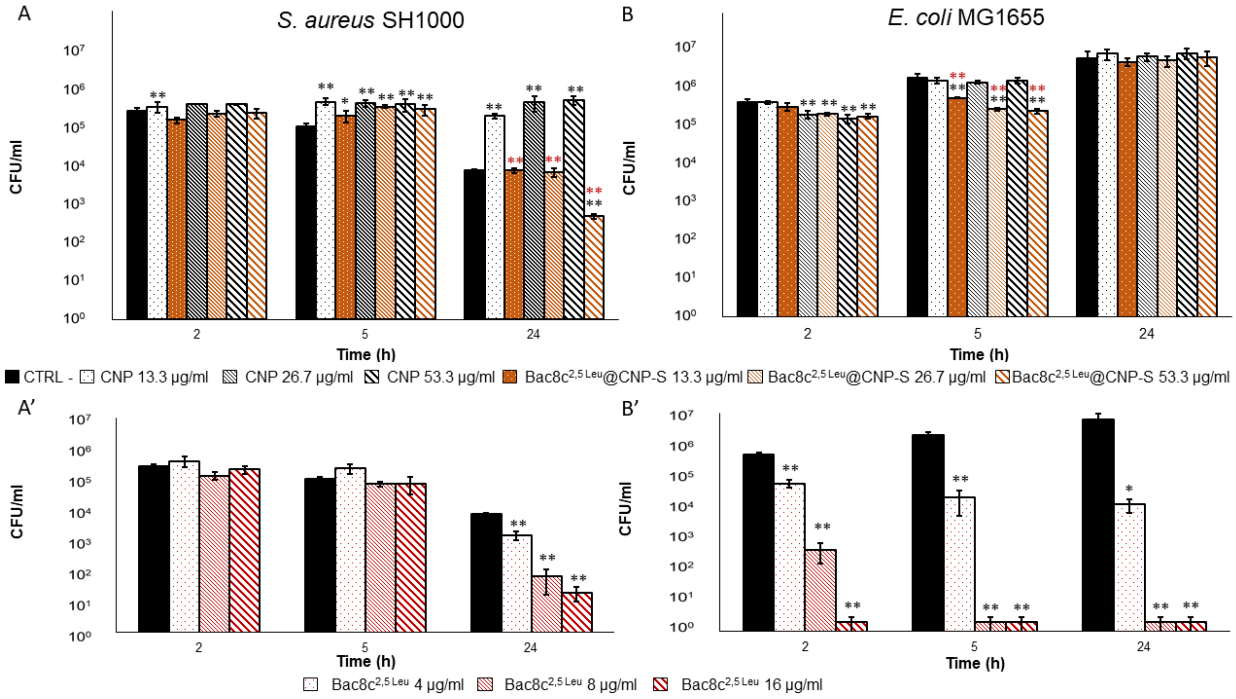

Figure 35: Activity of Bac8c^{2,5Leu} and Bac8c^{2,5Leu}@CNP-S against *S. aureus* and *E.coli*.

Left graphs are referred to *S. aureus* SH1000 and right graphs to *E. coli* MG1655. Upper panels: Effects of CNP (black) or Bac8c$^{2,5\ Leu}$@CNP-S (orange) at the concentrations of (53.3, 26.7, 13.3) µg/ml on (A) *S. aureus* and (B) *E. coli* viability after 2 h, 5 h and 24 h of exposition. Lower panels: effect of free Bac8c^{2,5Leu} (red) on A') *S. aureus* and B') *E. coli*. * *p-value* < 0.05; ** *p-value* < 0.01. red stars: comparison with bacteria treated with the same concentration of CNP-S, black stars: comparison with the CTRL–.

Aliquots of each sample were analysed after (2, 5 and 24) h from the inoculum performing a viability assay counting the CFU after each time point and comparing them with negative controls consisting of the selected bacterial strain grown in PBS only. The statistical significance of the difference between the colonies counted for each sample and the controls and between the CNP-S only and the nanosystem were evaluated performing a *t-test*.

These assays evinced once more that *S. aureus* showed a significant maintenance of the viability, in comparison with the CTRL–, since after 5 h of exposure to CNP-S. On the other hand, *E. coli* displayed a significant decrease of vitality already after 2 h at the highest CNP concentration that, as already seen previously, is lost over time, confirming a rapid interaction of the two bacteria with CNP which although leads to different effects.

Considering the Bac8c^{2,5Leu}@CNP-S system, for *S. aureus* it caused a significant reduction of vitality ($p < 0.01$) after 24 h from the inoculum at the highest concentration (Figure 35A). As concern *E. coli*, it did not show any particular bactericidal effect except from a very small reduction of bacterial growth after shorter time of exposition to the system at the highest concentrations (Figure 35B).

As regards the free peptide, tested at the same three concentrations loaded onto the CNP-S surface, (Figure 35B'), a significant ($p < 0.01$) reduction of bacterial viability (almost 3 log) by 99.9% in comparison with the CTRL– was detected for *E. coli* already after 2 hours from the inoculum for the highest concentration of Bac8c^{2,5Leu} (16 µg/ml) which become of 99.9999% after 24 hours. Furthermore, *E.coli* growth was significantly reduced by 90% also by the lowest AMP concentration (4 µg/ml). On the other hand, *S. aureus* showed a significant ($p < 0.01$) reduction of viability only after 24 hours for all the three concentrations tested (1 log for the lowest and more than 2 log for the highest).

These observed differences in the bactericidal behaviour of the free AMP against the two bacteria could be due to different reasons. First of all, as Bac8c^{2,5Leu} is positively charged, it is expected to target the negatively charged outer membrane of bacterial cell, with a lower efficiency toward Gram – due to the complexity of their surface organization in comparison with Gram + [250]. However, in literature examples of AMPs having high affinity for the negatively charged LPS, which are present in large amounts in the outer membrane of Gram – bacteria, are present [251]. For example, the group of Wu [251] explained the importance of this electrostatic interaction to promote the initial approach of the peptide with bacterial cells, which induces the permeabilization of the bacterial

outer membrane leading to an uptake of the peptide. This could be the reason of the higher bactericidal effects observed on *E. coli* at shorter times of exposition in respect to *S. aureus* at concentrations lower than the MIC for this bacterium. Moreover, the high ratio of hydrophobic to charged units in Bac8c^{2,5Leu} should benefit the anti-Gram – activity [252]. Furthermore, previous studies reported that even if *E. coli* exposed to sub-lethal concentrations of Bac8c peptides resulted in deleterious downstream events on the cell membrane almost immediately after the inoculum, its defence systems were sufficient for full recovery as time passed by, supporting the observed effects.

It is known that the peptide slowly desorbs by the particle surface over time, but here, an activity merely due to the release of the peptide in the medium should be excluded since the Bac8c^{2,5Leu}@CNP-S system action is different from that of the free peptide. In particular, when loaded on the surface of the CNP-S, it partially retains its efficacy against *S. aureus* but not against *E. coli* suggesting a different mechanism of action of the whole nanosystem. A hypothesis should be that the high amount of ECM matrix produced by *E. coli* when exposed to CNP, could act as a protection, reducing the bactericidal effects of the peptide thus reducing the Bac8c^{2,5Leu}@CNP-S activity and may also account for the reversal of selectivity toward the two strains. Indeed, previous study demonstrated that Bac8c^{2,5Leu} peptide (albeit in the D form) was significantly less active against bacterial biofilm than against the same planktonic bacteria [223].

4.5 Conclusions of Part II

In the second part of this thesis work, the antibacterial effects of silver and carbon nanoparticles were analysed. In particular, the physiochemical and antibacterial properties of differently sized AgNPs colloidal suspensions were characterized, confirming an inverse correlation between the antibacterial efficacy and the size. Then, they were successfully immobilized on glass slides at different surface coverage and, for the first time, a SMBC (the minimal moiety of silver required to kill more than 99.9999% of bacteria) was determined by ISO 22196:2011 adapted method for each of the three sizes. The obtained SMBC against *E. coli* for AgNPs (6, 30, 52) nm were (0.023, 0.026, 0.034) μg/cm^2, respectively. These amounts of silver revealed to be almost 100 times lower than the MBC found for colloidal AgNPs and 200 times lower than other comparable AgNPs modified glass systems, proving the importance of the SMBC to minimize the amount of silver on modified surface systems, thus reducing the costs of

production and the potential toxicity. Furthermore, since the SMBC values were obtained by an international standard procedure, the comparison between different non-porous surfaces results simplified and this method of calculation should be extended to a variety of new active materials in many fields.

As regards CNP, their interaction with *S. aureus* and *E. coli* was tested over time in a simplified system demonstrating a rapid association between CNP and bacteria without a significant antibacterial activity on both strains. On the contrary, *S. aureus* incubated with CNP maintained its cell vitality over time even in the absence of nutrients, suggesting the potential role of CNP as source of carbon or as positive stimulus effect on the bacterial growth. Moreover, the bacterial exposure to CNP evinced a particular effect of ECM production on both bacteria, almost immediately after the inoculum, which was verified by both DEP-Raman and SEM. This could be intended as a self-defence mechanism in response to an external stress or as a stimulus to biofilm production, which could suggest a positive effect of the CNP on bacterial vitality.

Then, the antibacterial properties of different concentrations of a novel nanosystem, obtained by the combination of the CNP with the AMP Bac8c^{2,5Leu}, were tested against the two bacterial strains. A significant ($p < 0.01$) cell viability reduction (about 1 log, 90%, in respect to the CTRL– and about 3 log, 99.9%, in respect to pristine CNP) was observed for *S. aureus* after 24 h of exposure at the highest concentration tested. This suggests that at shorter exposure times to the nanosystem, the positive effect of the CNP on *S. aureus* vitality is predominant but the antibacterial effect of the peptide becomes more evident over time, further demonstrating the close interaction between the nanosystem and the bacterial species. On the other hand, the nanosystem demonstrated low antibacterial effects on *E. coli* only at shorter times of exposure, which completely recovered after 24 hours. Since the free AMP showed a very high bactericidal efficacy against *E. coli,* even at the lowest concentration tested, the observed reduction of the bactericidal effect of the nanosystem over time should be due to the rapid interaction of bacteria with the CNP, which stimulates the very fast production of large amounts of ECM, thus enhancing the defence of the microorganism against external stress.

In conclusion, even if the conjugation of the AMP with the CNP resulted in a partially reduced antibacterial efficacy *in vitro*, it could enhance the peptide stability to degradation suggesting a better bioavailability *in vivo*. Furthermore, the rapid and evident interaction of the CNP with bacteria suggests that also different antibacterial agents could be loaded onto their surface to be driven directly in contact with cells, maximizing their effects and uptake. This, together

with their high biocompatibility and biodegradability, renders them particularly promising as active agents for the development of innovative antibacterial food packaging systems, in the perspective to exploit their photothermic and photodynamic properties by external irradiation.

Chapter 5

Production and characterization of a novel antioxidant active packaging based on natural extracts

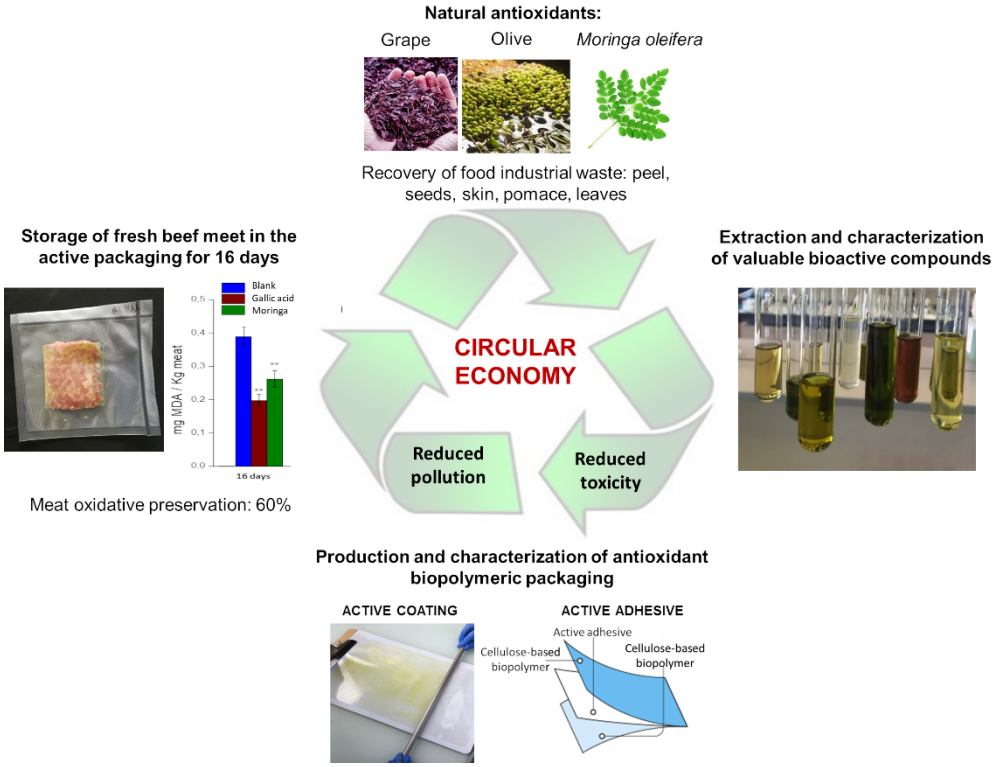

5.1 Olive, grape and moringa leaves extracts as natural antioxidant agents

One of the major issues of food industry is the management of huge amount of wastes. For instance for winery and olive oil production, from 10 to 20% of the total weight of plants material is discarded during the manufacturing processes, leading to the necessity of managing millions of tons of dregs per year [122]. Furthermore, it was demonstrated that most of the antioxidant active molecules such as phenolic compounds or flavonoids remain in the discarded plant materials such as skins, seeds and leaves [125]. It results clear how the employment of this waste as natural active additives in food packaging production has generated a great interest in the last few years in a context of circular economy and pollution's sources reduction. In addition, as natural plant derivatives, they can be considered as a safer and cost-effective alternative to synthetic antioxidant agents, improving health benefits for the consumers [43, 118]. In particular, in this work different fraction extracts from industrial waste of olive oil and wine production were obtained from Spanish industries by three different extractive methods: supercritical fluid extraction (SFE) by CO_2, subsequent supercritical antisolvent extraction (SAE) of the solid residues re-dissolved in ethanol, and maceration (MAC) for 10 days and 30 days in five different solvents (methanol, ethanol, acetone, water and dichloromethane). The same extractions were performed to obtain different fractions of *Moringa oleifera* leaves extracts. This tropical plant has indeed demonstrated to have valuable antioxidant, therapeutic and nutritional properties [137]. The presence of carboxylic groups on the conjugated ring structures of its polyphenols, flavonoids and vitamins contained in its leaves allow to neutralize free radicals or decompose peroxides [140] leading to the inhibition of lipid peroxidation [141]. Lipid peroxidation is one of the main mechanisms that lead to food degradation during its processing and storage. This phenomenon is a chain reaction process driven by the formation of secondary reaction products (like aldehydes or ketones) and free radicals that enhance the lipid auto-peroxidation while negatively influencing the overall quality of foods, including flavour, taste, nutritional values, and promoting the production of toxic compounds. The shelf-life prolongation of fresh meat is strictly bounded to a reduction or a slowdown of this reaction. Many studies have already focused their attention on the development of active films containing natural antioxidants which have demonstrated their efficiency on enhancing the myoglobin stability and fresh meat preservation from oxidation [253, 254]. These findings have driven the

research of new natural antioxidant active agents which can be incorporated in the meat package. They can act in different ways to interrupt the lipid peroxidation chain, for example as scavenger of free radicals or as autoxidation protectors [135]. The main advantage is the absence of need of any release or addition of the agent in the food, in compliance with European legislation. In the present study, the macerates fractions that have revealed the highest antioxidant efficacy *in vitro*, evaluated by the DPPH reduction assay and by ORAC, and the highest total phenols content, of each of the three plants materials were selected and incorporated in cellulose. This biopolymer was chosen because of its biodegradability and widespread use in food industry. Two innovative active packaging systems were here developed. The first one consisted on coating the cellulose foil with a food-safe resin incorporating 5% (w/w) of the moringa leaves and olive extracts for a direct food-contact action. The second one was a multilayer system in which 5% (w/w) of the grape extract was incorporated in the adhesive between two layers of cellulose for an indirect action avoiding the contact with the product. Their antioxidant efficacy was evaluated both *in vitro*, by the DPPH assay, and applied on hamburgers of fresh minced beef meat. The level of lipids oxidation was evaluated by both a classical indirect method, thiobarbituric acid reactive substances (TBARS) assay, and by Raman and FTIR spectroscopy. Vibrational spectroscopy, indeed, offers a direct and fast analysis of the molecular structure of the specimen without the need of any reagent or destructive sample preparation. Despite many works were already been published about classical and surface-enhanced Raman spectroscopy (SERS) [136], here the oxidation of lipids was directly monitored on the beef sample over 15 days, optimizing the acquisition conditions and avoiding any time-consuming lipid extraction step.

5.2 Materials and Methods

5.2.1 Reagents

2,2-Diphenyl-1-picrylhydrazyl (DPPH) powder was provided by Sigma-Aldrich. Methanol (HPLC grade), ethanol absolute anhydrous, acetone and glacial acetic acid (>99%), were provided by Carlo Erba and gallic acid (GA), 97.5-102.5%, by Sigma Aldrich.

AAPH (2,20-azobis(2methylpropionamide)dihydrochloride (97%); fluorescein (3,60-dihydroxypirol[isobenzofuran-1[3H],90[9H]-xanthen]-3one); and Trolox (6-hydroxy-2,5,7,8-tetramethylchroman-2-carboxylic acid; 98%);

potassium phosphate dibasic heptahydrate and potassium phosphate monobasic dihydrate were purchased from Sigma Aldrich. Working solutions for hydrophilic oxygen radical absorbance capacity (ORAC) assay were prepared following the AOAC standard method described by Ou et al. [255]. All the working solutions for the ORAC assay were prepared in sodium phosphate buffer (75 mM, pH 7.0). Aliquots of fluorescein stocks were prepared and stored at -80 °C and they were thawed once per time to prepare a stock solution 5.70 μM in ORAC buffer from which a working solution of 0.112 μM was obtained.

Folin-Ciocalteu's phenol reagent was purchased from Sigma Aldrich and sodium carbonate from Carlo Erba.

Hydrogen peroxide (>50%) was purchased from Scharlab (Barcelona, Spain), Sodium salicylate (>99.5%) and 2,5-dihydroxybenzoic acid (>99%) were supplied by Sigma-Aldrich, orthophosphoric acid (85%, reagent grade) and sodium hydroxide (0.01 mol/l) were purchased from Scharlab.

Trichloroacetic acid (TCA) (> 99%) and paraffin oil were purchased from Carlo Erba. Trichloroacetic acid 10% w/v was prepared dissolving it in Milli-Q® water. 4,6-dihydroxy-2-mercaptopyrimidine (2-thiobarbituric acid, TBA, 98%) was purchased from Acros organics (Rodano, Milan) and dissolved in Milli-Q® water to obtain two solutions with final concentrations of 4 mM for the calibration curve and 20 mM for the analysis of meat. Malondialdehyde tetrabutylammonium salt (MDA, > 96%), was purchased from Sigma Aldrich.

All the solutions described and the standard calibration solutions were prepared daily immediately before the starting of the analysis for all the tests.

For bacterial cultivation and assays Muller Hilton (MH) broth and agar purchased from Lickson, Phosphate Buffer Saline (PBS) tablets for 200 ml from PanReac AppliChem and NaCl by Carlo Erba were employed.

The following standard polyphenols and reagents were used for the UPLC-TQ-MS analysis, performed by the University of Zaragoza: Caffeine (CAS 58-08-2) (CAF), (+)catechin (> 99.0% (HPLC), CAS 154-23-4) (C), (−)epicatechin (> 95% (HPLC), CAS 490-46-0) (EC), (−)epicatechin gallate (> 98% (HPLC), CAS 1257-08-5) (ECG), (−)catechin gallate (>98% (HPLC), CAS 130405-40-2) (CG), (−)epigallocatechin (> 95% (HPLC), CAS 970-74-1) (EGC), (−)gallocatechin (> 98% (HPLC), CAS 3371-27-5) (GC), (−)gallocatechin gallate (> 98% (HPLC), CAS 4233-96-9) (GCG) and (−)epigallocatechin gallate (> 95% (HPLC), CAS 989-51-5) (ECG) were from Sigma Aldrich. Formic acid (MS solution) was from Waters (Waters; Manchester, UK). Methanol (LC-MS, CAS 67-56-1) was from

Honeywell (Barcelona, Spain). Ultrapure water was obtained from a Wasserlab Ultramatic GR system (Barbatáin, Spain).

5.2.2 Plant materials and extraction techniques

Moringa exsiccated leaves (*Moringa oleifera Lam.*) were purchased from Alesframa (Málaga, Spain). Olive fruits (*Olea europea*) collected after their harvesting in December 2020 were collected from trees located in Ayerbe (Spain, 42° 18’ 12’’ N 1° 57’ 53’’ O) and the olive cake was supplied by a local olive oil mill (Ayerbe). Grape waste (grape skin and seeds) obtained from the “*Garnacha*” kind of grape for red wine production were collected after the pressing of the fruits harvested in the zone of Rioja Baja, near Calahorra (Spain, 42° 16’ 36’’ N 0° 41’ 21’’ O) in October 2020.

The three plant materials were extracted in Zaragoza by three different methods: SFE using the CO_2 as critical solvent in three steps (see the scheme in Figure 36), the solid residues (mainly non-polar, this kind of extraction is indeed usually used as a cleaning step to remove fats and other non-polar compounds from the extracts) were collected manually from each of the two collectors, then hexane was employed to dissolve and collect the remaining residues in another two fractions. A part of the solid residues collected from SFE extractor were macerated in ethanol to solubilize them (this allows to obtain fractions containing the more polar compounds) and injected in a second extractor to perform a SAE employing CO_2 as supercritical solvent in two steps. Firstly, from the extractor two fractions were collected: one was collected manually and one after its solubilisation with ethanol.

Then, the remaining residues after another step of pressure regulation were collected manually from the collector. All the process is schematized in Figure 36.

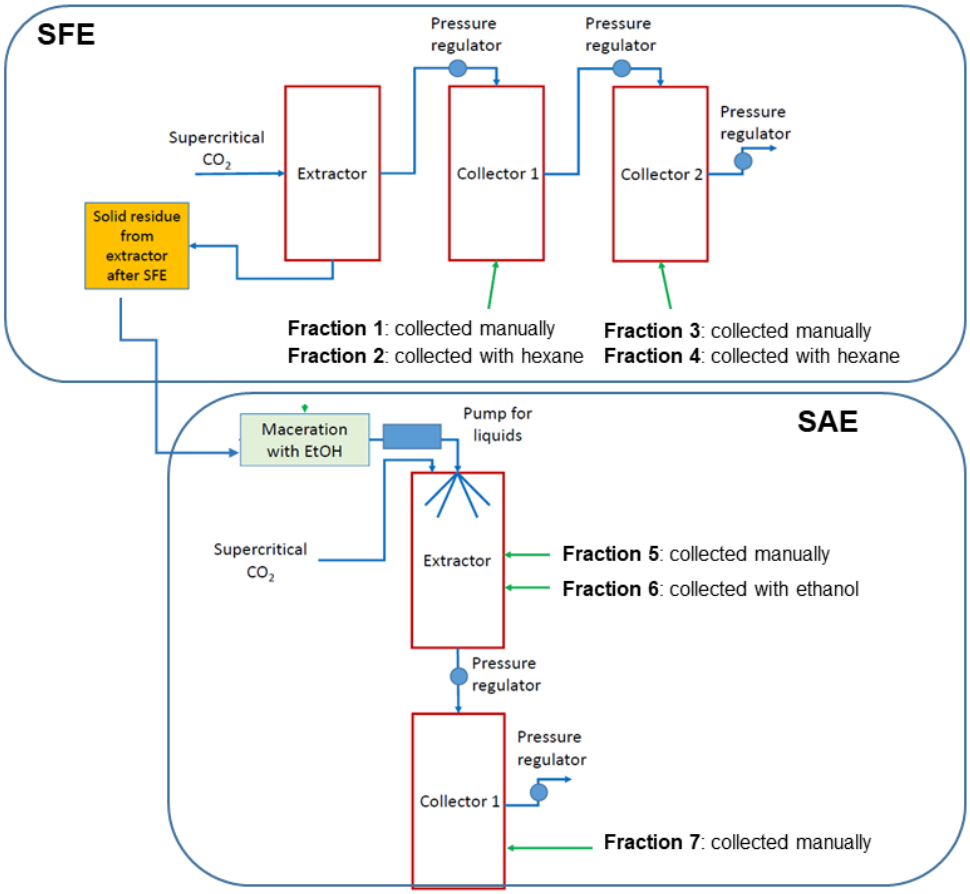

Figure 36: Scheme of SFE and SAE extractions and collected fractions. Upper panel: scheme of the SFE three steps extraction and of the 4 fractions collected for each plant material. Lower panel: scheme of the subsequent two steps SAE extraction from the solid residue collected from the extractor after the SFE and macerated in ethanol and of the three fractions collected for each plant material.

The other extraction technique employed was MAC for 10 days and 30 days in different solvents: ethanol, methanol, acetone, dichloromethane and water (the latter was employed only for grape residues due to their more polar nature). 100 g of material were put in contact with 500 ml of solvent. After the maceration time, solvent was recovered, put in a round flask and evaporated until dryness by means of a rotary evaporator Buchi R-300 (Flawil, Switzerland).

All the extractions were performed in the University of Zaragoza and the plants materials were purchased by the University of Zaragoza (Spain).

All the extracts fractions of grape and moringa were solubilized in ethanol at a final concentration of (1400 ± 5) mg/l, which was the maximum limit of solubilisation, except for the three grape's macerates for 10 days in ethanol, methanol and acetone which were solubilized at the same final concentration in a solution of Milli-Q® water and ethanol 1:1 because they resulted insoluble in ethanol only.

All the olive extracts fractions were solubilized in ethanol at a final concentration of (5000 ± 13) mg/l.

All these extracts solutions were placed in glass tubes, stirred and sonicated for at least 1 h at 300 W (Q-Sonica Q700 sonicator, 20 kHz, Newtown, CT, USA). Then the tubes were covered with aluminium foils, plugged and sealed with Parafilm® M and they were stored at 4 °C until their analysis.

A legend of all the fractions analysed is reported in Table 12.

Table 12: Legend of moringa, grape and olive extracts samples.

Extraction method	**Fraction**	**Symbol**		
Supercritical fluid extraction (SFE)	Collector 1 manually	SFE 1		
	Collector 1 with hexane	SFE 2		
	Collector 2 manually	SFE 3		
	Collector 2 with hexane	SFE 4		
Supercritical antisolvent extraction (SAE)	Extractor manually	SAE 1		
	Extractor with ethanol	SAE 2		
	Collector 1 manually	SAE 3		
Maceration		**Solvent**	**days**	**Symbol**
		Ethanol	10	MAC Et 10d
			30	MAC Et 30d

	Methanol	10	MAC Met 10d
		30	MAC Met 30d
	Acetone	10	MAC Ac 10d
		30	MAC Ac 30d
	Dicloromethane	10	MAC DCM 10d
		30	MAC DCM 30d
	Water	30	MAC W 30d

5.2.3 Chemical characterization of plant extracts

5.2.3.1 Determination of the total phenols content by Folin-Ciocalteu assay

This assay is based on the reaction between the phenols present in the extracts with the Folin-Ciocalteu reagent (a complex mixture of heteropolyphosphotungstate-molybdate) in the presence of sodium carbonate forming a blue-coloured complex. The intensity of the blue colour is proportional to the amount of reactive phenolic compounds in the sample. The phenolic content in percentage (w/w) is determined by measuring the absorbance of the sample solution at 765 nm and comparing it with a calibration curve built using gallic acid as a standard. This method allows quantifying total polyphenolic content of about 5% to 100% (w/w) in the extracts. The protocol was adapted by the official method described by Kupina et al. [256].

Briefly, a gallic acid stock solution (1 mg/ml) was prepared in Milli-Q® water and five dilutions from 40 mg/l to 200 mg/l were obtained to build the standard calibration curve. A series of test tubes, each containing 3 ml of water, 200 µl of Folin-Ciocalteu reagent were prepared and in each tube was added one of the following: 200 µl of sample test solution; 200 µl of calibration standard solution or 200 µl of water as blank. They were vortexed and allow to settle for 6 min.

Then, 200 µl of a 20% (w/v) sodium carbonate solution was added to each tube and mixed well. All the test tubes were incubated at (37 ± 1) °C for 30 min

and then 200 µl of each sample was placed in a well of a 96-wells plate in triplicate. The absorbance was measured at 765 nm in a multiwall reader, by subtracting the absorbance of the blank. A linear fit was calculated from the gallic acid calibration curve and the total phenolic content % (w/w) of each sample was calculated interpolating their average absorbance subtracted of the blank from the fit, normalizing the results by the concentration of the sample (mg/l). The relative uncertainty values were calculated for the linear fit considering all the uncertainty budget related both to the x-axis and to the y-axis. For the first, the sample pureness, each dilution performed (considering for the final volume uncertainty the propagation of the uncertainties related to each specific pipette used) and the weighing of the sample, were considered. For the second, a propagation of the calculated standard uncertainty values, derived from the three replicates absorbance measurements, was performed. Then the calculated uncertainties were propagated for each successive calculation performed.

5.2.3.2 UPLC-TQ-MS analysis of polyphenols

All the plant extracts already solubilized in ethanol as described in section 5.2.2 were analysed by UPLC-TQ-MS targeted for polyphenolic compounds using the standards listed in paragraph 5.2.1. Semi-quantitative analysis was carried out using an Acquity^{TM} UPLC chromatography system coupled to an electrospray interface (ESI) and Xevo TQ-S micro detector supplied by Waters (Manchester, UK). A UPLC BEH C18 column of 1.7 µm particle size (2.1 mm × 100 mm) was used with a flow rate of 0.3 ml/min and a column temperature of 35 ºC. The mobile phases were water (phase A) and methanol (phase B), both with 0.1% formic acid. The gradient used was 95% A and 5% B for 6 min; 5% A and 95% B up to 8 min; 95 A and 5% B up to 10 min. The volume of the sample injected was 10 µl.

The electrospray interface (ESI) was used in positive and negative ionization mode with a capillary voltage of 3.5 kV. The sampling cone voltage was optimized for each compound using standard, and it was set as 40 V. The temperatures used were 150 ºC and 350 ºC for source and desolvation gas, respectively, and the desolvation gas flow was 400 l/h. Selected Ion Recording (SIR) mode was used as an MS acquisition function. MassLynx v.4.1 software was used for data acquisition and processing. Results were expressed as the percentage ratio between the area of the peak of each specific compound (subtracted of the area of the same compound detected in the blank, solvent only, if present) and the total of the areas of all the target compounds detected for each sample. The analysis were performed in duplicate.

5.2.4 Antibacterial activity evaluation of plant extracts

Escherichia coli ATCC 8739 and *Staphylococcus aureus* ATCC 75380 were used for this work as a Gram – and a Gram + bacterial model, respectively.

5.2.4.1 Disk diffusion assay

Frozen stock cultures of *E. coli* and of *S. aureus* were revitalized on MHA and a single well separated colony was selected from each culture, suspended in 5 ml of physiologic solution (0.9% NaCl) with a sterile loop. The OD_{600} of the bacterial suspension was measured using physiologic solution without bacteria as blank and adjusted to a final OD_{600} of 0.1 (~1×10^8 CFU/ml). Then bacteria were spread on the surface of MHA plates using sterile cotton swabs taking care of covering all the surface of the plate and allowed to dry. 30 µl of each extract sample and of TCS 10 µg/ml as positive control were spotted on sterilized paper disks (Ø 6 mm) that were air-dried under the biological cabinet. The disks were placed on the top of the plates (in triplicate for both the bacterial strains) which were incubated overnight at (37 ± 1) °C. After 24 h the zones of inhibition were analysed on a dark background.

5.2.5 Antioxidant activity evaluation of plant extracts

5.2.5.1 DPPH radical scavenging activity

The antioxidant activity of all the extracts solubilized in ethanol, like described in paragraph 5.2.2, was determined by the DPPH assay. This is a colorimetric technique based on the capacity of the considered antioxidant agent to scavenge the DPPH radical. This reaction leads to the decolourization of the DPPH solution from dark violet (DPPH radical) to yellow (reduced DPPH) which is proportional to the decrease of the intensity of the absorbance at 516 nm, typical of the DPPH radical (Figure 37).

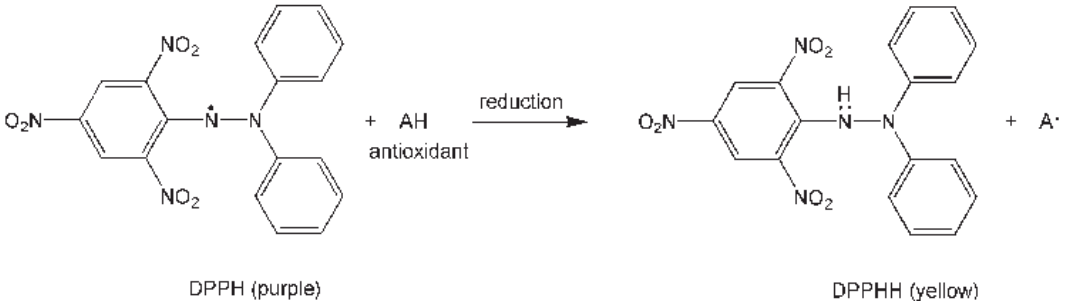

Figure 37: Reduction of free DPPH radical to 2,2-diphenyl-1-picrylhydrazine (DPPHH) by the presence of an antioxidant compound [257].

This measurement was performed using a multiplate reader (Varioskan, LUX Thermo Scientific) following the method previously described by Prieto [258]. Briefly, a DPPH stock solution was freshly prepared in methanol (final concentration 0.2 mM), sonicated in an ultrasonic bath for 5 min at 180 W, filtered with a 0.2 μm polystyrene filter. Then, it was stored in hermetically sealed amber glass bottle covered with aluminium foil and used over at least three hours from the preparation. In a 96-wells plate three kind of wells were prepared all with a final volume of 200 μl: i) blanks for each extract sample (100 μl of methanol and 100 μl of sample at each concentration tested); ii) DPPH controls (100 μl of methanol and 100 μl of DPPH stock solution); iii) test samples (100 μl of DPPH stock solution and 100 μl of sample at the chosen concentration). Each one of the wells containing the DPPH solution had a final concentration of DPPH of 0.1 mM. For each sample, 8 different concentrations were tested. All the measurements were performed in triplicate. The plate was left to stand in the dark under continuous shaking at 60 rpm and absorbance single lectures at 516 nm were collected every 10 min over 1 h. The radical scavenging activity or the antioxidant power (AP%) after one hour of incubation with the DPPH for each extract was expressed as the percentage of reduction of the free radical by the sample and calculated as follows:

Equation 9: Antioxidant power (AP%) = $[(A_{control} - A_{sample})/A_{control}] \times 100$

where $A_{control}$ is the mean of the DPPH controls (DPPH in methanol) absorbance values subtracted of methanol absorbance and A_{sample} is the mean of each samples replicates absorbance values (DPPH with extracts) subtracted of their blank absorbance values (extracts in methanol). The AP% was calculated for each sample concentrations (mg/l). The AP% of gallic acid at 8 different concentrations from 0.06 mg/l to 2.5 mg/l was measured as well as internal

control. The extracts that did not reached almost the 50% of AP were excluded from the subsequent analysis. For each sample, 5 concentrations which have demonstrated an AP% in the range between 20% and 70% were chosen and a linear fit was calculated from this five measurements points for each extract sample. The half maximal effective concentration (EC_{50}), the concentration of extract needed to reduce 50% of the DPPH radical, was calculated from the linear range of each sample. The relative uncertainty budget was calculated for each value taking into account, for each linear fit, all the uncertainties related both to the x-axis and to the y-axis. For the first, the sample pureness, each dilution performed (considering for the final volume uncertainty the propagation of the uncertainties related to each specific pipette used) and the weighing of the sample, were considered. For the second, a propagation of the calculated standard uncertainty values, derived from the three replicates absorbance measurements, was performed.

5.2.5.2 ORAC (oxygen radical absorbance capacity) assay

This assay measures the capacity of antioxidants to protect a fluorescent probe (fluorescein) from fluorescence intensity decay induced by the quenching with free peroxyl-radicals introduced by the addition in the well of AAPH which spontaneously decompose at (37 ± 1) °C. Fluorescence loss of the probe is measured over time. The efficacy of the antioxidants is determined by its capacity to prolong fluorescein fluorescence decay by measuring the average of the areas under the curve (AUC) of the sample in triplicate, subtracted of that of the blank (net AUC), in which no antioxidants are present. Trolox, a water-soluble analogue of vitamin E, was used as the calibration standard. In a unique assessment since as the reaction goes to completion, both the inhibition time and the inhibition degree are measured.

A stock solution of Trolox (100 µM) was obtained dissolving it in ORAC buffer. Then it was diluted to obtain a 25 mg/l solution from which seven different concentrations from 0.1 mg/l to 4.6 mg/l were obtained to build the calibration curve. A 96-wells plate was prepared placing 150 µl of a stock solution of fluorescein 11×10^{-2} mM, prepared diluting one aliquot from the frozen stock in ORAC working buffer. Then 25 µl of phosphate-diluted buffer as blank, three replicates of each of the eight Trolox different concentrations and 3 replicates for each sample were added to appropriate wells. The plate was incubated in the dark at 37 ± 1 °C for 30 min. A 25 µl amount of AAPH was added to all wells to reach a final volume of 200 µl. Timing is critical for the addition of AAPH as the

reaction begins immediately, and the rate is temperature-dependent, and for this reason, a multichannel pipette was used.

The plate was immediately transferred to the multiwell reader, agitated at 60 rpm before reading and the fluorescence was measured at the top of each well at 520 nm (excitation wavelength was 485 nm) every 90 seconds for 150 min. The net AUC was calculated for each sample including the Trolox dilutions by summation of all the fluorescence measurements over time, normalized by their initial fluorescence values. Then the Trolox calibration curve was obtained plotting the calculated net AUC over Trolox tested moieties (µmol). Each sample average AUC was interpolated in the calculated linear fit to obtain the relative Trolox equivalents (TE) (µmol). The results were expressed as ORAC values which are the calculated (TE) (µmol) per gram of sample. The relative uncertainty budget was calculated for each value taking into account, for the standard calibration curve linear fit, all the uncertainties related both to the x-axis and to the y-axis. For the first, the same factors mentioned in section 5.2.5.1 for the DPPH assay were taken into consideration. For the second, a propagation of the calculated standard uncertainty values, derived from the AUC measurements of the replicates, was performed.

5.2.6 Antioxidant packaging production

The developed packaging material was composed of cellulose-based biopolymer incorporated with a minimal amount of PVdC (polyvinylidene chloride) to optimise the moisture and gas barrier properties of the material and was purchased from the NatureFlex™ (45 NK) product range supplied by Futamura UK Ltd (Burgos, Spain). For the active film production with moringa leaves and olive extracts they were manually coated with a homogeneous layer of safe food-contact varnish methyl ethyl ketone-based, ADCOTE™ 17-3, courtesy of DOW Chemical Ibérica (Madrid, Spain) employing a wire close wound bar (bar number: 7; color code: brown; wire diameter: 1.02 mm; wet film deposit: 80 µM). Samples were prepared incorporating 5% (w/w) of the chosen active extracts of olive and moringa leaves directly in the varnish and all the samples were sonicated at the power of 300 W for 1 h. Samples with 5% (w/w) of gallic acid (GA) and with varnish only were prepared as well as positive control (CTRL+) and blank respectively. Then they were coated on the cellulose sheets and air-dried to get rid of the solvent (Figure 38).

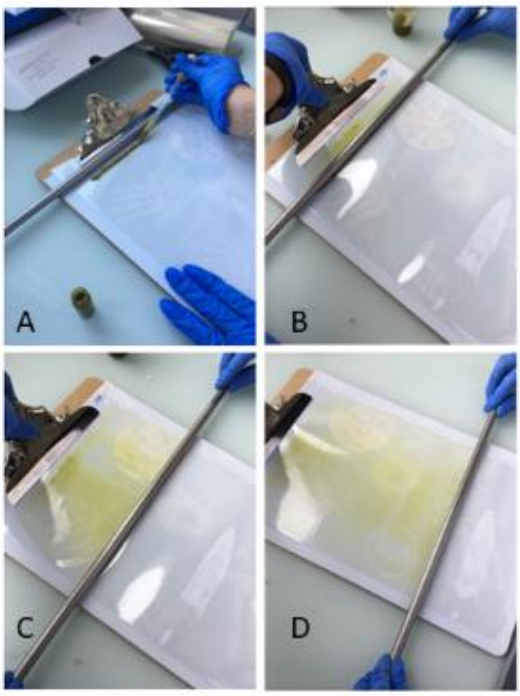

Figure 38: Scheme of the cellulose-based biopolymer coating procedure for the active packaging preparation.
A) About 2 g of safe food-contact varnish with 5% of the active agent were spotted in a line at the top of the cellulose film. B-C) The varnish was gently laminated on the surface of the cellulose foil using a wire close wound bar. D) The cellulose foil homogeneously coated with the active varnish was air-dried.

The grape macerates extracts, showed limited solubility in the solvent based varnish. Consequently, the corresponding developed packaging material was based on two cellulose polymer layers laminated together with a water-based biodegradable adhesive (Flex Tack 4M35) for food packaging applications from Samtack (Barcelona, Spain). Extracts were incorporated to the adhesive at 5% (w/w) concentration and homogenized by sonication using the same conditions previously described for moringa and olive samples. The active adhesive was spread on the cellulose sheet using the coating machine K control coater from RK print coat instruments (Litlington, UK). The same wire close wound bar described before was used for coating and the sheet was air-dried. The cellulose sheet with dry adhesive was covered by another cellulose layer. The developed multilayer biomaterial was placed in BiO 330 A3 Heavy Duty Laminator (South Korea), and it was pressed at 40 °C with a speed number 5.

5.2.7 Antioxidant packaging characterization

5.2.7.1 DPPH radical scavenging activity

The DPPH inhibition assay applied directly on active films was already previously described [259, 260]. Briefly, squares of 2 cm × 2 cm were cut in triplicate from each active film produced including the blank and the gallic acid as negative and positive control, respectively. Then, the volume of a solution (50 mg/l) of DPPH radical in methanol was calculated to maintain the proportion between the DPPH and the extracts molecules present in the area of the film the same of that used for the analysis of pure extracts. Therefore, the squares of active films were put in sterile 50 ml Falcon tubes and covered with aluminium foils, and then 12 ml of DPPH radical solution were put in each Falcon tube adding a falcon with DPPH solution only as control. Aliquots of 200 µl of each replicate of each sample were collected immediately after the addition of the DPPH and after 24 h. They were put in a 96-wells plate and their absorbance at 516 nm was measured. Then the AP% was calculated using the Equation 9 for all the samples including the blank at the two time points. The relative uncertainties were calculated by propagation of standard uncertainties obtained from the three measurement replicates.

5.2.7.2 Free radical scavenging assay

Antioxidant capacity of all the prepared cellulose-based active films was measured using a method developed by Pezo et al. [151] and a schematic representation of the apparatus used is shown in Figure 39.

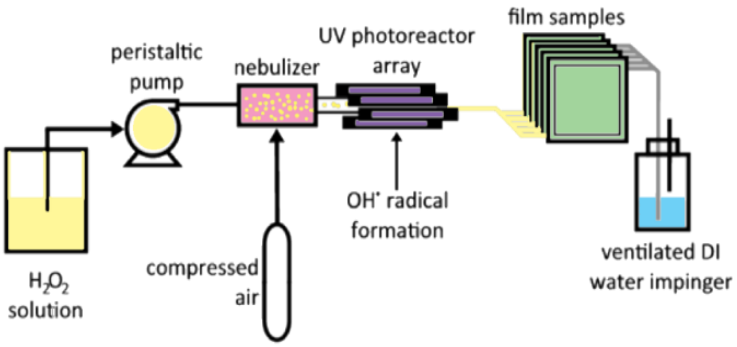

Figure 39: Schematic representation of generator of hydroxyl free radicals.

The method consists of the hydroxylation of salicylic acid by the free radicals generated from an aqueous H_2O_2 (0.29 M) aerosol, under UV-light irradiation. Samples of 1 dm^2 of each active cellulose films were placed inside PE bags with internal dimensions of 150 mm × 150 mm, internal volume was (420 ± 6) ml, and an impulse sealer PFS-200 Zhejiang Dongfeng Packing Machine Co (Wenzhou, Zhejiang, China) was used to thermo-seal the bags. The prepared bags were placed in a holder with separators that contained up to eight bags at the same time and the bags were then connected to the OH• radical generator. The generated atmosphere enriched in free radicals was carried by air through plastic bags with the active material inside, and finally bubbled into a salicylic acid solution. Salicylic acid reacts with the not scavenged free radicals and forms 2,5-dihydroxybenzoic acid (2,5-DHB) as major compound, which is fluorescent (Figure 40).

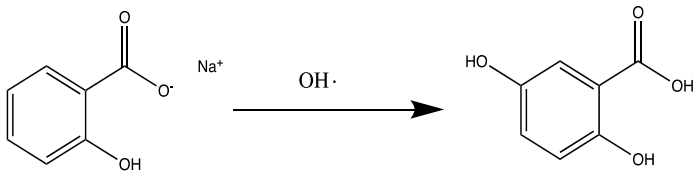

Figure 40: Reaction of sodium salicylate and hydroxyl radicals to form 2,5-DHB.

The setup comprised a Bio-Rad peristaltic pump (Hercules, CA, USA) set at 0.8 ml/min and a total air flow set at 3.76 l/min. The photoreactor used to generate OH• radicals from 1.66% (v/v) hydrogen peroxide solution consisted of a (300 mm × 30 mm cylindrical quartz tube that was irradiated with UV light generated by eight 250 mm × 15 mm Philips fluorescent UV lamps (TL 8W/08 F8T5/BLB Hg, Eindhoven, The Netherlands) that were placed axially around the quartz tube. Drechsler-type gas-washing bottles filled with 50 g of 2 μg/g of sodium salicylate solution were used to collect the flow-through gases. Three replicates of each sample have been analysed. The antioxidant samples have been compared to their targets. The oxidation of the samples has been carried out for 24 h.

Quantitative analysis of 2,5-DHB and the residual salicylic acid was performed by high-performance liquid chromatography (Alliance 2695 Separations Module (Waters, Milford, MA, USA)) with a 474 Scanning Fluorescence Detector. A Waters reversed phase column ((100 × 4.6) mm, 3 μm) Atlantis dC18 was used. The mobile phase was a mixture of aqueous acetate

buffer (35 mmol/l, pH 5.9, 1.0 ml/min) and methanol, 9:1 (v/v). The injection volume was 10 µl. Excitation and emission wavelengths were set at 324 nm and 448 nm, respectively.

As a result, the percentage of hydroxylation (H%), calculated from the rule of three, has been obtained where 100% is the peak area of 2,5-DHB in the blank sample (control) and x% is the area of the 2,5-DHB peak in a sample with antioxidant.

Equation 10: $H\% = [Area_{2,5DHB}\ (active\ film) / Area_{2,5DHB}\ (control)] \times 100$

5.2.7.3 TBARS assay on beef meat

This test is a colorimetric assay based on the reaction of thiobarbituric acid with malondialdehyde (MDA) molecules, a secondary product of the lipid peroxidation process, to form a pink product, as schematized in Figure 41, absorbance at 532 nm is measured.

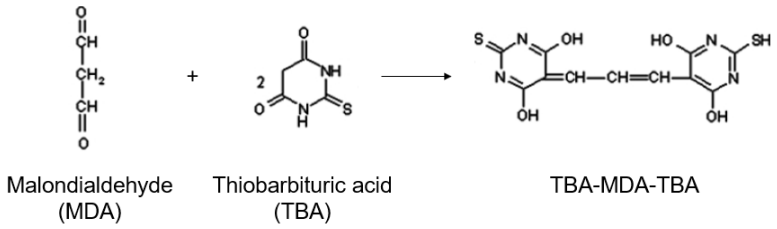

Figure 41: Scheme of the TBARS assay method reaction principle.

A scheme of the lipid peroxidation process is showed in Figure 42.

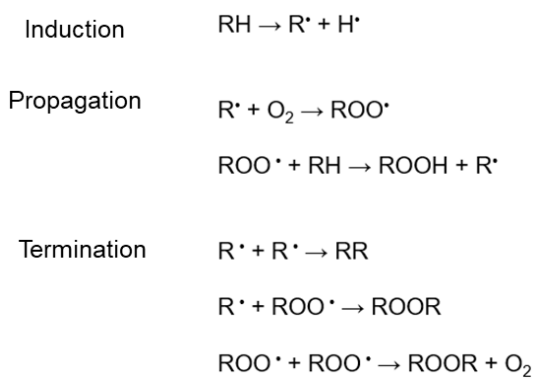

Figure 42: Scheme of the lipid peroxidation process.

Briefly, the oxidation of the double labile bondages in polyunsaturated fatty acids lead to the formation of peroxides, which could be further oxidised or decomposed in compounds with lower molecular weight such as ketones, short chain aldehydes like the MDA which could fasten the food degradation and also negatively influence its quality and safety [261].

In order to perform this assay 12 g of fresh beef meat minced twice with a content of about 50% of fat were weighted for each of the film samples (5% M MAC Met 30d, 5% GA, blank) and packaged individually in 2 squares of 6 cm × 6 cm of the films over and above the meat piece, flattening it to make sure that all the coated film area was in full contact with meat (Figure 43).

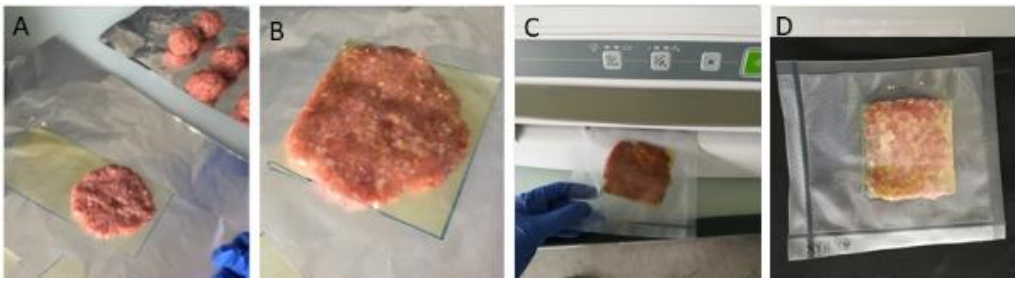

Figure 43: Packaging process of minced beef meat in active films.
A) 12 g of minced beef meat was weighted and placed in the centre of rectangles of each active films prepared with the coated layer in direct contact. B) Meat samples were flattened to cover the entire internal area of the film. C) The samples were inserted in PET thermos-sealable bags and sealed in normal atmosphere. D) Final packaged sample stored at 4 °C.

Each sample was inserted in a polyethylene terephthalate (PET) thermo-saleable bag of an external area of 12 cm × 14 cm and sealed aerobically with non-modified atmosphere air and stored in the fridge at 4 °C. Samples were prepared in triplicate for each kind of film tested, including the blank coated with varnish only, and for each time point of analysis (0, 3, 6, 9, 16) days, to follow the meat lipid peroxidation over time. The thiobarbituric acid index (TBARS value) was determined for each sample at each time point by adapting many previously described protocols [105, 262, 263, 264]. Briefly, the MDA was dissolved in Milli-Q® water to obtain a stock solution of 1 mM and diluted in different concentrations from 0.8 mM to 0.01 mM, and 1 ml of each standard dilution was mixed with 1 ml of TBA stock solution 4 mM, to build a calibration curve. 10 g of meat, from each packed sample in triplicate, were homogenized with 20 ml of

TCA 10% (w/v) for 30 s with a Brinkman Polytron (PT 10/35, Kinimatica, Switzerland) till a uniform slurry was obtained. Than the samples were centrifuged at 2000 rcf for 5 min at 10 °C. 1 ml of supernatant was collected from each sample and mixed with 1 ml of aqueous solution of TBA at a concentration 20 mM. All the samples, including the calibration curve dilutions, were kept in paraffin oil bath at 97 °C for 20 min, to allow the reaction between the MDA and the TBA. Then they were cooled in a water bath at 20 °C for at least 10 min to complete the colour change. The samples were then centrifuged at 2000 rcf for 15 min at 10°C and 200 µl were taken from each sample and put in a 96-wells plate including a column with water only as blank. The absorbance was measured at 532 nm and subtracted for the absorbance of the blank. The concentration of MDA in the samples was calculated interpolating the values in the linear fit obtained from the calibration curve. TBARS values were expressed as mg of MDA per kg of meat. All measurements were made in triplicate. The uncertainty budget for each measurement was obtained in the same way described for the DPPH assay in section 5.2.5.1. The statistical significance of the difference between the average of the measurements on the blank and the moringa samples was analysed performing a *t-test* and the relative *p*-value were calculated and represented in the graphs as a single star for $p < 0.05$ and two stars for $p < 0.01$.

5.2.7.4 Raman evaluation of meat oxidation

Pieces (2 g) of each meat sample at the first and final measurement time points were weighted and positioned on a microscope glass slide, flattening them as much as possible. Before data collection, the alignment and calibration of the Raman DXR™ Thermo Fisher Scientific microscope was performed using the instrument calibration tool, as described before. A 10× objective (0.25 NA) with a 20 µm slit aperture was employed. The analysed spectral range was (3500–200) cm^{-1}. All the spectra were acquired using the following conditions: laser wavelength 780 nm with a power of 5.0 mW, exposure time 5 s for 24 scans. All the spectra collected were manually corrected for the baseline and normalized for the intensity of the peak at 1000 cm^{-1} corresponding to the stretching vibrational mode of aromatic rings.

5.2.7.5 FT-IR evaluation of meat oxidation

The same meat samples on the glass slides were analysed by Fourier Transform-infrared (FT-IR) spectroscopy after the Raman measurements. For these measurements the Nicolet™ iN™10 infrared microscope equipped with a

DTGS detector was used. The spectra were collected by attenuated total reflection (ATR) collection mode using a Ge crystal, as they were solid, not transparent and not particularly reflecting samples. The tip was gently washed with ethanol between measurements. The background was collected in air before each measurement. 64 scans were acquired for 1 min of total collection time. Spectra were corrected for the baseline and deconvoluted for the amide 1 (1640–1680) cm^{-1} and amide II (1550–1530) cm^{-1} signals. Thermo Scientific Peak Resolve was use to fit a number of individual peaks to a complex set of overlapping peaks in the spectrum. The operation is performed on the selected region (1750–1350) cm-1 (where protein peaks appear) of the selected spectrum. Voigt function was selected as peak type initial guess. Once the peak shape is set, the peak characteristics are described by the location, height and full width at half height (FWHH=15). Find Peaks functions automatically defines a set of peaks based on the current sensitivity and FWHH (full width at half height) settings. The algorithm used to find peaks looks for minima in the Savitsky-Golay second derivative of the selected regions of the spectrum. The Sensitivity parameter determines the polynomial order used in calculating this derivative: we used medium sensitivity, which corresponds to a third order polynomial. Then the Fit Peaks function initiates the process of automatically adjusting the peak center, height and width to produce a composite spectrum that matches the original. The convergence routine in OMNIC is a Fletcher-Powell-McCormick algorithm. Convergence is determined by the ratio of the root mean square (RMS) of the residual to the RMS noise of the spectrum. Ideally, this should approach 1 as the RMS of the residual approaches the noise. The type of baseline component used in the fit operation was linear or none baseline. Baseline correction before fitting was however performed. The AUC of the deconvoluted spectra were calculated and their ratio was calculated for the evaluation of the proteins variation.

5.2.7.6 Migration test of active agents

For each active cellulose film including the blank and the CTRL+ a portion of 5 cm^2 were cut and put in amber glass bottle. then 8.33 ml of simulant (ethanol 10% or acetic acid 3%, considering that we want to simulate meat) were added, based on proportional relationship established by the European normative (1 dm^3 of simulant per 6 dm^2 of packaging), Regulation (EU) No 10/2011, and the bottles were carefully closed also by Parafilm® M to avoid evaporation of the simulant.

The migration test was carried out for 10 days at 40 °C, including hot-filling, according to Commission Regulation (EU) No 2016/1416 amending and

correcting chapter 2, section 2.1.4, of Regulation (EU) No 10/2011. After ten days, the films were removed from the bottles and the simulants were analysed by UV–Vis. Calibration curves of all the pure extracts tested were built making serial dilutions in both the food simulants. The amount of released compounds after 10 days was evaluated by interpolation in the linear fits following the Lambert-Beer law:

Equation 11: $A = \varepsilon \times b \times c$

Where A is the absorbance, ε is the molar absorptivity, b is the length of light path, and c is the concentration of sample detected.

5.3 Characterization of the antibacterial and antioxidant properties of the different natural extracts fractions

5.3.1 Evaluation of the antibacterial properties of the natural extracts by disk diffusion assay

Extracts were obtained from olives residues from olive oil production, grape residues from red wine production and from exsiccated *Moringa oleifera Lam*. leaves by the University of Zaragoza. All the fractions of extracts obtained by SFE, subsequent SAE and MAC in four different solvents for 10 days or 30 days of each plant material were dissolved in ethanol, or water and ethanol (1:1) at a fixed concentration (see paragraph 5.2.2). All these solutions were analysed for their antibacterial and antioxidant properties by different standard assays.

Firstly, their bactericidal effect against both *E. coli* and *S. aureus* standard strains, as a Gram – and a Gram + bacterial model, respectively, was tested by the disk diffusion assay. The zone of inhibition due to each test sample was evaluated and compared with a negative and a positive control of pure ethanol and TCS, respectively (Figure 44).

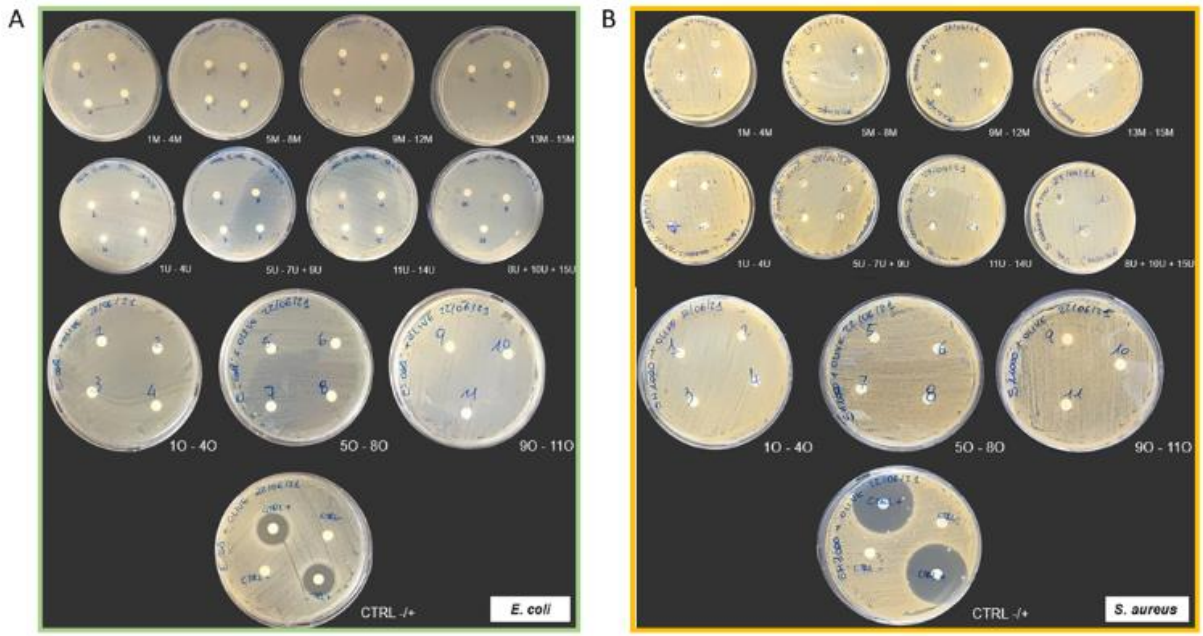

Figure 44: Disk diffusion assay results of all the pure extracts toward *E. coli* and *S. aureus*.

Disk diffusion assay most results of moringa leaves extracts (first line on the top), grape extracts (second line), olive extracts (third line) and comparison of the inhibition zone with positive (TCS) and negative (ethanol) controls (fourth line) towards A) *E. coli* ATCC 8739 and B) *S. aureus* ATCC 65380. In this image samples fractions were numerated from 1 to 15 or 11 to simplify their labelling on the plates.

As Figure 44 shows, no significant bactericidal effects were observed for each extract at the tested concentrations against both *E. coli* and *S. aureus.* Indeed, no inhibition zone was detected near all the extracts samples, which were comparable to the CTRL–, while a significant halo of inhibition was detected only around the CTRL+ for both the selected bacteria.

5.3.2 Evaluation of the antioxidant properties of the natural extracts by DPPH and ORAC assays

The antioxidant properties of all the ethanol solutions of the different fractions of the extracts were evaluated by both two standard assays: the DPPH scavenging capacity assay and the ORAC assay. As previously commented, these are two standard methods very commonly employed to assess the antioxidant efficacy of liquid compounds.

5.3.2.1 DPPH assay results

Different dilutions of all the ethanol solutions of the three plant materials were prepared and mixed with the DPPH radical solution. The reaction took place in the dark and the change of colour of the solution from violet to yellow was measured after one hour of incubation by UV-VIS absorbance at 516 nm. All the samples were analysed in triplicate, including gallic acid as reference standard compound since it is a phenolic simple molecule with very well characterized antioxidant properties. The antioxidant power percentage (AP%) was calculated for each sample using the Equation 9 and plotted against their different concentrations (Figure 45).

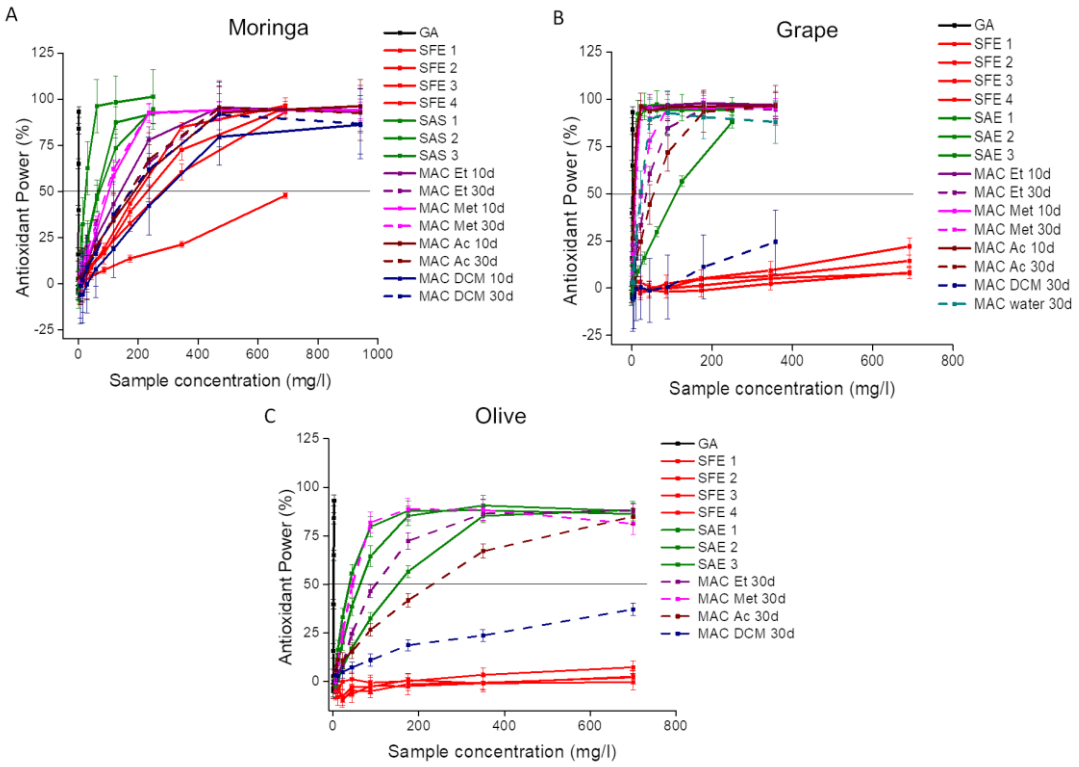

Figure 45: DPPH assays results expressed as antioxidant power percentage (AP%). Plots showing the calculated AP% against sample concentrations for each extraction fractions by SFE (red lines), SAE (green lines) and MAC for 10 days (solid lines) or 30 days (dashed lines) in the four different solvents of A) moringa leaves extracts, B) grape extracts and C) olive extracts.

Figure 45 shows that, as expected, the fractions obtained by SFE and maceration in dichloromethane exploited the lowest values of antioxidant power, which, in most of the cases, do not even reach the 50%. This is due to the mostly non-polar composition of these extracts, which do not contain the higher antioxidant active compounds such as polyphenols, flavonoids and tannins. These compounds are usually extracted by polar solvents such as water, ethanol or methanol. Indeed, the extraction with supercritical CO_2 is often employed to precipitate the polar fractions and eliminate the non-polar compounds that are not interesting for their antioxidant efficacy. Moreover, in this case the solid residues of this extraction were recovered with ethanol and then underwent an anti-solvent extraction which allowed to obtain extracts fractions with very high antioxidant efficacy (green lines in the plot), especially those collected immediately after the passage in the extractor (see the scheme in Figure 36). In addition, the macerates, especially those obtained after 30 days of maceration in ethanol or methanol showed good capability to reduce the DPPH radical, which again might be due to their more polar composition. The slope of the curves linearly reflects the antioxidant efficacy of the samples, since the higher is the pendency the lower concentration of sample is needed to reduce the same amount of DPPH. Consequently, it results evident that the highest efficacy is obtained by grape extracts, excluding the SFE and MAC in DCM fractions, followed by moringa extracts and lastly by olive.

This could be due to the more lipophilic composition of olive extracts, which could partially negatively influence their antioxidant efficacy in liquid assays conducted in hydrophilic conditions.

From these results, a linear range of at least 4 concentrations in the surrounding of the 50% of AP was analysed for each sample, in triplicate, excluding those that did not reach a 50% of AP and the relative linear fit were calculated (Figure 46).

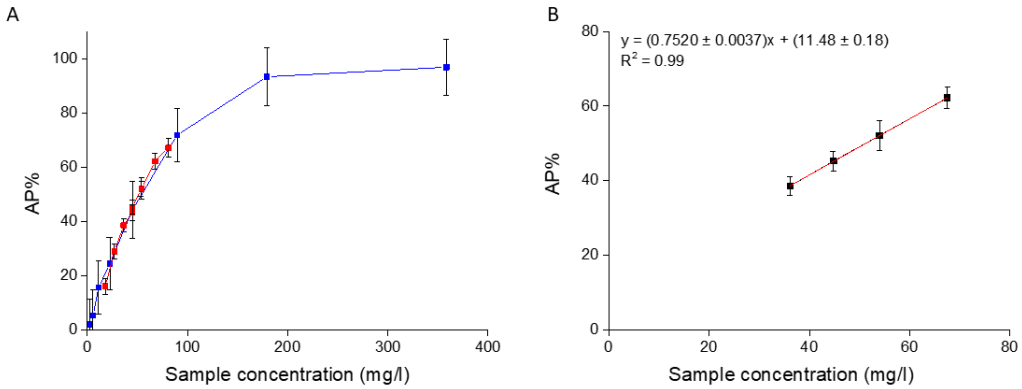

Figure 46: Example of the study of the linear range around 50% AP of a grape extract sample.

A) Antioxidant power (in %) plotted against concentration of a grape extract sample and example of the study of the linearity around 50% of AP (red points). B) Linear fit obtained from the 4 concentrations analysed on the sample in panel A.

From these fits, the half-maximal effective concentration (EC_{50}), that is, the minimal amount of antioxidant agent needed to reduce 50% of the radical DPPH, was obtained for each sample. The linear fits with their relative uncertainties and χ^2 values are shown in Table 13.

Table 13: Linear fits of olive, grape and moringa extracts obtained from the DPPH assay results around 50% of antioxidant power**.**

Sample	Extraction fraction	Linear fit equation (y = mx + q)	uncertainty(q)	uncertainty(m)	χ^2/(n-p)
Moringa	SFE 1	y = 0.145x + 17.8	9.1	0.039	0.107
	SFE 2	y = 0.176x + 15.2	7.4	0.029	0.312
	SFE 3	y = 0.476x - 4.9	8.4	0.067	0.237
	SAE 1	y = 0.63x + 6.3	11	0.16	0.044
	SAE 2	y = 0.526x + 2.3	5.7	0.079	0.154
	SAE 3	y = 0.371x - 1.5	6.5	0.081	0.110
	MAC Et 10d	y = 0.561x - 2.0	7.7	0.085	0.019
	MAC Et 30d	y = 0.302x + 0.6	6.9	0.038	0.368

	MAC Met 10d	y = 0.585x + 4.5	4.7	0.072	0.233
	MAC Met 30d	y = 0.633x + 15.8	5.1	0.069	0.236
	MAC Ac 10d	y = 0.521x + 2.3	7.6	0.080	0.113
	MAC Ac 30d	y = 0.472x - 1.0	5.9	0.070	0.090
	MAC DCM 10d	y = 0.290x + 6.8	13	0.065	0.018
	MAC DCM 30d	y = 0.279x + 0.7	13	0.084	0.006
Grape	SAE 1	y = 8.63x - 5.6	5.6	0.78	0.712
	SAE 2	y = 6.6x + 10.4	8.6	1.2	0.010
	SAE 3	y = 0.139x + 1.0	4.7	0.014	0.215
	MAC Et 10d	y = 5.7x + 2.7	7.2	1.0	0.005
	MAC Et 30d	y = 1.86x - 5.6	5.7	0.23	0.162
	MAC Met 10d	y = 5.92x + 10.3	4.9	0.74	0.013
	MAC Met 30d	y = 1.66x - 1.3	8.1	0.31	0.091
	MAC Ac 10d	y = 32.5x - 74.5	9.1	2.6	0.981
	MAC Ac 30d	y = 0.75x + 11.5	6.1	0.12	0.001
	MAC water 30d	y = 2.32x + 0	20	0.98	0.013
Olives	SAE 1	y = 0.96x + 6	11	0.24	0.003
	SAE 2	y = 0.56x + 14	13	0.19	0.007
	SAE 3	y = 0.334x + 3.7	8.3	0.050	0.134
	MAC Et 30d	y = 0.453x + 2	11	0.096	0.029
	MAC Met 30d	y = 0.80x + 13.1	9.9	0.19	0.112
	MAC Ac 30d	y = 0.165x + 14.8	9.2	0.034	0.018
Gallic acid		y = 46.2 x + 1.0	2.5	2.6	0.214

The EC_{50} of each sample was interpolated from their respective linear fit and the obtained values with the correspondent standard uncertainties are showed in Table 14. The samples that revealed the lower EC_{50} value have the higher antioxidant efficacy. The EC_{50} values were compared with the percentage of total content of polyphenols (w/w) determined for each sample by the Folin-Ciocalteu assay. For this assay, a calibration curve was built using gallic acid as standard polyphenolic compound (Figure 47). Then the total content of polyphenols in percentage (w/w) of each sample was calculated interpolating their absorbance measured at 765 nm in the calibration curve, obtaining the concentration in gallic acid equivalents and normalizing the results for the concentration of each sample.

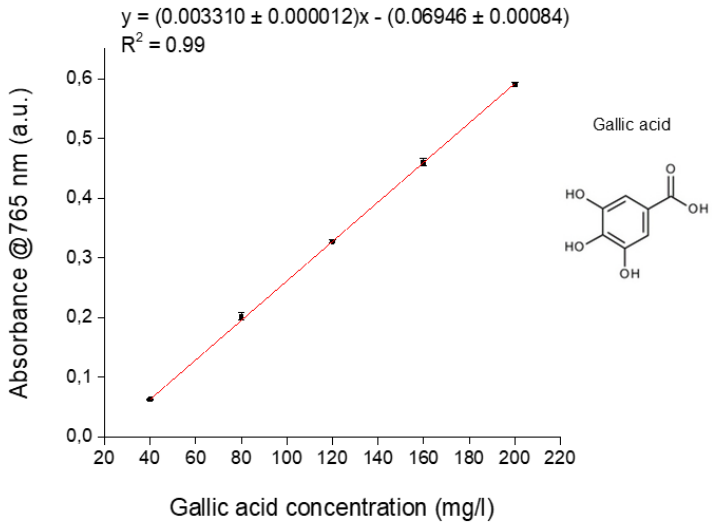

Figure 47: Gallic acid calibration curve obtained for the Folin-Ciocalteu assay.

Table 14: EC_{50} and total polyphenols content % (w/w) calculated for each olive, grape and moringa extract.

Sample	Extraction fraction	EC_{50}	Total polyphenols content % (w/w)
Moringa	SFE 1	223 ± 87	2.931 ± 0.052
	SFE 2	198 ± 53	2.83 ± 0.10
	SFE 3	115 ± 24	3.086 ± 0.057
	SAE 1	69 ± 25	10.693 ± 0.067

	SAE 2	91 ± 17	10.217 ± 0.081
	SAE 3	139 ± 35	3.479 ± 0.068
	MAC Met 10d	78 ± 13	7.476 ± 0.050
	MAC Ac 10d	92 ± 20	4.69 ± 0.20
	MAC Et 10d	93 ± 20	3.643 ± 0.029
	MAC DCM 10d	149 ± 55	3.688 ± 0.082
	MAC Met 30d	54 ± 10	7.60 ± 0.49
	MAC Et 30d	164 ± 30	5.652 ± 0.088
	MAC Ac 30d	108 ± 20	4.085 ± 0.046
	MAC DCM 30d	177 ± 71	3.968 ± 0.029
Grape	SAE 1	6.45 ± 0.91	45.0 ± 4.8
	SAE 2	6.0 ± 1.7	38.23 ± 0.74
	SAE 3	352 ± 50	10.34 ± 0.12
	MAC ac 10d	3.80 ± 0.42	47.34 ± 0.71
	MAC met 10d	6.7 ± 1.2	44.8 ± 1.9
	MAC et 10d	8.3 ± 1.9	31.78 ± 0.91
	MAC DCM 10d	21 ± 12	15.40 ± 0.21
	MAC water 30d	31.0 ± 7.6	16.35 ± 0.12
	MAC met 30d	29.8 ± 4.7	14.67 ± 0.21
	MAC et 30d	51 ± 12	14.74 ± 0.49
Olives	SAE 1	46 ± 16	5.05 ± 0.11
	SAE 2	66 ± 33	3.614 ± 0.081
	SAE 3	139 ± 33	3.41 ± 0.15
	MAC Met 30d	46 ± 16	3.78 ± 0.15
	MAC Et 30d	108 ± 34	3.309 ± 0.073

	MAC Ac 30d	214 ± 71	2.133 ± 0.039
Gallic acid	-	1.060 ± 0.079	-

The correlation between the obtained EC_{50} values and the total content of polyphenols of each extract was also evaluated (Figure 48) because a higher content of polyphenols is often related to a higher antioxidant efficacy due to the important antioxidant effect of those molecules and their capability to donate H^+ thus reducing radical compounds.

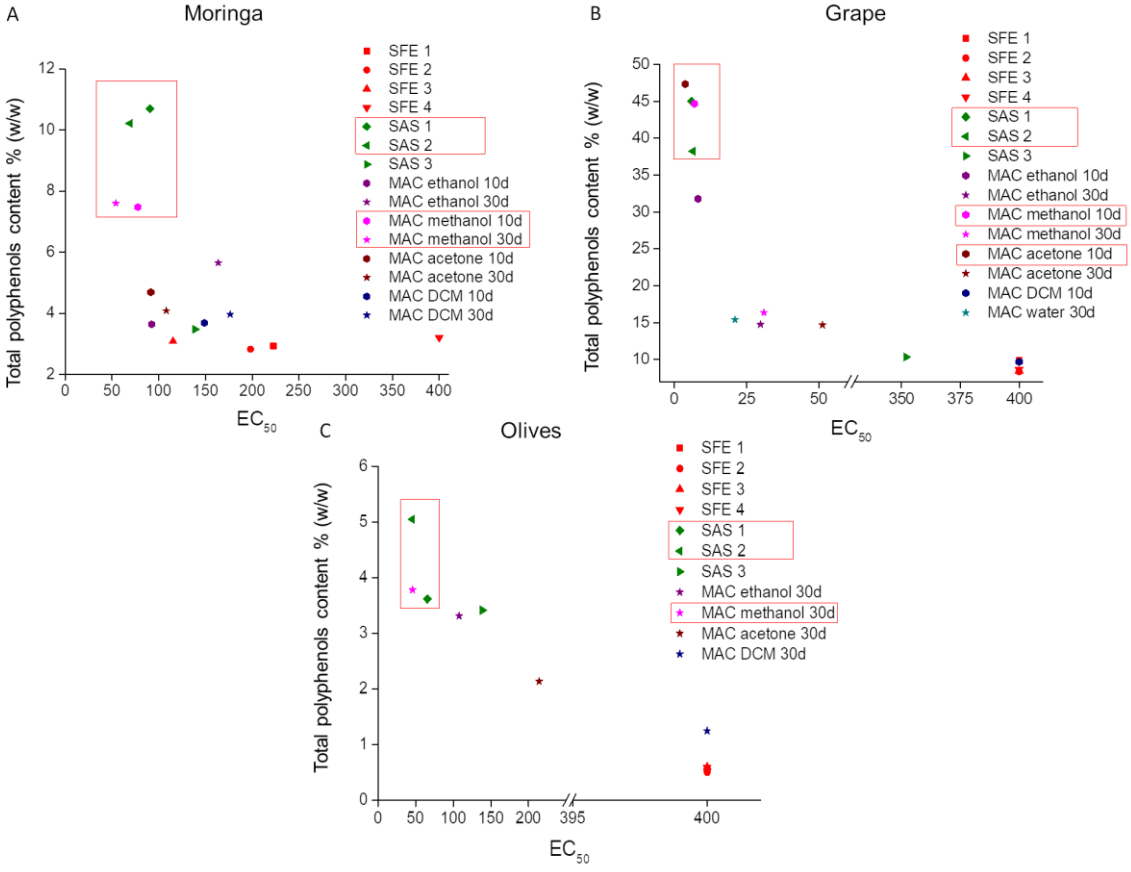

Figure 48: Comparison between the calculated EC_{50} and the total content of polyphenols% (w/w).

Total polyphenolic content plotted against the relative EC_{50} values of each extract sample of A) moringa leaves, B) grape industrial waste, and C) olive industrial waste. The samples with the most antioxidant efficacy were squared in red.

As showed in Figure 48, the samples with lower EC_{50} values are well correlated with a higher content of polyphenols. Furthermore, from this analysis it results clear that the extractions by SAE are those that produced the most antioxidant active extracts with the highest content of polyphenols, especially those collected from the first extractor. Those samples are immediately followed by macerates, especially those in methanol, confirming that this solvent resulted the one with the highest extractive capacity of active compounds. These findings are in line with literature data [265].

Additionally, grape extracts demonstrated the highest content of polyphenols with a relative very high antioxidant activity. This was a confirmed data because in the peel and seeds of red grapes huge amount of antioxidant active compounds are present [266].

For the maceration extracts, in particular, the time of maceration seems to influence the extraction of active compounds. Indeed, since for both moringa and olive the bests results in terms of antioxidant efficacy and polyphenolic content were obtained by the macerates for 30 days, this is not the case observed for grape, where the best samples were those macerated for 10 days. These results obtained for grape were confirmed also by the redder colour observed in the ethanolic solutions of the macerates for 10 days in all the 4 solvents, while the 30 days showed a loss of the red colour indicating a lower content of phenolic compounds. This phenomenon is confirmed in literature [267] because excessively prolonged time of exposition to the solvents could cause oxidation of phenolic compounds or their polymerization into insoluble compounds. Furthermore, it is known that the changes in the solid to liquid ratio occurring over time could influence the mass transfer of active compounds. So, the optimal extraction conditions, including solvent, temperature and time of extraction could be different between the plant materials due to their different compositions.

5.3.2.2 ORAC assay results

Firstly, Trolox at seven different concentrations was tested to obtain the standard calibration curve (Figure 49).

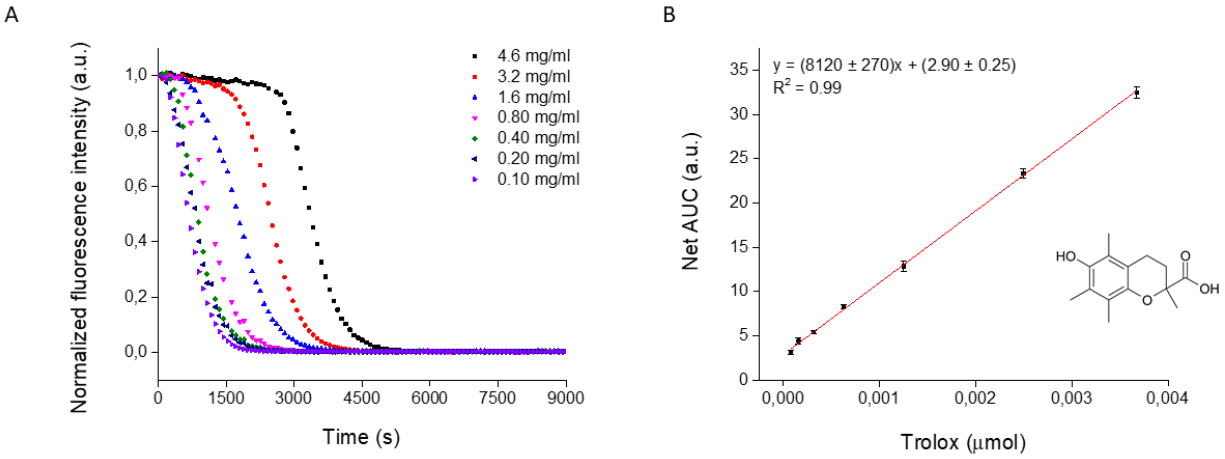

Figure 49: Trolox standard calibration curve and kinetics for the ORAC assay. A) Fluorescein kinetics of fluorescence intensity decay at 520 nm over time in presence of AAPH and seven different concentrations of Trolox. B) Trolox calibration curve obtained for the ORAC assay.

Then, all the plant extracts were analysed and the kinetics of fluorescence signal decay over time in presence of the oxidative molecule AAPH were measured for each sample in triplicate. The average of the calculated net areas under the curve of each sample were interpolated in the Trolox standard calibration curve and the TE were obtained and normalized for the sample concentration as explained in materials and methods paragraph 5.2.5. For each value the uncertainty budget was calculated propagating the standard uncertainty taking into consideration all the dilutions and weighed made. The results are summarized in Table 15.

Table 15: ORAC values obtained for each moringa, grape and olive extract expressed as μmol of Trolox equivalents (TE)/g of plant material.

Sample	Extraction fraction	ORAC values (μmol TE/g)
Moringa	SFE 1	21790 ± 610
	SFE 2	22990 ± 660
	SFE 3	24190 ± 670
	SFE 4	22880 ± 640
	SAE 2	46900 ± 1400
	SAE 3	43500 ± 1300
	MAC Et 10d	42900 ± 1200
	MAC Ac 10d	33900 ± 990
	MAC DCM 10d	30160 ± 890
	MAC Met 10d	26040 ± 750
	MAC Met 30d	42600 ± 1200
	MAC DCM 30d	31670± 950
	MAC Ac 30d	28300 ± 840
	MAC Et 30d	26240 ± 910
Grape	SFE 1	18730 ± 540
	SFE 2	23960 ± 760
	SFE 3	19530 ± 570
	SFE 4	31400 ± 860
	SAE 1	127700 ± 3700
	SAE 2	91600 ± 2600
	SAE 3	80900 ± 2400
	MAC Ac 10d	78000 ± 2300

	MAC Met 10d	74600 ± 2300
	MAC DCM 10d	72300 ± 2000
	MAC Et 10d	69000 ± 2000
	MAC water 30d	89400 ± 3500
	MAC ac 30d	75300 ± 2200
	MAC met 30d	75100 ± 2100
	MAC Et 30d	60600 ± 1800
Olives	SFE 1	2480 ± 130
	SFE 2	3000 ± 80
	SFE 3	3340 ± 150
	SFE 4	3530 ± 90
	SAE 1	4060 ± 110
	SAE 2	2950 ± 140
	SAE 3	3400 ± 180
	MAC Et 30d	4300 ± 110
	MAC Ac 30d	3420 ± 90
	MAC Met 30d	3340 ± 170
	Mac DCM 30d	3010 ± 170

In this case higher ORAC values (μmol TE / g_{sample}) correspond to higher antioxidant properties since the values represent how many times the sample works better than Trolox to protect fluorescein probe from oxidation induced by the presence of AAPH radical.

Despite minor differences from the DPPH assay results among the antioxidant efficacy of the MAC extracts with different solvents, which are included in the uncertainty values, and are mainly due to the different antioxidant mechanism measured by the two assays, it could be notice that also in this case all the grape

extracts showed the highest antioxidant properties followed by moringa and by olive, which as before, showed the lowest antioxidant effect also in this test. Furthermore, it was confirmed again that SAE is the extraction technique which allows to obtain the extracts with the highest antioxidant efficacy. Between the macerates, those that have already demonstrated the highest antioxidant power in the DPPH assay reconfirmed this result also by ORAC assay. In particular, the moringa MAC in methanol for 30 days, the grape MAC in acetone for 10 days and in water for 30 days, as well as the olive MAC in ethanol for 30 days showed the highest capability to protect fluorescein signal decay, which demonstrated once more their highest preservatives capabilities from oxidation among the other macerates.

5.3.3 UPLC-TQ-MS analysis of the polyphenolic content of the extracts

To better elucidate the relation between higher antioxidant properties and higher content of polyphenols a semi-quantitative analysis of the content of the principal polyphenolic molecules such as catechins, epicatechins and gallates was performed by targeted UPLC-TQ-MS. The results, expressed as relative peak ratio%, are summarized in Tables 16, 17 and 18, and in the graphs in Figure 50.

Table 16: Relative polyphenols content analysis of moringa extracts by UPLC-TQ-MS.

Compound	**GA**	**CAF**	**C**	**EC**	**CG**	**ECG**	**GC**	**EGC**	**GCG**	**EGCG**
ESI Mode	Negative	Positive	Negative	Negative	Negative	Negative	Negative	Negative	Negative	Negative
t_R (min)	0.76	3.00	2.63	3.09	3.46	3.37	1.99	2.32	3.06	4.98
m/z	169.02	195.1	289.07	289.07	441.08	441.08	305.07	305.07	457.08	457.08
MeOH (blank)	0	ND	ND	ND	ND	ND	ND	ND	ND	ND
SFE 1	100	ND	ND	ND	ND	ND	ND	ND	ND	ND
SFE 2	100	ND	ND	ND	ND	ND	ND	ND	ND	ND
SFE 3	65	ND	ND	ND	ND	ND	8	6	ND	21
SFE 4	96	ND	ND	ND	ND	ND	2	2	ND	ND
SAE 1	35	65	ND	ND	ND	ND	ND	ND	ND	ND
SAE 2	83	17	ND	ND	ND	ND	ND	ND	ND	ND
SAE 3	92	ND	ND	ND	ND	ND	ND	ND	ND	8
MAC Et 10d	100	ND	ND	ND	ND	ND	ND	ND	ND	ND

MAC Et 30d	60	40	ND	ND	ND	ND	ND	ND	ND	ND
MAC Met 10d	35	65	ND	ND	ND	ND	ND	ND	ND	ND
MAC Met 30d	90	10	ND	ND	ND	ND	ND	ND	ND	ND
MAC Ac 10d	100	ND	ND	ND	ND	ND	ND	ND	ND	ND
MAC Ac 30d	100	ND	ND	ND	ND	ND	ND	ND	ND	ND
MAC DCM 10d	100	ND	ND	ND	ND	ND	ND	ND	ND	ND
MAC DCM 30d	100	ND	ND	ND	ND	ND	ND	ND	ND	ND

*ND: non detected

Table 17: Relative polyphenols content analysis of grape extracts by UPLC-TQ-MS.

Compound	GA	CAF	C	EC	CG	ECG	GC	EGC	GCG	EGCG
ESI Mode	Negative	Positive	Negative	Negative	Negative	Negative	Negative	Negative	Negative	Negative
t_R (min)	0.76	3.00	2.63	3.09	3.46	3.37	1.99	2.32	3.06	4.98
m/z	169.02	195.1	289.07	289.07	441.08	441.08	305.07	305.07	457.08	457.08
MeOH (blank)	0	ND	ND	ND	ND	ND	ND	ND	ND	ND
SFE 1	ND	ND	ND	ND	ND	ND	ND	ND	ND	ND
SFE 2	100	ND	ND	ND	ND	ND	ND	ND	ND	ND
SFE 3	100	ND	ND	ND	ND	ND	ND	ND	ND	ND
SFE 4	100	ND	ND	ND	ND	ND	ND	ND	ND	ND
SAE 1	67	ND	22	11	ND	ND	ND	ND	ND	0
SAE 2	65	ND	23	10	ND	2	ND	ND	ND	ND
SAE 3	100	ND	ND	ND	ND	ND	ND	ND	ND	ND
MAC Et 10d	62	ND	22	12	ND	4	ND	ND	ND	ND

MAC Et 30d	66	ND	23	9	ND	1	ND	ND	ND	ND
MAC Met 10d	64	ND	22	12	ND	2	ND	ND	ND	ND
MAC Met 30d	90	ND	6	3	ND	1	ND	ND	ND	ND
MAC Ac 10d	53	ND	29	14	ND	4	ND	ND	ND	ND
MAC Ac 30d	53	ND	34	12	ND	1	ND	ND	ND	ND
MAC DCM 10d	100	ND	ND	ND	ND	ND	ND	ND	ND	ND
MAC water 30d	72	ND	17	11	ND	ND	1	0	ND	ND

*ND: non detected

Table 18: Relative polyphenols content analysis of olive extracts by UPLC-TQ-MS.

Compound	**GA**	**CAF**	**C**	**EC**	**CG**	**ECG**	**GC**	**EGC**	**GCG**	**EGCG**
ESI Mode	Negative	Positive	Negative	Negative	Negative	Negative	Negative	Negative	Negative	Negative
t_R (min)	0.76	3.00	2.63	3.09	3.46	3.37	1.99	2.32	3.06	4.98
m/z	169.02	195.1	289.07	289.07	441.08	441.08	305.07	305.07	457.08	457.08
MeOH (blank)	0	ND	ND	ND	ND	ND	ND	ND	ND	ND
SFE 1	100	ND	ND	ND	ND	ND	ND	ND	ND	ND
SFE 2	100	ND	ND	ND	ND	ND	ND	ND	ND	ND
SFE 3	100	ND	ND	ND	ND	ND	ND	ND	ND	ND
SFE 4	100	ND	ND	ND	ND	ND	ND	ND	ND	ND
SAE 1	37	ND	ND	ND	ND	ND	ND	63	ND	ND
SAE 2	22	ND	ND	ND	ND	ND	ND	72	1	5
SAE 3	100	ND	ND	ND	ND	ND	ND	ND	ND	ND

MAC Et 30d	46	ND	ND	ND	ND	ND	ND	54	ND	ND
MAC Met 30d	38	ND	ND	ND	ND	ND	ND	62	ND	ND
MAC Ac 30d	81	ND	ND	ND	ND	ND	ND	19	ND	ND
MAC DCM 30d	100	ND	ND	ND	ND	ND	ND	ND	ND	ND

*ND: non detected

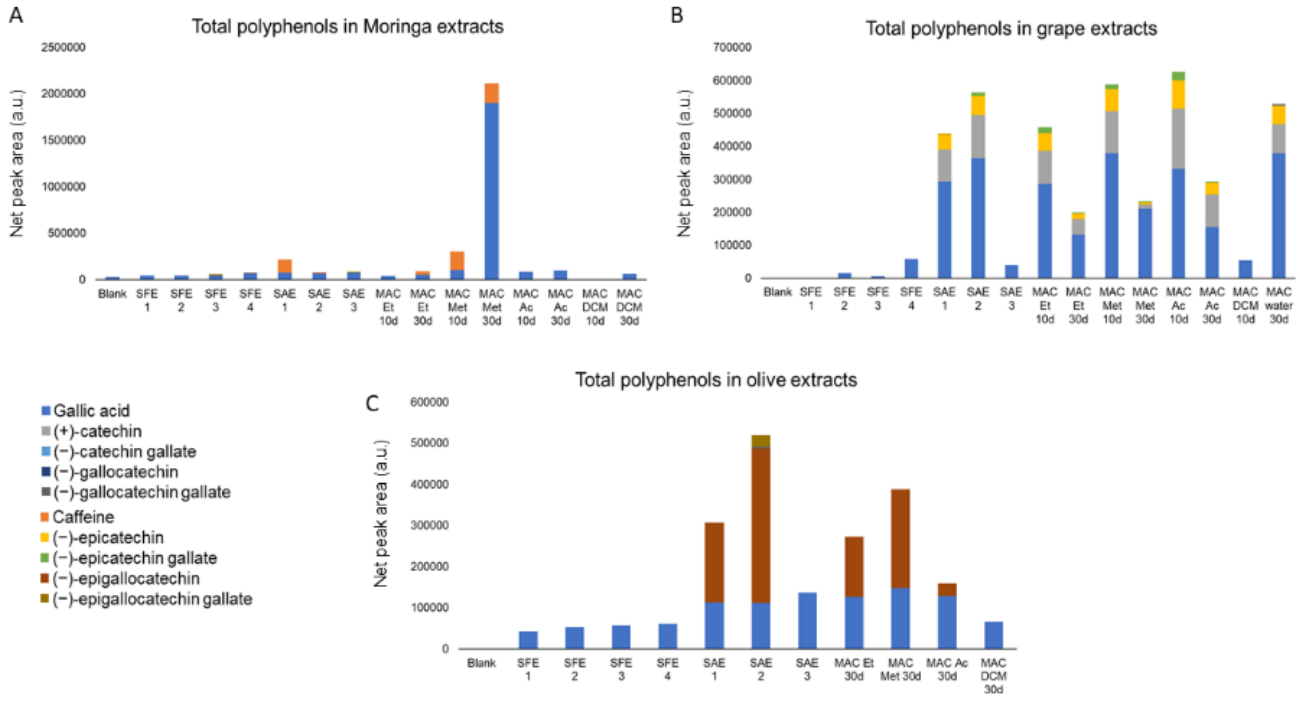

Figure 50: UPLC-TQ-MS results for all the moringa, grape and olive extracts. A-B-C) Plot resultant from the overlap of the UPLC-IMS results for each polyphenolic standard listed in the legend obtained by each extract of moringa leaves, grape and olive, respectively.

From this semi-quantitative analysis, it resulted that the polyphenolic content of all the three plants extracts is mostly composed of gallic acid, which is higher in the samples which have already evidenced a high polyphenolic content in the Folin-Ciocalteu assay such as the MAC and the SAE fractions. In particular, grape extracts confirmed again to be the ones with the highest content of polyphenolic compounds including catechin, epicatechin and epicatechin gallate. The highest values of those compounds were obtained once more by the two first SAE fractions and by the macerates for 10 days in acetone, followed by those in methanol and in ethanol. Also the MAC for 30 days in water showed a high content of polyphenolic molecules. Moringa leaves extracts showed also a predominance of gallic acid content, especially in the sample macerated for 30 days in methanol and also the presence of caffeine especially in the MAC in methanol and in the first SAE fraction. Again, olive extracts confirmed to contain the lower amount of polyphenols in comparison with the other two plants extracts

but they evidenced the presence of epigallocatechin and epigallocatechin gallate especially in the first two SAE fractions and in the macerates in ethanol and methanol. These results are perfectly in line with the DPPH, ORAC and Folin-Ciocalteu results confirming that the grape extracts are those with the highest total content of polyphenols, that the extracts which revealed the highest antioxidant effects in the DPPH and ORAC assays are also those with the highest content of polyphenols especially gallic acid. For all the three plants it results clear that the solvent that extracts the highest moiety of active compounds is methanol.

5.4 Active film production and antioxidant activity characterization

The active cellulose films, produced as described in detail in paragraph 5.2.6, with 5% (w/w) of the moringa leaves, grape and olive extracts which demonstrated the best antioxidant properties in the previous tests (moringa macerates for 10 days and 30 days in methanol, olive macerates in methanol and ethanol for 30 days and grape macerates in acetone and methanol for 10 days) were characterized for their antioxidant efficacy with different techniques. The macerates were chosen instead of the SAE best fractions because maceration represent a more sustainable and cheaper extraction process, since it do not need any particular high temperature or pressure and also the amount of solvent needed is reduced in comparison with other industrial extraction techniques [145].

5.4.1 DPPH radical scavenging assay

Firstly, a DPPH assay was performed directly on the films avoiding any extraction procedure by simply soaking squares of the active coated films in the DPPH radical solution (50 mg/l) in a volume calculated to maintain the same (DPPH / sample) molecules ratio of the tests on the pure extracts. The absorbance at 516 nm was measured almost immediately and after 24 h, and the AP% was calculated using the Equation 9. The results of the active cellulose films with moringa and olive extracts obtained by coating are presented in Table 19.

Table 19: Antioxidant power % (AP%) of the produced coated cellulose films obtained from the DPPH assay.

Sample	AP%
Blank	0.1 ± 5.9
Gallic acid	89.8 ± 3.0
Moringa MAC Met 10d	37.4 ± 4.9
Moringa MAC Met 30d	50.1 ± 7.8
Olive MAC Et 30d	13.3 ± 2.4
Olive MAC Met 30d	13.0 ± 2.9

This assay evidenced that the most effective DPPH radical scavenger resulted to be the cellulose film coated with 5% of the moringa macerate in methanol for 30 days. This sample, after 24 h of incubation was able to reduce (50.1 ± 7.8)% of the total radical DPPH molecules.

Then, the same assay was repeated with the cellulose double layer films with 5% of the two more promising grape macerates in the adhesive between the layers. The results are summarized in Table 20.

Table 20: Antioxidant power % (AP%) of the produced double-layer cellulose films obtained from the DPPH assay.

Sample	AP%
Blank	5.6 ± 6.9
Trolox	71.6 ± 6.7
Grape MAC Ac 10d	28.6 ± 6.7
Grape MAC Met 10d	48 ± 11

These results evinced that also these kind of packaging results active to reduce the DPPH radical present in the methanol solution. In particular, the cellulose-based packaging with 5% of the Trolox standard molecule in the adhesive resulted, as expected, more effective than the grape samples and with an antioxidant power percentage lower but comparable with that of gallic acid, which is a very good result considering that these samples are not in direct contact with the DPPH solution as for the coated ones. Furthermore, the sample with 5% of the grape extract by maceration in methanol for 10 days demonstrated an antioxidant efficacy very similar to that obtained by the moringa MAC Met 30d with an AP% of (48 ± 11)% suggesting a very promising antioxidant efficacy.

5.4.2 Free radical scavenging assay

All these produced active films were tested also for their ability to scavenge hydroxyl radicals by the method described by Pezo et al. [151]. Samples of active cellulose with moringa and olive extracts including also blanks (CTRL–) and gallic acid (CTRL+) in bags were prepared in triplicate. The fluorescence signal of the formed 2,5-DHB was measured and the percentage of hydroxylation (H%) was calculated by Equation 10. As previously described, the higher is the scavenging capacity of the active agent tested, the lower fluorescence signal is measured, so lower H% indicated better antioxidant efficacy of the film. The results are collected in Table 21.

Table 21: Free radical scavenging capacity of the active packaging materials expressed as average hydroxylation percentage (H%) of 2,5-DHB.

Active material	H%*	uncertainty%
Gallic acid	60.53 ± 0.16	0.3
Trolox	65.81 ± 0.13	0.2
Olive MAC Et 30d	74.01 ± 0.32	0.4
Olive MAC Met 30d	55.11 ± 0.19	0.3
Moringa MAC Met 10d	57.92 ± 0.10	0.2
Moringa MAC Met 30d	52.13 ± 0.17	0.3
Grape MAC Ac 10d	58.10 ± 0.18	0.3
Grape MAC Met 10d	66.84 ± 0.10	0.1

*blank: H% = 100%.

From this test resulted that the best radical scavenging capacity were obtained by the cellulose film coated with 5% of the moringa macerate in methanol for 30 days with a percentage of hydroxylation of 52 ± 0.17, which is even lower than that of gallic acid. This fact confirms again its higher antioxidant efficacy in respect to the other active film also applied in non-direct contact conditions. This test evidenced a good radical scavenging capacity also of the films coated with olive macerates, which with the DPPH test, in liquid, did not show satisfactory results. Furthermore, also the Trolox and grape extracts showed a good peroxyl radical scavenging capacity, comparable to that of gallic acid and moringa MAC Met 10d, even if their action was expected to be reduced in respect of that made by coating since their availability could be mitigated by the presence of another layer of cellulose-based biopolymer. In consequence, it must be pointed out that different tests are needed for a correct characterisation all the antioxidant effects of the produced active materials. Some of them are more indicated for the direct contact use since they are able to release larger amount of reducing compounds. On the contrary, other are more suitable as non-contact packaging materials

because they demonstrated higher scavenging activity, or because they are more active on different substances due to their more lipophilic behaviour.

However, in this work, since the cellulose-based biopolymer coated with moringa leaves macerated in methanol for 30 days demonstrated the higher antioxidant efficacy in all the performed assays, this sample was chosen to be applied on a case study of the oxidation of meat.

5.4.3 Analysis of oxidation of beef minced meat packed in the active film with Moringa leaves macerate extract

5.4.3.1 Evaluation of lipid peroxidation by TBARS assay

Since lipid peroxidation is one of the main cause of the degradation of meat, during transportation or storage, in this study minced beef meat containing about 50% of fat was wrapped with celluolose coated with 5% of moringa MAC Met 30d. Its oxidation was compared with meat packed in cellulose with only varnish without any active agent (blank) and in cellulose coated with 5% of GA as negative and positive controls respectively, over 16 days of storage in the fridge at 4 °C.

This particular active film was chosen to be tested in this experiment evaluating its ability to protect fresh meat oxidation because it demonstrated the highest antioxidant efficacy in the DPPH assay among the other active cellulose-based films produced by coating. Also the efficacy of the cellulose double layers films with grape macerates should be very interesting to test in the future but, they were not taken into consideration in the present work since they should involve more indirect process as non-contact active films.

The formation of the MDA as reference compound indicative of the lipid peroxidation of meat was quantitatively followed over time by the TBARS assay.

The MDA present in each sample was quantified as mg of MDA/kg of meat calculated interpolating the absorbance values in the MDA calibration curve.

The TBARS results are represented in Figure 51 and Table 22. The more MDA/kg is measured the more peroxidation of lipids took place on the analysed piece of meat.

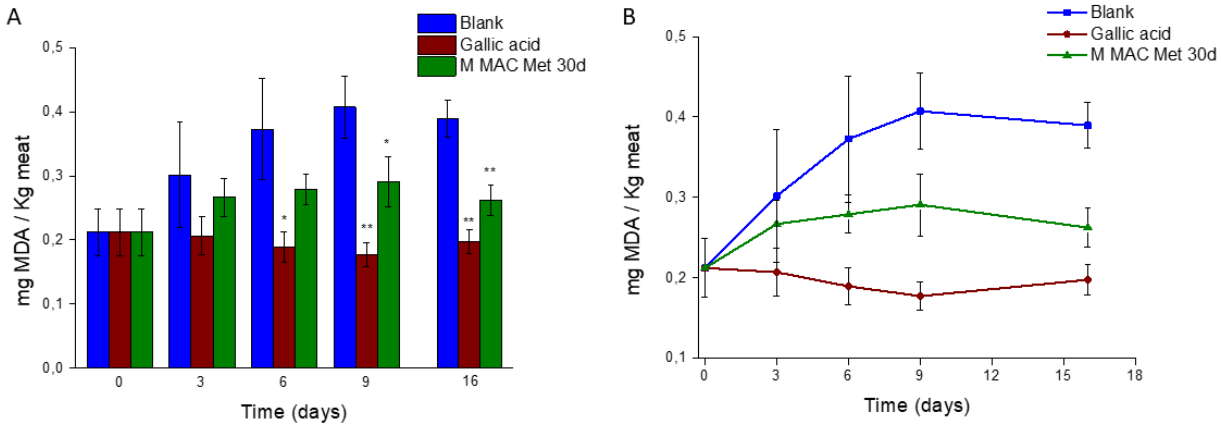

Figure 51: TBARS assay results of lipid oxidation of minced beef meat over time. TBARS assay analysis of minced beef meat packed in cellulose with moringa leaves 5% (green), gallic acid 5% (maroon) or blank (blue). The results are expressed as mg MDA/kg of meat. Absorbance measurements of the lipids extracts of each sample were taken at day 0, 3, 6, 9 and 16. Three different hamburgers were analysed for each sample at each measurement point and the relative uncertainties were calculated by propagation of standard uncertainty then a *t-test* was performed to determine the significance of the difference between the blank and the other samples mean values. Panel A) *: *p-value* < 0.05. **: *p-value* < 0.01.

Table 22: TBARS values of meat lipid peroxidation over time, expressed as mg malondialdehyde (MDA)/kg of meat.

Packaging used for the meat storage	**Blank**	**Cellulose coated with gallic acid 5% w/w**	**Cellulose coated with moringa leaves extract 5% w/w**
Day of analysis	**mg MDA/kg of meat**		
0	0.212 ± 0.036	0.212 ± 0.036	0.212 ± 0.036
3	0.302 ± 0.082	0.207 ± 0.029	0.267 ± 0.030
6	0.372 ± 0.079	0.189 ± 0.023	0.279 ± 0.024
9	0.407 ± 0.048	0.177 ± 0.018	0.291 ± 0.039
16	0.389 ± 0.028	0.197 ± 0.018	0.262 ± 0.024

The relatively high uncertainty values are reasonable, since three different hamburgers were analysed for each sample at each time point, so the total content of lipids could vary between each replicate. These results evidenced that a statistically significant difference of oxidation between the meat packed in the blank and the one packed in the cellulose with 5% of moringa leaves extract is visible from day 9 ($p < 0.05$) and even more evident after 16 days ($p < 0.01$). The results of the two controls showed the rightness of the test development. Indeed, the sample with 5% of gallic acid showed a maintenance of the meat integrity over all the time of storage tested, evidencing a significant difference of lipid peroxidation in comparison with the blank ($p < 0.05$) after only 6 days. On the other hand, the meat packed in the cellulose coated with the varnish without the addition of any antioxidant agent evidenced a clear meat oxidation, which reached the 84% of the total lipid content after 16 days. In contrast, the lipid peroxidation of the moringa sample was calculated to be only 24% and the one with gallic acid 7%. The percentages of oxidation were calculated using the Equation 12:

Equation 12: $[(A_{d0} - A_{d16}) / A_{d0}] \times 100$

Where A_{d0} is the absorbance of the sample measured at day 0 and A_{d16} is the absorbance of the sample measured at day 16.

Therefore, the minced beef meat packed in the cellulose coated with 5% of the moringa leaves extract by maceration in methanol for 30 days demonstrated to be able to protect lipid peroxidation by 60% over 16 days of storage in the fridge.

5.4.3.2 Raman analysis of meat oxidation

The TBARS assay is an indirect method to assess the oxidation of meat or other foods, which require a previous extraction of the lipids contained in the sample by meat homogenization followed by lipids extraction in trichloroacetic acid. Thus, many studies have focused their attention on the development of direct, rapid and non-destructive methods for the analysis of oxidation over time. In this case vibrational spectroscopy results to be a very suitable technique as it requires minimal sample preparation to obtain a detailed chemical fingerprint of the sample.

In particular, Raman spectroscopy was already reported to follow the lipid oxidation of meat over time [136, 268]. In the work described by Moudache et al. [136] a step of lipid extraction from the meat was included and the samples were analysed by a special sample holder with silver nanoparticles employing the surface enhanced Raman spectroscopy (SERS) configuration.

However, in this work hamburgers were analysed directly without using any preparative steps or extractions by simple Raman spectroscopy configuration as a rapid and non-contact technique.

The Raman spectra of minced beef meat showed in Figure 52 were collected at different times: immediately after buying the meat (t_0, fresh meat), after 3 days (t_1, dashed line) or 16 days (t_{fin}, solid line) of storage in the fridge at 4 °C packed in the active packaging with 5% of moringa leaves extract (green lines) or 5% of gallic acid (pink lines). The results were compared with the ones packed in the blank cellulose. All the spectra were pre-processed for baseline correction to eliminate fluorescence contribution and normalized by the intensity of the signal at 1000 cm^{-1} which corresponds to aromatic rings stretching modes (Socrates, 2001), which do not vary their Raman intensity from one sample to another. At least 5 spectra were taken in different part of each meat sample and the average spectrum is displayed.

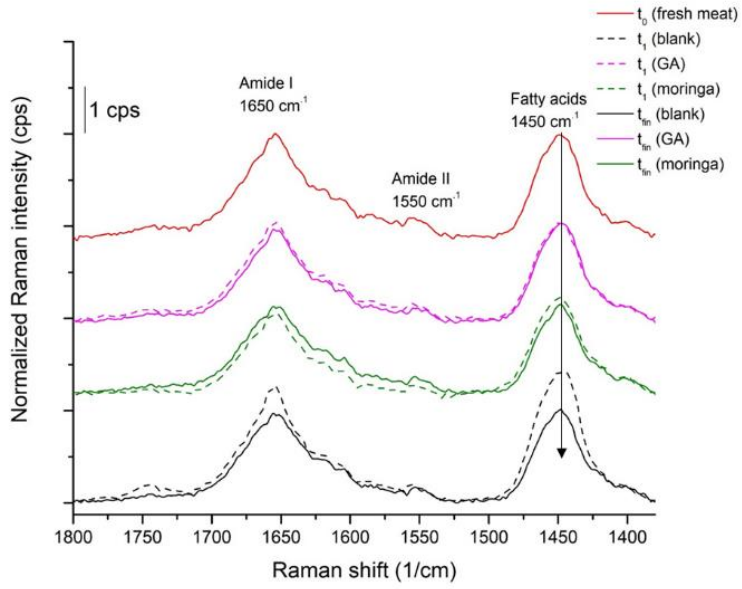

Figure 52: Raman *in situ* analysis of minced meat oxidation over time.
Raman spectra of minced beef meat immediately after buying it (red line, t_0), packed in blank (dark blue), in cellulose coated with moringa leaves extract (5%, green) or in cellulose coated with gallic acid (5%, pink) for 3 days (dashed lines, t_1) or 16 days (solid lines, t_{fin}). Spectra were corrected for the baseline and normalized for the intensity of the peak at 1000 cm^{-1} (aromatic rings). The Raman signals of amide I and II and of fatty acids were highlighted.

The Raman analysis of meat revealed that if the attention is focused on the bands relatives to fatty acids like the band at 1450 cm^{-1}, corresponding to $\delta(CH_2/CH_3)$, a significant decrease of the intensity over time could be detected. This effect is particulary evident in the blank sample, indicating an increasing of the total unsaturation of the fatty acids [136], due to the oxydation of meat over time. This decrease is drastically reduced in the sample packed in the cellulose with moringa extracts and even more in the sample packed in the cellulose with galic acid, in which the intensity of this signal after 16 days is nearly overlapped to that measured after 3 days. These results are perfectly in line with the findings reported by the TBARS assay and further confirm the protective action of cellulose with 5% of moringa leaves extract from lipid oxydation over time.

5.4.3.3 FT-IR analysis of meat oxydation

The same samples analysed by Raman spectroscopy were analysed also by FT-IR spectroscopy to obtain further information thanks to the complementarity of the two vibrational spectroscopy techniques. The ATR collection mode was used for better observation of protein conformation changes revealed by accurate comparison of the peaks associate to the amides. Thus, FT-IR spectra were collected in the range (400–4000) cm^{-1} and attention was focused on amide I (1640 cm^{-1}) and amide II (1570–1530) cm^{-1} signals [269]. As for proteins, the most evident changes are expected in this spectral region. These spectral changes, related to the O=C–NH peptidic bond of proteins, depend reasonably on structural changes involving intermolecular and intramolecular hydrogen bond interactions and on protein denaturation [270].

The spectra of the different samples of fresh meat, i.e. the day of purchase, (t_0) and after 16 days (t_{fin}) of storage in the fridge packed in the different cellulose-based samples were collected. After smoothing (Savitzky Golay filter, second order, 15 pt) and baseline correction (automatic weighted least squares regression performed by Omnic® software, the two amide peaks were deconvoluted as described in the materials and methods section (paragraph 5.2.7.5) and the ratios of the calculated areas under the curves were analysed (Figure 53).

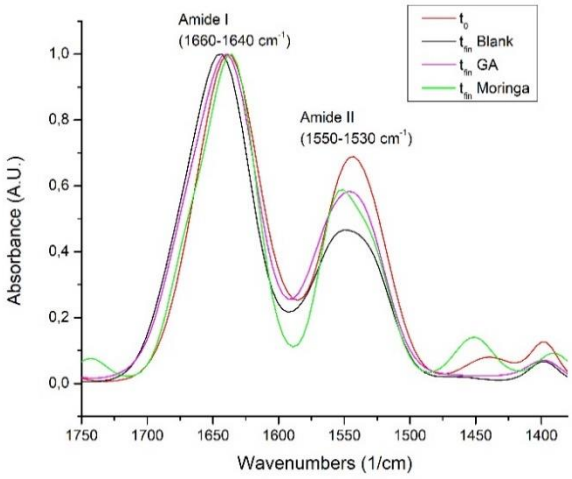

Figure 53: FT-IR spectra of Amide I and Amide II signals of minced beef meat over time.

FT-IR spectra of minced beef meat immediately after buying it (red line, t_0), packed in blank (dark blue), in cellulose coated with moringa leaves extract (5%, green) or in cellulose coated with gallic acid (5%, pink) for 16 days (t_{fin}).The spectra were smoothed and baseline corrected and normalized by the amide I band.

Table 23: Deconvoluted peak areas of Amide I and Amide II FT-IR signals of minced beef meat immediately after buying it (t_0) or stored in the cellulose packaging for 16 days (t_{fin}).

Sample	AmideI (1640-1680) cm^{-1}	Amide II (1570-1530) cm^{-1}	AmideII/AmideI
t_0	54.31	26.33	0.49
t_{fin} gallic acid	54.83	23.12	0.42
t_{fin} moringa	64.32	25.61	0.40
t_{fin} blank	61.20	18.23	0.30

Figure 53 showed a significant change in the ratio between amide II and amide I bands. In particular, this ratio reaches its maximum in the fresh meat, while it is significantly lower in the blank sample, i.e. the meat sample expected to deteriorate the most since it was stored in the absence of any antioxidant. The meat stored in contact with moringa extract and gallic acid showed intermediate values, with gallic acid being slightly more efficient in the meat freshness

preservation (Table 23). The decrease of the ratio of amide II over amide I due to the change of the whole protein pattern was previously reported in literature by Palaniappan (2009) [271], in accordance with the results here shown.

Moreover, a clear shift of amide I at higher frequency of the blank after 16 days in respect to time 0, which is less evident in the samples packed with moringa and gallic acid addictive films. The major shift registered for the blank sample, i.e. the meat stored in the absence of any antioxidant, attests the transition to a different protein conformation, which include the formation of more β-turns, which could be due to protein unfolding and denaturation process driven by oxidative phenomena [270]. The shift can be also partially due to a decrease of the component at (1630–1640) cm^{-1} (β-sheets) and it is observed in all the samples after 16 days but it is significantly more evident in the blank sample in respect to the samples stored in contact with gallic acid and moringa extract.

To confirm the previous observation, the amide I signal was further analysed by deconvoluting this band in two components at 1675 cm^{-1}, corresponding to turns, and at 1640 cm^{-1} relative to β sheets [271], to follow the proteins conformational changes over time (Figure 54 and Table 24).

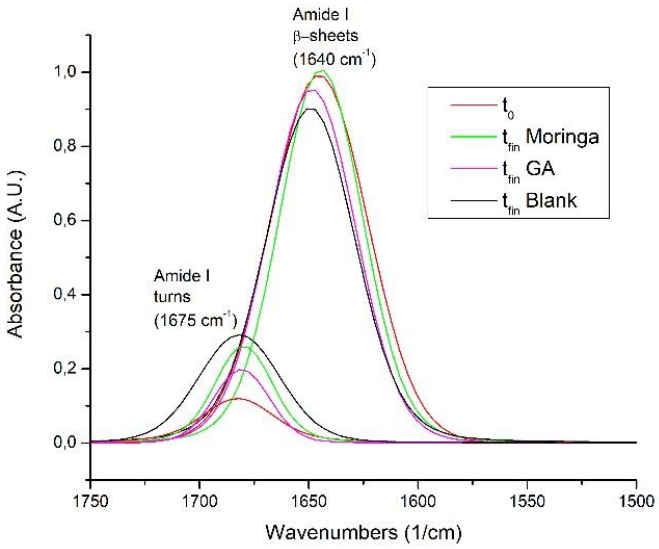

Figure 54: Deconvoluted components of FT-IR peak of Amide I in meat. Minced beef FT-IR analysis immediately after buying it (t_0) or after 16 days of storage in the cellulose packaging (t_{fin}) blank (blue line), with 5% of moringa (green line) or with 5% of GA (pink line).

Table 24: Deconvoluted FT-IR peak areas of Amide I signals in meat, immediately after buying it (t_0) or after 16 days (t_{fin}) of storage in the cellulose packaging.

Sample	AmideI (turns) 1680 cm^{-1}	Amide I (βsheet) 1640 cm^{-1}	Turns/βsheet
t_0	5.10	49.23	0.10
t_{fin} gallic acid	6.52	48.31	0.13
t_{fin} moringa	9.01	55.20	0.16
t_{fin} blank	13.72	47.51	0.29

The analysis of the area of the two deconvoluted components of the amide I band confirms the hypothesis that the (1670–1680) cm^{-1} component increases during the meat storage period, while a decrease of the component at 1640 cm^{-1} is registered. This demonstrates a change in the protein conformation over time, which is more evident for the blank sample and reduced for the meat stored in the presence of antioxidants. Again, the band area ratio attests that this effect is less severe in the meat stored into the packages with 5% (w/w) of moringa and gallic acid, confirming once more that the produced active package contributes to the preservation of meat over time reducing not only the oxidation of fats but also the protein degradation.

5.4.4 Polyphenols specific migration assay in food simulants

The extracts of moringa leaves, olive and grape that were chosen to be coated on the cellulose for their evident good antioxidant properties were used to build UV-VIS calibration curves, since they all contain polyphenolic molecules, they all present absorption bands at about 270-280 nm which demonstrated a trend proportional with extracts concentration. In particular, in this work the specific migration of polyphenols from the active films with moringa leaves, (M MAC Met 30d), olive, (O MAC Met 30d), and gallic acid was analysed. Acetic acid 3% (w/v) and ethanol 10% (v/v) were chosen as food simulants, indicated in the European normative (EU) No 10/2011 as food simulants A and B. They are assigned for foods that have a hydrophilic character and are able to extract hydrophilic substances and specified to be good simulants of meat ((EU) No 10/2011, table 2). UV-VIS measurements of the two solvents were taken after 10 days of contact with the active films at 40 °C, mimicking the worst foreseeable use possible.

For moringa extracts, a linear dynamic range at 268 nm was obtained between 36 mg/l and 175 mg/l in both the solvents with LOD and LOQ values of 4 mg/l

and 11 mg/l, respectively, for acetic acid, 10 mg/l and 29 mg/l for ethanol. For olive extracts the linear range was obtained at 279 nm between 16 mg/l and 420 mg/l in acetic acid, with LOD and LOQ values of 8 mg/l and 24 mg/l, respectively and between 156 mg/l and 420 mg/l for ethanol with LOD and LOQ values of 30 mg/l and 90 mg/l, respectively. Gallic acid was tested as well and a linearity range at 268 nm was found between 4 mg/l and 35 mg/l for acetic acid, with LOD and LOQ values of 1 mg/l and 2 mg/l, respectively, and between 8 mg/l and 47 mg/l for ethanol, with LOD and LOQ values of 0.3 mg/l and 1 mg/l, respectively. The results of the migration test are presented in Table 25.

Table 25: Selective polyphenols migration test results of moringa, olive, and gallic acid active films expressed as mg of polyphenols per kg of meat and per dm^2 of film.

Sample	Migration (mg/kg) in simulant A (ethanol 10%)	Migration (mg/dm^2)	Migration (mg/kg) in simulant B (acetic acid 3%)	Migration (mg/dm^2)
Olive MAC Met 30d	229 ± 149	38 ± 25	28 ± 10	5 ± 2
Moringa MAC Met 30d	51 ± 7	8 ± 1	64 ± 18	11 ± 3
Gallic acid	43 ± 13	7 ± 2	34 ± 7	6 ± 1

From this analysis it resulted that the cellulose-based active film with 5% of moringa leaves extract showed a migration of its polyphenolic component in simulant A, of (51 ± 7) mg/kg of simulant, which corresponds to (8 ± 1) mg/dm^2 of active packaging. However, in simulant B it showed a higher release. This could be due to the higher pH and higher polarity of this kind of simulant. The olive active packaging revealed a migration in simulant B which is far lower than that evidenced in simulant A. Indeed, celluolose with olive extract coating demonstrated to be the one which released the higher quantity of polyphenols in ethanol 10%. This could be a good property if the positive effect in food preservation of polyphenolic compounds is considered, but could also represent an issue to face when a total migration analysis is performed and the results must be below the normative limits of 10 mg/cm^2. On the other hand, gallic acid active

film showed a release of polyphenols that is comparable to that observed for moringa active film.

5.5 Conclusion of part III

Extracts of *Moringa oleifera* leaves and olives and grapes industrial waste obtained by SAE and MAC revealed to have the highest antioxidant efficacy, by both DPPH and ORAC assays, due to their highest content of polyphenols and other active molecules such as gallic acid. However, grape extracts exhibited the lowest EC_{50} and the highest ORAC values related to higher total content of polyphenols, determined by both the Folin-Ciocalteu assay and UPLC-TQ-MS, followed by moringa leaves and by olive extracts. The latter demonstrated the lowest antioxidant activity and a lower content of active molecules which could be due to their more lipophilic composition.

Among all macerates, methanol revealed to be the solvent with the highest extraction yield of active compounds, followed by ethanol and acetone thanks to their higher polarity and affinity with phenolic molecules. As for grapes, also water resulted to extract fractions with high antioxidant efficacy.

Active cellulose films with 5% (w/w) of the two macerates of each plant material which exhibited the highest antioxidant properties were produced by coating (moringa and olive extracts) or by inclusion of the active agent in the adhesive between two layers of cellulose (grape extracts). The film coated with moringa MAC Met 30d showed the highest antioxidant properties in both DPPH and free radical scavenging assays. Then, the TBARS assay analysis of minced beef meat, packed with this active film and stored in the fridge for 16 days, revealed significantly reduced lipid peroxidation over time in comparison with samples packed in simple cellulose without moringa (blank). The produced active packaging demonstrated to protect meat from lipid peroxidation by 60% over 16 days. This protective action was also confirmed by *in situ* vibrational spectroscopy analysis, i.e. Raman and FT-IR spectroscopies, measuring the lipids oxidation and changing of protein conformation over time directly on the meat, avoiding any extractive step.

Additionally, the specific release of polyphenols from the moringa active packaging in food simulant (acetic acid 3%) resulted to be (8 ± 1) mg/dm^2. This could be a very good result, but needed to be further investigated by a total migration analysis to assess if this packaging material complies with the migration limits settled by the European normative (EU) No 10/2011.

In conclusion, this work demonstrated the comparability and reliability of data obtained employing many different analytical techniques. Furthermore, novel natural active agents revealed their antioxidant efficacy in different food packaging systems both *in vitro* or applied on minced beef meat. Therefore, this work could open the way to the production of innovative, safer and sustainable active packaging systems suggesting a novel way to employ food industry related waste.

Chapter 6

General Conclusions

In this Doctoral thesis a novel DEP-Raman approach, which allows to rapidly identify and classify different bacterial strains, thanks to their specific Raman chemical fingerprint, was developed. This method was optimized to analyse bacteria directly in liquid suspension enabling dynamic analysis of living cells in their natural environment. Thus, their response to different treatments, including antibiotic or biocides, can be followed real-time without the need of any staining, minimizing sample preparation process. Furthermore, this method, coupled with machine learning techniques, was used to build statistical models able to evaluate bacterial susceptibility to antibiotics and to reveal the insurgence of cross-induced tolerance phenomena with high sensitivity and specificity within hours, reducing the time consuming steps required by classical microbiological techniques. The reliability of this method was confirmed by comparing the results with those obtained by standard microbiological assays.

Moreover, it was demonstrated that Raman hyperspectral imaging combined with machine learning allows to detect the spatial distribution of different biomolecules at sub-micrometre level, enabling to detect actually dividing single bacterial cells.

Innovative active antibacterial materials based on silver and carbon nanoparticles were here developed and characterized. In particular, the SMBC of differently sized AgNPs attached on glass surfaces was evaluated, for the first time, by the ISO 22196:2011. The introduction of a value that determines the minimum concentration of antibacterial agent needed on a surface to eliminate the 99.9999% of bacteria, which is measurable by an international standard method,

facilitates comparisons between different measurements, materials and laboratories. This assumes a great importance, for instance, during the development of innovative active food packaging materials because it enables to obtain an optimal characterization of their antibacterial properties and to minimize the concentration of antibacterial agents present on the materials' surface, thus reducing their eventual toxicity and the cost of production.

Novel CNP, obtained from glucose by a green synthesis process, were also tested against both Gram + and Gram – bacteria as more biocompatible and safer nanomaterial. Their interaction with bacterial cells was dynamically followed directly in the culture medium by the developed DEP-Raman method. This allowed investigating the cells defensive mechanisms to external stimuli by the presence of specific Raman signals related to ECM production. Starting from these observations, new strategies for the production of an efficient CNP-based antibacterial system could be defined. For instance, their combination with antimicrobial peptides, which was here demonstrated to be a successful path, especially against Gram + bacteria, or, in future projects, by exploiting their proved photothermic and photodynamic activity. These characteristics, together with their possible degradability by the human body, offer a fertile ground for their employment in novel antibacterial food packaging systems.

Another important study was focused on natural active agents to be included in more sustainable active packaging systems. In particular, extracts of grapes and olives from food industry waste and moringa leaves, obtained by different extraction methods, including SFE, SAE and MAC, were characterized and compared for their antioxidant properties by different techniques. The highest antioxidant efficacy was highlighted in fractions obtained by SAE and MAC, which was related to a higher content of polyphenols, in particular gallic acid. Active cellulose-based packaging systems, here chosen as model biodegradable biopolymer, were produced by coating and multilayer techniques, including 5% (w/w) of the highest effective macerates, as more sustainable extraction process. The active packaging produced by coating of moringa MAC Met 30d demonstrated to protect minced beef meat from lipid oxidation by 60% over 16 days, as confirmed by TBARS assay.

Moreover, an *in situ* analysis of the meat oxidation over time was performed by vibrational spectroscopy techniques, involving Raman spectroscopy for the direct evaluation of the lipids oxidation, avoiding any destructive extraction steps, and FT-IR spectroscopy to investigate the conformational changes related to the degradation of the biological matrix over time.

The specific migration of polyphenols from the produced active packaging materials after 10 days of incubation at 40 °C, as the worst storage condition possible for meat, was analysed in two food simulants. The values of polyphenols migration measured resulted to be reasonably low for all the materials tested, a part from the olive active packaging in ethanol 10%. Although, to demonstrate that novel materials are in compliance with the (EU) No 10/2011 limits, a total migration analysis is needed and it will be further performed.

In summary, a huge variety of materials were here analysed for their antibacterial and antioxidant properties with many different techniques.

In particular, the importance to compare results obtained by different antioxidant assays was highlighted here by the fact that distinct properties of the natural extracts were considered, obtaining a more global evaluation of their antioxidant activity. Some differences that emerged between the results underline the importance of adopting a metrological approach of characterization, employing standard procedures, including AOAC methods and ISO, and a proper evaluation of the measurement uncertainty budget in order to ensure the data comparability and their traceability to the SI.

As regards novel active packaging development, it emerged that the analysis of their actual application on real biological matrices is fundamental to understand their real effectiveness and functioning.

Furthermore, this work stressed out the versatility of direct, non-destructive and rapid methods, such as vibrational spectroscopies, in many application fields from the study of microorganisms, and their interactions with nanomaterials, to *in situ* real-time assays in order to dynamically follow different effects over time.

Also in this case, in which innovative methodologies are proposed, metrology resulted fundamental to validate them and ensure the reliability of data obtained with these techniques by constant comparisons with standard methodologies.

References

[1] Arvanitoyannis, I. (2005) 'Food packaging technology. Edited by R Coles, D McDowell and MJ Kirwan. Blackwell Publishing, CRC Press, Oxford, 2003. 346 pp ISBN 0-8493-97788-X', *Journal of the Science of Food and Agriculture*. doi:10.1002/jsfa.2089.

[2] Marsh, K. and Bugusu, B. (2007) 'Food packaging - Roles, materials, and environmental issues: Scientific status summary', *Journal of Food Science*. doi:10.1111/j.1750-3841.2007.00301.x.

[3] Miltz, J., Raz, I. and Passy, N. (1995) 'Shelf-life of grapefruit segments in multilayer plastic trays', *LWT - Food Science and Technology*. doi:10.1016/0023-6438(95)90029-2.

[4] Rooney, M.L. (1995) 'Overview of active food packaging', in *Active Food Packaging*. doi:10.1007/978-1-4615-2175-4_1.

[5] Hotchkiss, J.H. (1997) 'Food-packaging interactions influencing quality and safety', *Food Additives and Contaminants*. doi:10.1080/02652039709374572.

[6] Mane, K.A. (2016) 'A Review on Active Packaging: An Innovation in Food Packaging', *International Journal of Environment, Agriculture and Biotechnology*. doi:10.22161/ijeab/1.3.35.

[7] Mills, A. and Hazafy, D. (2009) 'Nanocrystalline SnO2-based, UVB-activated, colourimetric oxygen indicator', *Sensors and Actuators, B: Chemical*. doi:10.1016/j.snb.2008.12.048.

[8] Robertson, G.L. (2013) 'Food Packaging: Principles and Practice, Third Edition', *Taylor & Francis Group*.

[9] Restuccia, D., Spizzirri, U.G., Parisi, O.I., Cirillo, G., Curcio, M., Iemma, F., Puoci, F., Vinci, G. and Picci, N. (2010) 'New EU regulation aspects and global market of active and intelligent packaging for food industry applications', *Food Control*. doi:10.1016/j.foodcont.2010.04.028.

[10] Sivertsvik, M. (2007) 'Lessons from other commodities: Fish and meat', in *Intelligent and Active Packaging for Fruits and Vegetables*. doi:10.1201/9781420008678-12.

[11] Floros, Dock and Han (2000) 'Active packaging technologies and applications.', *Food, Cosmetics and Drug Packaging*.

[12] Brody, A.L., Bugusu, B., Han, J.H., Sand, C.K. and McHugh, T.H. (2008) 'Innovative food packaging solutions', *Journal of Food Science*. doi:10.1111/j.1750-3841.2008.00933.x.

[13] Biji, K.B., Ravishankar, C.N., Mohan, C.O. and Srinivasa Gopal, T.K. (2015) 'Smart packaging systems for food applications: a review', *Journal of Food Science and Technology*. doi:10.1007/s13197-015-1766-7.

[14] Rhim, J.W., Park, H.M. and Ha, C.S. (2013) 'Bio-nanocomposites for food packaging applications', *Progress in Polymer Science*. doi:10.1016/j.progpolymsci.2013.05.008.

[15] Caillol, S. (2020) 'Special Issue "Natural Polymers and Biopolymers II"', *Molecules (Basel, Switzerland)*. doi:10.3390/molecules26010112.

[16] Ammala, A., Bateman, S., Dean, K., Petinakis, E., Sangwan, P., Wong, S., Yuan, Q., Yu, L., Patrick, C. and Leong, K.H. (2011) 'An overview of degradable and biodegradable polyolefins', *Progress in Polymer Science (Oxford)*. doi:10.1016/j.progpolymsci.2010.12.002.

[17] Chen, G.Q. and Patel, M.K. (2012) 'Plastics derived from biological sources: Present and future: A technical and environmental review', *Chemical Reviews*. doi:10.1021/cr200162d.

[18] Karak, N. (2012) *Vegetable oil-based polymers: Properties, processing and applications*, *Vegetable Oil-Based Polymers: Properties, Processing and Applications*. doi:10.1533/9780857097149.

[19] Liu, C., Wang, Shujun, Chang, X. and Wang, Shuo (2015) 'Structural and functional properties of starches from Chinese chestnuts', *Food Hydrocolloids*. doi:10.1016/j.foodhyd.2014.07.014.

[20] Heinze, T. (2016) *Cellulose Chemistry and Properties: Fibers, Nanocelluloses and Advanced Materials*, *Advances in Polymer Science 271*.

[21] Rinaudo, M. (2006) 'Chitin and chitosan: Properties and applications', *Progress in Polymer Science (Oxford)*. doi:10.1016/j.progpolymsci.2006.06.001.

[22] Yarnpakdee, S., Benjakul, S. and Kingwascharapong, P. (2015) 'Physico-chemical and gel properties of agar from Gracilaria tenuistipitata from the lake of Songkhla, Thailand', *Food Hydrocolloids*. doi:10.1016/j.foodhyd.2015.05.004.

[23] Lee, K.Y. and Mooney, D.J. (2012) 'Alginate: Properties and biomedical applications', *Progress in Polymer Science (Oxford)*. doi:10.1016/j.progpolymsci.2011.06.003.

[24] Guiraldo, R.D., Berger, S.B., Consani, R.L.X., Consani, S., De Carvalho, R.V., Lopes, M.B., Meneghel, L.L., Da Silva, F.B. and Sinhoreti, M.A.C. (2014) 'Characterization of morphology and composition of inorganic fillers in dental alginates', *BioMed Research International*. doi:10.1155/2014/178064.

[25] Zhang, Y., Rempel, C. and McLaren, D. (2014) 'Chapter 16 – Thermoplastic Starch', in *Innovations in Food Packaging*.

[26] Fischer, S., Thümmler, K., Volkert, B., Hettrich, K., Schmidt, I. and Fischer, K. (2008) 'Properties and applications of cellulose acetate', in *Macromolecular Symposia*. doi:10.1002/masy.200850210.

[27] Nabipour Chakoli, A. (2019) 'Poly(L-Lactide) Bionanocomposites', in *Peptide Synthesis*. doi:10.5772/intechopen.85035.

[28] Israni, N. and Shivakumar, S. (2019) 'Polyhydroxybutyrate: Development and applications as a biodegradable biotextile', in *Materials for Biomedical Engineering: Biopolymer Fibers*. doi:10.1016/B978-0-12-816872-1.00014-5.

[29] Pachekoski, W.M., Agnelli, J.A.M. and Belem, L.P. (2009) 'Thermal, mechanical and morphological properties of poly (hydroxybutyrate) and polypropylene blends after processing', *Materials Research*. doi:10.1590/S1516-14392009000200008.

[30] Tebaldi, M.L., Maia, A.L.C., Poletto, F., de Andrade, F.V. and Soares, D.C.F. (2019) 'Poly(-3-hydroxybutyrate-co-3-hydroxyvalerate) (PHBV): Current advances in synthesis methodologies, antitumor applications and biocompatibility', *Journal of Drug Delivery Science and Technology*. doi:10.1016/j.jddst.2019.02.007.

[31] Bruna, J.E., Galotto, M.J., Guarda, A. and Rodríguez, F. (2014) 'A novel polymer based on MtCu2+/cellulose acetate with antimicrobial activity', *Carbohydrate Polymers*. doi:10.1016/j.carbpol.2013.11.038.

[32] Emblem, A. (2012) 'Plastics properties for packaging materials', in *Packaging Technology*. doi:10.1533/9780857095701.2.287.

[33] Cao, J., Sun, X., Lu, C., Zhou, Z., Zhang, X. and Yuan, G. (2016) 'Water-soluble cellulose acetate from waste cotton fabrics and the aqueous processing of all-cellulose composites', *Carbohydrate Polymers*. doi:10.1016/j.carbpol.2016.04.086.

[34] Cao, L., Luo, G., Tsang, D.C.W., Chen, H., Zhang, S. and Chen, J. (2018) 'A novel process for obtaining high quality cellulose acetate from green landscaping waste', *Journal of Cleaner Production*. doi:10.1016/j.jclepro.2017.12.077.

[35] Marrez, D.A., Abdelhamid, A.E. and Darwesh, O.M. (2019) 'Eco-friendly cellulose acetate green synthesized silver nano-composite as antibacterial packaging system for food safety', *Food Packaging and Shelf Life*. doi:10.1016/j.fpsl.2019.100302.

[36] Ach, A. (1993) 'Biodegradable plastics based on cellulose acetate', *Journal of Macromolecular Science, Part A*. doi:10.1080/10601329308021259.

[37] Malhotra, B., Keshwani, A. and Kharkwal, H. (2015) 'Antimicrobial food packaging: Potential and pitfalls', *Frontiers in Microbiology*. doi:10.3389/fmicb.2015.00611.

[38] Muriel-Galet, V., López-Carballo, G., Gavara, R. and Hernández-Muñoz, P. (2012) 'Antimicrobial food packaging film based on the release of LAE from EVOH', *International Journal of Food Microbiology*. doi:10.1016/j.ijfoodmicro.2012.05.009.

[39] Suppakul, P., Miltz, J., Sonneveld, K. and Bigger, S.W. (2003) 'Active packaging technologies with an emphasis on antimicrobial packaging and its applications', *Journal of Food Science*. doi:10.1111/j.1365-2621.2003.tb05687.x.

[40] Kuorwel, K.K., Cran, M.J., Sonneveld, K., Miltz, J. and Bigger, S.W. (2011) 'Essential Oils and Their Principal Constituents as Antimicrobial Agents for Synthetic Packaging Films', *Journal of Food Science*. doi:10.1111/j.1750-3841.2011.02384.x.

[41] Fang, Z., Zhao, Y., Warner, R.D. and Johnson, S.K. (2017) 'Active and intelligent packaging in meat industry', *Trends in Food Science and Technology*. doi:10.1016/j.tifs.2017.01.002.

[42] Kerry, J.P., O'Grady, M.N. and Hogan, S.A. (2006) 'Past, current and potential utilisation of active and intelligent packaging systems for meat and muscle-based products: A review', *Meat Science*. doi:10.1016/j.meatsci.2006.04.024.

[43] Realini, C.E. and Marcos, B. (2014) 'Active and intelligent packaging systems for a modern society', *Meat Science*. doi:10.1016/j.meatsci.2014.06.031.

[44] Jayasena, D.D. and Jo, C. (2013) 'Essential oils as potential antimicrobial agents in meat and meat products: A review', *Trends in Food Science and Technology*. doi:10.1016/j.tifs.2013.09.002.

[45] Han, J.H. (2000) 'Antimicrobial Food Packaging', *Food Technology*. doi:10.1533/9781855737020.1.50.

[46] Quintavalla, S. and Vicini, L. (2002) 'Antimicrobial food packaging in meat industry', *Meat Science*. doi:10.1016/S0309-1740(02)00121-3.

[47] Mauriello, G., De Luca, E., La Storia, A., Villani, F. and Ercolini, D. (2005) 'Antimicrobial activity of a nisin-activated plastic film for food packaging', *Letters in Applied Microbiology*. doi:10.1111/j.1472-765X.2005.01796.x.

[48] Han, J.H. (2003) 'Antimicrobial food packaging', in *Novel Food Packaging Techniques*. doi:10.1016/B978-1-85573-675-7.50008-0.

[49] López, P., Sánchez, C., Batlle, R. and Nerín, C. (2007) 'Development of flexible antimicrobial films using essential oils as active agents', *Journal of Agricultural and Food Chemistry*. doi:10.1021/jf071737b.

[50] Hyldgaard, M., Mygind, T. and Meyer, R.L. (2012) 'Essential oils in food preservation: Mode of action, synergies, and interactions with food matrix components', *Frontiers in Microbiology*. doi:10.3389/fmicb.2012.00012.

[51] Youssef, A.M. and El-Sayed, S.M. (2018) 'Bionanocomposites materials for food packaging applications: Concepts and future outlook', *Carbohydrate Polymers*. doi:10.1016/j.carbpol.2018.03.088.

[52] Zhang, L., Jiang, Y., Ding, Y., Povey, M. and York, D. (2007) 'Investigation into the antibacterial behaviour of suspensions of ZnO nanoparticles (ZnO nanofluids)', *Journal of Nanoparticle Research*. doi:10.1007/s11051-006-9150-1.

[53] Slavin, Y.N., Asnis, J., Häfeli, U.O. and Bach, H. (2017) 'Metal nanoparticles: Understanding the mechanisms behind antibacterial activity', *Journal of Nanobiotechnology*, 15(1), pp. 1–20. doi:10.1186/s12951-017-0308-z.

[54] Torres-Giner, S., Wilkanowicz, S., Melendez-Rodriguez, B. and Lagaron, J.M. (2017) 'Nanoencapsulation of Aloe vera in Synthetic and Naturally Occurring Polymers by Electrohydrodynamic Processing of Interest in Food Technology and Bioactive Packaging', *Journal of Agricultural and Food Chemistry*. doi:10.1021/acs.jafc.7b01393.

[55] Perinelli, D.R., Fagioli, L., Campana, R., Lam, J.K.W., Baffone, W., Palmieri, G.F., Casettari, L. and Bonacucina, G. (2018) 'Chitosan-based nanosystems and their exploited antimicrobial activity', *European Journal of Pharmaceutical Sciences*. doi:10.1016/j.ejps.2018.01.046.

[56] Almasi, H., Jafarzadeh, P. and Mehryar, L. (2018) 'Fabrication of novel nanohybrids by impregnation of CuO nanoparticles into bacterial cellulose and chitosan nanofibers: Characterization, antimicrobial and release properties', *Carbohydrate Polymers*. doi:10.1016/j.carbpol.2018.01.067.

[57] Hoseinnejad, M., Jafari, S.M. and Katouzian, I. (2018) 'Inorganic and metal nanoparticles and their antimicrobial activity in food packaging applications', *Critical Reviews in Microbiology*. doi:10.1080/1040841X.2017.1332001.

[58] Huang, Z., Jiang, X., Guo, D. and Gu, N. (2011) 'Controllable synthesis and biomedical applications of silver nanomaterials', *Journal of Nanoscience and Nanotechnology*, pp. 9395–9408. doi:10.1166/jnn.2011.5317.

[59] Kim, J.S., Kuk, E., Yu, K.N., Kim, J.H., Park, S.J., Lee, H.J., Kim, S.H., Park, Y.K., Park, Y.H., Hwang, C.Y., Kim, Y.K., Lee, Y.S., Jeong, D.H. and Cho, M.H. (2007) 'Antimicrobial effects of silver nanoparticles', *Nanomedicine: Nanotechnology, Biology, and Medicine*, 3(1), pp. 95–101. doi:10.1016/j.nano.2006.12.001.

[60] P., G., C., G., X., S., Q., Z., S.S., L., C., T., Y., C., M.B., C.-P., M.W., C., K., W., R., X., Gunawan, P., Guan, C., Song, X., Zhang, Q., Leong, S.S., Tang, C., Chen, Y., Chan-Park, M.B., Chang, M.W., Wang, K. and Xu, R. (2011) 'Hollow fiber membrane decorated with Ag/MWNTs: toward effective water disinfection and biofouling control', *ACS nano*, 5(12), pp. 10033–10040. doi:10.1021/nn2038725; 10.1021/nn2038725.

[61] Siddiqi, K.S., Husen, A. and Rao, R.A.K. (2018) 'A review on biosynthesis of silver nanoparticles and their biocidal properties', *Journal of Nanobiotechnology*. doi:10.1186/s12951-018-0334-5.

[62] Zhao, G. and Stevens, S.E. (1998) 'Multiple parameters for the comprehensive evaluation of the susceptibility of Escherichia coli to the silver ion', *BioMetals*, 11(1), pp. 27–32.

doi:10.1023/A:1009253223055.

[63] Drake, P.L. and Hazelwood, K.J. (2005) 'Exposure-related health effects of silver and silver compounds: A review', *Annals of Occupational Hygiene*. doi:10.1093/annhyg/mei019.

[64] Mijnendonckx, K., Leys, N., Mahillon, J., Silver, S. and Van Houdt, R. (2013) 'Antimicrobial silver: Uses, toxicity and potential for resistance', *BioMetals*. doi:10.1007/s10534-013-9645-z.

[65] Li, W.R., Xie, X.B., Shi, Q.S., Zeng, H.Y., Ou-Yang, Y.S. and Chen, Y. Ben (2010) 'Antibacterial activity and mechanism of silver nanoparticles on Escherichia coli', *Applied Microbiology and Biotechnology*, 85(4), pp. 1115–1122. doi:10.1007/s00253-009-2159-5.

[66] Chernousova, S. and Epple, M. (2013) 'Silver as antibacterial agent: Ion, nanoparticle, and metal', *Angewandte Chemie - International Edition*, pp. 1636–1653. doi:10.1002/anie.201205923.

[67] Cho, K.H., Park, J.E., Osaka, T. and Park, S.G. (2005) 'The study of antimicrobial activity and preservative effects of nanosilver ingredient', in *Electrochimica Acta*, pp. 956–960. doi:10.1016/j.electacta.2005.04.071.

[68] Knetsch, M.L.W. and Koole, L.H. (2011) 'New strategies in the development of antimicrobial coatings: The example of increasing usage of silver and silver nanoparticles', *Polymers*. doi:10.3390/polym3010340.

[69] Gangadharan, D., Harshvardan, K., Gnanasekar, G., Dixit, D., Popat, K.M. and Anand, P.S. (2010) 'Polymeric microspheres containing silver nanoparticles as a bactericidal agent for water disinfection', *Water Research*. doi:10.1016/j.watres.2010.06.057.

[70] Carbone, M., Donia, D.T., Sabbatella, G. and Antiochia, R. (2016) 'Silver nanoparticles in polymeric matrices for fresh food packaging', *Journal of King Saud University - Science*. doi:10.1016/j.jksus.2016.05.004.

[71] Ghiazza, M., Vietti, G. and Fenoglio, I. (2014) 'Carbon nanotubes: Properties, applications, and toxicity', in *Health and Environmental Safety of Nanomaterials: Polymer Nancomposites and Other Materials Containing Nanoparticles*. doi:10.1533/9780857096678.3.147.

[72] Galadari, S., Rahman, A., Pallichankandy, S. and Thayyullathil, F. (2017) 'Reactive oxygen species and cancer paradox: To promote or to suppress?', *Free Radical Biology and Medicine*. doi:10.1016/j.freeradbiomed.2017.01.004.

[73] Liu, X., Sen, S., Liu, J., Kulaots, I., Geohegan, D., Kane, A., Puretzky, A.A., Rouleau, C.M., More, K.L., Palmore, G.T.R. and Hurt, R.H. (2011) 'Antioxidant deactivation on graphenic nanocarbon surfaces', *Small*. doi:10.1002/smll.201100651.

[74] Kokalari, I., Gassino, R., Giovannozzi, A.M., Croin, L., Gazzano, E., Bergamaschi, E., Rossi, A.M., Perrone, G., Riganti, C., Ponti, J. and Fenoglio, I. (2019) 'Pro- and anti-oxidant properties of near-infrared (NIR) light responsive carbon nanoparticles', *Free Radical Biology and Medicine*. doi:10.1016/j.freeradbiomed.2019.01.013.

[75] Miao, Z.H., Wang, H., Yang, H., Li, Z., Zhen, L. and Xu, C.Y. (2016) 'Glucose-Derived Carbonaceous Nanospheres for Photoacoustic Imaging and Photothermal Therapy', *ACS Applied Materials and Interfaces*. doi:10.1021/acsami.6b03652.

[76] Kumar, P., Huo, P., Zhang, R. and Liu, B. (2019) 'Antibacterial properties of graphene-based nanomaterials', *Nanomaterials*. doi:10.3390/nano9050737.

[77] Demir-Cakan, R., Baccile, N., Antonietti, M. and Titirici, M.M. (2009) 'Carboxylate-rich carbonaceous materials via one-step hydrothermal carbonization of glucose in the presence of acrylic acid', *Chemistry of Materials*. doi:10.1021/cm802141h.

[78] Yi, Z., Liang, Y., Lei, X., Wang, C. and Sun, J. (2007) 'Low-temperature synthesis of nanosized disordered carbon spheres as an anode material for lithium ion batteries', *Materials Letters*. doi:10.1016/j.matlet.2007.01.054.

[79] Kokalari, I., Keshavan, S., Rahman, M., Gazzano, E., Barzan, G., Mandrile, L., Giovannozzi, A., Ponti, J., Antonello, G., Monopoli, M., Perrone, G., Bergamaschi, E., Riganti, C., Fadeel, B. and Fenoglio, I. (2021) 'Efficacy, biocompatibility and degradability of carbon nanoparticles for photothermal therapy of lung cancer', *Nanomedicine*. doi:10.2217/nnm-2021-0009.

[80] Soddu, L., Trinh, D.N., Dunne, E., Kenny, D., Bernardini, G., Kokalari, I., Marucco, A., Monopoli, M.P. and Fenoglio, I. (2020) 'Identification of physicochemical properties that modulate nanoparticle aggregation in blood', *Beilstein Journal of Nanotechnology*. doi:10.3762/bjnano.11.44.

[81] Burt, S. (2004) 'Essential oils: Their antibacterial properties and potential applications in foods - A review', *International Journal of Food Microbiology*. doi:10.1016/j.ijfoodmicro.2004.03.022.

[82] Busatta, C., Vidal, R.S., Popiolski, A.S., Mossi, A.J., Dariva, C., Rodrigues, M.R.A., Corazza, F.C., Corazza, M.L., Vladimir Oliveira, J. and Cansian, R.L. (2008) 'Application of Origanum majorana L. essential oil as an antimicrobial agent in sausage', *Food Microbiology*. doi:10.1016/j.fm.2007.07.003.

[83] Grower, J.L., Cooksey, K. and Getty, K.J.K. (2004) 'Development and characterization of an antimicrobial packaging film coating containing nisin for inhibition of Listeria monocytogenes', *Journal of Food Protection*. doi:10.4315/0362-028X-67.3.475.

[84] Ćwiek-Ludwicka, K. and Ludwicki, J.K. (2017) 'Nanomaterials in food contact materials; considerations for risk assessment', *Roczniki Panstwowego Zakladu Higieny*.

[85] Piperigkou, Z., Karamanou, K., Engin, A.B., Gialeli, C., Docea, A.O., Vynios, D.H.,

Pavão, M.S.G., Golokhvast, K.S., Shtilman, M.I., Argiris, A., Shishatskaya, E. and Tsatsakis, A.M. (2016) 'Emerging aspects of nanotoxicology in health and disease: From agriculture and food sector to cancer therapeutics', *Food and Chemical Toxicology*. doi:10.1016/j.fct.2016.03.003.

[86] Nerin, C., Alfaro, P., Aznar, M. and Domeño, C. (2013) 'The challenge of identifying non-intentionally added substances from food packaging materials: A review', *Analytica Chimica Acta*, 775, pp. 14–24. doi:10.1016/j.aca.2013.02.028.

[87] Klančnik, A., Piskernik, S., Jeršek, B. and Možina, S.S. (2010) 'Evaluation of diffusion and dilution methods to determine the antibacterial activity of plant extracts', *Journal of Microbiological Methods*. doi:10.1016/j.mimet.2010.02.004.

[88] Ando, Y., Miyamoto, H., Noda, I., Miyaji, F., Shimazaki, T., Yonekura, Y., Miyazaki, M., Mawatari, M. and Hotokebuchi, T. (2010) 'Effect of bacterial media on the evaluation of the antibacterial activity of a biomaterial containing inorganic antibacterial reagents or antibiotics', *Biocontrol Science*. doi:10.4265/bio.15.15.

[89] Kumar, R., Howdle, S. and Münstedt, H. (2005) 'Polyamide/silver antimicrobials: Effect of filler types on the silver ion release', *Journal of Biomedical Materials Research - Part B Applied Biomaterials*. doi:10.1002/jbm.b.30306.

[90] Wiegand, C., Völpel, A., Ewald, A., Remesch, M., Kuever, J., Bauer, J., Griesheim, S., Hauser, C., Thielmann, J., Tonndorf-Martini, S., Sigusch, B.W., Weisser, J., Wyrwa, R., Elsner, P., Hipler, U.C., Roth, M., Dewald, C., Lüdecke-Beyer, C. and Bossert, J. (2018) 'Critical physiological factors influencing the outcome of antimicrobial testing according to ISO 22196 / JIS Z 2801', *PLoS ONE*. doi:10.1371/journal.pone.0194339.

[91] Who (2014) 'ANTIMICROBIAL RESISTANCE Global Report on Surveillance 2014', *World Health Organization*.

[92] Chapman, J.S. (2003) 'Disinfectant resistance mechanisms, cross-resistance, and co-resistance', in *International Biodeterioration and Biodegradation*, pp. 271–276. doi:10.1016/S0964-8305(03)00044-1.

[93] Jutkina, J., Marathe, N.P., Flach, C.F. and Larsson, D.G.J. (2018) 'Antibiotics and common antibacterial biocides stimulate horizontal transfer of resistance at low concentrations', *Science of the Total Environment*, 616–617, pp. 172–178. doi:10.1016/j.scitotenv.2017.10.312.

[94] Jorgensen, J.H. and Ferraro, M.J. (2002) 'Antimicrobial Susceptibility Testing: Special Needs for Fastidious Organisms and Difficult-to-Detect Resistance Mechanisms', *Clinical Infectious Diseases*, 30(5), pp. 799–808. doi:10.1086/313788.

[95] Sibley, C.D., Peirano, G. and Church, D.L. (2012) 'Molecular methods for pathogen and microbial community detection and characterization: Current and potential application in diagnostic microbiology', *Infection, Genetics and Evolution*. doi:10.1016/j.meegid.2012.01.011.

[96] Lupo, A., Papp-Wallace, K.M., Bonomo, R.A. and Endimiani, A. (2015) 'Non-Phenotypic Tests to Detect and Characterize Antibiotic Resistance Mechanisms in Enterobacteriaceae', in *Antimicrobial Resistance and Food Safety: Methods and Techniques*. doi:10.1016/B978-0-12-801214-7.00012-0.

[97] Schröder, U.C., Beleites, C., Assmann, C., Glaser, U., Hübner, U., Pfister, W., Fritzsche, W., Popp, J. and Neugebauer, U. (2015) 'Detection of vancomycin resistances in enterococci within 3 1/2; Hours', *Scientific Reports*, 5, pp. 1–7. doi:10.1038/srep08217.

[98] Kirchhoff, J., Glaser, U., Bohnert, J.A., Pletz, M.W., Popp, J. and Neugebauer, U. (2018) 'Simple Ciprofloxacin Resistance Test and Determination of Minimal Inhibitory Concentration within 2 h Using Raman Spectroscopy', *Analytical Chemistry*, 90(3), pp. 1811–1818. doi:10.1021/acs.analchem.7b03800.

[99] Schröder, U.C., Ramoji, A., Glaser, U., Sachse, S., Leiterer, C., Csaki, A., Hübner, U., Fritzsche, W., Pfister, W., Bauer, M., Popp, J. and Neugebauer, U. (2013) 'Combined dielectrophoresis-Raman setup for the classification of pathogens recovered from the urinary tract', *Analytical Chemistry*, 85(22), pp. 10717–10724. doi:10.1021/ac4021616.

[100] Pethig, R. and Markx, G.H. (1997) 'Applications of dielectrophoresis in biotechnology', *Trends in Biotechnology*. doi:10.1016/S0167-7799(97)01096-2.

[101] Gómez-Estaca, J., López-de-Dicastillo, C., Hernández-Muñoz, P., Catalá, R. and Gavara, R. (2014) 'Advances in antioxidant active food packaging', *Trends in Food Science and Technology*. doi:10.1016/j.tifs.2013.10.008.

[102] Harris, W.S. (2007) 'Omega-3 fatty acids and cardiovascular disease: A case for omega-3 index as a new risk factor', *Pharmacological Research*. doi:10.1016/j.phrs.2007.01.013.

[103] Masuda, T., Inaba, Y., Maekawa, T., Takeda, Y., Tamura, H. and Yamaguchi, H. (2002) 'Recovery mechanism of the antioxidant activity from carnosic acid quinone, an oxidized sage and rosemary antioxidant', *Journal of Agricultural and Food Chemistry*. doi:10.1021/jf025605o.

[104] Amakura, Y., Umino, Y., Tsuji, S. and Tonogai, Y. (2000) 'Influence of jam processing on the radical scavenging activity and phenolic content in berries', *Journal of Agricultural and Food Chemistry*. doi:10.1021/jf000849z.

[105] Nerín, C. (2010) 'Antioxidant active food packaging and antioxidant edible films', in *Oxidation in Foods and Beverages and Antioxidant Applications*. doi:10.1533/9780857090331.3.496.

[106] Ahmed, I., Lin, H., Zou, L., Brody, A.L., Li, Z., Qazi, I.M., Pavase, T.R. and Lv, L. (2017) 'A comprehensive review on the application of active packaging technologies to muscle foods', *Food Control*. doi:10.1016/j.foodcont.2017.06.009.

[107] López-Rubio, A., Almenar, E., Hernandez-Muñoz, P., Lagarón, J.M., Catalá, R. and

Gavara, R. (2004) 'Overview of active polymer-based packaging technologies for food applications', *Food Reviews International*. doi:10.1081/FRI-200033462.

[108] Mastromatteo, Marcella, Mastromatteo, Marianna, Conte, A. and Del Nobile, M.A. (2010) 'Advances in controlled release devices for food packaging applications', *Trends in Food Science and Technology*. doi:10.1016/j.tifs.2010.07.010.

[109] COMA, V. (2008) 'Bioactive packaging technologies for extended shelf life of meat-based products', *Meat Science*. doi:10.1016/j.meatsci.2007.07.035.

[110] Han, J.W., Ruiz-Garcia, L., Qian, J.P. and Yang, X.T. (2018) 'Food Packaging: A Comprehensive Review and Future Trends', *Comprehensive Reviews in Food Science and Food Safety*. doi:10.1111/1541-4337.12343.

[111] Ong, G., Kasi, R. and Subramaniam, R. (2021) 'A review on plant extracts as natural additives in coating applications', *Progress in Organic Coatings*. doi:10.1016/j.porgcoat.2020.106091.

[112] Siripatrawan, U. and Harte, B.R. (2010) 'Physical properties and antioxidant activity of an active film from chitosan incorporated with green tea extract', *Food Hydrocolloids*. doi:10.1016/j.foodhyd.2010.04.003.

[113] Wang, Y.C., Lu, L. and Gunasekaran, S. (2017) 'Biopolymer/gold nanoparticles composite plasmonic thermal history indicator to monitor quality and safety of perishable bioproducts', *Biosensors and Bioelectronics*. doi:10.1016/j.bios.2017.01.047.

[114] Peng, Y., Wu, Y. and Li, Y. (2013) 'Development of tea extracts and chitosan composite films for active packaging materials', *International Journal of Biological Macromolecules*. doi:10.1016/j.ijbiomac.2013.04.019.

[115] Bentayeb, K., Rubio, C., Batlle, R. and Nerín, C. (2007) 'Direct determination of carnosic acid in a new active packaging based on natural extract of rosemary', *Analytical and Bioanalytical Chemistry*. doi:10.1007/s00216-007-1570-y.

[116] López-De-Dicastillo, C., Alonso, J.M., Catalá, R., Gavara, R. and Hernández-Munoz, P. (2010) 'Improving the antioxidant protection of packaged food by incorporating natural flavonoids into ethylene-vinyl alcohol copolymer (EVOH) films', *Journal of Agricultural and Food Chemistry*. doi:10.1021/jf1022324.

[117] Granda-Restrepo, D.M., Soto-Valdez, H., Peralta, E., Troncoso-Rojas, R., Vallejo-Córdoba, B., Gámez-Meza, N. and Graciano-Verdugo, A.Z. (2009) 'Migration of α-tocopherol from an active multilayer film into whole milk powder', *Food Research International*. doi:10.1016/j.foodres.2009.07.007.

[118] Barbosa-Pereira, L., Aurrekoetxea, G.P., Angulo, I., Paseiro-Losada, P. and Cruz, J.M. (2014) 'Development of new active packaging films coated with natural phenolic compounds to improve the oxidative stability of beef', *Meat Science*. doi:10.1016/j.meatsci.2014.02.006.

[119] López-De-Dicastillo, C., Pezo, D., Nerín, C., López-Carballo, G., Catalá, R., Gavara, R. and Hernández-Muñoz, P. (2012) 'Reducing oxidation of foods through antioxidant active packaging based on ethyl vinyl alcohol and natural flavonoids', *Packaging Technology and Science*. doi:10.1002/pts.992.

[120] Robards, K., Prenzler, P.D., Tucker, G., Swatsitang, P. and Glover, W. (1999) 'Phenolic compounds and their role in oxidative processes in fruits', *Food Chemistry*. doi:10.1016/S0308-8146(99)00093-X.

[121] Carrizo, D., Taborda, G., Nerín, C. and Bosetti, O. (2016) 'Extension of shelf life of two fatty foods using a new antioxidant multilayer packaging containing green tea extract', *Innovative Food Science and Emerging Technologies*. doi:10.1016/j.ifset.2015.10.018.

[122] Lafka, T.I., Sinanoglou, V. and Lazos, E.S. (2007) 'On the extraction and antioxidant activity of phenolic compounds from winery wastes', *Food Chemistry*. doi:10.1016/j.foodchem.2007.01.068.

[123] Teissedre, P.L., Frankel, E.N., Waterhouse, A.L., Peleg, H. and Bruce German, J. (1996) 'Inhibition of in vitro human LDL oxidation by phenolic antioxidants from grapes and wines', *Journal of the Science of Food and Agriculture*. doi:10.1002/(sici)1097-0010(199601)70:1<55::aid-jsfa471>3.3.co;2-o.

[124] Jayaprakasha, G.K., Selvi, T. and Sakariah, K.K. (2003) 'Antibacterial and antioxidant activities of grape (Vitis vinifera) seed extracts', *Food Research International*. doi:10.1016/S0963-9969(02)00116-3.

[125] Rodis, P.S., Karathanos, V.T. and Mantzavinou, A. (2002) 'Partitioning of olive oil antioxidants between oil and water phases', *Journal of Agricultural and Food Chemistry*. doi:10.1021/jf010864j.

[126] Pereira, A.P., Ferreira, I.C.F.R., Marcelino, F., Valentão, P., Andrade, P.B., Seabra, R., Estevinho, L., Bento, A. and Pereira, J.A. (2007) 'Phenolic compounds and antimicrobial activity of olive (Olea europaea L. Cv. Cobrançosa) leaves', *Molecules*. doi:10.3390/12051153.

[127] Jerman Klen, T. and Mozetič Vodopivec, B. (2012) 'The fate of olive fruit phenols during commercial olive oil processing: Traditional press versus continuous two- and three-phase centrifuge', *LWT - Food Science and Technology*. doi:10.1016/j.lwt.2012.03.029.

[128] Lozano-Sánchez, J., Giambanelli, E., Quirantes-Piné, R., Cerretani, L., Bendini, A., Segura-Carretero, A. and Fernández-Gutiérrez, A. (2011) 'Wastes generated during the storage of extra virgin olive oil as a natural source of phenolic compounds', *Journal of Agricultural and Food Chemistry*. doi:10.1021/jf202596q.

[129] Bulotta, S., Oliverio, M., Russo, D. and Procopio, A. (2013) 'Biological activity of oleuropein and its derivatives', in *Natural Products: Phytochemistry, Botany and Metabolism of Alkaloids, Phenolics and Terpenes*. doi:10.1007/978-3-642-22144-6_156.

[130] El-Abbassi, A., Kiai, H. and Hafidi, A. (2012) 'Phenolic profile and antioxidant activities of olive mill wastewater', *Food Chemistry*. doi:10.1016/j.foodchem.2011.11.013.

[131] Suárez, M., Romero, M.P. and Motilva, M.J. (2010) 'Development of a phenol-enriched olive oil with phenolic compounds from olive cake', *Journal of Agricultural and Food Chemistry*. doi:10.1021/jf102203x.

[132] Visioli, F., Bellomo, G. and Galli, C. (1998) 'Free radical-scavenging properties of olive oil polyphenols', *Biochemical and Biophysical Research Communications*. doi:10.1006/bbrc.1998.8735.

[133] Araújo, M., Pimentel, F.B., Alves, R.C. and Oliveira, M.B.P.P. (2015) 'Phenolic compounds from olive mill wastes: Health effects, analytical approach and application as food antioxidants', *Trends in Food Science and Technology*. doi:10.1016/j.tifs.2015.06.010.

[134] Kim, T.J., Kim, J.H., Jin, Y.R. and Yun, Y.P. (2006) 'The inhibitory effect and mechanism of luteolin 7-glucoside on rat aortic vascular smooth muscle cell proliferation', *Archives of Pharmacal Research*. doi:10.1007/BF02977471.

[135] Moudache, M., Colon, M., Nerín, C. and Zaidi, F. (2016) 'Phenolic content and antioxidant activity of olive by-products and antioxidant film containing olive leaf extract', *Food Chemistry*. doi:10.1016/j.foodchem.2016.06.001.

[136] Moudache, M., Nerín, C., Colon, M. and Zaidi, F. (2017) 'Antioxidant effect of an innovative active plastic film containing olive leaves extract on fresh pork meat and its evaluation by Raman spectroscopy', *Food Chemistry*. doi:10.1016/j.foodchem.2017.02.023.

[137] Khalafalla, M.M., Abdellatef, E., Dafalla, H.M., Nassrallah, A.A., Aboul-Enein, K.M., Lightfoot, D.A., El-Deeb, F.E. and El-Shemy, H.A. (2010) 'Active principle from Moringa oleifera Lam leaves effective against two leukemias and a hepatocarcinoma', *African Journal of Biotechnology*. doi:10.4314/ajb.v9i49.

[138] Makkar, H.P.S. and Becker, K. (1996) 'Nutrional value and antinutritional components of whole and ethanol extracted Moringa oleifera leaves', *Animal Feed Science and Technology*. doi:10.1016/S0377-8401(96)01023-1.

[139] Fahey, J. (2005) 'Moringa oleifera: A Review of the Medical Evidence for Its Nutritional, Therapeutic, and Prophylactic Properties. Part 1.', *Trees for life Journal*.

[140] Adedapo, A.A., Jimoh, F.O., Koduru, S., Afolayan, A.J. and Masika, P.J. (2008) 'Antibacterial and antioxidant properties of the methanol extracts of the leaves and stems of Calpurnia aurea', *BMC Complementary and Alternative Medicine*. doi:10.1186/1472-6882-8-53.

[141] Oyedemi, S.O., Bradley, G. and Afolayan, A.J. (2010) 'In -vitro and -vivo antioxidant

activities of aqueous extract of Strychnos henningsii Gilg', *African Journal of Pharmacy and Pharmacology*.

[142] Wright, R.J., Lee, K.S., Hyacinth, H.I., Hibbert, J.M., Reid, M.E., Wheatley, A.O. and Asemota, H.N. (2017) 'An investigation of the antioxidant capacity in extracts from Moringa oleifera plants grown in Jamaica', *Plants*. doi:10.3390/plants6040048.

[143] Rahman, M. Mashiar, Sheikh, M.M.I., Sharmin, S.A., Islam, M.S., Rahman, M.A., Rahman, M. Mizanur and Alam, M.F. (2009) 'Antibacterial activity of leaf juice and extracts of Moringa oleifera Lam. against some human pathogenic bacteria', *Chiang Mai University Journal of Natural Sciences*.

[144] Handa, S.S., Khanuja, S.P.S., Longo, G. and Rakesh, D.D. (2008) *Extraction Technologies for Medicinal and Aromatic Plants*, *Journal of natural products*.

[145] Vongsak, B., Sithisarn, P., Mangmool, S., Thongpraditchote, S., Wongkrajang, Y. and Gritsanapan, W. (2013) 'Maximizing total phenolics, total flavonoids contents and antioxidant activity of Moringa oleifera leaf extract by the appropriate extraction method', *Industrial Crops and Products*. doi:10.1016/j.indcrop.2012.09.021.

[146] 'A Review on the Extraction Methods Use in Medicinal Plants, Principle, Strength and Limitation' (2015) *Medicinal & Aromatic Plants*. doi:10.4172/2167-0412.1000196.

[147] Kaufmann, B. and Christen, P. (2002) 'Recent extraction techniques for natural products: Microwave-assisted extraction and pressurised solvent extraction', *Phytochemical Analysis*. doi:10.1002/pca.631.

[148] Baldino, L. and Reverchon, E. (2018) 'Challenges in the production of pharmaceutical and food related compounds by SC-CO2 processing of vegetable matter', *Journal of Supercritical Fluids*. doi:10.1016/j.supflu.2017.11.034.

[149] Floris, T., Filippino, G., Scrugli, S., Pinna, M.B., Argiolas, F., Argiolas, A., Murru, M. and Reverchon, E. (2010) 'Antioxidant compounds recovery from grape residues by a supercritical antisolvent assisted process', *Journal of Supercritical Fluids*. doi:10.1016/j.supflu.2010.04.006.

[150] Baldino, L., Della Porta, G., Osseo, L.S., Reverchon, E. and Adami, R. (2018) 'Concentrated oleuropein powder from olive leaves using alcoholic extraction and supercritical CO2 assisted extraction', *Journal of Supercritical Fluids*. doi:10.1016/j.supflu.2017.09.026.

[151] Pezo, D., Salafranca, J. and Nerín, C. (2006) 'Design of a method for generation of gas-phase hydroxyl radicals, and use of HPLC with fluorescence detection to assess the antioxidant capacity of natural essential oils', *Analytical and Bioanalytical Chemistry*. doi:10.1007/s00216-006-0395-4.

[152] Prior, R.L., Wu, X. and Schaich, K. (2005) 'Standardized methods for the determination of antioxidant capacity and phenolics in foods and dietary supplements', *Journal of*

Agricultural and Food Chemistry. doi:10.1021/jf0502698.

[153] Hussain, M.A. and Dawson, C.O. (2013) 'Economic impact of food safety outbreaks on food businesses', *Foods*. doi:10.3390/foods2040585.

[154] Fletcher, E.N.R. (2012) 'ANCIENT METROLOGY', *Survey Review*. doi:10.1179/003962668791976209.

[155] *Metrofood* (2021). Available at: http://www.metrofood.eu/.

[156] Mridha, Z. (2013) 'Food safety-A global concern', *Bangladesh Journal of Medical Biochemistry*. doi:10.3329/bjmb.v4i2.13768.

[157] Pinstrup-Andersen, P. (2009) 'Food security: definition and measurement', *Food Security*. doi:10.1007/s12571-008-0002-y.

[158] De Prins, J. (2014) 'Book review on Edible insects: Future prospects for food and feed security', *Advances in Entomology*. doi:10.4236/ae.2014.21008.

[159] Aung, M.M. and Chang, Y.S. (2014) 'Traceability in a food supply chain: Safety and quality perspectives', *Food Control*. doi:10.1016/j.foodcont.2013.11.007.

[160] Regattieri, A., Gamberi, M. and Manzini, R. (2007) 'Traceability of food products: General framework and experimental evidence', *Journal of Food Engineering*. doi:10.1016/j.jfoodeng.2006.10.032.

[161] *Aims of EU quality schemes* (no date fe). Available at: https://ec.europa.eu/agriculture/quality/.

[162] *A European Green Deal* (2021). Available at: https://ec.europa.eu/info/strategy/priorities-2019-2024/european-green-deal_en.

[163] Uzunbajakava, N., Lenferink, A., Kraan, Y., Volokhina, E., Vrensen, G., Greve, J. and Otto, C. (2003) 'Nonresonant confocal Raman imaging of DNA and protein distribution in apoptotic cells', *Biophysical Journal*. doi:10.1016/S0006-3495(03)75124-8.

[164] Li, M., Xu, J., Romero-Gonzalez, M., Banwart, S.A. and Huang, W.E. (2012) 'Single cell Raman spectroscopy for cell sorting and imaging', *Current Opinion in Biotechnology*. doi:10.1016/j.copbio.2011.11.019.

[165] Smekal, A. (1923) 'Zur Quantentheorie der Dispersion', *Die Naturwissenschaften*. doi:10.1007/BF01576902.

[166] Raman, C. V. and Krishnan, K.S. (1928) 'A new type of secondary radiation [11]', *Nature*. doi:10.1038/121501c0.

[167] 'Eine neue Erscheinung bei der Lichtzerstreuung in Krystallen' (1928) *Die Naturwissenschaften*. doi:10.1007/BF01506807.

[168] Lu, X., Al-Qadiri, H.M., Lin, M. and Rasco, B.A. (2011) 'Application of Mid-infrared and Raman Spectroscopy to the Study of Bacteria', *Food and Bioprocess Technology*, 4(6), pp. 919–935. doi:10.1007/s11947-011-0516-8.

[169] Piqueras, S., Duponchel, L., Tauler, R. and De Juan, A. (2011) 'Resolution and segmentation of hyperspectral biomedical images by Multivariate Curve Resolution-Alternating Least Squares', *Analytica Chimica Acta*. doi:10.1016/j.aca.2011.05.020.

[170] de Juan, A. and Tauler, R. (2006) 'Multivariate Curve Resolution (MCR) from 2000: Progress in concepts and applications', *Critical Reviews in Analytical Chemistry*. doi:10.1080/10408340600970005.

[171] Mandrile, L., Rotunno, S., Miozzi, L., Vaira, A.M., Giovannozzi, A.M., Rossi, A.M. and Noris, E. (2019) 'Nondestructive Raman Spectroscopy as a Tool for Early Detection and Discrimination of the Infection of Tomato Plants by Two Economically Important Viruses', *Analytical Chemistry*. doi:10.1021/acs.analchem.9b01323.

[172] Mandrile, L., Amato, G., Marchis, D., Martra, G. and Rossi, A.M. (2017) 'Species-specific detection of processed animal proteins in feed by Raman spectroscopy', *Food Chemistry*. doi:10.1016/j.foodchem.2017.02.089.

[173] Clemente, I., Aznar, M., Salafranca, J. and Nerín, C. (2017) 'Raman spectroscopy, electronic microscopy and SPME-GC-MS to elucidate the mode of action of a new antimicrobial food packaging material', *Analytical and Bioanalytical Chemistry*. doi:10.1007/s00216-016-0022-y.

[174] Fenn, M.B., Xanthopoulos, P., Pyrgiotakis, G., Grobmyer, S.R., Pardalos, P.M. and Hench, L.L. (2011) 'Raman spectroscopy for clinical oncology', *Advances in Optical Technologies*. doi:10.1155/2011/213783.

[175] Barzan, G., Sacco, A., Mandrile, L., Giovannozzi, A.M., Brown, J., Portesi, C., Alexander, M.R., Williams, P., Hardie, K.R. and Rossi, A.M. (2020) 'New frontiers against antibiotic resistance: A Raman-based approach for rapid detection of bacterial susceptibility and biocide-induced antibiotic cross-tolerance', *Sensors and Actuators, B: Chemical*, 309. doi:10.1016/j.snb.2020.127774.

[176] Clemente, I., Aznar, M. and Nerín, C. (2016) 'Raman Imaging Spectroscopy as a Tool to Investigate the Cell Damage on Aspergillus ochraceus Caused by an Antimicrobial Packaging Containing Benzyl Isothiocyanate', *Analytical Chemistry*. doi:10.1021/acs.analchem.6b00116.

[177] Wiegand, I., Hilpert, K. and Hancock, R.E.W. (2008) 'Agar and broth dilution methods to determine the minimal inhibitory concentration (MIC) of antimicrobial substances', *Nature Protocols*, 3(2), pp. 163–175. doi:10.1038/nprot.2007.521.

[178] *Performance Standards for Antimicrobial Susceptibility Testing* (2007) *Clinical and Laboratory Standards Institute - NCCLS*. doi:1-56238-525-5.

[179] Smilde, A.K., Jansen, J.J., Hoefsloot, H.C.J., Lamers, R.J.A.N., van der Greef, J. and Timmerman, M.E. (2005) 'ANOVA-simultaneous component analysis (ASCA): A new tool for analyzing designed metabolomics data', *Bioinformatics*, 21(13), pp. 3043–3048. doi:10.1093/bioinformatics/bti476.

[180] Zwanenburg, G., Hoefsloot, H.C.J., Westerhuis, J.A., Jansen, J.J. and Smilde, A.K. (2011) 'ANOVA–principal component analysis and ANOVA–simultaneous component analysis: A comparison', *Journal of Chemometrics*. doi:10.1002/cem.1400.

[181] Lindgren, P.K., Karlsson, Å. and Hughes, D. (2003) 'Mutation rate and evolution of fluoroquinolone resistance in Escherichia coli isolates from patients with urinary tract infections', *Antimicrobial Agents and Chemotherapy*, 47(10), pp. 3222–3232. doi:10.1128/AAC.47.10.3222-3232.2003.

[182] Fasugba, O., Gardner, A., Mitchell, B.G. and Mnatzaganian, G. (2015) 'Ciprofloxacin resistance in community- and hospital-acquired Escherichia coli urinary tract infections: A systematic review and meta-analysis of observational studies', *BMC Infectious Diseases*. doi:10.1186/s12879-015-1282-4.

[183] Carey, D.E. and McNamara, P.J. (2014) 'The impact of triclosan on the spread of antibiotic resistance in the environment', *Frontiers in Microbiology*, 5(DEC), pp. 1–11. doi:10.3389/fmicb.2014.00780.

[184] Inagaki, F., Tasumi, M. and Miyazawa, T. (1975) 'Vibrational analysis of polyene chains. Assignments of the resonance Raman lines of poly (acetylene) and β-carotene', *Journal of Raman Spectroscopy*. doi:10.1002/jrs.1250030404.

[185] Naumann, D. (1998) 'Infrared and NIR Raman spectroscopy in medical microbiology', *Proceedings of SPIE*, 3257(i), pp. 245–257. doi:10.1117/12.306089.

[186] Harz, M., Rösch, P., Peschke, K.D., Ronneberger, O., Burkhardt, H. and Popp, J. (2005) 'Micro-Raman spectroscopic identification of bacterial cells of the genus Staphylococcus and dependence on their cultivation conditions', *Analyst*. doi:10.1039/b507715j.

[187] Movasaghi, Z., Rehman, S. and Rehman, I.U. (2007) 'Raman spectroscopy of biological tissues', *Applied Spectroscopy Reviews*, 42(5), pp. 493–541. doi:10.1080/05704920701551530.

[188] Harz, M., Kiehntopf, M., Stöckel, S., Rösch, P., Straube, E., Deufer, T. and Popp, J. (2009) 'Direct analysis of clinical relevant single bacterial cells from cerebrospinal fluid during bacterial meningitis by means of micro-Raman spectroscopy', *Journal of Biophotonics*. doi:10.1002/jbio.200810068.

[189] Socrates, G. (2001) *Infrared and Raman characteristic group frequencies. Tables and charts*, *Journal of Raman Spectroscopy*.

[190] Kloß, S., Kampe, B., Sachse, S., Rösch, P., Straube, E., Pfister, W., Kiehntopf, M. and Popp, J. (2013) 'Culture independent raman spectroscopic identification of urinary tract

infection pathogens: A proof of principle study', *Analytical Chemistry*, 85(20), pp. 9610–9616. doi:10.1021/ac401806f.

[191] Pätzold, R., Keuntje, M., Theophile, K., Müller, J., Mielcarek, E., Ngezahayo, A. and Anders-von Ahlften, A. (2008) 'In situ mapping of nitrifiers and anammox bacteria in microbial aggregates by means of confocal resonance Raman microscopy', *Journal of Microbiological Methods*, 72(3), pp. 241–248. doi:10.1016/j.mimet.2007.12.003.

[192] Deng, H., Bloomfield, V.A., Benevides, J.M. and Thomas, G.J. (1999) 'Dependence of the raman signature of genomic B-DNA on nucleotide base sequence', *Biopolymers*, 50(6), pp. 656–666. doi:10.1002/(SICI)1097-0282(199911)50:6<656::AID-BIP10>3.0.CO;2-9.

[193] De Gelder, J., De Gussem, K., Vandenabeele, P. and Moens, L. (2007) 'Reference database of Raman spectra of biological molecules', *Journal of Raman Spectroscopy*, 38(9), pp. 1133–1147. doi:10.1002/jrs.1734.

[194] Fisher, L.M., Lawrence, J.M., Josty, I.C., Hopewell, R., Margerrison, E.E.C. and Cullen, M.E. (1989) 'Ciprofloxacin and the fluoroquinolones. New concepts on the mechanism of action and resistance', *The American Journal of Medicine*. doi:10.1016/0002-9343(89)90010-7.

[195] Smart, A., de Lacy Costello, B., White, P., Avison, M., Batty, C., Turner, C., Persad, R. and Ratcliffe, N. (2019) 'Sniffing out resistance – Rapid identification of urinary tract infection-causing bacteria and their antibiotic susceptibility using volatile metabolite profiles', *Journal of Pharmaceutical and Biomedical Analysis*. doi:10.1016/j.jpba.2019.01.044.

[196] Carey, D.E. and McNamara, P.J. (2014) 'The impact of triclosan on the spread of antibiotic resistance in the environment', *Frontiers in Microbiology*. doi:10.3389/fmicb.2014.00780.

[197] Westfall, C., Flores-Mireles, A.L., Robinson, J.I., Lynch, A.J.L., Hultgren, S., Henderson, J.P. and Levin, P.A. (2019) ' The widely used antimicrobial triclosan induces high levels of antibiotic tolerance in vitro and reduces antibiotic efficacy up to 100-fold in vivo ', *Antimicrobial Agents and Chemotherapy*, pp. 1–31. doi:10.1128/aac.02312-18.

[198] Calafat, A.M., Ye, X., Wong, L.Y., Reidy, J.A. and Needham, L.L. (2008) 'Urinary concentrations of triclosan in the U.S. population: 2003-2004', *Environmental Health Perspectives*. doi:10.1289/ehp.10768.

[199] MacIsaac, J.K., Gerona, R.R., Blanc, P.D., Apatira, L., Friesen, M.W., Coppolino, M. and Janssen, S. (2014) 'Health care worker exposures to the antibacterial agent triclosan', *Journal of Occupational and Environmental Medicine*, 56(8), pp. 834–839. doi:10.1097/JOM.0000000000000183.

[200] Amigo, J.M., Martí, I. and Gowen, A. (2013) 'Hyperspectral Imaging and Chemometrics. A Perfect Combination for the Analysis of Food Structure, Composition

and Quality', in *Data Handling in Science and Technology*. doi:10.1016/B978-0-444-59528-7.00009-0.

[201] Eriksson, L., Antti, H., Gottfries, J., Holmes, E., Johansson, E., Lindgren, F., Long, I., Lundstedt, T., Trygg, J. and Wold, S. (2004) 'Using chemometrics for navigating in the large data sets of genomics, proteomics, and metabonomics (gpm)', *Analytical and Bioanalytical Chemistry*. doi:10.1007/s00216-004-2783-y.

[202] Barzan, G., Sacco, A., Mandrile, L., Giovannozzi, A.M., Portesi, C. and Rossi, A.M. (2021) 'Hyperspectral chemical imaging of single bacterial cell structure by raman spectroscopy and machine learning', *Applied Sciences (Switzerland)*. doi:10.3390/app11083409.

[203] Kloß, S., Kampe, B., Sachse, S., Rösch, P., Straube, E., Pfister, W., Kiehntopf, M. and Popp, J. (2013) 'Culture independent raman spectroscopic identification of urinary tract infection pathogens: A proof of principle study', *Analytical Chemistry*. doi:10.1021/ac401806f.

[204] Tamotsu, K., Shinji, F., Akemi, F., Wataru, S., Masahira, H., Jun, K., Hiroshi, O. and Ohara, O. (2014) 'Multiple omics uncovers host-gut microbial mutualism during prebiotic fructooligosaccharide supplementation', *DNA Research*. doi:10.1093/dnares/dsu013.

[205] Motegi, H., Tsuboi, Y., Saga, A., Kagami, T., Inoue, M., Toki, H., Minowa, O., Noda, T. and Kikuchi, J. (2015) 'Identification of Reliable Components in Multivariate Curve Resolution-Alternating Least Squares (MCR-ALS): A Data-Driven Approach across Metabolic Processes', *Scientific Reports*. doi:10.1038/srep15710.

[206] Niki, H., Yamaichi, Y. and Hiraga, S. (2000) 'Dynamic organization of chromosomal DNA in Escherichia coli', *Genes and Development*.

[207] Gordon, G.S. and Wright, A. (2000) 'DNA segregation in bacteria', *Annual Review of Microbiology*. doi:10.1146/annurev.micro.54.1.681.

[208] Shapiro, L. and Losick, R. (2000) 'in the Bacterial Cell', *Cell*, 100(1), pp. 89–98.

[209] Laxminarayan, R., Duse, A., Wattal, C., Zaidi, A.K.M., Wertheim, H.F.L., Sumpradit, N., Vlieghe, E., Hara, G.L., Gould, I.M., Goossens, H., Greko, C., So, A.D., Bigdeli, M., Tomson, G., Woodhouse, W., Ombaka, E., Peralta, A.Q., Qamar, F.N., Mir, F., Kariuki, S., Bhutta, Z.A., Coates, A., Bergstrom, R., Wright, G.D., Brown, E.D. and Cars, O. (2013) 'Antibiotic resistance-the need for global solutions', *The Lancet Infectious Diseases*. doi:10.1016/S1473-3099(13)70318-9.

[210] Agnihotri, S., Mukherji, Soumyo and Mukherji, Suparna (2014) 'Size-controlled silver nanoparticles synthesized over the range 5-100 nm using the same protocol and their antibacterial efficacy', *RSC Advances*, 4(8), pp. 3974–3983. doi:10.1039/c3ra44507k.

[211] Baker, C.N., Stocker, S.A., Culver, D.H. and Thornsberry, C. (1991) 'Comparison of the

E test to agar dilution, broth microdilution, and agar diffusion susceptibility testing techniques by using a special challenge set of bacteria', *Journal of Clinical Microbiology*, 29(3), pp. 533–538.

[212] Morones, J.R., Elechiguerra, J.L., Camacho, A., Holt, K., Kouri, J.B., Ramírez, J.T. and Yacaman, M.J. (2005) 'The bactericidal effect of silver nanoparticles', *Nanotechnology*, 16(10), pp. 2346–2353. doi:10.1088/0957-4484/16/10/059.

[213] Amato, E., Diaz-Fernandez, Y.A., Taglietti, A., Pallavicini, P., Pasotti, L., Cucca, L., Milanese, C., Grisoli, P., Dacarro, C., Fernandez-Hechavarria, J.M. and Necchi, V. (2011) 'Synthesis, characterization and antibacterial activity against gram positive and gram negative bacteria of biomimetically coated silver nanoparticles', *Langmuir*, 27(15), pp. 9165–9173. doi:10.1021/la201200r.

[214] Sotiriou, G.A. and Pratsinis, S.E. (2010) 'Antibacterial activity of nanosilver ions and particles', *Environmental Science and Technology*. doi:10.1021/es101072s.

[215] Pal, S., Tak, Y.K. and Song, J.M. (2015) 'Does the antibacterial activity of silver nanoparticles depend on the shape of the nanoparticle? A study of the gram-negative bacterium Escherichia coli', *Journal of Biological Chemistry*, 290(42), pp. 1712–1720. doi:10.1128/AEM.02218-06.

[216] Ostermeyer, A.K., Kostigen Mumuper, C., Semprini, L. and Radniecki, T. (2013) 'Influence of bovine serum albumin and alginate on silver nanoparticle dissolution and toxicity to Nitrosomonas europaea', *Environmental Science and Technology*. doi:10.1021/es4033106.

[217] Kvítek, L., Panáček, A., Soukupová, J., Kolář, M., Večeřová, R., Prucek, R., Holecová, M. and Zbořil, R. (2008) 'Effect of surfactants and polymers on stability and antibacterial activity of silver nanoparticles (NPs)', *Journal of Physical Chemistry C*, 112(15), pp. 5825–5834. doi:10.1021/jp711616v.

[218] Furno, F., Morley, K.S., Wong, B., Sharp, B.L., Arnold, P.L., Howdle, S.M., Bayston, R., Brown, P.D., Winship, P.D. and Reid, H.J. (2004) 'Silver nanoparticles and polymeric medical devices: A new approach to prevention of infection?', *Journal of Antimicrobial Chemotherapy*. doi:10.1093/jac/dkh478.

[219] Durán, N., Marcato, P.D., De Souza, G.I.H., Alves, O.L. and Esposito, E. (2007) 'Antibacterial effect of silver nanoparticles produced by fungal process on textile fabrics and their effluent treatment', *Journal of Biomedical Nanotechnology*. doi:10.1166/jbn.2007.022.

[220] Taglietti, A., Arciola, C.R., D'Agostino, A., Dacarro, G., Montanaro, L., Campoccia, D., Cucca, L., Vercellino, M., Poggi, A., Pallavicini, P. and Visai, L. (2014) 'Antibiofilm activity of a monolayer of silver nanoparticles anchored to an amino-silanized glass surface', *Biomaterials*. doi:10.1016/j.biomaterials.2013.11.047.

[221] Liu, G., Shen, H., Mao, J., Zhang, L., Jiang, Z., Sun, T., Lan, Q. and Zhang, Z. (2013)

'Transferrin modified graphene oxide for glioma-targeted drug delivery: In vitro and in vivo evaluations', *ACS Applied Materials and Interfaces*. doi:10.1021/am402128s.

[222] Xu, G., Liu, S., Niu, H., Lv, W. and Wu, R. (2014) 'Functionalized mesoporous carbon nanoparticles for targeted chemo-photothermal therapy of cancer cells under near-infrared irradiation', *RSC Advances*. doi:10.1039/c4ra03993a.

[223] Zapotoczna, M., Forde, É., Hogan, S., Humphreys, H., O'gara, J.P., Fitzgerald-Hughes, D., Devocelle, M. and O'Neill, E. (2017) 'Eradication of staphylococcus aureus biofilm infections using synthetic antimicrobial peptides', *Journal of Infectious Diseases*. doi:10.1093/infdis/jix062.

[224] Wan, Y., Guo, Z., Jiang, X., Fang, K., Lu, X., Zhang, Y. and Gu, N. (2013) 'Quasi-spherical silver nanoparticles: Aqueous synthesis and size control by the seed-mediated Lee-Meisel method', *Journal of Colloid and Interface Science*, 394(1), pp. 263–268. doi:10.1016/j.jcis.2012.12.037.

[225] Mandrile, L., Cagnasso, I., Berta, L., Giovannozzi, A.M., Petrozziello, M., Pellegrino, F., Asproudi, A., Durbiano, F. and Rossi, A.M. (2020) 'Direct quantification of sulfur dioxide in wine by Surface Enhanced Raman Spectroscopy', *Food Chemistry*. doi:10.1016/j.foodchem.2020.127009.

[226] Mandrile, L., Vona, M., Giovannozzi, A.M., Salafranca, J., Martra, G. and Rossi, A.M. (2020) 'Migration study of organotin compounds from food packaging by surface-enhanced Raman scattering', *Talanta*. doi:10.1016/j.talanta.2020.121408.

[227] Abràmoff, M.D., Magalhães, P.J. and Ram, S.J. (2004) 'Image processing with imageJ', *Biophotonics International*. doi:10.1201/9781420005615.ax4.

[228] Barzan, G., Rocchetti, L., Portesi, C., Pellegrino, F., Taglietti, A., Rossi, A.M. and Giovannozzi, A.M. (2021) 'Surface Minimal Bactericidal Concentration: A comparative study of active glasses functionalized with different-sized silver nanoparticles', *Colloids and Surfaces B: Biointerfaces*. doi:10.1016/j.colsurfb.2021.111800.

[229] Quan, F., Mao, A., Ding, M., Ran, S., Wang, J., Yang, G. and Yan, Y. (2018) 'Combustion synthesis and formation mechanism of silver nanoparticles', *International Journal of Materials Research*, 109(8), pp. 751–755. doi:10.3139/146.111666.

[230] Chen, M., Feng, Y.G., Wang, X., Li, T.C., Zhang, J.Y. and Qian, D.J. (2007) 'Silver nanoparticles capped by oleylamine: Formation, growth, and self-organization', *Langmuir*. doi:10.1021/la700553d.

[231] He, R.X., Liang, R., Peng, P. and Norman Zhou, Y. (2017) 'Effect of the size of silver nanoparticles on SERS signal enhancement', *Journal of Nanoparticle Research*. doi:10.1007/s11051-017-3953-0.

[232] Tang, S. and Zheng, J. (2018) 'Antibacterial Activity of Silver Nanoparticles: Structural Effects', *Advanced Healthcare Materials*. doi:10.1002/adhm.201701503.

[233] Long, Y.M., Hu, L.G., Yan, X.T., Zhao, X.C., Zhou, Q.F., Cai, Y. and Jiang, G. Bin (2017) 'Surface ligand controls silver ion release of nanosilver and its antibacterial activity against Escherichia coli', *International Journal of Nanomedicine*. doi:10.2147/IJN.S132327.

[234] Radniecki, T.S., Stankus, D.P., Neigh, A., Nason, J.A. and Semprini, L. (2011) 'Influence of liberated silver from silver nanoparticles on nitrification inhibition of Nitrosomonas europaea', *Chemosphere*. doi:10.1016/j.chemosphere.2011.06.039.

[235] Agnihotri, S., Mukherji, Soumyo and Mukherji, Suparna (2013) 'Immobilized silver nanoparticles enhance contact killing and show highest efficacy: Elucidation of the mechanism of bactericidal action of silver', *Nanoscale*. doi:10.1039/c3nr00024a.

[236] Pallavicini, P., Taglietti, A., Dacarro, G., Antonio Diaz-Fernandez, Y., Galli, M., Grisoli, P., Patrini, M., Santucci De Magistris, G. and Zanoni, R. (2010) 'Self-assembled monolayers of silver nanoparticles firmly grafted on glass surfaces: Low Ag+ release for an efficient antibacterial activity', *Journal of Colloid and Interface Science*, 350(1), pp. 110–116. doi:10.1016/j.jcis.2010.06.019.

[237] Dacarro, G., Cucca, L., Grisoli, P., Pallavicini, P., Patrini, M. and Taglietti, A. (2012) 'Monolayers of polyethilenimine on flat glass: A versatile platform for cations coordination and nanoparticles grafting in the preparation of antibacterial surfaces', *Dalton Transactions*. doi:10.1039/c1dt11373a.

[238] Noviello, S., Ianniello, F., Leone, S. and Esposito, S. (2002) 'Attività batteriostatica e battericida di levofloxacina e ciprofloxacina verso uropatogeni determinata mediante MIC, MBC, time-kill curves e analisi dell'indice di batteriocidia', *Infezioni in Medicina*.

[239] You, Y., Das, K.K., Guo, H., Chang, C.W., Navas-Moreno, M., Chan, J.W., Verburg, P., Poulson, S.R., Wang, X., Xing, B. and Yang, Y. (2017) 'Microbial Transformation of Multiwalled Carbon Nanotubes by Mycobacterium vanbaalenii PYR-1', *Environmental Science and Technology*. doi:10.1021/acs.est.6b04523.

[240] Zhang, L., Petersen, E.J., Habteselassie, M.Y., Mao, L. and Huang, Q. (2013) 'Degradation of multiwall carbon nanotubes by bacteria', *Environmental Pollution*. doi:10.1016/j.envpol.2013.05.058.

[241] Chen, M., Qin, X. and Zeng, G. (2017) 'Biodegradation of Carbon Nanotubes, Graphene, and Their Derivatives', *Trends in Biotechnology*. doi:10.1016/j.tibtech.2016.12.001.

[242] Kang, S., Pinault, M., Pfefferle, L.D. and Elimelech, M. (2007) 'Single-walled carbon nanotubes exhibit strong antimicrobial activity', *Langmuir*. doi:10.1021/la701067r.

[243] Zhao, C., Deng, B., Chen, G., Lei, B., Hua, H., Peng, H. and Yan, Z. (2016) 'Large-area chemical vapor deposition-grown monolayer graphene-wrapped silver nanowires for broad-spectrum and robust antimicrobial coating', *Nano Research*. doi:10.1007/s12274-016-0984-2.

[244] Tu, Y., Lv, M., Xiu, P., Huynh, T., Zhang, M., Castelli, M., Liu, Z., Huang, Q., Fan, C., Fang, H. and Zhou, R. (2013) 'Destructive extraction of phospholipids from Escherichia coli membranes by graphene nanosheets', *Nature Nanotechnology*. doi:10.1038/nnano.2013.125.

[245] McEwen, G.D., Wu, Y. and Zhou, A. (2010) 'Probing nanostructures of bacterial extracellular polymeric substances versus culture time by Raman microspectroscopy and atomic force microscopy', *Biopolymers*. doi:10.1002/bip.21315.

[246] Lombardi, L., Maisetta, G., Batoni, G. and Tavanti, A. (2015) 'Insights into the antimicrobial properties of hepcidins: Advantages and drawbacks as potential therapeutic agents', *Molecules*. doi:10.3390/molecules20046319.

[247] Chung, P.Y. and Khanum, R. (2017) 'Antimicrobial peptides as potential anti-biofilm agents against multidrug-resistant bacteria', *Journal of Microbiology, Immunology and Infection*. doi:10.1016/j.jmii.2016.12.005.

[248] Tang, Z., Ma, Q., Chen, X., Chen, T., Ying, Y., Xi, X., Wang, L., Ma, C., Shaw, C. and Zhou, M. (2021) 'Recent Advances and Challenges in Nanodelivery Systems for Antimicrobial Peptides (AMPs)', *Antibiotics*. doi:10.3390/antibiotics10080990.

[249] Devocelle, M. (2012) 'Targeted antimicrobial peptides', *Frontiers in Immunology*. doi:10.3389/fimmu.2012.00309.

[250] Romeo, D., Skerlavaj, B., Bolognesi, M. and Gennaro, R. (1988) 'Structure and bactericidal activity of an antibiotic dodecapeptide purified from bovine neutrophils', *Journal of Biological Chemistry*. doi:10.1016/s0021-9258(19)81553-3.

[251] Wu, M. and Hancock, R.E.W. (1999) 'Interaction of the cyclic antimicrobial cationic peptide bactenecin with the outer and cytoplasmic membrane', *Journal of Biological Chemistry*. doi:10.1074/jbc.274.1.29.

[252] Haug, B.E., Stensen, W., Stiberg, T. and Svendsen, J.S. (2004) 'Bulky nonproteinogenic amino acids permit the design of very small and effective cationic antibacterial peptides', *Journal of Medicinal Chemistry*. doi:10.1021/jm049582b.

[253] Nerín, C., Tovar, L., Djenane, D., Camo, J., Salafranca, J., Beltrán, J.A. and Roncalés, P. (2006) 'Stabilization of beef meat by a new active packaging containing natural antioxidants', *Journal of Agricultural and Food Chemistry*. doi:10.1021/jf060775c.

[254] Nerín, C., Tovar, L. and Salafranca, J. (2008) 'Behaviour of a new antioxidant active film versus oxidizable model compounds', *Journal of Food Engineering*. doi:10.1016/j.jfoodeng.2007.05.027.

[255] Ou, B., Chang, T., Huang, D. and Prior, R.L. (2013) 'Determination of total antioxidant capacity by oxygen radical absorbance capacity (ORAC) using fluorescein as the fluorescence probe: First action 2012.23', *Journal of AOAC International*. doi:10.5740/jaoacint.13-175.

[256] Kupina, S., Fields, C., Roman, M.C. and Brunelle, S.L. (2018) 'Determination of total phenolic content using the Folin-C assay: Single-laboratory validation, first action 2017.13', *Journal of AOAC International*. doi:10.5740/jaoacint.18-0031.

[257] Gajić, I., Stanojević, L., Dinić, A., Stanojević, J., Nikolić, L., Nikolić, V. and Savić, V. (2020) 'The chemical composition of the essential oil and volatile compounds from caraway fruit (Carum carvi L.) extracted by headspace-solid phase microextraction and the antioxidant activity', *Advanced Technologies*. doi:10.5937/savteh2001037g.

[258] Prieto, J.M. (2012) 'Dr Prieto's DPPH Microplate Protocol Procedure: Preparation of DPPH Radical, and antioxidant scavenging assay', *Dr Prieto's DPPH Microplate Protocol*.

[259] Benbettaïeb, N., Tanner, C., Cayot, P., Karbowiak, T. and Debeaufort, F. (2018) 'Impact of functional properties and release kinetics on antioxidant activity of biopolymer active films and coatings', *Food Chemistry*. doi:10.1016/j.foodchem.2017.09.065.

[260] Busolo, M.A. and Lagaron, J.M. (2015) 'Antioxidant polyethylene films based on a resveratrol containing Clay of Interest in Food Packaging Applications', *Food Packaging and Shelf Life*. doi:10.1016/j.fpsl.2015.08.004.

[261] Atarés, L. and Chiralt, A. (2016) 'Essential oils as additives in biodegradable films and coatings for active food packaging', *Trends in Food Science and Technology*. doi:10.1016/j.tifs.2015.12.001.

[262] Henriott, M.L., Herrera, N.J., Ribeiro, F.A., Hart, K.B., Bland, N.A., Eskridge, K. and Calkins, C.R. (2020) 'Impact of myoglobin oxygenation state prior to frozen storage on color stability of thawed beef steaks through retail display', *Meat Science*. doi:10.1016/j.meatsci.2020.108232.

[263] Ribeiro, F.A., Lau, S.K., Furbeck, R.A., Herrera, N.J., Henriott, M.L., Bland, N.A., Fernando, S.C., Subbiah, J., Sullivan, G.A. and Calkins, C.R. (2021) 'Ultimate pH effects on dry-aged beef quality', *Meat Science*. doi:10.1016/j.meatsci.2020.108365.

[264] Ahn, D.U., Olson, D.G., Jo, C., Chen, X., Wu, C. and Lee, J.I. (1998) 'Effect of muscle type, packaging, and irradiation on lipid oxidation, volatile production, and color in raw pork patties', *Meat Science*. doi:10.1016/S0309-1740(97)00101-0.

[265] Babbar, N., Oberoi, H.S., Sandhu, S.K. and Bhargav, V.K. (2014) 'Influence of different solvents in extraction of phenolic compounds from vegetable residues and their evaluation as natural sources of antioxidants', *Journal of Food Science and Technology*. doi:10.1007/s13197-012-0754-4.

[266] Lapornik, B., Prošek, M. and Wondra, A.G. (2005) 'Comparison of extracts prepared from plant by-products using different solvents and extraction time', *Journal of Food Engineering*. doi:10.1016/j.jfoodeng.2004.10.036.

[267] Shi, J., Yu, J., Pohorly, J., Young, J.C., Bryan, M. and Wu, Y. (2003) 'Optimization of

the extraction of polyphenols from grape seed meal by aqueous ethanol solution', *Journal of Food Agriculture & Environment*.

[268] Olsen, E.F., Rukke, E.O., Flåtten, A. and Isaksson, T. (2007) 'Quantitative determination of saturated-, monounsaturated- and polyunsaturated fatty acids in pork adipose tissue with non-destructive Raman spectroscopy', *Meat Science*. doi:10.1016/j.meatsci.2007.02.004.

[269] Kong, J. and Yu, S. (2007) 'Fourier transform infrared spectroscopic analysis of protein secondary structures', *Acta Biochimica et Biophysica Sinica*. doi:10.1111/j.1745-7270.2007.00320.x.

[270] Mecozzi, M., Sturchio, E., Boccia, P., Zanellato, M., Meconi, C. and Peleggi, F. (2017) 'Molecular and structural changes induced by essential oil treatments in Vicia faba roots detected by FTIR and FTNIR spectroscopy', *Environmental Science and Pollution Research*. doi:10.1007/s11356-016-8232-6.

[271] Palaniappan, P.R. and Vijayasundaram, V. (2009) 'The effect of arsenic exposure on the biochemical and mineral contents of Labeo rohita bones: An FT-IR study', *Infrared Physics and Technology*. doi:10.1016/j.infrared.2008.11.002.